Model-based Source Partitioning of Eddy Covariance Flux Measurements

Anne Klosterhalfen

Energie & Umwelt / Energy & Environment
Band / Volume 461
ISBN 978-3-95806-401-0

Mitglied der Helmholtz-Gemeinschaft

JÜLICH
Forschungszentrum

Schriften des Forschungszentrums Jülich
Reihe Energie & Umwelt / Energy & Environment Band / Volume 461

Forschungszentrum Jülich GmbH
Institut für Bio- und Geowissenschaften
Agrosphäre (IBG-3)

Model-based Source Partitioning of Eddy Covariance Flux Measurements

Anne Klosterhalfen

Schriften des Forschungszentrums Jülich
Reihe Energie & Umwelt / Energy & Environment Band / Volume 461

ISSN 1866-1793 ISBN 978-3-95806-401-0

Bibliografische Information der Deutschen Nationalbibliothek.
Die Deutsche Nationalbibliothek verzeichnet diese Publikation in der Deutschen Nationalbibliografie; detaillierte Bibliografische Daten sind im Internet über http://dnb.d-nb.de abrufbar.

Herausgeber und Vertrieb:	Forschungszentrum Jülich GmbH Zentralbibliothek, Verlag 52425 Jülich Tel.: +49 2461 61-5368 Fax: +49 2461 61-6103 zb-publikation@fz-juelich.de www.fz-juelich.de/zb
Umschlaggestaltung:	Grafische Medien, Forschungszentrum Jülich GmbH
Druck:	Grafische Medien, Forschungszentrum Jülich GmbH
Copyright:	Forschungszentrum Jülich 2019

Schriften des Forschungszentrums Jülich
Reihe Energie & Umwelt / Energy & Environment, Band / Volume 461

D 5 (Diss., Bonn, Univ., 2019)

ISSN 1866-1793
ISBN 978-3-95806-401-0

Vollständig frei verfügbar über das Publikationsportal des Forschungszentrums Jülich (JuSER) unter www.fz-juelich.de/zb/openaccess.

This is an Open Access publication distributed under the terms of the Creative Commons Attribution License 4.0, which permits unrestricted use, distribution, and reproduction in any medium, provided the original work is properly cited.

ABSTRACT

Terrestrial ecosystems constantly exchange momentum, energy, and mass (e.g., water vapor, CO_2) with the atmosphere above. This exchange is commonly measured with a micrometeorological technique, the eddy covariance (EC) method. Various components of the measured net fluxes, such as transpiration, evaporation, gross primary production, and soil respiration, cannot be depicted separately by the EC approach. Thus, so-called source partitioning approaches have to be applied to CO_2 and water vapor EC data to gain a better understanding of the prevailing processes and their interrelations in terrestrial ecosystems. A large variety of partitioning procedures with diverse model approaches have been developed, including various driving variables, necessity of different input data and parameterizations. The most robust and commonly used source partitioning tools for CO_2 flux components, often primarily developed to fill gaps in EC measurements, are based on the notion that during night respiration fluxes prevail. They use non-linear regressed relationships of these nighttime observations and physical drivers (e.g., temperature in the approach after Reichstein et al. 2005). Here, the challenge lies within extrapolating the nighttime relationship to daytime conditions, and analogous methods for water fluxes are lacking. In this thesis, next to the approach after Reichstein et al. (2005) various data-driven source partitioning approaches for H_2O and CO_2 fluxes were applied, compared, modified, and evaluated for multiple ecosystems to get a better understanding of the methods' functionality, dependencies, uncertainties, advantages, and shortcomings.

We first describe the coupling and extension of the complex terrestrial ecosystem model AgroC. Further, we conducted a comprehensive model-data fusion study to clarify the CO_2 exchange in agroecosystems and estimate their annual carbon balance. For three test sites in Western Germany, AgroC was calibrated based on soil water content, soil temperature, biometric, and soil respiration measurements for each site, and validated sufficiently in terms of hourly net ecosystem exchange (NEE) measured with the EC technique. Moreover, AgroC reproduced the flux dynamics very effectively after sudden changes in the grassland canopy due to mowing. In a second step, AgroC was optimized with the EC measurements to examine the effect of various objective functions, constraints, and data-transformations on the estimated carbon balance and to compare the results to the established gap-filling approach after Reichstein et al. (2005). It was found that modeled NEE showed a distinct sensitivity to the choice of objective function and the inclusion of soil respiration data in the optimization process. Even though the model performance of the selected optimization strategies did not diverge substantially, the resulting cumulative NEE over simulation time period differed extensively. Therefore, it is concluded that data-transformations, definitions of objective functions, and data sources have to be considered cautiously when a terrestrial ecosystem model is used to determine NEE by means of EC measurements.

Second, we applied the source partitioning approaches after Scanlon and Kustas (2010; SK10) and after Thomas et al. (2008; TH08) to high frequency EC measurements estimating transpiration, evaporation, net primary production, and soil respiration, of various ecosystems (croplands, grasslands, and forests). Both partitioning methods are based on higher-order statistics of the H_2O and CO_2 fluctuations, but proceed differently. SK10 had the tendency to overestimate and TH08 to underestimate soil flux components, where the partitioning of CO_2 fluxes was more irregular than of H_2O fluxes. Results derived with SK10 showed relatively large dependencies on estimated water use efficiency (WUE) on leaf-level, which is needed as an input. Measurements of outgoing longwave radiation used for the estimation of foliage temperature and WUE could slightly increase the quality of the partitioning results. A modification of the TH08 approach, by applying a cluster analysis for the conditional sampling of respiration/evaporation events, performed sufficiently, but did not result in significant advantages compared to the other method versions. The performance of each partitioning approach was dependent on meteorological conditions, plant development, canopy height, canopy density, and measurement height. Foremost, the performance of SK10 correlated negatively with the ratio between measurement and canopy height. The performance of TH08 was more dependent on canopy height and leaf area index. It was found, that all site characteristics which increase dissimilarities between scalars enhance partitioning performance for SK10 and TH08.

Also, we conducted large eddy simulations (LES), simulating the turbulent transport of H_2O and CO_2. SK10 was applied to the synthetic high frequency data generated by LES, and the effects of canopy type, measurement height, given scalar sink-source-distributions, and estimated WUE input were tested regarding the partitioning performance. The LES-based analysis revealed that for a satisfying performance of SK10, a certain degree of decorrelation of the H_2O and CO_2 fluctuations was needed and a correct WUE estimation was favorable. Furthermore, another possible error source, which was so far not yet discussed in the literature, could be detected for the partitioning approach. In the special case of the LES experiments, validity of an essential assumption about the prevailing transport efficiencies of the scalars in the method's derivation was found to be a crucial point for a correct application of SK10.

The application of different source partitioning methods including their various involved assumptions, required input data and work effort showed that still uncertainties and unknowns prevail for the source partitioning of water vapor and CO_2 fluxes. An assessment and evaluation of the partitioning results can only be conducted with additional measurements of flux components on differing spatial and temporal scales independent of the EC measurements. Further, the application of multiple partitioning methods (usage of an ensemble) to the same data can give a better idea about uncertainties in the results.

ZUSAMMENFASSUNG

Terrestrische Ökosysteme tauschen ständig Impuls, Energie und Masse (z.B. Wasserdampf, CO_2) mit der darüber liegenden Atmosphäre aus. Dieser Austausch wird üblicherweise mit einer mikrometeorologischen Methode, der Eddy-Kovarianz-Methode (EC), gemessen. Die einzelnen Komponenten der gemessenen Nettoflüsse, wie Transpiration, Evaporation, Bruttoprimärproduktion und Bodenatmung, können durch die EC-Methode nicht erfasst werden. Daher müssen sogenannte Quellpartitionierungsmethoden (engl. „source partitioning methods“) auf CO_2- und Wasserdampf-EC-Daten angewendet werden, um die vorherrschenden Prozesse und deren Wechselwirkungen in terrestrischen Ökosystemen besser zu verstehen. Eine Vielzahl von Partitionierungsverfahren mit unterschiedlichen Modellansätzen unter Berücksichtigung verschiedener Einflussfaktoren wurde entwickelt. Die am häufigsten verwendeten Partitionierungsmethoden, die nur auf CO_2-Flussmessungen anwendbar sind und oft in erster Linie zum Füllen von Lücken in den EC-Messungen entwickelt wurden, basieren auf der Vorstellung, dass in der Nacht nur Respirationsflüsse vorherrschen. Sie nutzen nichtlineare Regressionen zwischen diesen nächtlichen Messungen und Umweltfaktoren (z.B. Temperatur in der Methode nach Reichstein et al. 2005). Hier liegt die Herausforderung in der Extrapolation der nächtlichen Verhältnisse zu den Tagesbedingungen und zudem fehlt es an analogen Methoden für Wasserflüsse. In dieser Arbeit wurden neben der Methode nach Reichstein et al. (2005) verschiedene analytische Ansätze zur Quellpartitionierung von Wasser- und CO_2-Flüssen angewandt, verglichen, modifiziert und für mehrere Ökosysteme ausgewertet, um ein besseres Verständnis der Funktionalität, ihrer Abhängigkeiten, Unsicherheiten, Vor- und Nachteile zu erhalten.

Zunächst beschreiben wir die Entwicklung und Erweiterung des komplexen terrestrischen Ökosystemmodells AgroC, mit dem wir dann eine umfassende Modell-Daten-Fusionsstudie durchführten, um den CO_2-Austausch in Agrarökosystemen zu klären und deren jährliche Kohlenstoffbilanz abzuschätzen. Für drei Messstandorte in Westdeutschland wurde AgroC auf Basis von Messungen des Bodenwassergehalts, der Bodentemperatur, des Pflanzenwachstums und der Bodenatmung für jeden Standort kalibriert und im Hinblick auf den stündlichen, mit der EC-Methode gemessenem Nettoökosystemaustausch (NEE) erfolgreich validiert. Zudem reproduzierte AgroC die CO_2-Flüsse eines Graslands effektiv nach plötzlichen Änderungen der Vegetation durch Mahd. In einem zweiten Schritt wurde AgroC mit den EC-Messungen optimiert, um die Auswirkungen verschiedener Zielfunktionen, Restriktionen und Datentransformationen auf die simulierte Kohlenstoffbilanz zu untersuchen und die Ergebnisse mit der etablierten Partitionierungsmethode nach Reichstein et al. (2005) zu vergleichen. Es wurde festgestellt, dass die Wahl der Zielfunktion und die Einbeziehung von Bodenatmungsmessungen in den Optimierungsprozess die Simulation von NEE deutlich beeinflussten. Auch wenn die Modellperformance der verschiedenen Optimierungsstrategien nicht wesentlich voneinander abwich, war die resultierende, über den Simulationszeitraum

kumulierte NEE sehr unterschiedlich. Somit sollte die Anwendung von verschiedenen Datentransformationen, Zielfunktionen und Datenquellen gut bedacht sein, wenn ein terrestrisches Ökosystemmodell zur Bestimmung von NEE mittels EC-Messungen verwendet werden soll.

Des Weiteren haben wir die Quellpartitionierungsmethoden nach Scanlon und Kustas (2010; SK10) und nach Thomas et al. (2008; TH08) auf hochfrequente EC-Messungen verschiedener Ökosysteme (Ackerland, Grasland und Wald) angewandt, die die Transpiration, Evaporation, Nettoprimärproduktion und Bodenatmung schätzen. Beide Partitionierungsmethoden basieren auf einer statistischen Analyse der H_2O- und CO_2-Fluktuationen, unterscheiden sich jedoch in der Vorgehensweise. SK10 tendierte zur Überschätzung und TH08 zur Unterschätzung der Bodenflusskomponenten, wobei die Partitionierung der CO_2-Flüsse unregelmäßiger war als die der H_2O-Flüsse. Die mit SK10 gewonnenen Ergebnisse zeigten relativ große Abhängigkeiten von der geschätzten Wassernutzungseffizienz (WUE) auf Blattebene, die als Input benötigt wird. Messungen der langwelligen Ausstrahlung zur Abschätzung der Blatttemperatur zur WUE-Schätzung konnten die Plausibilität der Partitionierungsergebnisse leicht erhöhen. Eine Modifikation der TH08-Methode durch die Anwendung einer Clusteranalyse für die Erfassung von Atmungs-/Verdunstungsereignissen ergab zufriedenstellende Ergebnisse, brachte aber keine signifikanten Vorteile gegenüber den anderen Methodenversionen. Die Güte der Partitionierungsergebnisse beider Methoden war abhängig von den meteorologischen Bedingungen, der Vegetationshöhe und -dichte, der Pflanzenentwicklung und der Messhöhe. In erster Linie korrelierte die Güte der Partitionierung durch SK10 negativ mit dem Verhältnis zwischen Mess- und Vegetationshöhe. Die Partitionierungsperformance durch TH08 war stärker abhängig vom Blattflächenindex und der Vegetationshöhe. Es wurde festgestellt, dass alle Standortmerkmale, die die Wahrscheinlichkeit einer Mischung der Skalarsignale vor Erreichen der EC-Station erhöhen, die Partitionierungsgüte für SK10 und TH08 verschlechtern.

Außerdem haben wir Large Eddy Simulationen (LES) durchgeführt, die den turbulenten Transport von H_2O und CO_2 simulieren. SK10 wurde auf die von LES generierten, hochfrequenten Daten angewendet und die Auswirkungen von Vegetationsstruktur, Messhöhe, Senken- und Quellenverteilung der Skalare und unterschiedliche WUE Inputs wurden hinsichtlich der Partitionierungsgüte getestet. Die LES-basierte Analyse ergab, dass für ein zufriedenstellendes Ergebnis von SK10 eine gewisse Dekorrelation der H_2O- und CO_2-Fluktuationen erforderlich und eine korrekte WUE-Schätzung förderlich war. Darüber hinaus konnte eine weitere mögliche Fehlerquelle, die bisher in der Literatur noch nicht diskutiert wurde, für den Partitionierungsansatz entdeckt werden. Im speziellen Fall der LES-Experimente wurde die Validität einer wesentlichen Annahme über die vorherrschenden Transporteffizienzen der Skalare in der Methodenherleitung als entscheidender Punkt für eine korrekte Anwendung von SK10 ermittelt.

Die Anwendung verschiedener Partitionierungsmethoden mit ihren unterschiedlichen Ansätzen, den damit verbundenen Annahmen, den erforderlichen Eingangsdaten und dem Arbeitsaufwand hat gezeigt, dass für die Quellenaufteilung von Wasserdampf- und CO_2-Flüssen noch Unsicherheiten und Ungewissheiten bestehen. Eine Beurteilung und Auswertung der Partitionierungsergebnisse kann nur mit zusätzlichen Messungen von Flusskomponenten auf unterschiedlichen räumlichen und zeitlichen Skalen unabhängig von den EC-Messungen erfolgen. Weiterhin kann die Anwendung mehrerer Partitionierungsmethoden (Verwendung eines Ensembles) auf die gleichen Daten eine bessere Vorstellung von den Unsicherheiten in den Ergebnissen geben.

TABLE OF CONTENTS

Abstract I

Zusammenfassung III

Table of Contents VII

List of Figures IX

List of Tables XII

List of Abbreviations and Variables XIII

1. General Introduction and Motivation 1

1.1. Land-atmosphere exchange of carbon dioxide and water vapor 2

1.1.1. Water cycle and water vapor fluxes 2

1.1.2. Carbon cycle and carbon dioxide fluxes 3

1.2. Eddy covariance flux measurements 5

1.3. Source partitioning approaches 7

1.4. Motivation and objective 9

2. Multi-site Calibration and Validation of a Net Ecosystem Carbon Exchange Model for Croplands 11

2.1. Introduction 12

2.2. Material and methods 14

2.2.1. The AgroC model 14

2.2.2. Study sites and data availability 15

2.2.3. Model setup and initialization 16

2.2.4. Model calibration 17

2.3. Results and discussion 19

2.3.1. Calibration and validation of AgroC 19

2.3.2. Calibration with NEE data 27

2.4. Conclusions 32

2.5. Acknowledgements 32

3. Sensitivity Analysis of a Source Partitioning Method for H_2O and CO_2 Fluxes Based on High Frequency Eddy Covariance Data: Findings from Field Data and Large Eddy Simulations 33

3.1. Introduction 34

3.2. Material and methods 36

3.2.1. Study sites 36

3.2.2. Source partitioning based on high frequency data - SK10 37

3.2.3. Large eddy simulations 41
3.3. Results and discussion 44
3.3.1. Source partitioning of field data 44
3.3.2. Large eddy simulations 50
3.4. Summary and conclusions 58
3.5. Acknowledgements 59

4. Source Partitioning of H_2O and CO_2 Fluxes Based on High Frequency Eddy Covariance Data: a Study Sites Comparison 61
4.1. Introduction 62
4.2. Material and methods 63
4.2.1. Source partitioning after Scanlon and Kustas (2010) - SK10 63
4.2.2. Source partitioning after Thomas et al. (2008) - TH08 64
4.2.3. Study sites and data processing 66
4.2.4. Evaluation of source partitioning results 68
4.2.5. Analysis of source partitioning approaches 68
4.3. Results and discussion 69
4.3.1. Evaluation of source partitioning results 71
4.3.2. Analysis of source partitioning approaches 77
4.4. Conclusions 81
4.5. Acknowledgements 82

5. Final Conclusions 83

Appendix 87
A. The AgroC model 87
B. Source partitioning based on high frequency data 98
C. Study sites comparison 107
References 121
Acknowledgements 131

LIST OF FIGURES

Fig. 1.1: Exchange of CO_2/carbon and water vapor/water in the soil-vegetation-atmosphere continuum. 4

Fig. 1.2: Instrumentation to measure heat, water vapor, and CO_2 exchange between land surface and atmosphere at a cropland in Selhausen and a spruce forest in Wüstebach in Western Germany. 7

Fig. 2.1: Carbon fluxes and partitioning in AgroC. 14

Fig. 2.2: Observed and simulated soil temperature in several depths in Selhausen, Merzenhausen, and Rollesbroich. 20

Fig. 2.3: Observed and simulated soil water content at various depths in Selhausen, Merzenhausen, and Rollesbroich. 21

Fig. 2.4: Observed and simulated leaf area index in Selhausen, Merzenhausen, and Rollesbroich. 22

Fig. 2.5: Observed and simulated dry matter in Selhausen, Merzenhausen, and Rollesbroich. 22

Fig. 2.6: Observed CO_2 efflux at soil surface and simulated stacked CO_2 production in soil profile for several source terms in Selhausen, Merzenhausen, and Rollesbroich. 23

Fig. 2.7: Observed and simulated soil CO_2 concentration at various depths in Rollesbroich. 24

Fig. 2.8: Observed and simulated net ecosystem exchange in Selhausen, Merzenhausen, and Rollesbroich. 26

Fig. 2.9: Observed and simulated net ecosystem exchange with reduced major axis regression in Selhausen, Merzenhausen, and Rollesbroich. 26

Fig. 2.10: Root mean square error, model efficiency, Pearson product-moment correlation coefficient, Bias, and cumulated net ecosystem exchange (cum NEE) over simulation time period, calculated in "gap-filling mode", for each optimization strategy, for the simulation without calibration to NEE, and for the gap-filling method after Reichstein et al. (2005) at all three study sites. 28

Fig. 2.11: Correlations between observed and simulated net ecosystem exchange for all optimization strategies at test site Selhausen. 30

Fig. 3.1: Vertical profiles of the crop plant area density, cumulative plant area index, and variations of sink-source-distributions for H_2O and CO_2 used to scale the LES scalar fields (ModelV, after Sellers et al. 1992; ModelB, after Ney et al. 2017), each with ten canopy sinks/sources and one soil source. 43

Fig. 3.2: Source partitioning results of the approach after Scanlon and Kustas (2010) for H_2O fluxes at the two study sites Wüstebach (forest) and Selhausen (cropland) for varying time periods. 45

Fig. 3.3: Comparison of source partitioning results of the approaches after Reichstein et al. (2005) and after Scanlon and Kustas (2010) for CO_2 fluxes at the two study sites Wüstebach (forest) and Selhausen (cropland) for varying time periods. 46

Fig. 3.4: Comparison of source partitioning results of the approach after Scanlon and Kustas (2010) depending on different water use efficiency inputs for both study sites. 48

Fig. 3.5: Mean vertical profiles of streamwise and crosswise velocity (u, v), vertical momentum flux, variances of u, v, and vertical wind velocity, and skewness of vertical wind, scaled by friction velocity at canopy top. 50

Fig. 3.6: Vertical profiles of H_2O and CO_2 flux, and their components resulting from LES scaled with the four variations of sink-source-distributions (ModelV or ModelB; low or high soil source) for the crop canopy. Also shown are the partitioning results of the approach after Scanlon and Kustas (2010) for each grid height. 52

Fig. 3.7: a)-c) Vertical profiles of $\rho_{q'c'}$, $\rho_{c_p'c_r'}$, and $\sigma_{c_p}^2$ resulting from LES scaled with the four variations of sink-source-distributions (ModelV or ModelB; low or high soil source) for the crop canopy, compared to results of the approach after Scanlon and Kustas (2010). d)-e) Comparison of the two sides of Equations 3.2 and 3.3 checking the transfer assumption and corresponding correction factors ($fact_q$, $fact_c$, defined in Equation 3.5 and 3.6). 53

Fig. 3.8: Comparison of H_2O and CO_2 flux components, $\rho_{q'c'}$, $\rho_{c_p'c_r'}$, and $\sigma_{c_p}^2$ resulting from LES scaled with the four variations of sink-source-distributions (ModelV or ModelB; low or high soil source) and the partitioning results of the approach after Scanlon and Kustas (2010) at a 'measurement' height of 2.5 canopy heights for the crop canopy. 54

Fig. 3.9: Vertical profiles of H_2O and CO_2 flux components, $\rho_{q'c'}$, $\rho_{c_p'c_r'}$, and $\sigma_{c_p}^2$ resulting from LES scaled with the four variations of sink-source-distributions (ModelV or ModelB; low or high soil source) for the crop canopy. Also, the partitioning results of the approach after Scanlon and Kustas (2010) including the correction of the transfer assumption are shown for each grid height. 55

Fig. 3.10: Results of partitioning fractions for H_2O (T/ET) and CO_2 (NPP/NEE) fluxes in relation to the input water use efficiency. 57

Fig. 4.1: Exemplary scatterplots of w', q', and c' from WU_FR, May 18th, 2015, 12:00-12:30 p.m. including results of the cluster analysis by Gaussian Mixture Model for the conditional sampling. 65

Fig. 4.2: Source partitioning results of H_2O and CO_2 fluxes in half-hourly time steps for the Loobos study site (forest) in The Netherlands and for every method version. 70

Fig. 4.3: Diurnal dynamics of source partitioning results of H_2O and CO_2 fluxes and water use efficiency for the Waldstein study site (forest) in Germany for 4-10 July, 2016 and for every method version. 72

Fig. 4.4: Diurnal dynamics of source partitioning results of H_2O and CO_2 fluxes for all study sites and for the approach after Scanlon and Kustas (2010) with WUE_{OLR} and after Thomas et al. (2008) with REA H. 73

Fig. 4.5: Averages of source partitioning results of H_2O and CO_2 fluxes, a) for the Metolius Mature Pine study site (forest) in US and for every method version, b) for all study sites and for the approach after Scanlon and Kustas (2010) with WUE_{OLR}, and c) after Thomas et al. (2008) with REA H. 74

Fig. 4.6: Error quantities of source partitioning results for each study site and method version. 76

Fig. 4.7: a)-c) Setup of conceptual model for synthetic fluctuations (q' and c') originating from soil, canopy, or boundary layer with differing degrees of mixing (no, complete, or partial mixing between soil and canopy sink/source) including water use efficiency, reduced major axis regression after Webster (1997), hyperbolic threshold criteria after Thomas et al. (2008; TH08) (H = 0.25) and correlation coefficient between q' and c'. d)-e) True known partitioning ratios and source partitioning results of all TH08 method versions for each degree of mixing. 80

Fig. A.1: Correlations between observed and simulated net ecosystem exchange for all optimization strategies at test site Merzenhausen. 95

Fig. A.2: Correlations between observed and simulated net ecosystem exchange for all optimization strategies at test site Rollesbroich. 96

Fig. A.3: Cumulated net ecosystem exchange (cum NEE) over simulation time period, calculated in "gap-filling mode", for each optimization strategy, for the simulation without calibration to NEE, and for the gap-filling method after Reichstein et al. (2005) in Selhausen, Merzenhausen, and Rollesbroich. 97

Fig. B.1: Source partitioning results of the approach after Scanlon and Kustas (2010) for H_2O fluxes with various water use efficiency inputs at the two study sites Wüstebach (forest) and Selhausen (cropland) for varying time periods. 99

Fig. B.2: Source partitioning results of the approach after Scanlon and Kustas (2010) for CO_2 fluxes with various water use efficiency inputs at the two study sites Wüstebach (forest) and Selhausen (cropland) for varying time periods. 99

Fig. B.3: Examples of sampled synthetic high frequency data of H_2O and CO_2 fluctuations for the crop canopy in different 'measurement' heights and for the two sink-source-distributions ModelV and ModelB each with the strong soil source. 100

Fig. B.4: Absolute and relative residuals between H_2O and CO_2 flux components, $\rho_{q'c'}$, $\rho_{c_p'c_r'}$, and $\sigma_{c_p}^2$ resulting from LES scaled with the four variations of sink-source-distributions (ModelV or ModelB; low or high soil source) and the partitioning results of the approach after Scanlon and Kustas (2010) at a 'measurement' height of 2.5 canopy heights for the crop canopy. 101

Fig. B.5: Vertical profiles of the forest plant area density, cumulative plant area index, and variations of sink-source-distributions for H_2O and CO_2 used to scale the LES scalar fields (ModelV, after Sellers et al. 1992; ModelB, after Ney et al. 2017), each with ten canopy sinks/sources and one soil source. 101

Fig. B.6: Vertical profiles of H_2O and CO_2 flux, and their components resulting from LES scaled with the four variations of sink-source-distributions (ModelV or ModelB; low or high soil source) for the forest canopy. Also shown are the partitioning results of the approach after Scanlon and Kustas (2010) for each grid height. 102

Fig. B.7: a)-c) Vertical profiles of $\rho_{q'c'}$, $\rho_{c_p'c_r'}$, and $\sigma_{c_p}^2$ resulting from LES scaled with the four variations of sink-source-distributions (ModelV or ModelB; low or high soil source) for the forest canopy, compared to results of the approach after Scanlon and Kustas (2010). d)-e) Comparison of the two sides of Equation 3.2 and 3.3 checking the transfer assumption and corresponding correction factors ($fact_q$, $fact_c$, defined in Equation 3.5 and 3.6). 103

Fig. B.8: Comparison of H_2O and CO_2 flux components, $\rho_{q'c'}$, $\rho_{c_p'c_r'}$, and $\sigma_{c_p}^2$ resulting from LES scaled with the four variations of sink-source-distributions (ModelV or ModelB; low or high soil source) and the partitioning results of the approach after Scanlon and Kustas (2010) at a 'measurement' height of 2.5 canopy heights for the forest canopy. 103

Fig. B.9: Vertical profiles of H_2O and CO_2 flux components, $\rho_{q'c'}$, $\rho_{c_p'c_r'}$, and $\sigma_{c_p}^2$ resulting from LES scaled with the four variations of sink-source-distributions (ModelV or ModelB; low or high soil source) for the forest canopy. Also, the partitioning results of the approach after Scanlon and Kustas (2010) including the correction of the transfer assumption are shown for each grid height. 104

Fig. B.10: Results of partitioning fractions for H_2O (T/ET) and CO_2 (NPP/NEE) fluxes in relation to the input water use efficiency. 105

Fig. B.11: Absolute and relative residuals between H_2O and CO_2 flux components, $\rho_{q'c'}$, $\rho_{c_p'c_r'}$, and $\sigma_{c_p}^2$ resulting from LES scaled with the four variations of sink-source-distributions (ModelV or ModelB; low or high soil source) and the partitioning results of the approach after Scanlon and Kustas (2010) at a 'measurement' height of 2.5 canopy heights for the forest canopy. 106

Fig. C.1: Source partitioning results of H_2O and CO_2 fluxes in half-hourly time steps for the Hohes Holz study site (forest) in Germany and for every method version. 109

Fig. C.2: Source partitioning results of H_2O and CO_2 fluxes in half-hourly time steps for the Wüstebach study site (forest) in Germany and for every method version. 110

Fig. C.3: Source partitioning results of H_2O and CO_2 fluxes in half-hourly time steps for the Waldstein study site (forest) in Germany and for every method version. 111

Fig. C.4: Source partitioning results of H_2O and CO_2 fluxes in half-hourly time steps for the Lackenberg study site (forest) in Germany and for every method version. 112

Fig. C.5: Source partitioning results of H_2O and CO_2 fluxes in half-hourly time steps for the Metolius Mature Pine study site (forest) in United States and for every method version. 113

Fig. C.6: Source partitioning results of H_2O and CO_2 fluxes in half-hourly time steps for the Sta. Clotilde study site (forest) in Spain and for every method version. 114

Fig. C.7: Source partitioning results of H_2O and CO_2 fluxes in half-hourly time steps for the Rollesbroich study site (grassland) in Germany and for every method version. 115

Fig. C.8: Source partitioning results of H_2O and CO_2 fluxes in half-hourly time steps for the Wüstebach study site (clear cut) in Germany and for every method version. 116

Fig. C.9: Source partitioning results of H_2O and CO_2 fluxes in half-hourly time steps for the Fendt study site (grassland) in Germany and for every method version. 117

Fig. C.10: Source partitioning results of H_2O and CO_2 fluxes in half-hourly time steps for the Dijkgraaf study site (cropland, maize) in The Netherlands and for every method version. 118

Fig. C.11: Source partitioning results of H_2O and CO_2 fluxes in half-hourly time steps for the Selhausen study site (cropland, sugar beet) in Germany and for every method version. 119

Fig. C.12: Source partitioning results of H_2O and CO_2 fluxes in half-hourly time steps for the Selhausen study site (cropland, 06/2015: winter wheat, 05/2016: barley, 09/2016: intercrop) in Germany and for every method version. 120

LIST OF TABLES

Tab. 2.1: Site-specific characteristics, meteorological conditions, and crop management. 16

Tab. 2.2: Applied optimization strategies and their objective functions, used data streams and data transformation. 18

Tab. 3.1: Root mean square error, bias in µmol m^{-2} s^{-1}, and number of found solutions of the source partitioning results for soil respiration after the approach of Scanlon and Kustas (2010) with various water use efficiencies compared to chamber measurements at the two study sites Selhausen (cropland) and Wüstebach (forest). 47

Tab. 4.1: Study sites and their characteristics. 67

Tab. 4.2: Correlation coefficients between partitioning performance of each method version regarding HiR GPP and study site characteristics considering all, only forest, or only crop- and grassland sites. 77

Tab. 4.3: Correlation coefficients between partitioning performance of each method version regarding HiR TER and study site characteristics considering all, only forest, or only crop- and grassland sites. 78

Tab. A.1: Site-specific soil properties and calibrated hydraulic parameters. 93

Tab. A.2: Selection of most important fitted plant parameters for the calibration of the plant growth module of AgroC. 94

Tab. C.1: Count of half-hourly time steps during daylight (CoD) per considered time period for each study site, corresponding relative fractions of CoD of high-quality (HQ) and relative fractions of these HQ-time steps with a successful partitioning solution for each method version. 107

LIST OF ABBREVIATIONS AND VARIABLES

AgroC	one-dimensional agroecosystem model
a.s.l.	above sea level
BA	barley
BIO	microbial biomass
c, c'	CO_2 concentration or fluctuation (mg m^{-3})
C_d	drag coefficient
c_i	internal (inter-stomatal) concentration of CO_2 (mg m^{-3})
c_p, c_p'	CO_2 concentration or fluctuation related to photosynthesis (mg m^{-3})
c_r, c_r'	CO_2 concentration or fluctuation related to R_{soil} (mg m^{-3})
c_s	external (within canopy) concentration of CO_2 (mg m^{-3})
CFL	Courant-Friedrichs-Lewy number
CL	cropland
CoD	count of daylight timesteps
cum NEE	cumulated NEE
CV	covariance (for flux calculation)
DALES	Dutch Atmospheric Large-Eddy Simulation model
DI_CL	study site Dijkgraaf, Gelderland, NL (cropland)
DM	dry matter (kg ha^{-1})
DPM	decomposable plant material
E	evaporation (W m^{-2}, mmol m^{-2} s^{-1})
E_{soil}	soil evaporation estimated based on Beer's law (W m^{-2}, mmol m^{-2} s^{-1})
EC	eddy covariance
ET	evapotranspiration (W m^{-2}, mmol m^{-2} s^{-1})
$fact_c$, $fact_q$	correction factors for transfer assumption
FE_GL	study site Fendt, BY, DE (grassland)
FLUXNET	global network of micrometeorological tower sites
FR	forest
GL	grassland
GMM	conditional sampling using Gaussian Mixture Model
GPP	gross primary production (µmol m^{-2} s^{-1}, mg m^{-2} s^{-1})
H	conditional sampling using hyperbolic threshold criterion (H = 0.25)
h_c	canopy height (m)
HH_FR	study site Hohes Holz, ST, DE (forest)
HiR	hits in range
HQ	high-quality
HUM	humified organic matter
IC	intercrop
ICOS	Integrated Carbon Observation System
k	exponent
LA_FR	study site Lackenberg, BY, DE (forest)
LAI	leaf area index (m^2 m^{-2})
LE	latent heat flux (W m^{-2})
LES	large eddy simulation
LINGRA	grassland productivity model (Schapendonk et al. 1998)
LO_FR	study site Loobos, Gelderland, NL (forest)
lv	leaves (subscript)
MA	maize
ME	model efficiency (Nash and Sutcliff 1970)
meanT	measured mean air temperature (°C)
meas	measurement
MMP_FR	study site Metolius Mature Pine, PNW, US (forest)
ModelB	beta-function-shaped sink-source-distribution inferred from profile measurements in winter barley on June 9th, 2016 (Ney et al. 2017; Ney and Graf 2018)
ModelV	v-shaped sink-source distribution taken from Sellers et al. (1992)
MOST	Monin-Obukhov similarity theory
N	total number of
NEE	net ecosystem exchange (µmol m^{-2} s^{-1}, mg m^{-2} s^{-1}, mol ha^{-1} h^{-1})
NEE_{BSc} (+ R_{soil})	optimization strategy including RMSE and bias in NEE (and R_{soil})
NEE_{Cum} (+ R_{soil})	optimization strategy including RMSE in cumulated NEE (and R_{soil})
NEE_{inst} (+ R_{soil})	optimization strategy including RMSE in instantaneous NEE (and R_{soil})
NEE_{Log} (+ R_{soil})	optimization strategy including RMSE in log-transformed NEE (and R_{soil})
NPP	net primary production (µmol m^{-2} s^{-1}, mg m^{-2} s^{-1})

obs_N, obs_R	NEE or R_{soil} observations
OLR	outgoing longwave radiation (W m^{-2})
P	precipitation (mm)
PAD	plant area density (m^2 m^{-3})
PAI	plant area index (m^2 m^{-2})
q, q'	H_2O concentration or fluctuation (g m^{-3})
Q1	conditional sampling within quadrant 1
q_e, q_e'	H_2O concentration or fluctuation related to E (g m^{-3})
q_i	internal (inter-stomatal) concentration of H_2O (g m^{-3})
q_s	external (within canopy) concentration of H_2O (g m^{-3})
q_t, q_t'	H_2O concentration or fluctuation related to T (g m^{-3})
r	Pearson product-moment correlation coefficient
R^2	coefficient of determination
R_a	respiration by autotrophs
R_{ABG}	above-ground respiration
R_{BG}	below-ground respiration
R_{gr}	growth respiration
R_h	respiration by heterotrophs
R_m	maintenance respiration
R_{rhizo}	rhizosphere respiration
R_{soil}	soil respiration (µmol m^{-2} s^{-1}, mg m^{-2} s^{-1})
RE05	source partitioning approach after Reichstein et al. (2005)
REA	relaxed eddy accumulation
redmaj	reduced major axis regression (Webster 1997)
RMSE	Root mean square error
$RMSE_{ln}$	RMSE in log-transformed data
RO_GL	study site Rollesbroich, NRW, DE (grassland)
RothC	soil carbon turnover model (Coleman and Jenkinson 2008)
RPM	resistant plant material
rt	roots (subscript)
SB	sugar beet
SCE	Shuffled Complex Evolution (Duan et al. 1993)
SC_FR	study site Sta. Clotilde, ES (oak savanna)
SE_CL	study site Selhausen, NRW, DE (cropland)
sim_N, sim_R	NEE or R_{soil} simulations
SK10	source partitioning approach after Scanlon and Kustas (2010)
Sk_w	skewness of vertical wind
so	storage organs (subscript)
SOILCO2	one-dimensional soil water, heat, and CO_2 flux model (Šimůnek and Suarez 1993)
st	stems (subscript)
SUCROS	crop growth model (Spitters et al. 1989)
T	transpiration (W m^{-2}, mmol m^{-2} s^{-1})
T_f	foliage temperature (°C, K)
T_{soil}	soil temperature (°C)
Temp	temperature
TER	terrestrial ecosystem respiration (µmol m^{-2} s^{-1}, mg m^{-2} s^{-1})
TERENO	Terrestrial Environmental Observatories
TH08	source partitioning approach after Thomas et al. (2008)
u	streamwise wind velocity (m s^{-1})
u_*	friction velocity (m s^{-1})
$\overline{u'u'}$, $\overline{v'v'}$, $\overline{w'w'}$	variances of u, v, or w
$\overline{u'w'}$	vertical momentum flux (m^2 s^{-2})
v	crosswise wind velocity (m s^{-1})
w, w'	vertical wind velocity or fluctuation (m s^{-1})
$\overline{w'_+}$, $\overline{w'_-}$	mean vertical velocities of updrafts or downdrafts
$\overline{w'c'}$	covariance of vertical wind and CO_2 fluctuations, CO_2 flux (µmol m^{-2} s^{-1}, mg m^{-2} s^{-1})
$\overline{w'q'}$	covariance of vertical wind and H_2O fluctuations, H_2O flux (mmol m^{-2} s^{-1}, g m^{-2} s^{-1})
WA_FR	study site Waldstein, BY, DE (forest)
WB	winter barley
WUE	water use efficiency (on leaf-level, mg g^{-1})
WUE_{MAX}	WUE estimated with T_f equal to mean air temperature minus 2 K and c_i equal to 200 ppm
WUE_{meanT}	WUE estimated with T_f equal to mean air temperature
$WUE_{meanT±2K}$	WUE estimated with T_f equal to mean air temperature plus or minus 2 K

WUE_{MIN}	WUE estimated with T_f equal to mean air temperature plus 5 K and c_i equal to 300 ppm
WUE_{MOST}	WUE estimated with T_f derived by logarithmic mean profile implementing MOST
WUE_{OLR}	WUE derived with T_f derived by means of measured outgoing longwave radiation
WU_FR	study site Wüstebach, NRW, DE (forest)
WU_GL	study site Wüstebach, NRW, DE (clear cut)
WW	winter wheat
z	measurement height (m)
z_0	roughness length (m)
β	empirical constant in REA approach
$\rho_{c_p'c_r'}$	correlation coefficient between CO_2 fluctuations related to photosynthesis and R_{soil}
$\rho_{q'c'}$	correlation coefficient between H_2O and CO_2 fluctuations
$\rho_{q_e'c_r'}$	correlation coefficient between fluctuations related to E and R_{soil} (non-stomatal processes)
$\rho_{q_t'c_p'}$	correlation coefficient between fluctuations related to T and photosynthesis (stomatal processes)
$\rho_{q_t'q_e'}$	correlation coefficient between H_2O fluctuations related to T and E
$\rho_{w'c'}$, $\rho_{w'c_p'}$, $\rho_{w'c_r'}$	transport efficiency of CO_2 fluctuations, total or related to photosynthesis or R_{soil}
$\rho_{w'q'}$, $\rho_{w'q_t'}$, $\rho_{w'q_e'}$	transport efficiency of H_2O fluctuations, total or related to T or E
$\rho_{w'\theta'}$	transport efficiency of temperature
$\rho_{\theta'q'}$	correlation coefficient between temperature and humidity
$\sigma_{c'}^2$	variance of CO_2 fluctuations ($mg^2\ m^{-6}$)
$\sigma_{c_p'}^2$	variance of the CO_2 fluctuations related to photosynthesis ($mg^2\ m^{-6}$)
$\sigma_{q'}^2$	variance of H_2O fluctuations ($g^2\ m^{-6}$)
$\sigma_{w'}$	standard deviation of vertical wind velocity
θ	soil water content ($cm^3\ cm^{-3}$)

1

GENERAL INTRODUCTION AND MOTIVATION

1.1. LAND-ATMOSPHERE EXCHANGE OF CARBON DIOXIDE AND WATER VAPOR

Terrestrial ecosystems constantly exchange momentum, energy, and mass with the atmosphere above. These land-atmosphere interactions are mainly driven by incoming solar radiation and they play essential roles in both local and global climatology. Complex interrelations exist between atmosphere and land surface influencing physical, biogeochemical, and biological properties and conditions, and can be observed and contemplated on differing temporal and spatial scales (Dickinson 2002; Moene and van Dam 2014).

During a typical daylight situation, the incoming solar energy is absorbed by the land surface, which heats up and thereby adjusts its properties to balance the received energy. Further, the solar energy drives photosynthesis and the evaporation of water from soil and water surfaces. When atmospheric water vapor condenses in a certain height, clouds are formed, which can have a cooling effect by reducing the incoming solar radiation (via reflection) and a warming effect by increasing downward thermal radiation. Moreover, clouds are a source of fluid and solid precipitation, which supplies water to the terrestrial ecosystem filling the soil water storage, ground water, rivers, and above-ground reservoirs. Plants take up soil water through roots to maintain their growth and release water by transpiration for the assimilation of CO_2. Next to the radiative and hydrological input, the energy balance of the land surface further depends on wind, temperature, and humidity of the atmosphere, which in turn is also affected by the land surface. The main pathway for the energy exchange from the land surface to the atmosphere is turbulence motion (eddies) in the surface layer, the lowest layer of the atmosphere. The intensity of turbulence is determined by convection (surface heating) and mechanical mixing. The latter is imposed by wind strength and surface roughness (Dickinson 2002; Jones and Rotenberg 2001; Moene and van Dam 2014).

The focus in this study lies on the mass exchange of water vapor and CO_2 within the soil-vegetation-atmosphere continuum.

1.1.1. Water Cycle and Water Vapor Fluxes

In regard of terrestrial ecosystems as part of the global water cycle, precipitation (P) on the land surface can be lost to surface runoff towards the oceans, lateral flow through soil towards rivers and lakes, percolation and subsequent groundwater recharge, and evapotranspiration (ET) to the atmosphere (Fig. 1.1). ET consists of two components: the physical evaporation (E) from soil, surface water and wet canopies, and the biological transpiration (T) via soil water uptake by roots and loss of water vapor through plant stomata, which is typically accompanied by photosynthesis (Bales 2002; Eamus 2001; Moene and van Dam 2014; Schlesinger and Jasechko 2014; Reichstein et al. 2012). E is controlled by atmospheric conditions, such as solar radiation, air temperature, humidity, and wind speed, as well as by the actual water supply. Next to the micrometeorological conditions in the canopy, T is

determined additionally by stomatal conductance, and more general by plant type and ecological conditioning. T locally exerts a cooling effect in canopies, and accounts for 60-80% of ET of terrestrial ecosystems, thus being a dominant part of the global water cycle. A portion of precipitation can be temporarily stored on vegetation surfaces (interception), and subsequently evaporate or reach the ground as throughfall (Bales 2002; Dickinson 2002; Moene and van Dam 2014; Reichstein et al. 2012; Schlesinger and Jasechko 2014).

Net radiation, the sum of incoming solar shortwave radiation and thermal longwave radiation minus radiation reflected or emitted upward, is the main energy source for water and land surfaces. Depending on physical and ecological conditions of the surface, this energy is partitioned mainly between the soil heat flux, the sensible, and the latent (LE) heat flux to the atmosphere. A minor part goes into chemical energy during photosynthesis. The sensible heat flux describes the heat transfer from an area of higher temperature to one of lower temperature by conduction (between adjacent molecules without mass transfer) and convection (transfer of molecules themselves and their kinetic energy). The latent heat can only be extracted by a phase change. Sensible heat is transferred to latent heat when it leads to the evaporation of formerly liquid water to the atmospheric water vapor. When the water molecules condense (e.g., during cloud formation), the latent heat is gained again. Water vapor can be transported in air parcels over large vertical and horizontal distances, enabling an effective latent heat exchange in the soil-vegetation-atmosphere continuum (Moene and van Dam 2014; Jones and Rotenberg 2001).

Due to its involvement in both the water and energy budget, evapotranspiration can be quantified by using a water balance estimation, using an energy balance to determine the amount of latent heat, or directly by assessing water vapor fluxes (Kool et al. 2014).

1.1.2. Carbon Cycle and Carbon Dioxide Fluxes

The global carbon cycle includes five large carbon storages: oceans, atmosphere, vegetation and soil of terrestrial ecosystems, and fossil fuel deposits. The amount of carbon currently stored in the terrestrial vegetation is estimated to be as large as the amount stored in the complete atmosphere. The amount stored in the soil is uncertain but estimated to be at least twofold larger. The oceans hold most of the carbon (about 50 times more than the atmosphere), mostly dissolved as bicarbonates and carbonates in sea water (Dickinson 2002; Houghton 2014).

Carbon can be exchanged between the various storages very fast in a few seconds (e.g., fixation due to photosynthesis, fire) or over millennia (e.g., accumulation of fossil carbon), where the exchange between terrestrial ecosystems and atmosphere is relatively rapid. Plants (and other autotrophic organisms) transform radiative energy into chemical energy during photosynthesis (Fig. 1.1). CO_2 is assimilated through the stomata and converted to glucose, cellulose, carbohydrates, proteins, and fats, all forms of organic matter, which, whether in

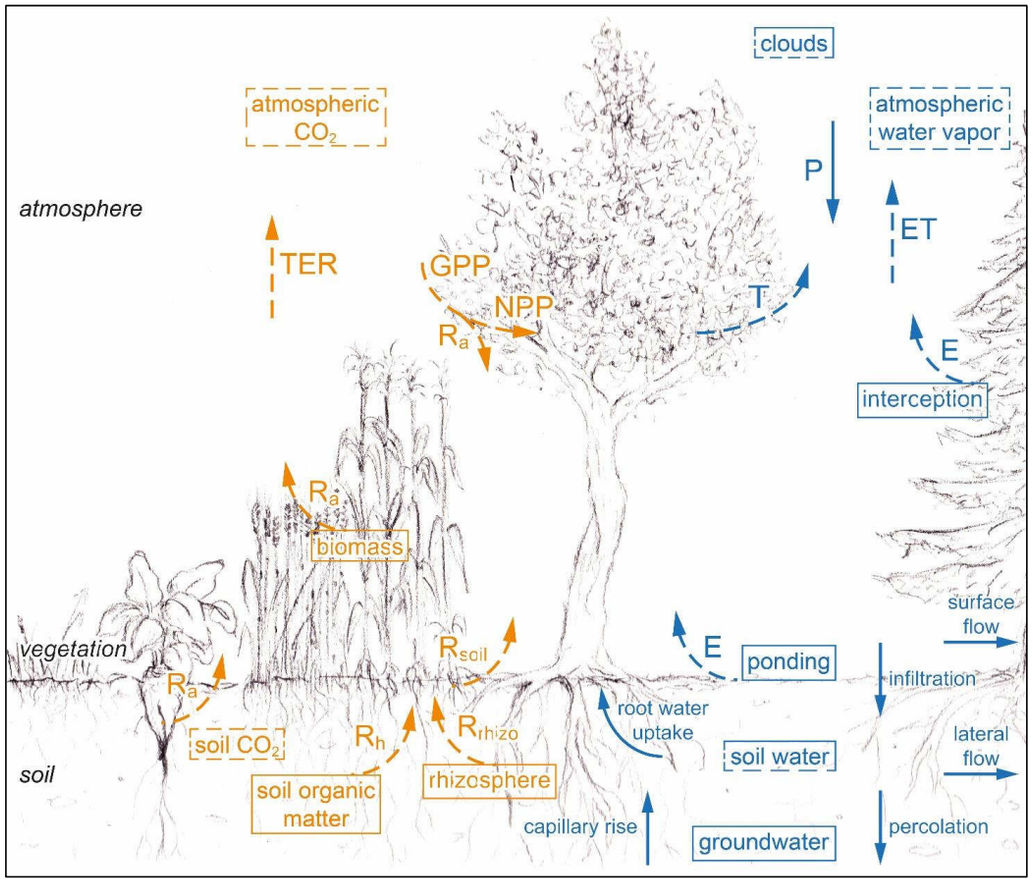

Fig. 1.1: Exchange of CO_2/carbon (*orange*) and water vapor/water (*blue*) in the soil-vegetation-atmosphere continuum. *Arrows* represent fluxes for typical daytime conditions. *Boxes* represent storages or sinks. *Dashed lines* refer to transport or storage of matter in gas phase and *non-dashed lines* to transport or storage of fluid or solid matter (for abbreviations see text).

living organisms or in dead organic material, support food chains in natural ecosystems. Organic Carbon of terrestrial ecosystems can exist in form of living plant tissue, such as leaves, wood or roots, animals, microbes, decaying material, and as soil humus. In soil ecosystems, dead organic matter is decomposed by heterotrophic organisms, mostly bacteria and fungi, to access the stored chemical energy, and CO_2 is respired back to the atmosphere (respiration by heterotrophs R_h). Also, plants respire. At a cellular level, the synthesized carbohydrates are metabolized (oxidized) by mitochondria into energy and CO_2 (dark respiration). The energy is used to maintain growth and to convert carbohydrates to more complex molecules, which can be stored (Dickinson 2002; Houghton 2014; Kirschbaum et al. 2001; Moene and van Dam 2014; Reichstein et al. 2012). CO_2 is released by above-ground plant organs and below-ground by roots (respiration by autotrophs R_a; Fig. 1.1). The sum of R_h and R_a compose the so-called total ecosystem respiration (TER). Soil respiration (R_{soil}) consists of the below-ground CO_2 sources, R_h and root respiration. Furthermore, microbial

respiration of root exudates and rhizodeposition is considered as an additional CO_2 source in soils. In this study, we refer to the autotrophic source of direct root respiration and the heterotrophic decomposition of root deposits, both occurring in the root zone, as "rhizosphere respiration" (R_{rhizo}; Kirschbaum et al. 2001; Kuzyakov 2006; Reichstein et al. 2012; Suleau et al. 2011; Subke et al. 2006). The counterpart (and ultimate source) of all these respiration fluxes is the removal of CO_2 from the atmosphere by photosynthesis, also termed as gross primary production (GPP, true photosynthesis minus photorespiration), and the net flux of GPP and TER is the net ecosystem exchange (NEE). The term net primary production (NPP) describes the difference between GPP and R_a, i.e. the part of GPP leading to biomass growth. All described flux components are sensitive to changes in the soil-vegetation-atmosphere continuum. They strongly depend on the physical environment, biological factors, the overlying atmosphere, and the supply of energy and heat by the sun (Dickinson 2002; Eamus 2001; Houghton 2014; Kirschbaum et al. 2001; Kuzyakov 2006; Moene and van Dam 2014).

The natural fluxes of carbon between oceans, atmosphere, and land are considered to have been almost balanced, with the land approximately taking up as much carbon via CO_2 assimilation as it releases via respiration. Currently, this terrestrial balance is shifted, because the CO_2 content of the atmosphere is increased by the human combustion of fossil fuels, making CO_2 assimilation by plants more efficient (CO_2 'fertilization effect'). The magnitude of transpiration is decreased and the ecosystem water use efficiency (ratio between CO_2 assimilation and water vapor loss) is increased. The additional removal and storage of atmospheric CO_2 by the terrestrial ecosystems is an ecosystem service decelerating climate change, but we cannot foresee when and under what conditions this removal would cease or even be reversed (Baldocchi et al. 2001; Dickinson 2002). Changes in the amount of carbon in terrestrial ecosystems are difficult to measure and more difficult to model and predict, because the land surface is not as well-mixed as the atmosphere or the oceans and thus more spatially heterogeneous, background levels are relatively high, and consequently upscaling of local measurements to global sums is very challenging. Thus, changes in storage and fluxes of terrestrial carbon are usually estimated by taking the differences from global carbon mass and the other three big reservoirs. The uncertainty of these estimations is still relatively high, and a deeper understanding, accurate observations, and better model predictions of the prevailing processes regarding carbon in terrestrial ecosystems are necessary (Houghton 2014).

1.2. EDDY COVARIANCE FLUX MEASUREMENTS

Atmospheric turbulence in the surface layer effectively exchanges momentum, heat, water vapor, and CO_2 between land surface and atmosphere. A direct way to observe this flux exchange is the so-called eddy covariance (EC) technique. The concentration of H_2O and/or CO_2 in air parcels and the wind speed in three orthogonal directions can be obtained in high temporal resolution (usually in 10 or 20 Hz) via a gas analyzer and a sonic anemometer

(Fig. 1.2a). These instruments can be installed on a tower, causing only a minimal disturbance to the ecosystem. The calculation of the covariance between the measured vertical wind and one of the concentrations (after corrections and quality tests on the applicability of underlying assumptions) yield the net flux (LE or NEE, respectively) between ecosystem and atmosphere (Baldocchi et al. 2001; Baldocchi 2003; Foken 2006; Houghton 2014; Moene and van Dam 2014). In this calculation the Reynolds decomposition is used, which separates the mean and the fluctuating part of a variable. Individual eddies in the turbulent atmosphere are characterized by a temperature, scalar concentrations, and a wind velocity vector different from the mean air flow. For the calculation of the covariance between vertical wind and scalar fluctuations, a time interval of usually one or one half hour of high frequency data is used. This time interval should be long enough to capture the most important eddy scales (up to a certain size), and short enough to exclude large-scale fluctuations. Ideally, the average vertical wind over that time interval is zero and conditions are stationary (Baldocchi 2003; Foken 2006; Moene and van Dam 2014). The EC technique is a direct method to measure water vapor and CO_2 exchange, but in the derivation of the algorithm several assumptions are made, making instrument- and data-related corrections and quality tests necessary. Due to these quality assessments, inadequate meteorological conditions, and required instrument maintenance gaps in the data record of EC measurements are to be expected and frequent. The number of gaps and the quality of EC measurements mainly depend on the atmospheric conditions, the homogeneity of the surface, and the correct application of data corrections and quality assessment tools. Furthermore, the spatial source of the measured fluxes has to be taken into account. An EC station can receive signals from a mostly upwind lying footprint area of over several 100 m^2 (Baldocchi et al. 2001; Baldocchi 2003; Foken 2006).

In micrometeorology so-called similarity theories were developed to understand and estimate the relationship between surface fluxes, vertical gradients, and fluxes in the atmospheric surface layer, which starts at a distance above the plant canopy, can reach various heights and is characterized by approximately height-constant vertical fluxes. Similarity theories assume that two flows behave similar if certain dimensionless characteristics are identical in these situations. The so-called Monin-Obukhov Similarity Theory (MOST) is commonly used to describe flow behavior in the surface layer based on dimensional analysis. The theory relates turbulence properties (velocity and scalar gradients, variances, and covariances) with surface fluxes of mass and energy. Derived relations between atmospheric variables and surface properties for certain situations can be applied to all similar situations with the universal functions derived from MOST. The theory assumes a flat, homogeneous surface and stationarity (Foken 2006; Moene and van Dam 2014; Patton and Finnigan 2012; van de Boer et al. 2014; Williams et al. 2007). In the so-called roughness sublayer, where a more direct and extreme influence of the canopy on the turbulence is observed, MOST requires adjustment. Within a canopy MOST is no longer applicable (Patton and Finnigan 2012).

The so-called flux-variance similarity theory leads to a second approach to estimate fluxes from measured variances and a known functional dependency of turbulent characteristics, expecting a similar transport for passive scalars (Foken 2006; Williams et al. 2007). The correlation coefficient between two passive scalars gives insight to which degree these two scalars conform these similarity assumptions. Dissimilarities between scalars can be provoked by turbulent structures and processes, horizontal heterogeneity of the canopy, its vertical structure, the sink-source-distribution of the scalars, their transport efficiencies, and source strength (Huang et al. 2013; Moene and Schüttemeyer 2008).

1.3. SOURCE PARTITIONING APPROACHES

With the EC technique the net exchange of H_2O and CO_2 between ecosystem and atmosphere is obtained. LE and NEE give valuable measures of ecosystem water availability and carbon sequestration, but the various flux components responsible for the net balance cannot be depicted separately by the EC approach. Quantifications of T, E, GPP, TER, R_h, R_a, R_{soil}, their dynamics, variabilities, and feedbacks with environmental drivers give a better insight of the biosphere's sensitivity towards global change. Thus, so-called source partitioning approaches have to be applied to EC data to estimate these flux components. Applicable to both LE and NEE measurements, or to each separately, a large variety of procedures with diverse model approaches including various driving variables, necessity of different input data, and different parameterization including the cost function have been developed (Desai et al. 2008; Reichstein et al. 2012; Stoy et al. 2006).

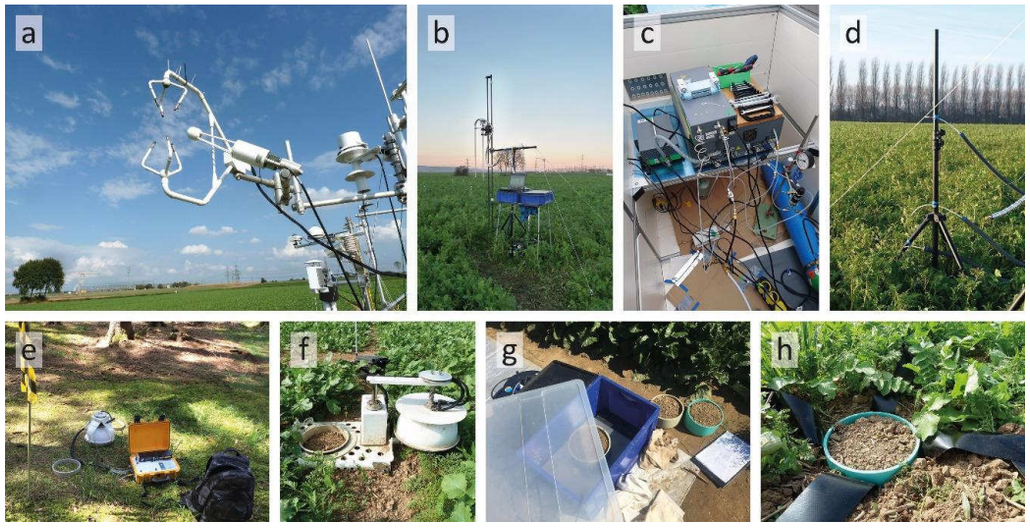

Fig. 1.2: Instrumentation to measure heat, water vapor, and CO_2 exchange between land surface and atmosphere at a cropland in Selhausen (a-d, f-h) and a spruce forest in Wüstebach (e) in Western Germany: a) eddy covariance station and b) profile lift (Patrizia Ney) for high frequency scalar measurements, c)-d) instrumentation for stable water isotope measurements (Maria Quade), e)-f) survey and longterm soil respiration chambers (Patrizia Ney), and g)-h) microlysimeters for soil evaporation.

Source partitioning methods can be classified as data-driven or instrumental approaches. Instrumental approaches require next to the EC instrumentation additional measurements in different parts of ecosystems and with different methods and instruments, e.g. chamber measurements (for soil surface and at leaf-level), profile measurements (Ney and Graf 2018), sub-canopy EC measurements, or tracer measurements (isotopes; Quade et al. 2019) (Fig. 1.2). The latter are very promising for flux partitioning, but because of their high costs, elaborated technical setups, and maintenance requirements they are usually not used for spatially widespread and longterm measurements. With flux chambers, sap flux sensors, and microlysimeters, sources and sinks of CO_2 or H_2O, respectively, can be derived in an ecosystem, but they are associated with scaling issues in comparison to the EC footprint (Kool et al. 2014; Reichstein et al. 2012; Schlesinger and Jasechko 2014).

Data-driven approaches use existing (raw or processed) data of typical EC stations. The most popular source partitioning tools for CO_2 flux components, often primarily developed to fill gaps in EC measurements of NEE, belong to such approaches, which are often based on the notion that during night respiration fluxes prevail. They use regressed relationships of EC measurements and physical drivers, e.g., between nighttime (respiration) fluxes and air temperature (e.g., approach after Reichstein et al. 2005). Here, the challenge lies within extrapolating the nighttime relationship to daytime conditions. The approach after Lasslop et al. (2010), for instance, deduces additionally the rate of photosynthesis with light response curves from daytime flux measurements to consider additionally the effects of radiation and vapor pressure deficit. The various non-linear regression gap-filling methods differ in choice of functional form, parameter fitting and time dependencies, time window size, and use of nighttime, daytime, or all NEE data (Desai et al. 2008; Falge et al. 2001; Moffat et al. 2007; Reichstein et al. 2012; Stoy et al. 2006). Several comparison studies concerning these data-driven approaches have been conducted presenting discrepancies and uncertainties (e.g., Desai et al. 2008; Falge et al. 2001; Moffat et al. 2007). Similar to the CO_2 gap-filling models, LE can be partitioned via time intervals without any T, such as for croplands shortly after harvest or in deciduous forests after leaf fall. However, most of the data-driven approaches are well developed for the partitioning of carbon fluxes, but analogous methods for water fluxes are lacking (Kool et al. 2014; Reichstein et al. 2012; Schlesinger and Jasechko 2014).

Considering the coupling between the water and carbon cycle in the process of photosynthesis, new source partitioning approaches have been developed in the last decade to partition H_2O and CO_2 fluxes simultaneously using high frequency EC data. Scanlon and Sahu (2008) and Scanlon and Kustas (2010) suggest that air parcels originating from stomatal and non-stomatal (soil surface) processes have specific compositions of the two scalars and can be detected and quantified with the additional information about the water use efficiency (WUE) on leaf-level. Thomas et al. (2008) applied conditional sampling methods to identify turbulent events originating from the sub-canopy. These two different approaches proceed without any

assumptions about dependencies of the flux components on physical drivers, which makes them very interesting.

Complex process-based ecosystem models can also be used for source partitioning applications and to get a better insight of interrelations and flux contributions of included processes, e.g., the response of photosynthesis and respiration to temperature fluctuations. Especially, model-data fusion frameworks allow an estimation of uncertainty in the measurements and model formulation. Furthermore, multiple driving variables can be included or chosen in such model simulations, such as rapid, seasonal, or annual changes in canopy characteristics, soil moisture, nutrient levels, and management strategies (Desai et al. 2008; Reichstein et al. 2012).

1.4. MOTIVATION AND OBJECTIVE

The main goal of this thesis was to apply, evaluate, and improve various data-driven source partitioning approaches using EC measurements of LE and NEE, and to get a better understanding of their functionality, dependencies, uncertainties, advantages, and shortcomings. Therefore, the transport of momentum and matter (water vapor, CO_2) in the soil-vegetation-atmosphere continuum were especially of interest. Here, ecosystem processes and source partitioning results are usually contemplated in a half-hourly or hourly time step making diurnal dynamics apparent.

First, we describe the coupling and extension of the complex terrestrial ecosystem model AgroC. Further, we conducted a comprehensive model-data fusion study to clarify the CO_2 exchange in agroecosystems and estimate their annual carbon balance (Chapter 2). AgroC contains detailed process descriptions of CO_2 and carbon exchange between soil and crop. The model is calibrated using several measurements of heat, water, and CO_2 fluxes at three test sites in Germany, and then validated with hourly NEE measured with the EC technique. In a second step, AgroC is optimized with these EC measurements to examine the effect of various objective functions and data-transformations on the simulated carbon balance. Also, the effect of including R_{soil} measurements as an additional constraint to the fitting procedure is investigated.

Second, we applied the source partitioning approaches after Scanlon and Kustas (2010) and after Thomas et al. (2008) to EC measurements of several study sites including forests, croplands, grasslands, and to synthetic data (Chapter 3, 4). Applying higher-order statistics, these methods focus on the correlation of water vapor and CO_2 fluctuations to estimate the contributions of T, E, NPP, and R_{soil}. Thus, these methods can be used for the partitioning of water and CO_2 fluxes, and they (only) require high frequency raw data of common EC stations. The partitioning results are compared among each other and to the commonly used source partitioning approach after Reichstein et al. (2005), and are evaluated on the basis of additional measurements (Chapter 3, 4). In Chapter 3 the partitioning approach after Scanlon

and Kustas (2010) is applied to high frequency data synthesized by large eddy simulations (LES) to validate and further understand the functioning of the approach. In Chapter 4 conditions and site characteristics for a high performance of both methods are identified via a site comparison study involving multiple sites in different ecosystems, and usage of a conceptual model.

Chapter 2 of this thesis was published, Chapter 3 has been under review in a scientific journal, and Chapter 4 has been in preparation for submission, when this thesis was finalized (since 2019, all three Chapters are published in scientific journals). The individual chapters are presented as published/submitted and each contains an introduction, a methodology description, results, discussion, and conclusions. Therefore, some contents, especially methodology descriptions, slightly overlap. Concluding remarks and an outlook are given in Chapter 5.

2

MULTI-SITE CALIBRATION AND VALIDATION OF A NET ECOSYSTEM CARBON EXCHANGE MODEL FOR CROPLANDS

This chapter is based on a journal article published as:
Klosterhalfen, A., Herbst, M., Weihermüller, L., Graf, A., Schmidt, M., Stadler, A., Schneider, K., Subke, J.-A., Huisman, J.A., Vereecken, H., 2017. Multi-site calibration and validation of a net ecosystem carbon exchange model for croplands. Ecological Modelling 363, 137-156, https://doi.org/10.1016/j.ecolmodel.2017.07.028.

2.1. INTRODUCTION

Terrestrial ecosystems play an important role in the global carbon cycle. Photosynthesis by vegetation and respiration from autotrophic and heterotrophic organisms represent the two major carbon fluxes between atmosphere and terrestrial biosphere. Terrestrial ecosystems store large amounts of carbon, and especially soils contain about twice as much carbon as the atmosphere (Rustad et al. 2000). Over 37% of the world's landmass is agricultural land (FAO Statistical Yearbook 2014). Thus, carbon fluxes in agroecosystems constitute a significant part of the global carbon cycle. The quantification and prediction of terrestrial carbon sinks and sources and their dynamics, variabilities, and controls are of major importance for climate change research and the optimization of management strategies affecting the ecosystem's carbon budget (e.g., Baldocchi 2003; Kuzyakov 2006; Subke et al. 2006). The net ecosystem exchange (NEE) of carbon dioxide and its two components, gross primary production (GPP) and terrestrial ecosystem respiration (TER), are of particular interest (Suleau et al. 2011; Sus et al. 2010). The total CO_2 efflux from soils, one of the major compartments of TER (Moureaux et al. 2008; Suleau et al. 2011), derives from decomposition of soil organic matter and dead plant material by microorganisms, from direct root respiration, and from microbial respiration of root exudates and rhizodepositions (Kuzyakov 2006; Kuzyakov and Domanski 2000). In this study, we consider the last two CO_2 sources as one sum, and refer to it as "rhizosphere respiration".

NEE is increasingly being monitored using the eddy covariance (EC) technique, which provides information on net carbon fluxes for a relatively large area with a high temporal resolution (Baldocchi 2003). This allows to investigate the relation between CO_2 efflux and weather conditions or crop development stages (Sus et al. 2010). Due to methodological and technical constraints, significant gaps occur in high-quality EC data, which prohibits direct computation of annual NEE. Gap-filling methods (e.g., Reichstein et al. 2005) and their application with meteorological and EC data overcome this limitation, but e.g., they cannot be used for predictive modeling of carbon balances addressing climate change effects. Alternatively, terrestrial ecosystem models that provide a physical description of processes in the agroecosystem can be used to assess annual NEE sums. An additional advantage of such models is that they allow to quantify interrelations and feedbacks in biogeochemical processes and fluxes of agricultural systems. Mechanistic models like ORCHIDEE-STICS (de Noblet-Ducoudré et al. 2004), DNDC (Li et al. 2005), or SPAc (Sus et al. 2010) were developed for this purpose and have been successfully applied in a number of studies (e.g., Sus et al. 2010; Wattenbach et al. 2010; Wu et al. 2009; Yuan et al. 2012). In most of these studies, the carbon assimilation by plants was captured well by the models, but a significant bias in the simulation of the respiratory fluxes was observed. This inevitably causes systematic errors in the estimation of the overall carbon balance. An improved representation of processes linked to respiration may help to decrease systematic errors and in combination with soil

respiration (R_{soil}) measurements, it may help to reduce the uncertainty in the estimation of annual NEE. For this purpose, we coupled a one-dimensional soil water, heat, and CO_2 flux model (SOILCO2; Šimůnek and Suarez 1993), a pool concept of soil carbon turnover (RothC; Coleman and Jenkinson 2008), and a crop growth module (SUCROS; Spitters et al. 1989). In addition, the coupled model, further referred to as AgroC, was extended with routines for root exudation, root decay, as well as for a managed grassland system. The main motivation for the coupling was a more detailed representation of sources and locations of CO_2 production, the gas transport in the soil, and the fluxes in the ecosystem.

Various sources of measured data are available for validation, calibration, evaluation, and structural improvement of terrestrial ecosystem models. In the last decade, substantial progress has been made in implementing model-data fusion techniques to make optimal use of available measurements (e.g., Richardson et al. 2010; Sus et al. 2010; Trudinger et al. 2007; Wu et al. 2009; Yuan et al. 2012). Such model-data fusion techniques, including calibration techniques, require the formulation and minimization of an objective function that quantifies the mismatch between model predictions and observations (Evans 2003; Herbst et al. 2008; Wang et al. 2009). Detailed measurements of biotic and abiotic processes and fluxes allow to improve process models on various spatiotemporal scales, and to verify model assumptions, parameters, and performance (Richardson et al. 2010; Williams et al. 2009; Yuan et al. 2012). However, the use of multiple objective functions or constraints in model calibration may be challenging because of the need to combine measurements with variable spatial scale, temporal scale, magnitude, and uncertainty. For example, optimizing the simulation regarding one data source (e.g., NEE) can lead to a low model performance (trade-off) regarding another data source (e.g., heterotrophic soil respiration) (Richardson et al. 2010). Other important decisions to be made before model calibration include the selection and appropriate weighting of observations, the choice of an optimization algorithm (Trudinger et al. 2007), and the selection of model parameters being altered during calibration (Wu et al. 2009). These decisions differ between model studies, which will influence the results of NEE predictions (Evans 2003; Trudinger et al. 2007).

The main goal of this study is to present the mechanistic model AgroC and to evaluate its model performance simulating biophysical processes and interactions in agroecosystems. In a first step, AgroC was calibrated with soil moisture, soil temperature, biometric, and soil CO_2 flux measurements of three test sites in Germany cropped with winter wheat, barley, or grass. After calibration, it was evaluated how well AgroC simulates the hourly NEE through comparison with EC measurements. In the next step, we optimized the AgroC model using EC measurements by estimating plant and R_{soil} parameters. In addition, we evaluated how joint use of EC and R_{soil} measurements in the calibration affected the estimated cumulative NEE and model performance. Finally, we evaluated the effect of data-transformation (e.g., log-transformation) on the model results with a focus on estimated NEE.

2.2. MATERIAL AND METHODS

2.2.1. The AgroC Model

AgroC is a coupled model developed from the SOILCO2/RothC model (Herbst et al. 2008) and the SUCROS model for crop growth (Spitters et al. 1989). The SOILCO2/RothC model simulates vertical water, heat, and CO_2 fluxes in a soil column, and the source term of heterotrophic respiration over soil depth and time, which is given by the turnover of depth-specific carbon pools (Coleman and Jenkinson 2008; Šimůnek and Suarez 1993; Šimůnek et al. 1996). The carbon turnover rates depend on the soil water content and temperature. The SOILCO2/RothC model was validated in several laboratory and field studies (Bauer et al. 2008, 2012; Herbst et al. 2008; Palosuo et al. 2012; Weihermüller et al. 2009). The coupling with SUCROS is expected to allow for an improved simulation of the soil autotrophic respiration source term, since temporal development of root growth and related growth and maintenance respiration is simulated by SUCROS in a mechanistic way. In addition, AgroC was extended with routines for the simulation of root exudation, root decay, and managed grassland. The latter routine follows the sink/source approach suggested by Schapendonk et al. (1998) for the grassland productivity model LINGRA. The final coupled model allows closing the one-dimensional carbon balance and to estimate NEE, since carbon assimilation as well as organ-specific growth and maintenance respiration are now included. Figure 2.1 provides a summary of the carbon cycling in AgroC.

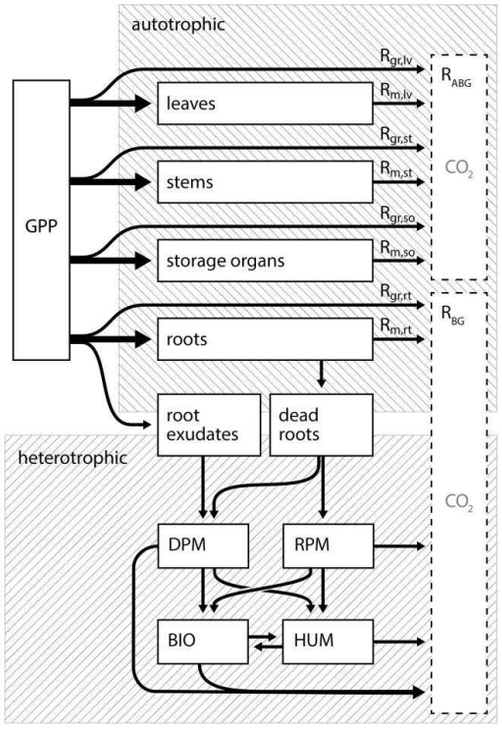

Fig. 2.1: Carbon fluxes and partitioning in AgroC. Gross primary production (GPP) is partitioned to the different plant organs, leaves (subscript lv), stems (st), storage organs (so), and roots (rt). CO_2 is lost due to growth (R_{gr}) and maintenance respiration (R_m). The sum of these autotrophic CO_2 source terms by the shoot organs account for the above-ground respiration (R_{ABG}). Carbon and CO_2 is added to the soil profile by autotrophic root respiration, root exudates, and dead roots. The latter two are transferred to the decom-posable and resistant plant material pool (DPM, RPM) of the RothC model and decomposed. The hetero-trophic CO_2 source term consists of microbial decom-position of those and further soil organic matter pools (humified organic matter HUM, microbial biomass BIO). The root respiration and the heterotrophic components are part of the below-ground respiration (R_{BG}).

The coupled SOILCO2/RothC model allows the use of user-specified length and time units, whereas the SUCROS module uses fixed units. For the coupled AgroC model, we preserved the flexibility in terms of length ([L]) and time units ([T]), but we kept the fixed mass and area units (kg, ha) of the original SUCROS code. Also, the final coupled AgroC model works with an hourly time step. Further information about the coupling and the modifications to the original models regarding the hourly time step, the water fluxes, the carbon fluxes, and the grassland routines are given in Appendix A.

2.2.2. Study Sites and Data Availability

AgroC was applied to three experimental sites in the western part of Germany: Selhausen and Merzenhausen, both located in the southern part of the Lower Rhine Embayment (Schmidt et al. 2012; Stadler et al. 2015), and Rollesbroich, located in the low mountain range Eifel (Gebler et al. 2015). The dominant land use at the first two test sites is cropland. Rollesbroich is a managed grassland site, which is mown three times per year (Borchard et al. 2015). All three study sites are included in the Terrestrial Environmental Observatories (TERENO) network of highly instrumented field sites (Zacharias et al. 2011). An overview of soil properties, meteorological conditions, and crop management is given in Tables 2.1 and A.1 for all three sites.

At the two cropland sites, EC and ancillary environmental measurements were conducted in the center of the agricultural fields. Measurements of NEE, latent heat, wind components, global radiation, air temperature, soil (surface) temperature at a depth of -1 cm, precipitation, and relative humidity were collected. A detailed description of the sites, measurement setup, EC post-processing, and footprint modelling is given by Schmidt et al. (2012), Graf et al. (2013), Post et al. (2015), Mauder et al. (2013) and Kormann and Meixner (2001). Soil water content and soil temperature were measured in various depths at several soil profiles per site. Biometric measurements were carried out bi-weekly to monitor crop development, and R_{soil} data were obtained with closed-chamber measurements during summer (Prolingheuer et al. 2014; Schmidt et al. 2012; Stadler et al. 2015). Prolingheuer et al. (2014) also measured the heterotrophic contribution to the CO_2 flux by root exclusion experiments at 61 sample points at the Selhausen test site.

In Rollesbroich, the EC tower was placed between two neighboring grasslands (A and B) with different management in terms of mowing dates. Thus, measured fluxes were dominated by one of the two grasslands depending on the wind direction and the resulting flux footprint distribution. Data processing was similar to the two agricultural fields. Borchard et al. (2015) conducted detailed surveys of the Rollesbroich site. At 21 sample points in grassland A, soil samples were taken, and the total leaf area index (LAI) and harvested dry matter were also determined during the growing season. Eleven of the sampling points were mown following the management of grassland A, and the remaining 10 points were sampled following the

management of grassland B. R_{soil} was again determined from closed-chamber measurements during summer. Soil moisture, soil temperature, and CO_2 concentration in several depths were observed at three profiles near the EC tower.

Tab. 2.1: Site-specific characteristics, meteorological conditions, and crop management (WW: winter wheat; WB: winter barley; GL: grassland) (Borchard et al. 2015; Gebler et al. 2015; Prolingheuer et al. 2014; Schmidt et al. 2012; Séquaris et al. 2013; Stadler et al. 2015).

	Selhausen	**Merzenhausen**	**Rollesbroich**
Site characteristics			
coordinates	50°52’14’’N, 6°26’59’’E	50°55’47’’N, 6°17’49’’E	50°37’19’’N, 6°18’15’’E
elevation (m a.s.l.)	103	93	515
soil type*	Luvisol	Luvisol	Cambisol
soil texture	silt loam	silt loam	silty clay
Climate conditions			
mean annual temperature (°C)	9.9	9.9	7.7
annual precipitation (mm)	698	698	1033
Simulation period	Oct 2008 - Dec 2009	Oct 2011 - Dec 2014	Jan 2013 - Dec 2013
Land management			
crop sequence	WW tilled every autumn	WW - WW - WB tilled every autumn	GL mowed 3x annually

*according to soil taxonomy of the FAO (I.U.S.S. Working Group WRB 2006)

2.2.3. Model Setup and Initialization

AgroC requires gap-filled meteorological data (air temperature, soil surface temperature, precipitation, solar radiation, and potential grass reference evapotranspiration), plant-specific parameters, and soil characteristics. Potential grass reference evapotranspiration was estimated with the Penman-Monteith approach according to the FAO guidelines (Allen et al. 1998). Plant-specific parameters for cereals and grass were mainly taken from literature (e.g., Boons-Prins et al. 1993; Gonzales et al. 1989; Goudriaan et al. 1997; Kuzyakov and Domanski 2000; Parsons 1988; Parsons and Robson 1981; Prud’homme et al. 1992; Schapendonk et al. 1998; Spitters et al. 1989; Swinnen et al. 1995; Vanclooster et al. 1995; van Keulen et al. 1997). These plant parameters have been extensively used in other simulation studies with the models SUCROS and LINGRA. Root biomass measurements were not available, thus the proportion of the root system (root/shoot ratio) was also derived from literature (e.g., Bolinder et al. 1997, 2002; López et al. 2013).

In AgroC, appropriate boundary conditions have to be specified for CO_2, water, and heat flow at the top and bottom of the simulation domain. The upper boundary condition for CO_2 flow was the atmospheric concentration of 0.038%. Meteorological measurements were used to describe the upper boundary for water and heat flux. Soil profile characteristics were available

from Séquaris et al. (2013), Herbst et al. (2005), and Borchard et al. (2015) for Selhausen, Merzenhausen, and Rollesbroich, respectively (Tab. A.1 in Appendix A). The simulated profile depths varied from 1.0 to 1.2 m. A no-flow boundary was used at the bottom of the soil profile for heat and CO_2. For water, a prescribed pressure head following a sine wave over the course of the year with a minimum in autumn was used as a Dirichlet boundary condition at the bottom of the simulation domain (Bauer et al. 2008; Scharnagl et al. 2011).

Initial carbon pool sizes were derived from measured soil organic carbon contents for each soil horizon. In Selhausen and Rollesbroich, measured soil carbon fractions were available from previous studies (Bauer et al. 2012; Séquaris et al. 2013; Nils Borchard and Henning Schiedung, personal communication). For these two sites, initial pool sizes were calculated following Falloon et al. (1998), Skjemstad et al. (2004), and Zimmermann et al. (2007). For Merzenhausen, initial pool sizes were determined with pedotransfer functions according to Weihermüller et al. (2013), assuming a state of equilibrium. The reference temperature required for the estimation of the soil heterotrophic CO_2 source term was set to the mean annual temperature at each site.

2.2.4. Model Calibration

In a first step, AgroC was calibrated with the downhill Nelder-Mead Simplex algorithm (Nelder and Mead 1965), since only a small number of parameters were considered. The root mean square error (*RMSE*) between measurements and simulations was minimized. In addition, the Pearson product-moment correlation coefficient (r) and the model efficiency (*ME*; Nash and Sutcliffe 1970) were calculated as model quality criteria. A *ME* close to 1 indicates that the simulation describes the observations well without systematic bias. If *ME* is lower than 0, the mean of the observations is a better predictor than the simulation.

First, the soil hydraulic parameters were calibrated. Then, plant development and growth were adjusted. Here, mainly the plant development rate depending on temperature, the effectiveness of CO_2 assimilation, the partitioning factors of assimilates between the different plant organs, especially between shoot and root system, and the specific leaf area (conversion factor between plant dry matter and LAI) were modified (Tab. A.2 in Appendix A).

CO_2 production in the soil profile was estimated in dependence of several physical processes and conditions. For soil temperature, we used the default reduction function of the SOILCO2 model, which is a modified form of the Arrhenius relationship (Šimůnek and Suarez 1993; Šimůnek et al. 1996). To describe the soil moisture dependency of respiration, we applied a bell-shaped curve as suggested by Bauer et al. (2012), Moyano et al. (2012), and Skopp et al. (1990). The simulation of R_{soil} was improved by calibrating the reference temperature used in the temperature scaling function, the turnover rate of the resistant plant material (RPM) pool, and the parameters of the water reduction function. For Rollesbroich, soil CO_2 concentration measurements in different depths were available, so the gaseous diffusion through the soil

matrix could also be adjusted. Here, we implemented the gas diffusivity and transport model of Kristensen et al. (2010), which accounts for preferential diffusion through fractures and macropores in the soil matrix. Appendant parameters, the fracture porosity, the fracture tortuosity factor, and the matrix tortuosity factor, were adjusted.

Tab. 2.2: Applied optimization strategies and their objective functions, used data streams and data transformation (obs_N: NEE observation; sim_N: NEE simulation; obs_R: R_{soil} observation; sim_R: R_{soil} simulation).

label	objective function	data streams	data trans-formation	*obs* or *sim*
NEE_{inst}	$E = \sqrt{\frac{1}{n}\sum_{i=1}^{n}\left(obs_{N_i} - sim_{N_i}\right)^2}$	NEE	instan-taneous	with x_i
NEE_{Cum}			cumulative	$x_i = \sum_{j=1}^{i} x_j$
NEE_{Log}			log-trans-formed	$x_i = \ln(x_i + \lvert\min\rvert + 1)$
RMSE				
$NEE_{inst} + R_{soil}$	$E = \frac{\sqrt{\frac{1}{n}\sum_{i=1}^{n}\left(obs_{N_i} - sim_{N_i}\right)^2}}{\frac{1}{n}\sum_{i=1}^{n} obs_{N_i}} + \frac{\sqrt{\frac{1}{m}\sum_{j=1}^{m}\left(obs_{R_j} - sim_{R_j}\right)^2}}{\frac{1}{m}\sum_{j=1}^{m} obs_{R_j}}$	NEE and R_{soil}	instan-taneous	x_i
$NEE_{Cum} + R_{soil}$			cumulative	$x_i = \sum_{j=1}^{i} x_j$ *
$NEE_{Log} + R_{soil}$			log-trans-formed	$x_i = \ln(x_i + \lvert\min\rvert + 1)$
NEE_{BSc}	$E = \sqrt{\frac{1}{n}\sum_{i=1}^{n}\left(obs_{N_i} - sim_{N_i}\right)^2} + \left\lvert\frac{1}{n}\sum_{i=1}^{n}\left(obs_{N_i} - sim_{N_i}\right)\right\rvert$	NEE	instan-taneous	x_i
RMSE + Bias				
$NEE_{BSc} + R_{soil}$	$E = \sqrt{\frac{1}{n}\sum_{i=1}^{n}\left(obs_{N_i} - sim_{N_i}\right)^2} + \left\lvert\frac{1}{n}\sum_{i=1}^{n}\left(obs_{N_i} - sim_{N_i}\right)\right\rvert + \sqrt{\frac{1}{m}\sum_{j=1}^{m}\left(obs_{R_j} - sim_{R_j}\right)^2}$	NEE and R_{soil}	instan-taneous	x_i

* only applied to NEE data, R_{soil} data was used instantaneous.

After soil water, soil heat, and CO_2 flux, as well as plant development were calibrated, we compared the NEE estimates with the EC measurements at each test site. NEE measurements were handled according to the quality assessment strategy suggested by Mauder et al. (2013), and only data with high quality was used for validation purposes (28% of data in Selhausen, 55% of data in Merzenhausen, 33% of data in Rollesbroich).

In a second step, several model runs were conducted where simulated NEE was optimized with EC measurements by estimating plant parameters (regarding the light use efficiency, the potential CO_2 assimilation rate, their dependence on crop development stage and air temperature, and the biomass partitioning factors between shoot and root), and model parameters affecting R_{soil} (as above: reference temperature, turnover rate of RPM, and parameters of the water reduction function). Here, parameter calibration was conducted with the Shuffled Complex Evolution (SCE) algorithm (Duan et al. 1993), which is a global optimization strategy that was shown to be effective for a wide range of non-linear optimization problems. Two different objective functions were considered: (i) the *RMSE* and (ii) the sum of the *RMSE* and the *Bias*. The former was calculated on the basis of various data expressions (instantaneous data, cumulative data, or instantaneous log-transformed data). Additional calibrations were conducted that not only considered NEE data for the optimization, but also measurements of R_{soil}. Therefore, we considered a total of eight different calibration strategies (see Tab. 2.2). Because of the different magnitude of NEE and R_{soil} (and resulting misfits), the error was transformed by division with the respective observed mean flux (with the exception of NEE_{BSc} approach). For each test site, these eight calibrations were conducted to examine the sensitivity of estimated cumulative NEE to the different objective functions and to the inclusion of R_{soil} measurements. Estimated cumulative NEE based on each optimization strategy was compared to the well-established gap-filling method by Reichstein et al. (2005), which is based on linear regressions between EC measurements and physical drivers.

2.3. RESULTS AND DISCUSSION

2.3.1. Calibration and Validation of AgroC

Soil Temperature and Water Content

All simulations described measured soil temperature very well using the default settings. The *RMSE* was below 1.0°C and the *ME* larger than 0.93 when measurements for all depths and sites were considered (see Fig. 2.2).

After calibration, the soil moisture dynamics were reproduced well by the AgroC model (Fig. 2.3). Estimated soil hydraulic parameters are summarized in Table A.1 in Appendix A. The *RMSE* was below 0.020 cm^3 cm^{-3}, the *ME* above 0.74 and the *r* above 0.86 for all sites and profile depths. For Merzenhausen, the model was calibrated for 2012 and the following

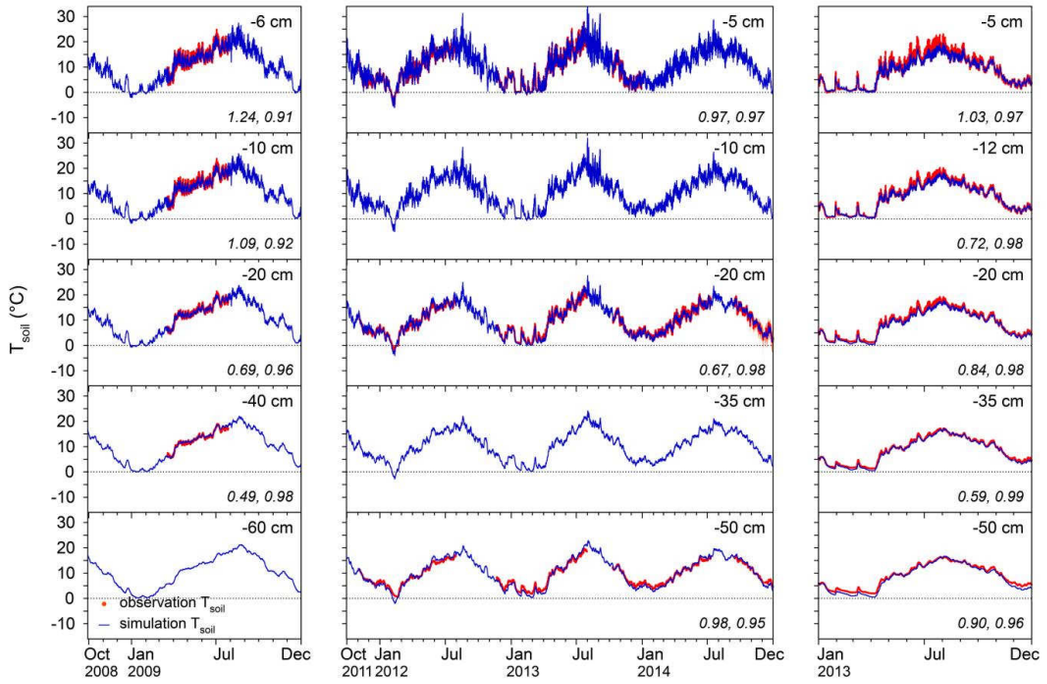

Fig. 2.2: Observed (*dots*; *orange area*: standard deviation) and simulated (*lines*) soil temperature (T_{soil}) in several depths in Selhausen (*left*), Merzenhausen (*middle*), and Rollesbroich (*right*). Root mean square error (RMSE) and model efficiency (ME) (in this order) are given for each soil depth and location.

two years were used for validation. The performance of the model decreased for the validation period, but overall dynamics were still reproduced well (Fig. 2.3). Some near-surface peaks in soil moisture were not captured by the model, which is probably related to inaccuracies in the meteorological data used for the upper boundary condition. Furthermore, static hydraulic properties were assumed for the AgroC simulations, which is a simplification because hydraulic properties of managed topsoils are typically variable due to ploughing, seedbed preparation, and subsequent re-compaction. For the Rollesbroich site, soil moisture simulations at -5 cm differed from the observations during winter. This is partly related to the presence of a snow cover, which results in delayed infiltration not represented in the model, and frozen soil, which affects soil water content measurements with the dielectric sensors used in this study.

Crop Development and Growth

Without calibration, simulated crop development and dry matter accumulation over time were already close to the observations (not shown). For further improvement, plant-specific parameters were manually adjusted (Fig. 2.4, 2.5). In general, the assimilation rate, the

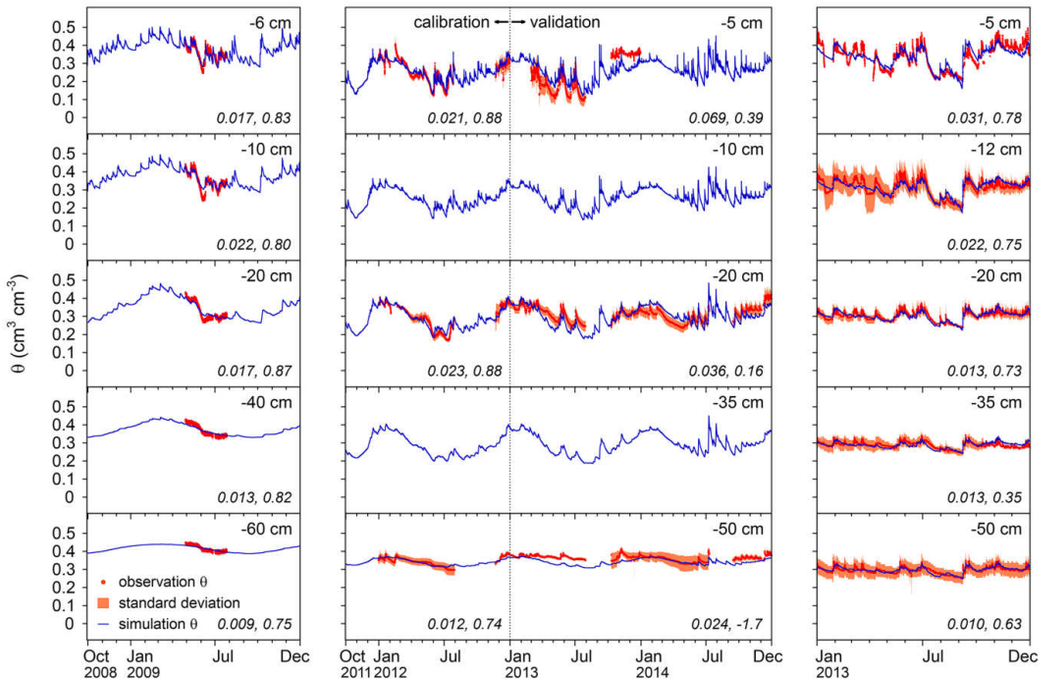

Fig. 2.3: Observed (*dots*; *orange area*: standard deviation) and simulated (*lines*) soil water content (θ) at various depths in Selhausen (*left*), Merzenhausen (*middle*), and Rollesbroich (*right*). Root mean square error (RMSE) and model efficiency (ME) (in this order) are given for each soil depth and location. In Merzenhausen, RMSE and ME are given for the calibration (until end of 2012) and the validation period.

fraction of the root biomass, and the specific leaf area were increased for all crops at all test sites. In Table A.2 in Appendix A, the most relevant plant parameters are summarized. For total LAI, the lowest *ME* was 0.63, *RMSE* was lower than 0.82 ha ha^{-1}, and *r* was larger than 0.93 for all sites. Site-specific errors for green and brown LAI are provided in Figure 2.4. As can be seen, green LAI was well reproduced over the growing season, while the course of brown LAI was simulated less well. As indicated by the *ME* in Figure 2.5, the simulation of dry matter was adequate too, especially for winter wheat in Selhausen. However, the simulations progressively diverged from the measurements towards crop maturity. For cereals, this might be due to the fact that reallocation of assimilates from leaves and stem to storage organs was not implemented in AgroC (Spitters et al. 1989).

In Merzenhausen, LAI and biomass measurements were only conducted at harvest in 2012 and during the entire growing season in 2013 (both winter wheat). For model calibration over the complete simulation period, measurements of plant height were therefore considered. A relation between LAI and plant height was determined for 2013. Plant height showed distinct differences between 2012 and 2013. In 2013, a smaller height and consequently a lower LAI and dry matter allocation were observed. This could not be reproduced by the model when only differences in meteorological conditions between the two years were considered. Winter

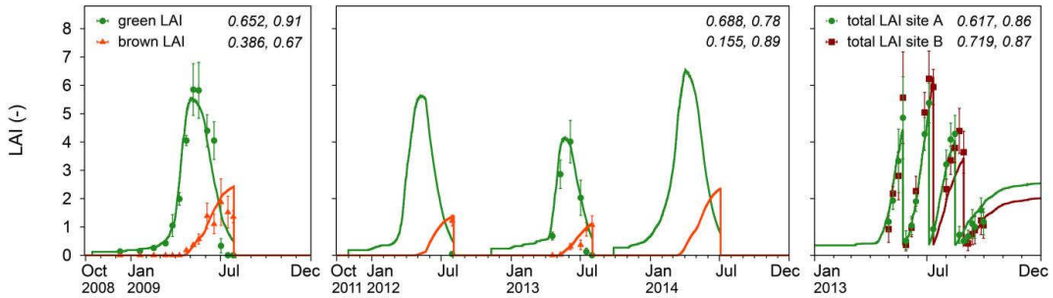

Fig. 2.4: Observed (*dots*; *error bars*: standard deviation) and simulated (*lines*) leaf area index (LAI) in Selhausen (*left*), Merzenhausen (*middle*), and Rollesbroich (*right*). For the two cropped fields green and brown LAI were measured and simulated. Root mean square error (RMSE) and model efficiency (ME) (in this order) are given for each quantity and location.

Fig. 2.5: Observed (*dots*; *error bars*: standard deviation) and simulated (*lines*) dry matter (DM) in Selhausen (*left*), Merzenhausen (*middle*), and Rollesbroich (*right*; AGB: above-ground biomass). Root mean square error (RMSE) and model efficiency (ME) (in this order) are given for each quantity and location.

wheat varieties and management differed between the two cultivation periods, and according to Spitters et al. (1989), plant parameters can vary substantially between species. In addition, it needs to be considered that the spring of 2013 was much drier than usual. Even though water stress was explicitly accounted for in AgroC, irreversible damages (e.g., by heat stress) of plant tissue might have caused a reduced growth beyond the water stress period. Furthermore, the root system may have preferably been expanded relative to the shoots due to the water deficit. These effects were not directly considered in AgroC, and could only be captured by different parameterizations. Therefore, we ran AgroC with crop parameter sets for winter wheat that differed between the two cultivation periods.

The Rollesbroich grassland site was covered by snow until the beginning of April 2013, thus plant growth was delayed. The model was fitted to the plant development and growth on parcel A. For the simulation of parcel B, only the dates of mowing were adjusted. This resulted in an adequate simulation for LAI and dry matter allocation of both grassland parcels (Fig. 2.4, 2.5).

At the day of harvest, the simulations for Selhausen and Merzenhausen resulted in mean root/shoot dry matter ratios of 0.08 and 0.16, respectively. Bolinder et al. (1997, 2002) determined root/shoot ratios between 0.13 and 0.20 for winter wheat. Compared to this, the simulated root/shoot ratio for Selhausen was rather low. However, observations of rhizospheric respiration at this test site (Fig. 2.6) confirmed the estimated partitioning of assimilates between shoot and roots. For the Rollesbroich grassland site, the mean root/shoot ratio was 0.58. This corresponds well with López et al. (2013), who reported a root/shoot ratio of 0.56 for *Lolium perenne*.

Soil Respiration

Magnitude and dynamics of soil CO_2 efflux were captured adequately by AgroC, as shown by *ME* values larger than 0.58, *RMSE* values lower than 45.4 mol ha^{-1} h^{-1}, and an *r* larger than 0.77 across all sites. For the Selhausen site, observations of efflux due to heterotrophic respiration were available separately (Prolingheuer et al. 2014). Therefore, Figure 2.6 not only shows modeled total respiration, but also the simulated partitioning in root and rhizosphere respiration and heterotrophic respiration. Since this partitioning is available only for the production terms but not for efflux at the surface, the errors reported in Figure 2.6 differ slightly from those presented above. Parameters of the reduction functions for heterotrophic CO_2 production in the soil profile were also calibrated. The start parameter for the reference temperature was set to the annual mean temperature at each site as suggested by Coleman and Jenkinson (2008). In the optimization process, all reference temperatures were decreased, thus CO_2 production was increased at any temperature. As reported by Bauer et al. (2012) and Moyano et al. (2012), the approach after Skopp et al. (1990) provided the best results for the response of CO_2 production to soil moisture. Therefore, the two control parameters of this response function were calibrated. The estimated optimal water content (maximum of reduction function curve) was 0.41, 0.29, and 0.28 cm^3 cm^{-3} in Selhausen, Merzenhausen, and Rollesbroich, respectively. The optimum water contents were very close to the mean soil water

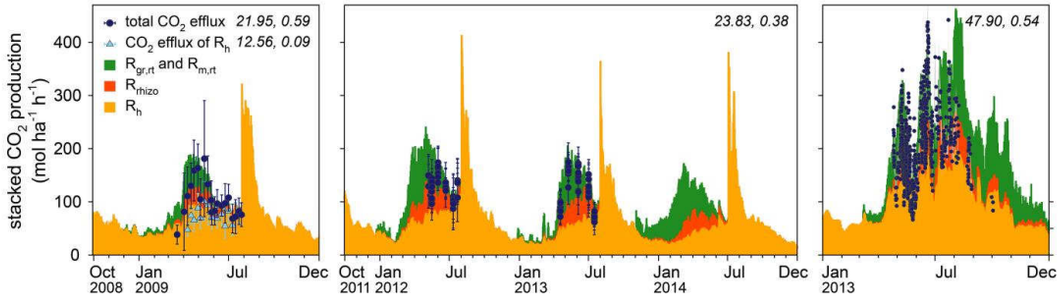

Fig. 2.6: Observed (*dots*; *error bars*: standard deviation) CO_2 efflux at soil surface and simulated stacked CO_2 production in soil profile (*areas*) for several source terms (*green*: growth and maintenance respiration by roots ($R_{gr,rt}$, $R_{m,rt}$); *orange*: respiration in rhizosphere (R_{rhizo}) due to root exudates and root decay; *yellow*: respiration by heterotrophs (R_h)) in Selhausen (*left*), Merzenhausen (*middle*), and Rollesbroich (parcel A, *right*). Root mean square error (RMSE) and model efficiency (ME) (in this order) are given for each location.

content of each simulation (0.38, 0.29, and 0.32 cm^3 cm^{-3}, respectively).

As shown in Figure 2.6, CO_2 production at the grassland site was higher than at the cropped sites, which is attributed to the higher soil organic carbon content (Tab. A.1 in Appendix A) and an extensive perennial root system. However, the magnitude of the simulated rhizospheric respiration turned out to be quite similar for all sites, even though the grassland accumulates root biomass over the years. The root/shoot ratios reported above showed that the below-ground translocation of assimilated carbon was much higher for grassland than for cereal crops. Hence, the relative fraction of assimilates partitioned to the root system is larger in grasslands (Kuzyakov and Domanski 2000). Considering the same growth period, the absolute translocation of carbon is the same for both ecosystems; whilst cereals have a higher productivity per unit area and time, their carbon assimilation is restricted to a shorter growth period compared to grasslands. Further, grasslands are not ploughed, so they are potentially a larger sink for atmospheric carbon (Kuzyakov and Domanski 2000).

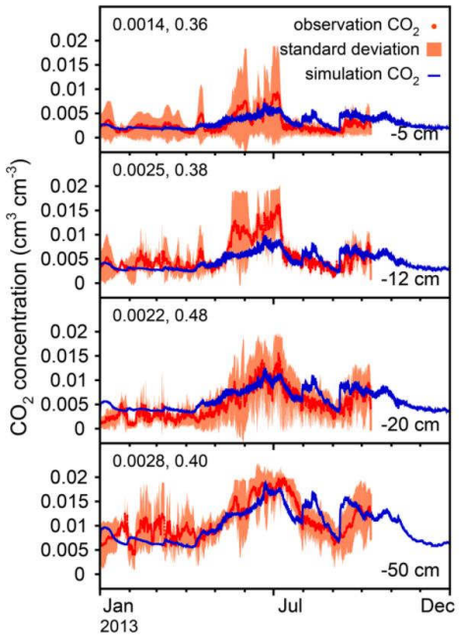

Fig. 2.7: Observed (*dots*; *orange area*: standard deviation) and simulated (*lines*) soil CO_2 concentration at various depths in Rollesbroich. Root mean square error (RMSE) and model efficiency (ME) (in this order) are given for each soil depth.

An extensive peak of soil CO_2 emission was simulated right after harvest of the cereals, because a large amount of fresh plant material was added to the carbon pools of the soil. Unfortunately, no chamber-based R_{soil} observations were available for those critical time periods to validate these model predictions.

The estimated mean annual ratio between rhizospheric respiration and total R_{soil} was 0.12 for Selhausen, 0.21 for Merzenhausen, and 0.34 for Rollesbroich. Wang and Fang (2009) analyzed 36 grassland sites and reported a corresponding average ratio of 0.36, which agrees well with results for our grassland site in Rollesbroich. For winter wheat, Moureaux et al. (2008) obtained a ratio between below-ground respiration by autotrophs and total R_{soil} of 0.56 for the vegetation period only. Suleau et al. (2011) found ratios between 0.40 and 0.48 using root exclusion experiments. The simulated ratios for the vegetation period were 0.18 for Selhausen and between 0.33 and 0.38 for Merzenhausen. It seems that the simulated fraction of rhizospheric respiration in Selhausen is too low compared to previous studies. However, these values were confirmed by measurements from root exclusion experiments at this site

(Prolingheuer et al. 2014). Subke et al. (2006) compared numerous respiration ratios derived by various methods from several studies, and report that the heterotrophic source term may be overestimated by root exclusion, because of increased dead root biomass (for experiments conducted within perennial vegetation), a change of irradiation, and a decreased water uptake by roots. In our study, those error sources were mostly excluded, due to installation of the exclusion rings before cereal growth, a small ring size that enables representative growth and shading around/above the measurement points, and the correction for the soil moisture effects (Prolingheuer et al. 2014).

For Rollesbroich, measurements of soil CO_2 concentration in different depths were available, which allowed calibration of the CO_2 flux through the soil. The approach after Kristensen et al. (2010), which additionally accounts for diffusion through fractures and macropores, provided the best results with a *ME* of 0.44 (Fig. 2.7).

Net Ecosystem Exchange

After calibrating soil water flux, plant development, and CO_2 flux, we compared the NEE simulations to the EC measurements at each test site. At this point, NEE measurements were not used to calibrate the model. Figure 2.8 and 2.9 show the AgroC estimates in comparison to the NEE flux measurements. With a *RMSE* between 113 and 128 mol ha^{-1} h^{-1}, a *ME* between 0.78 and 0.83, and an *r* between 0.91 and 0.96, AgroC performed reasonably well at all three test sites. However, some discrepancies could also be observed. As already discussed for R_{soil}, the estimated peaks of R_{soil} and corresponding NEE after harvest were also not observed in the EC measurements (Fig. 2.8). Fluxes from adjacent and cropped fields could have distorted the measurements of the area of interest (e.g., Massman and Lee 2002). In Merzenhausen in autumn 2012, negative CO_2 fluxes were measured even though the crop was harvested. This was not captured by the AgroC model, because it was assumed that the field was bare fallow. In reality, weeds and wheat emerged again during this post-harvest period and assimilated CO_2 until ploughing (cf., Sus et al. 2010).

At the Rollesbroich site, the EC tower was located at the border between two differently managed grassland parcels, so that the contribution of CO_2 fluxes originating from each of the two parcels varied according to the flux footprint (Kormann and Meixner 2001; Mauder et al. 2013; Post et al. 2015). For validation, two AgroC model runs were made for grassland parcels A and B. The two NEE estimates were weighted according to the relative fraction of the footprint within each parcel, and subsequently compared to the observations. Consequently, simulated fluxes could only be attained for time steps at which measurements and thus information about the footprint distribution were available. The consideration of the footprint distribution improved the performance of the NEE simulations significantly compared to a single model run. This was especially true for time periods between two mowing events, since parcel B was always mown a few days later than parcel A. Generally,

AgroC reproduced the dynamics of the grassland NEE including the effect of mowing and regrowth. At the time of mowing, leaf area was reduced substantially, canopy photosynthesis decreased, and the site temporarily turned from a CO_2 sink to a CO_2 source. From the first to the third mowing, peak assimilation declined consistently. This has previously also been reported for other grassland sites (Schmitt et al. 2010; Wohlfahrt et al. 2008).

The ratios between the annual sum of TER and GPP were 0.79 for Selhausen, between 0.67 and 0.75 for Merzenhausen, and 1.06 for Rollesbroich. The ratios for the growing period only were 0.64 for Selhausen and between 0.52 and 0.62 for Merzenhausen. The value higher than 1 for Rollesbroich indicates that this site was a CO_2 source in 2013. The annual ratios between respiration by heterotrophs and TER varied between 0.51 and 0.58 (ratios for growing period: 0.35 - 0.48). Moureaux et al. (2008) and Suleau et al. (2011) report TER/GPP ratios between 0.49 and 0.66 for cereals, and R_h/TER ratios between 0.2 and 0.24, again only considering the plant growth phase. Our simulations generally agree well with these values, although the heterotrophic component appears to be larger in this study. Again, this reflects the lower

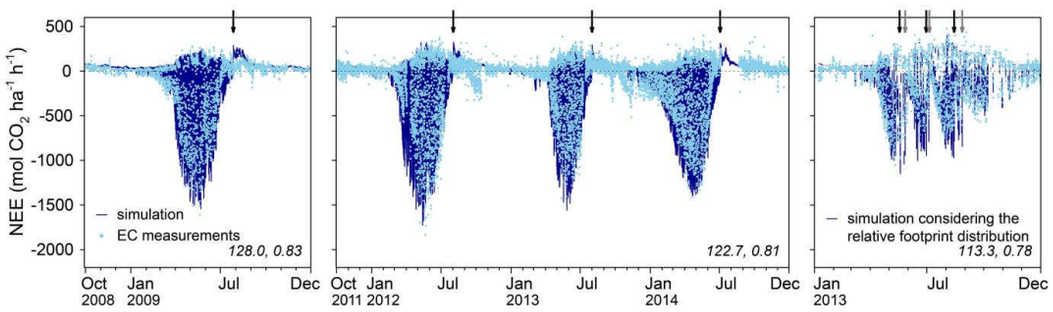

Fig. 2.8: Observed (*dots*) and simulated (*lines*) net ecosystem exchange (NEE) in Selhausen (*left*; EC: eddy covariance), Merzenhausen (*middle*), and Rollesbroich (*right*). In Rollesbroich NEE was simulated for each grassland (parcel A and B) and then allocated with the relative fraction of the footprint on each grassland. Arrows indicate dates of harvest or mowing (*black*: parcel A; *grey*: parcel B), respectively. Root mean square error (RMSE) and model efficiency (ME) (in this order) are given for each location.

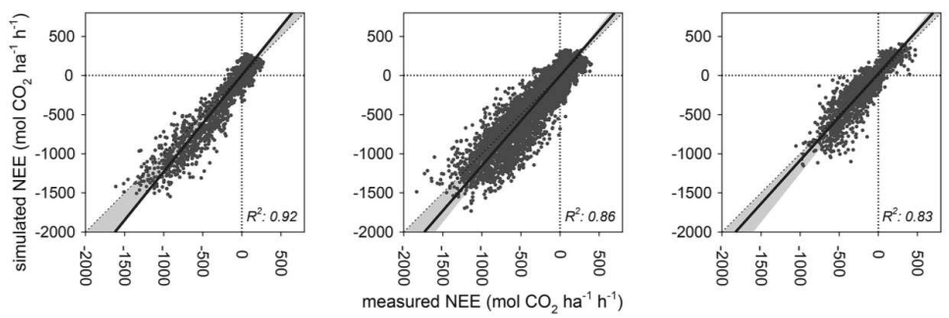

Fig. 2.9: Observed and simulated net ecosystem exchange (NEE) with reduced major axis regression (*black line*) in Selhausen (*left*), Merzenhausen (*middle*), and Rollesbroich (*right*). In Rollesbroich NEE was simulated for each grassland (parcel A and B) and then weighted according to the relative fraction of the footprint. A potential NEE gap of up to 20% in the measurements is indicated by the *grey area*. Coefficient of determination (R^2) is given for each location.

contribution of rhizospheric respiration as already discussed above.

The 1:1 plots between observed and simulated NEE (Fig. 2.9) show that on average AgroC overestimated the CO_2 fluxes by less than 20%, since the regression lines fall within the *grey area*. Turbulence fluxes can be systematically underestimated by EC measurements, and energy balance closure gaps of this magnitude have previously been reported (Eder et al. 2015; Schmidt et al. 2012; Twine et al. 2000). Therefore, underestimation of CO_2 fluxes can be expected (Ingwersen et al. 2015; Massman and Lee 2002; Mauder et al. 2013). This inability to close the surface energy balance, the various approaches to correct for the balance gaps, uncertainties due to instrumentation, and differing data-processing strategies complicate cross-site and longterm comparisons of NEE (Massman and Lee 2002; Mauder et al. 2013; Schmidt et al. 2012; Twine et al. 2000).

Wattenbach et al. (2010) compared the efficiency of four models to simulate NEE, and reported *ME* values between -0.15 and 0.87. The *ME* values for AgroC for the three sites compare favorably with this wide range (0.78 - 0.83). Wattenbach et al. (2010) also reported more substantial discrepancies between observations and simulations for positive NEE fluxes. Such an underestimation of positive NEE fluxes was also observed in this study, but to a much smaller extent, which is very likely a result of our more advanced approach towards the simulation of CO_2 fluxes and the calibration of R_{soil} with chamber measurements.

2.3.2. Calibration with NEE Data

After calibration to NEE measurements, the *RMSE* was reduced by up to 43%, and *Bias* also decreased strongly (Fig. 2.10). Depending on the optimization strategy, the cumulative NEE over the simulation period differed strongly (Fig. 2.10, A.3 in Appendix A). The calibration based on the instantaneous NEE data (NEE_{inst}) yielded the best results in terms of *RMSE*, *ME*, and *r* at all sites, because the reduction of the squared residual error between NEE prediction and measurements was the only criterion. *Bias* was the lowest in the NEE_{BSc} approach with and without inclusion of R_{soil} data because the *Bias* was now part of the objective function. Apart from that, model performance and NEE prediction by the NEE_{BSc} (+ R_{soil}) approach were very similar to NEE_{inst} (+ R_{soil}). The NEE_{Cum} and NEE_{Log} + R_{soil} approaches resulted in the poorest model performances at each study site. In almost all cases, model performance for NEE slightly deteriorated when R_{soil} measurements were included in the optimization process due to trade-offs between fitting multiple objective functions, with the exception of the approach that considered NEE_{Cum} + R_{soil} (Fig. 2.10).

Figure 2.11 shows reduced major axis regression (Webster 1997) for measured and simulated day- and nighttime (nighttime hours with global radiation < 20 W m^{-2} after Reichstein et al. 2005) NEE fluxes for the test site Selhausen. The corresponding figures for Merzenhausen and Rollesbroich are given in Appendix A (Fig. A.1, A.2). Compared to the NEE predictions obtained without calibration (Fig. 2.9), the calibrated daytime fluxes were generally closer to

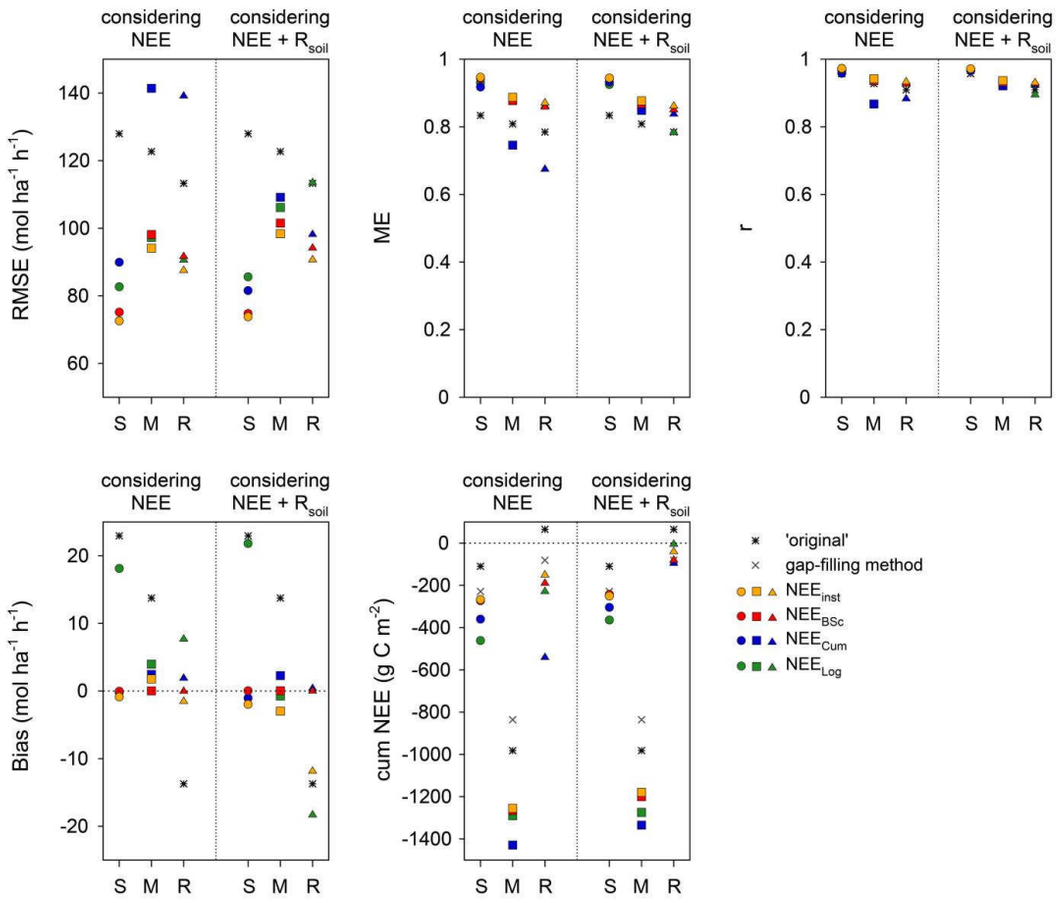

Fig. 2.10: Root mean square error (RMSE), model efficiency (ME), Pearson product-moment correlation coefficient (r), Bias, and cumulated net ecosystem exchange (cum NEE) over simulation time period, calculated in "gap-filling mode", for each optimization strategy, for the simulation without calibration to NEE ('original'), and for the gap-filling method after Reichstein et al. (2005) (gap-filling method) at all three study sites (S: Selhausen; M: Merzenhausen; R: Rollesbroich). For description of optimization strategies see text.

the 1:1 line and tended to only slightly underestimate daytime NEE fluxes as indicated by regression slopes slightly lower than 1. In general, nighttime NEE fluxes (dominated by respiratory fluxes) were better captured by the approaches that used an objective function including R_{soil} data, irrespective of the error weighting in the objective function or the transformation of the raw NEE data. Including R_{soil} data in the calibration clearly improved the simulation of diurnal and annual dynamics of the measured R_{soil}. The approaches only considering NEE measurements did not reproduce those dynamics (not shown). Even with the inclusion of R_{soil} data, nighttime NEE was still underestimated as indicated by regression slopes between 0.75 and 0.85 (Fig. 2.11, A.1, A.2).

In Figure 2.10 (*bottom right panel*) and A.3 in Appendix A, cumulative NEE over the corresponding simulation period (referred to as "cumulative NEE" in the following) is shown for all optimization strategies, for the simulations without calibration, and for the gap-filling method by Reichstein et al. (2005). For this comparison, cumulative NEE estimated with AgroC was also calculated in a "gap-filling mode", keeping the EC measurements and only filling the gaps with AgroC results. The cumulative NEE varied between -462 and -243 g C m^{-2} in Selhausen, -1429 and -1180 g C m^{-2} in Merzenhausen, and -541 and -5 g C m^{-2} in Rollesbroich. Cumulative NEE was mostly lower for the calibrated model runs than for the uncalibrated simulation. For all sites, the NEE_{Cum} or NEE_{Log} approach with and without R_{soil} measurements resulted in the lowest cumulative NEE. The $NEE_{inst} + R_{soil}$ approach resulted in the highest NEE, except for the Rollesbroich site. Generally, cumulative NEE of approaches including R_{soil} data in the objective function showed better agreement with the gap-filling method after Reichstein et al. (2005) than the approaches that did not consider R_{soil} measurements (Fig. 2.10).

Neglecting carbon removal due to harvest, the simulations suggest that all sites are CO_2 sinks, except for the simulation without calibration to NEE in Rollesbroich, which showed a very small positive annual NEE. Pastures are usually considered to be sinks for atmospheric CO_2 (Kuzyakov and Domanski 2000). Soussana et al. (2007) estimated an average annual carbon budget of -247 ± 67 g C m^{-2} and a net biome productivity (= NEE minus carbon loss due to disturbances, such as harvest) of -104 ± 73 g C m^{-2} for nine grasslands in Europe. Wohlfahrt et al. (2008) reported alternating positive and negative annual NEE for one grassland (gap-filled EC measurements), varying between -42 g C m^{-2} a^{-1} and 69 g C m^{-2} a^{-1}, and concluded that meteorological variations or differing biotic responses could easily lead to a positive carbon balance in some years. Also, the large amount of carbon stored in grassland soils (Tab. A.1 in Appendix A) can easily cause large respiratory fluxes that exceed plant carbon uptake. For Selhausen, estimated NEE matches cumulative values reported by Schmidt et al. (2012) and Wattenbach et al. (2010). Anthoni et al. (2004) found annual NEE in a range from -185 to -245 g C m^{-2} for a winter wheat field in Germany in 2001, which is in good agreement with our findings.

Since the true cumulative NEE is unknown due to measurement gaps, modelling can provide valuable information about the carbon balance. The best calibration approach that provides the 'true' cumulative NEE cannot be determined at this point. However, our results suggest that the cumulative NEE obtained from the calibrated model runs is more realistic than the cumulative NEE obtained with a model run not calibrated to NEE. The well-established gap-filling method after Reichstein et al. (2005) and AgroC produced somewhat different carbon balances, although NEE was derived from the same weather data. Especially after harvest or mowing, AgroC provided more reasonable predictions because it considers the changes in crop characteristics that directly influence GPP. Nevertheless, a better representation of respiration processes is still required, because even after calibration with EC and chamber

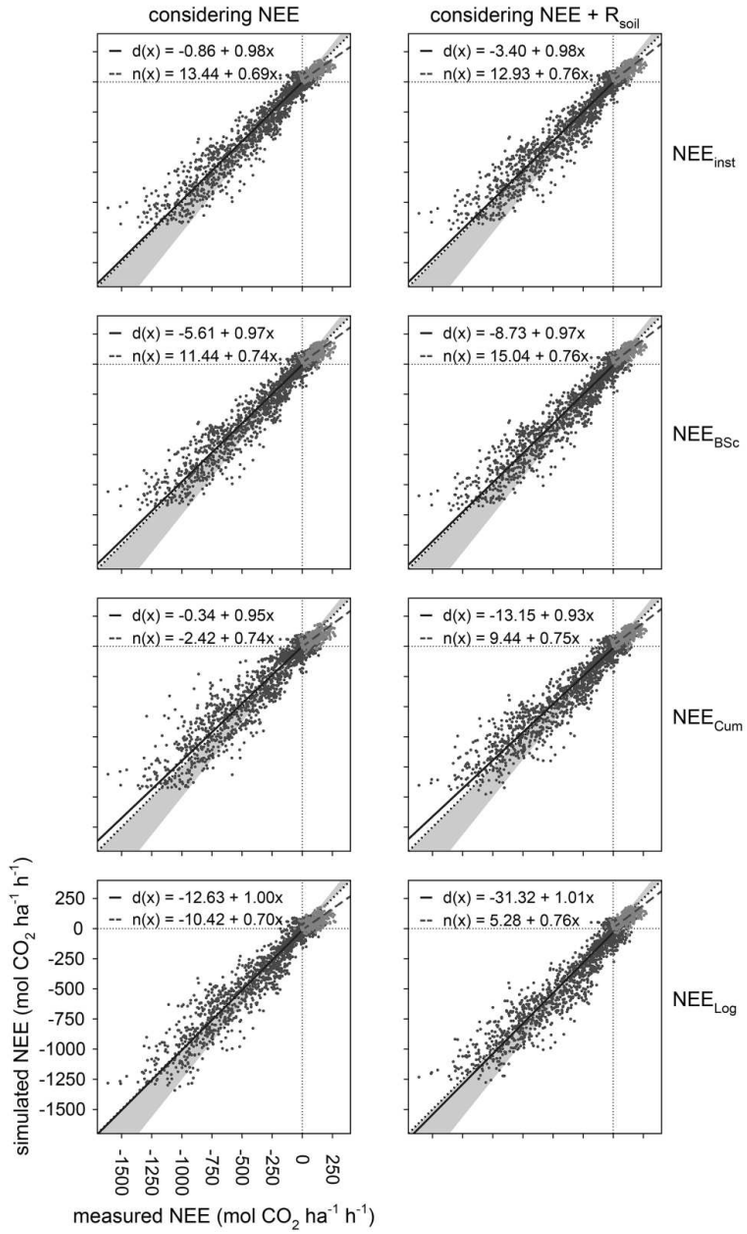

Fig. 2.11: Correlations between observed and simulated net ecosystem exchange (NEE) for all optimization strategies at test site Selhausen. Reduced major axis regression was derived for each strategy distinguished between day- (d) and nighttime (n) CO_2 fluxes, whereat nighttime was designated to a measured global radiation lower than 20 W m^{-2}. For description of optimization strategies see text.

measurements the respiration by heterotrophs and autotrophs was still underestimated. This bias between measured and modelled respiration may indicate a wrong process representation

in the model, errors in model parameterization, or may also be related to a disparity in the measurement footprint between chamber and EC measurements (Richardson et al. 2010). Obviously, an underestimation of respiratory fluxes will shift NEE to more negative values, as observed for the simulation results in Figure 2.10.

The cumulative NEE obtained after calibration with EC measurements was sensitive to the definition of the objective function and the data-transformation. As expected, explicit consideration of *Bias* in the objective function reduced it substantially (Fig. 2.10), with the NEE_{BSc} approach being most effective. The NEE_{Cum} approach often led to overestimation of negative and underestimation of positive fluxes (Fig. 2.10, 2.11, A.1, A.2). The use of cumulative data is known to enhance systematic errors and reduce noise (Hess and Schmidt 1995; Mandel 1957), and might not provide statistically valid information about associated errors and results if non-random auto-correlated residuals prevail. Compared to using the *Bias* as a criterion, it gives more weight to early observations that affect all succeeding cumulative values in the simulation period.

High-quality (hourly) EC measurements obtained after data processing usually consist of a large number of large negative fluxes during daytime and a smaller number of small positive nighttime fluxes, the latter being underrepresented. During calibration, the negative fluxes will on average have a higher weight, since they are more frequent and larger than positive fluxes. Therefore, a log-transformation of the NEE data could partly compensate for this, and provide more equal weighting. However, our results suggest the effect of this transformation on the performance of the calibration was weak. The slope of the regression between observed and simulated positive NEE was just slightly closer to 1 for the NEE_{Log} ($+ R_{soil}$) approach (Fig. 2.11, A.1, A.2).

The model performance for small positive fluxes improved strongly when considering R_{soil} measurements as an additional data source (Fig. 2.11, A.1, A.2). Similar findings were reported by Richardson et al. (2010), Wang et al. (2009), and Yuan et al. (2012). Williams et al. (2009) stated that the use of multiple data streams in calibration reduces the sensitivity to biases and internal inconsistencies in each data stream. Including R_{soil} measurements in the optimization process notably reduced the bias in the simulated nighttime NEE more than any of the modifications of the objective function or the use of data-transformation.

The $NEE_{inst} + R_{soil}$ approach provided the best results regarding both day- and nighttime fluxes at all three test sites. On average, model bias was one of the lowest for this optimization strategy at all sites. Even though overall model performance of the eight calibration approaches differed only marginally, it was found that resulting cumulative NEE diverged strongly. Considering additional data sources such as biomass measurements should help to further decrease the uncertainty of the cumulative NEE estimation (Richardson et al. 2010).

2.4. CONCLUSIONS

The present study demonstrates that a crop growth module coupled to a model of soil CO_2 production, soil water and heat flux can be used to simulate hourly NEE in agricultural systems. After calibrating the model for soil moisture, crop development, and R_{soil}, the simulation of hourly NEE agreed well to EC measurements. For further validation, the application of AgroC to cropping systems in different European climate regions would be interesting.

An additional calibration based on EC measurements further improved the model in terms of the performance criteria. Even more importantly, systematic errors between EC data and model were reduced. However, the various calibration approaches reveal that particularly the cumulative NEE over the entire simulation period is rather strongly affected by the choice of the objective criterion. Based on the evaluation of different optimization strategies, we recommend the use of the *RMSE* and non-transformed instantaneous EC-derived fluxes in combination with R_{soil} measurements (if available) by equally weighted errors. Our results indicate that cumulative NEE obtained using calibration and gap-filling methods is associated with considerable uncertainty, which can be decreased when R_{soil} measurements are included in the optimization process. At the same time, inclusion of R_{soil} also provided a substantial reduction of bias in the simulation of the respiratory fluxes.

2.5. ACKNOWLEDGEMENTS

This research was supported by FACCE MACSUR - Modelling European Agriculture with Climate Change for Food Security and by the German Federal Ministry of Education and Research BMBF, project IDAS-GHG [grant number 01LN1313A]. The measurement infrastructure providing observational data was supported by the German Research Foundation DFG through the Transregional Collaborative Research Centre 32 (TR 32) and Terrestrial Environmental Observatories (TERENO). We thank Axel Knaps (Sicherheit und Strahlenschutz - Umwelt, Meteorologie (S-UM), Forschungszentrum Jülich GmbH) for providing climate information, Ludger Bornemann (Institute of Crop Science and Resource Conservation (INRES) - Division of Soil Science, University of Bonn) for the analysis of black carbon, Henning Schiedung (INRES - Division of Soil Science, University of Bonn) for providing soil carbon fractions. The authors thank all technicians, engineers, and laboratory assistants in TR32 and TERENO for providing measurements of the test sites. We are also grateful to Daniel Farber and Horst Hardelauf for modifications of the model source code. Finally, we thank the reviewers for their helpful comments that improved the quality of this manuscript.

3

SENSITIVITY ANALYSIS OF A SOURCE PARTITIONING METHOD FOR H_2O AND CO_2 FLUXES BASED ON HIGH FREQUENCY EDDY COVARIANCE DATA: FINDINGS FROM FIELD DATA AND LARGE EDDY SIMULATIONS

This chapter is based on a journal article published as:
Klosterhalfen, A., Moene, A.F., Schmidt, M., Scanlon, T.M., Vereecken, H., Graf, A., 2019. Sensitivity analysis of a source partitioning method for H_2O and CO_2 fluxes based on high frequency eddy covariance data: findings from field data and large eddy simulations. Agricultural and Forest Meteorology 265, 152-170, https://doi.org/10.1016/j.agrformet.2018.11.003.

3.1. INTRODUCTION

The eddy covariance (EC) method is a convenient measurement technique for energy, water vapor, and carbon dioxide exchange between atmosphere and biosphere. It is routinely used for a better understanding of the exchange of greenhouse gases, providing, among others, fluxes of H_2O and CO_2 based on high-resolution (10 - 20 Hz) raw data of the concentrations of these gases and the vertical wind velocity. The method yields net fluxes; to gain deeper insight into the underlying biophysical processes, source partitioning methods have to be applied to the data to distinguish between the fluxes from the various compartments of the biosphere. Measured net ecosystem exchange (NEE) of CO_2 and its two components gross primary production (GPP) and total ecosystem respiration (TER) are of particular interest (Reichstein et al. 2012; Stoy et al. 2006). In addition, elements of the water cycle, their dynamics, and magnitudes have to be considered to comprehend the interrelation between atmosphere and terrestrial systems more completely. Particularly the study of evapotranspiration (ET), with its two components evaporation (E) and transpiration (T), and its feedbacks with the carbon cycle should be incorporated in environmental studies (Scanlon and Kustas 2010).

A large variety of source partitioning procedures with diverse approaches and necessity of different input data have been developed (Kool et al. 2014; Reichstein et al. 2012; Stoy et al. 2006). The most popular partitioning tools use regressed relationships of EC measurements (typically averaged over half-hourly periods) and physical drivers, in particular temperature (e.g., approach after Reichstein et al. 2005). The approach after Lasslop et al. (2010) additionally constrains the rate of photosynthesis with light response curves from daytime flux measurements. These approaches are well developed for the partitioning of carbon fluxes, but analogous methods for water fluxes are lacking yet (Reichstein et al. 2012; Stoy et al. 2006). Instrumental approaches of source partitioning require, next to EC data, additional measurements at different parts of ecosystems and with different methods, e.g., soil-flux chamber measurements, profile measurements (Ney and Graf 2018), or tracer measurements (isotopes). The latter are promising for flux partitioning, but associated with high costs, elaborate technical setups, and maintenance requirements that are usually not possible at most stations (Kool et al. 2014; Reichstein et al. 2012). With flux chambers, sap flux sensors, and microlysimeters sources and sinks of H_2O and/or CO_2 can be derived in an ecosystem, but are associated with scaling issues in comparison to the EC footprint.

As a data-driven method only requiring existing data from a typical EC station, Scanlon and Sahu (2008) and Scanlon and Kustas (2010) proposed a method to estimate the contributions of T, E, photosynthesis, and soil respiration (R_{soil}, autotrophic and heterotrophic sources) using measured high frequency time series of water vapor and CO_2 concentrations. This method (further called SK10) is based on the dissimilarities of sources and sinks of water vapor and CO_2 among sub-canopy, canopy, and atmosphere, which lead to unique “signals” in EC measurements for air transported from differing locations. The flux-variance similarity theory

is separately applied to the stomatal and non-stomatal components of the regarded scalars. The discrepancy between the perfect correlation between H_2O and CO_2 at leaf-level (via the water use efficiency WUE) and the imperfect correlation between H_2O and CO_2 fluctuations above the canopy is used to determine the relative strength of each flux component. SK10 requires that the correlation coefficient between stomatal and non-stomatal scalar fluctuations is determined by the ratio of the transfer efficiencies of these scalar components, an assumption (transfer assumption in the following) made by Scanlon and Sahu (2008) in the method's derivation.

Scanlon and Kustas (2012) applied SK10 to a corn field (eastern USA) and showed that the performance of ET partitioning is consistent, can give insights for calculation of canopy conductance, and therefore, has the potential to improve land surface models. A comparison between isotopic H_2O flux partitioning and SK10 was conducted by Good et al. (2014). Wang et al. (2016) analyzed H_2O flux partitioning by SK10 at a suburban grassland site (western USA), that yielded similar diurnal and seasonal dynamics compared to simulations with the Noah Land Surface Model. Sulman et al. (2016) compared SK10 with other partitioning methods (sub-canopy EC measurements, non-linear regression method, and potential evapotranspiration) and evaluated its performance in a forest site in a decadal time scale. Considering ten day moving averages the multiple methods showed a good agreement for T and GPP and a higher variability in E and TER.

Sulman et al. (2016) suggested further investigation of SK10 via large eddy simulation (LES) studies identifying potential sources of errors in the application of the partitioning method. Various LES studies including a canopy have been conducted studying the influence of canopy properties and canopy edges on airflow above and in the canopy (e.g., Cassiani et al. 2008; Dupont and Brunet 2008; Finnigan et al. 2009). Huang et al. (2013) studied the influence of coherent structures on the scalar dissimilarity in the air space just above the canopy via LES. They investigated the scalar-scalar-correlation in forest canopies with differing densities. Edburg et al. (2012) simulated the transport of passive scalars for a forest canopy and concluded that scalar concentration profiles, fluxes, correlation coefficients, and scalar segregation are affected by the sink-source-distribution of the scalars. We assumed that these differing characteristics also influence the performance of SK10.

In spite of the partly successful applications of SK10 (see above), the method is still not widely used and robustness issues have been reported (mostly personal communication). We aim to identify the key assumptions behind the method that, if not properly met, can lead to its failure. To this end, we applied the partitioning method to data of two contrasting field sites with various WUE assumptions derivable from meteorological measurements. Furthermore, we applied SK10 to data obtained on synthetic high frequency data by LES, checked scalar statistics, the validity of the transfer assumption, and evaluated the partitioning method.

3.2. MATERIAL AND METHODS

3.2.1. Study Sites

The measurements were obtained at Selhausen (50°51'N, 6°26'E, 103 m a.s.l., ICOS code DE-RuS) and Wüstebach (50°30'N, 6°19'E, 610 m a.s.l., ICOS code DE-RuW) in western Germany. These study sites are included in the Terrestrial Environmental Observatories (TERENO) network of highly instrumented field sites.

Selhausen is located in the southern part of the Lower Rhine Embayment. The underlying sediments are Quaternary fluvial deposits from the Rhine/Meuse and Rur river system, and were covered by floodplain sediments and loess in the Pleistocene and Holocene. The major soil type was classified as a Luvisol according to the soil taxonomy of the FAO (I.U.S.S. Working Group WRB 2006). The soil texture is a silt loam and fairly homogeneous in the area (Weihermüller et al. 2007). The climate conditions are temperate maritime with a mean annual temperature of 9.9 °C and an annual precipitation of 698 mm (1961-2009; Graf et al. 2012). The dominant land use in the region is cropland and in 2015 winter wheat (*Triticum aestivum* L.) was cultivated in Selhausen. The crop height was between 0.57 and 0.81 m and the leaf area index (LAI) between 5.7 and 6.8 m^2 m^{-2} on the considered days. EC measurements (measurement height 2.43 m) and ancillary environmental measurements were conducted in the center of the field. Measurements of H_2O, CO_2, wind components, sensible heat, global radiation, air temperature, precipitation, and relative humidity were available for the regarded time periods. A detailed description of the measurement setups is given by Ney and Graf (2018). All observations were averaged in half-hourly time steps, while the measurement frequency of the EC method was 20 Hz. Here, we use the micrometeorological convention, where downward fluxes from atmosphere to biosphere are negative and upward fluxes positive (Stoy et al. 2006).

The Wüstebach catchment is part of the low mountain range Eifel and covers an area of ~38.5 ha; the altitude ranges from 595 m to 628 m a.s.l. The underlying bedrock consists of fractured Devonian slate with sporadic sandstone inclusions. Soil types vary from Cambisols and Planosols to Gleysols and Histosols depending on the average groundwater level. Soil texture is a silty clay loam (Bogena et al. 2015). The mean annual temperature is 7.5 °C and the annual precipitation is 1220 mm (1979-1999; Bogena et al. 2015; Ney et al. in press). The dominant vegetation type is Norway spruce (*Picea abis* L.). EC and ancillary environmental measurements (same as in Selhausen) were taken in a height of 38 m above ground, over a spruce canopy of 25 m height and a LAI of about 3.9 m^2 m^{-2}.

SK10 is applied to half-hourly time series of pre-processed high frequency EC data of vertical wind velocity, total H_2O, and CO_2 concentrations. Beforehand, physically not possible values and spikes were excluded in the high frequency data, the time delay was corrected, missing raw data in one 30 minutes period was gap-filled by linear interpolation and a planar-fit rotation was conducted.

For the application of the source partitioning method, days with a high productive state of the vegetation and fair-weather conditions (sunny, almost no precipitation, clear diurnal dynamics of all meteorological variables) were chosen to ensure that all flux components contributed to the measured total fluxes and to exclude processes and factors further disturbing the stationarity of turbulence and the expected behavior of the stomata (e.g., cloud cover). Also, the method was only applied to time periods, where the quality assessment scheme during EC processing (after Mauder et al. 2013) assigned the highest or intermediate out of three quality flag levels. Furthermore, for Selhausen half-hour periods have been excluded, if the relative contribution of the target field to the footprint (after Kormann and Meixner 2001) was smaller than 80%. For Wüstebach time periods with wind directions between 70° and 162° were excluded to receive only flux measurements of the desired target area. Furthermore, the source partitioning method was merely applied to daytime data because the SK10 method requires the presence of photosynthesis. Here, sunrise and sunset times were calculated by means of local time, and in addition, daytime was designated to a measured global radiation higher than 20 W m^{-2} after Reichstein et al. (2005).

For validation purposes, R_{soil} data were obtained with closed-chamber measurements at both sites. In Selhausen, half-hourly measurements of four longterm-chambers were available for the considered time periods. In Wüstebach, R_{soil} was measured with survey-chambers at several measurement points in the forest on June 10th, 2015 (9 a.m. - 1 p.m.), so a spatial and temporal average for that day could be calculated. Furthermore, soil evaporation E_{soil} was estimated as a fraction of measured ET based on Beer's law depending on LAI (E_{soil} = ET exp(-0.6 LAI); Campbell and Norman 1998; Denmead et al. 1996; Kool et al. 2014) to compare to the partitioned H_2O components by SK10 at both study sites.

3.2.2. Source Partitioning Based on High Frequency Data - SK10

The source partitioning method after Scanlon and Sahu (2008) and Scanlon and Kustas (2010) is based, among others, on the Monin-Obukhov similarity theory (MOST). In the atmospheric surface layer above a horizontally homogenous surface, scalar statistics in a particular height are expected to depend on the surface fluxes, surface shear stress, and buoyancy determined by sensible and latent heat flux (Scanlon and Kustas 2010; Scanlon and Sahu 2008). Strictly, MOST implies that scalar time series measured at the same position in the atmospheric surface layer should correlate perfectly, which is consistent with the concept of flux-variance similarity (Hill 1989). These expectations are not always met under field conditions because of a non-steadiness of time series, the influence of entrainment, and heterogeneous distribution of sinks and sources (Scanlon and Kustas 2010; Scanlon and Sahu 2008).

With the EC method high frequency measurements of water vapor and CO_2 concentrations are collected and their turbulence-driven dynamics are monitored. During the day T and photosynthesis are usually the main contributors to measured H_2O and CO_2 fluxes, and both

derive from stomatal exchange. In the absence of non-stationarity and entrainment, the correlation coefficient $\rho_{q_t'c_p'}$, between the two stomatal scalars is equal to -1 according to the flux-variance similarity theory (subscripts q_t and c_p indicate moisture and CO_2 concentrations related to T and photosynthesis; likewise, subscripts q_e and c_r indicate moisture and CO_2 concentrations related to E and R_{soil}, respectively). This relationship between H_2O loss and CO_2 uptake on leaf-level by vegetation is described by the WUE. When in a hypothetical case the fluctuations of H_2O and CO_2 (R_{soil} and direct E disregarded) are plotted against each other, they would correlate perfectly and the linear slope would be equivalent to the WUE (WUE is defined to be negative, see Eq. 3.4; Scanlon and Kustas 2010; Scanlon and Sahu 2008), from which follows:

$$c_p' = \mathrm{WUE} \cdot q_t' \tag{3.1}$$

The non-stomatal processes, direct E and R_{soil}, are expected to also adhere to flux-variance similarity. These fluxes originate primarily from the sub-canopy, are enriched in both H_2O and CO_2, and it is assumed that they are transported similarly with one another, but different from the stomatal components. Since both fluxes are positive during daytime, they correlate positively and $\rho_{q_e'c_r'}$ would be equal to +1 (Scanlon and Kustas 2010; Scanlon and Sahu 2008).
For the natural case in which both stomatal and non-stomatal processes contribute to the fluxes, the correlation between water vapor fluctuations (q') and CO_2 fluctuations (c') is reduced. The slope of the q' versus c' relationship becomes less than WUE, such that the magnitude of the ecosystem-level WUE is smaller (less negative) than WUE at leaf-level (Palatella et al. 2014). The reduced correlation and deviation from WUE at leaf-level provides information about the composition and magnitudes of the measured fluxes (Scanlon and Kustas 2010; Scanlon and Sahu 2008). Scanlon and Sahu (2008) state that, to obtain accurate source partitioning from this extra information, the vegetation has to be distributed homogeneously in a horizontal sense and the vertical heterogeneity and spatial distribution of stomatal and non-stomatal sinks and sources have to be significant to reduce the degree of correlation.
Figure 8 in Scanlon and Sahu (2008, page 10) shows an overview of the main analysis steps of SK10. The first step in this time series analysis is the correction for density fluctuations in the raw data of H_2O and CO_2 fluxes. Such fluctuations can arise due to external factors such as changes in air temperature or water vapor density. Scanlon and Kustas (2010) use the approach after Detto and Katul (2007). As mentioned before, the correlation between q' and c' is very sensitive to advection, entrainment, and large-scale weather effects. Therefore, large-scale fluctuations should be eliminated from measurements, in this case, by orthonormal wavelet transform using the discrete Haar wavelet. For 20 Hz data sets of 30 minutes (36000 data points) 15 wavelet levels can be derived (2^{15} data points in the first 27.3 min; Scanlon and Albertson 2001). In this study, the first two wavelet levels representing the low frequency

eddies have always been removed by default to reduce the influence of large-scale processes as suggested by Scanlon and Kustas (2010). In the process of finding a valid solution, additional wavelet levels can be excluded progressively, if necessary (see below). The application of wavelet transform gives an insight, how $\rho_{q'c'}$, ecosystem-level WUE, and scalar transport efficiencies vary across scales of turbulent eddies. The derived eddy frequencies could be converted to eddy diameters using Taylor's frozen turbulence hypothesis (Scanlon and Kustas 2010).

To compute the exact combination of flux contributions, Scanlon and Sahu (2008) derived a system of equations for this approach, in which most parameters ($\overline{w'q'}$, $\overline{w'c'}$, $\rho_{q'c'}$, $\rho_{w'q'}$, $\rho_{w'c'}$, $\sigma_{q'}^2$, $\sigma_{c'}^2$) are known from measurements. To further reduce the number of unknowns, the following equations are assumed to be reasonable approximations (transfer assumption; Bink and Meesters 1997; Katul et al. 1995; Scanlon and Kustas 2010; Scanlon and Sahu 2008):

$$\rho_{q_t'q_e'} \approx \frac{\rho_{w'q_e'}}{\rho_{w'q_t'}} \tag{3.2}$$

$$\rho_{c_p'c_r'} \approx \frac{\rho_{w'c_r'}}{\rho_{w'c_p'}} \tag{3.3}$$

where w' is the vertical wind fluctuation. These equations imply that transport efficiencies of q_e' and c_r' coming from the soil surface are smaller than the efficiencies of q_t' and c_p' from the canopy airspace, respectively, because $|\rho_{q_t'q_e'}|$ and $|\rho_{c_p'c_r'}|$ should be smaller than 1 (Bink and Meesters 1997). This is consistent with the results of Lamaud and Irvine (2006) and Moene and Schüttemeyer (2008) who found that for the scalar pair temperature-humidity the relative transport efficiency $\rho_{w'\theta'}/\rho_{w'q'}$ is equal to $\rho_{\theta'q'}$ for well-watered conditions (small heat flux) and $1/\rho_{\theta'q'}$ for dry conditions (small moisture flux). They also show that in general $\rho_{w'\theta'}/\rho_{w'q'}$ can be described as $(\rho_{\theta'q'})^k$ with k ranging between -1 and 1.

Besides, WUE can be estimated (see below), such that only two parameters in the essential equation of the approach (Scanlon and Sahu 2008, Equation 15, page 5; Eq. B.1 in Appendix B) are unknown: the correlation coefficient of the CO_2 concentrations related to photosynthesis and R_{soil} ($\rho_{c_p'c_r'}$) and the variance of photosynthesis-related CO_2 ($\sigma_{c_p'}^2$). The equation can be further manipulated to solve for $\sigma_{c_p}^2 = f(\rho_{c_p'c_r'})$ (Eq. B.2). To obtain results for $\sigma_{c_p}^2$ and the corresponding magnitudes of each flux component, values of $\rho_{c_p'c_r'}$ in a physically meaningful range of $-1 \leq \rho_{c_p'c_r'} \leq 0$ are inserted into the function. To obtain the exact partitioning solution, $\rho_{q'c'}$ is derived as a function of $\rho_{c_p'c_r'}$ and the other variables. If this calculated $\rho_{q'c'}$ matches the observed $\rho_{q'c'}$, (misfit is less than 0.005), then actual values for $\rho_{c_p'c_r'}$, $\sigma_{c_p}^2$ and the partitioning factors are found (Scanlon and Kustas 2010; Scanlon and Sahu 2008). As a further check, WUE is calculated again as a function of the derived partitioning factors and compared to the input WUE. If those 'input' and 'control' WUEs differ too much (misfit larger than 1%), the solution is disregarded. If no solution for $\rho_{c_p'c_r'}$ and $\sigma_{c_p}^2$ is attained,

the next wavelet level is removed progressively to further reduce the influence of large-scale processes until a valid solution is reached or none at all. The estimated partitioning factors are then applied to the post-processed half-hourly EC data.

For a detailed analytical description of SK10 see Palatella et al. (2014), Scanlon and Albertson (2001), Scanlon and Kustas (2010, 2012), and Scanlon and Sahu (2008). Our implementation deviates from the procedure of Palatella et al. (2014) and Scanlon and Kustas (2010) in terms of finding valid solutions with a minimal error in $\rho_{q'c'}$ and WUE. Because we converted Equation 15 in Scanlon and Sahu (2008) solving for $\sigma_{c_p}^2$ directly (see Appendix B), we were left with only one unknown variable: $\rho_{c_p'c_r'}$. By insisting upon very low errors in $\rho_{q'c'}$ and WUE we found almost always the same solutions as the approach after Palatella et al. (2014), even though we passed on the implementation of the globally convergent Newton's method. Aside from this, Skaggs et al. (2018) developed an algebraic solution simplifying the source partitioning procedure and implemented SK10 in the open source Python 3 module Fluxpart. Using the analytical approach would not significantly change our results, but it might improve the rate of convergence to a solution.

One disadvantage of SK10 is that the autotrophic CO_2 source term (growth and maintenance respiration by plants) cannot be quantified. Thus, not GPP but the above-ground net primary production (NPP; GPP minus above-ground respiration by autotrophs) is result of this approach. Furthermore, SK10 can only be applied to daytime fluxes, because it is based on the assumptions that photosynthesis is active and E positive. Also, no evaporation of intercepted rain water in the plant canopy should be present, because the method cannot discriminate between T and E from water at leaf-level.

Water Use Efficiency

A key element of the source partitioning method after Scanlon and Kustas (2010) is the WUE at leaf-scale, which describes the relation between the amount of CO_2 uptake through stomata (photosynthesis) and the corresponding amount of H_2O loss (T) (not to be confused with the ecosystem WUE, the ratio between NEE and ET).

One way to derive WUE is to relate the difference in mean CO_2 concentration between air (just outside the leaf) and stomata to the difference in mean humidity concentration between air and stomata:

$$\mathrm{WUE} = 0.7 \cdot \frac{c_s - c_i}{q_s - q_i} \tag{3.4}$$

where the subscripts "s" and "i" indicate the external (within canopy) and internal (intra-stomatal) concentration of H_2O (q) and CO_2 (c) averaged over the regarded time period. The factor 0.7 (mg g^{-1}) accounts for the difference in diffusion and convection between H_2O and CO_2 through the stomatal aperture (Campbell and Norman 1998). c_i should be lower than c_s to

maintain CO_2 uptake and q_i larger (saturated) than q_s, leading to a negative fraction (Scanlon and Kustas 2010, 2012; Scanlon and Sahu 2008).

As mentioned before, WUE should be evaluated for the leaf-level, where the exchange between plants and atmosphere takes place. c_s and q_s at displacement height can be inferred from EC measurements by considering logarithmic mean concentration profiles implementing MOST (Scanlon and Kustas 2010, 2012; Scanlon and Sahu 2008). For c_i a constant value of 270 ppm was presumed, a typical value for C3 plants (Špunda et al. 2005; Williams et al. 1996; Xue et al. 2004). Values for q_i were estimated based on 100% relative humidity at foliage temperature (T_f). Measurements of T_f were not available at our study sites, so for the source partitioning T_f was set equal to measured air temperature (Scanlon and Sahu 2008). Additionally, to investigate the sensitivity of WUE, T_f was derived by different strategies: it was assumed to be 2 K lower or higher than air temperature ($WUE_{meanT-2K}$ or $WUE_{meanT+2K}$, respectively) as suggested by Scanlon and Sahu (2008), as well as calculated by means of measured outgoing longwave radiation (WUE_{OLR}; with a surface emissivity of 0.98), or calculated similar to c_s and q_s by considering a logarithmic mean profile implementing MOST (WUE_{MOST}).

Because the chosen inputs of c_i and T_f comprise an uncertainty, we conducted two additional runs with quantities of c_i and T_f on the outer margins of their reasonable ranges for a very low or very high WUE, respectively. Following Equation 3.4, if c_i and/or T_f (and with it q_i) increases, the magnitude of WUE decreases (WUE gets less negative), and the plant is assumed to be less efficient. For Norway spruce Špunda et al. (2005) calculated values of c_i between 180 and 400 ppm based on measured air CO_2, assimilation rate and stomatal conductance in a diurnal cycle. Xue et al. (2004) measured c_i for four different winter wheat cultivars under differing conditions and obtained a range between 120 and 300 ppm. Thus here, 200 and 300 ppm were chosen for a minimal or maximal magnitude of c_i, respectively. The calculated T_f by means of measured outgoing longwave radiation was during the day about 3 K or 6 K higher at the forest or crop site, respectively, than the mean air temperature. Thus, for a minimal value, q_i was calculated based on the mean air temperature minus 2 K and for a maximal value, based on air temperature plus 5 K. For the two additional applications of SK10 to the study sites, on the one hand the small values of c_i and T_f were chosen for a maximal magnitude of WUE (WUE_{MAX}) and on the other hand the larger values for a minimal magnitude of WUE (WUE_{MIN}) (Tab. 3.1). Note that tentatively choosing even more extreme values for c_i or T_f mostly led to no valid solutions of the SK10 procedure.

3.2.3. Large Eddy Simulations

LES were undertaken to study the impact of different canopy types on the vertical exchange of scalars. The effect of the vertical scalar sink-source-distribution and of the relative importance of canopy and soil source on correlation coefficients were of interest. The simulations have

been performed with the Dutch Atmospheric Large-Eddy Simulation (DALES) model (Heus et al. 2010; Ouwersloot et al. 2016). The default version was extended to enable closer control of the source distribution in the canopy.

We conducted experiments with neutral flow conditions (i.e., all scalars are passive with respect to buoyancy). A frictionless rigid lid (zero-gradient boundary conditions for horizontal velocity components and all scalars, and $w = 0$) was applied as upper boundary condition. A periodic boundary condition was set in each horizontal direction for both velocity and all scalars. The external forcing was a constant horizontal pressure gradient. This setup was slightly different from the variable momentum forcing (targeting a constant mean velocity) used in the studies conducted by Ouwersloot et al. (2016) and Edburg et al. (2012).

A domain size of $72\ h_c \times 36\ h_c \times 32\ h_c$ with $720 \times 360 \times 144$ nodes in the x-, y-, and z-directions with a grid resolution of 0.1 canopy heights (h_c) was used for the numerical experiments. In the vertical direction the grid cells were equally spaced up to a height of five times the h_c and above stretched progressively to a total domain height of 32 times the h_c.

The total simulation runtime for each experiment was $720\ h_c\ u_*^{-1}$ (u_* is the friction velocity at the canopy top), of which the last $120\ h_c\ u_*^{-1}$ were sampled. For the statistics of turbulence profiles, quantities were sampled every $1\ h_c\ u_*^{-1}$ and averaged over $120\ h_c\ u_*^{-1}$, respectively. Fields of momentum and scalars were sampled every $6\ h_c\ u_*^{-1}$. The Courant-Friedrichs-Lewy (CFL) number was smaller than 0.5 for all runs. The time steps and the maximum horizontal velocity in x-direction were variable in these simulations, but were in average about $0.0042\ h_c\ u_*^{-1}$ and $0.46\ h_c\ u_*^{-1}$, respectively[1].

The plant area density (PAD) profile was prescribed, with a smooth transition at the top of the canopy over four grid points, and the canopy was resolved vertically by 10 grid points, both as recommended by Ouwersloot et al. (2016). The drag coefficient C_d was set to 0.5 describing the drag on the flow induced by canopy elements, and we prescribed the roughness length of the underlying soil as $z_0 = 0.005$ m. The canopy was homogeneous in the horizontal direction.

Two LES experiments with contrasting PAD profiles were conducted: on the one hand with a canopy similar to a crop (winter wheat) and on the other hand with a canopy similar to a coniferous forest (Fig. 3.1, B.5 in Appendix B). These canopy profiles were taken from measurements at our study sites and literature (Edburg et al. 2012; Gspaltl et al. 2013; Weiskittel et al. 2009). The LAI was set to $2\ m^2\ m^{-2}$ in both cases, which is a typical magnitude for forests, while winter wheat usually has a considerably denser canopy. In the following, only results of the experiment with the crop-like canopy are shown. The corresponding figures of the experiments with forest-like canopy can be found in Appendix B (Fig. B.5-B.11).

[1] In dimensional terms, the various simulation characteristics are: $h_c = 1$ m, $u_* = 0.2\ m\ s^{-1}$, total simulation run time 3600 s, of which the last 600 s were sampled; time steps and the maximum horizontal velocity in x-direction were in average about 0.021 s and $2.3\ m\ s^{-1}$, respectively.

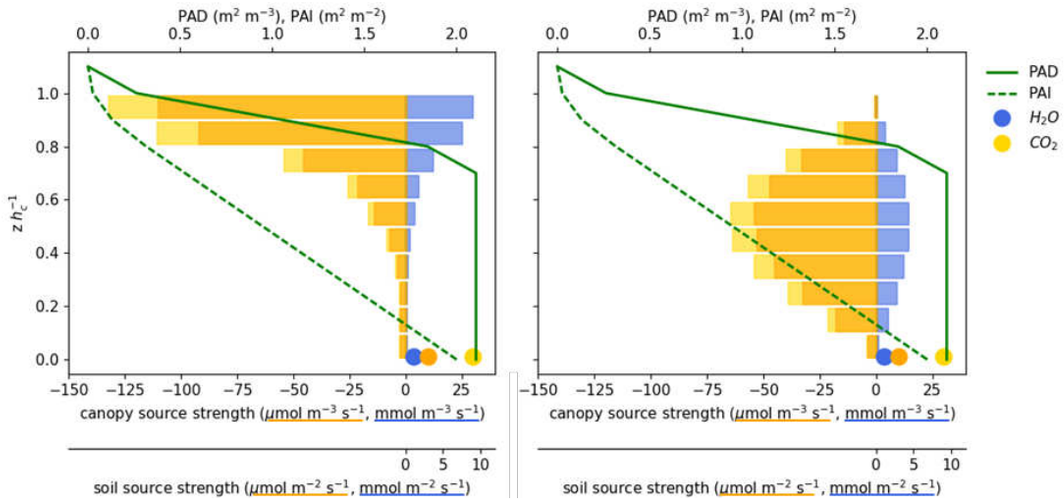

Fig. 3.1: Vertical profiles of the crop plant area density (PAD), cumulative plant area index (PAI), and variations of sink-source-distributions for H_2O and CO_2 used to scale the LES scalar fields (*left*: ModelV, after Sellers et al. 1992; *right*: ModelB, after Ney et al. 2017), each with ten canopy sinks/sources (*bars*) and one soil source (*circle*). For CO_2, two different soil sources and accordingly differing canopy sinks were used, in which the flux at canopy top for each distribution is the same.

In the simulations passive scalars were emitted homogeneously from the soil surface and from ten canopy sources (one for each grid cell in vertical direction). So, in total eleven fields of arbitrary scalars were simulated. Each of these fields can be scaled with a desired source strength for the respective source level. A scalar with sources at multiple levels can be constructed by adding these fluctuation fields, each scaled with a height-specific source strength derived from a desired vertical source strength distribution. This could be repeated for an arbitrary number of scalars and vertical source distributions after the actual LES runs. Thus, fields for both H_2O and CO_2 were created, assuming a water vapor source and a carbon sink in the canopy and a source for both scalars at the soil surface. Two different variations of distributions were applied: on the one hand a v-shaped distribution taken from Sellers et al. (1992) (ModelV, Fig. 3.1 *left*) and on the other hand a beta-function-shaped distribution inferred from profile measurements in winter barley on June 9th, 2016 (Ney et al. 2017; Ney and Graf 2018) (ModelB, Fig. 3.1 *right*). Finally, the relative strength of the CO_2 soil source was varied: the soil sources were set to 1 mmol m^{-2} s^{-1} for H_2O and to 3 or 9 µmol m^{-2} s^{-1}, respectively, for CO_2. The total flux at canopy top was for each distribution the same and matched EC measurements of the same day in June 2016 (ET = 9.2 mmol m^{-2} s^{-1}, NEE = -27.26 µmol m^{-2} s^{-1}). So, in total we had for each canopy type four different combinations of sink-source-distributions: ModelV with low or higher CO_2 soil source and ModelB with low or higher CO_2 soil source. This setup was chosen to study the influence of the separation between soil sources and canopy sink/source and of their relative magnitudes on scalar-scalar-correlations and flux profiles. Also, the impact of differing magnitudes of ecosystem- and

canopy-level WUE could be studied. Ecosystem WUE was for all LES experiments identical, and the WUE on canopy-level did not differ between ModelV and ModelB under identical soil source strength. Furthermore, the setup allowed to separately study and compare the effect of the different PADs and the resulting turbulence on the one hand, and of differing scalar sink-source-distributions on the other hand.

After scaling the scalar fields with the chosen sink-source-distributions, variances and covariances could be sampled from the LES experiments in any chosen virtual measurement height. To calculate the required fluxes, simulation data of vertical wind and scalar concentrations were sampled from each field (fields collected every $6\ h_c\ u_*^{-1}$ in the last $120\ h_c\ u_*^{-1}$ of runtime) for every tenth grid point in x- and y-direction in each corresponding height, so data for one virtual measurement height consisted of 51840 data points. After calculating the necessary H_2O and CO_2 fluxes, the variances and correlation of q' and c', and WUE, the SK10 approach could be applied to this 'virtual EC data'. SK10 was only applied to the resolved scale statistics, assuming any correlation structure found in the resolved scale would be valid for the subgrid scale as well. The source partitioning results could then be validated to the known fluxes and statistics of the components q_t, q_e, c_p, and c_r from the LES experiments.

3.3. RESULTS AND DISCUSSION

The first objective of our study was the application of SK10 to data of our study sites and the analysis of the partitioning results depending of the WUE input. The second objective was the application of SK10 to synthetic high frequency data generated by LES and the analysis of the partitioning performance depending on canopy type, measurement height, and given sink-source-distribution. Also here, dependence of the partitioning result to the WUE input was analyzed. Of particular interest was the assessment of the transfer assumption involved in SK10 (Eq. 3.2, 3.3), which was only possible with the LES experiments.

3.3.1 Source Partitioning of Field Data

The selected time period for the forest site included 247 daytime hours and the three periods for the cropland 359 daytime hours in total. After checking the data quality (excluding periods with precipitation events, worst quality flag, and insufficient fraction of footprint on target area) SK10 could be applied to 70% and 86% of these daytime hours for the forest and cropland site, respectively. Subsequently, SK10 found valid partitioning solutions for 75% and 58% of these high-quality daytime periods for the forest and cropland site.

Figures 3.2 and 3.3 show source partitioning results of SK10 for H_2O and CO_2 fluxes at the two study sites for certain time periods. The partitioned H_2O fluxes were compared to estimated E_{soil} computed as a fraction of measured ET based on Beer's law depending on LAI

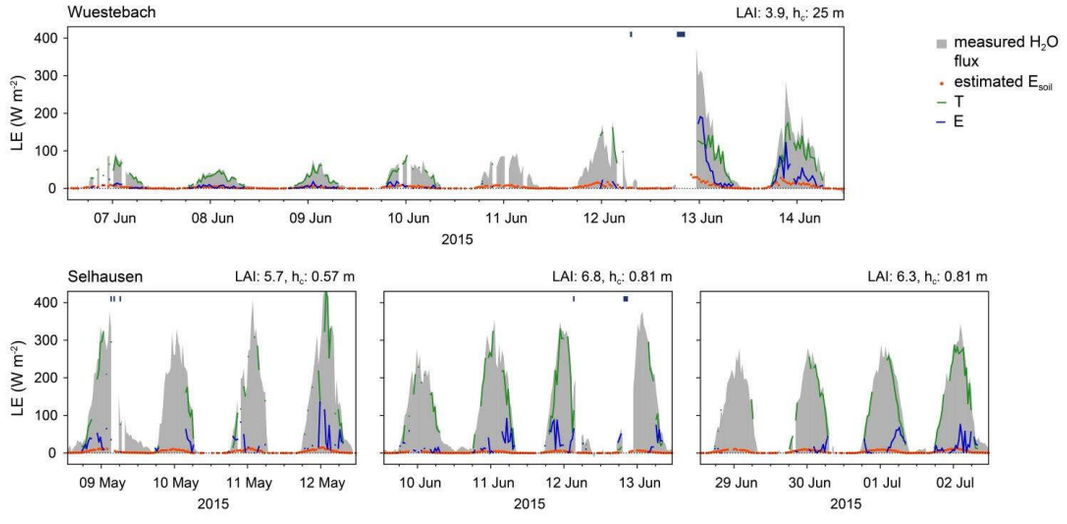

Fig. 3.2: Source partitioning results of the approach after Scanlon and Kustas (2010) for H_2O fluxes at the two study sites Wüstebach (forest; *top*) and Selhausen (cropland; *bottom*) for varying time periods (LE: latent heat flux; T: transpiration; E: evaporation; E_{soil}: soil evaporation calculated based on Beer's law depending on LAI; LAI: leaf area index; h_c: canopy height; *blue bars*: precipitation events).

(Fig. 3.2; Campbell and Norman 1998; Denmead et al. 1996; Kool et al. 2014). The partitioned CO_2 fluxes were compared to results of the approach after Reichstein et al. (2005) and to R_{soil} chamber measurements (Fig. 3.3). The root mean square error (*RMSE*) and the *bias* between measured and SK10-based R_{soil} are given in Table 3.1. For the calculation of the error quantities, outliers were excluded which deviated from the mean by more than ten times the standard deviation. Concerning the different chamber measurement setups, one area average from four chamber measurements was given per considered half-hour at the crop site, while at the forest site only one space-time average from 36 consecutive manual chamber measurements in different locations was assumed to be approximately applicable for June 10th, 2015 from 9 a.m. till 1 p.m.

SK10 reasonably partitioned water vapor fluxes into larger fractions of T than E (Fig. 3.2). The comparison between E and estimated E_{soil} based on Beer's law showed a good agreement for the forest and larger discrepancies for the cropland. For the latter, SK10 seemed to overestimate E up to the tenfold in most time periods and matched the magnitude of E_{soil} perfectly in only a few time periods, keeping in mind that E_{soil} was also just an approximation. The large variations in E decreased with maturity of the crop. The median of the partitioning fraction E/ET was 0.16 for the forest and between 0.09 and 0.23 for the cropland in the three time periods. At the forest site E/ET increased to a median of 0.29 on the two days after the precipitation events during the night from June 12th to June 13th. Thereby, T was reduced due to an increased q_s and a decreased humidity gradient at leaf-level. This effect was also observed by Scanlon and Kustas (2012). Kool et al. (2014) reviewed 52 studies about ET partitioning and found values of E/ET between 0.05 and 0.53 for forests and between 0.1 and

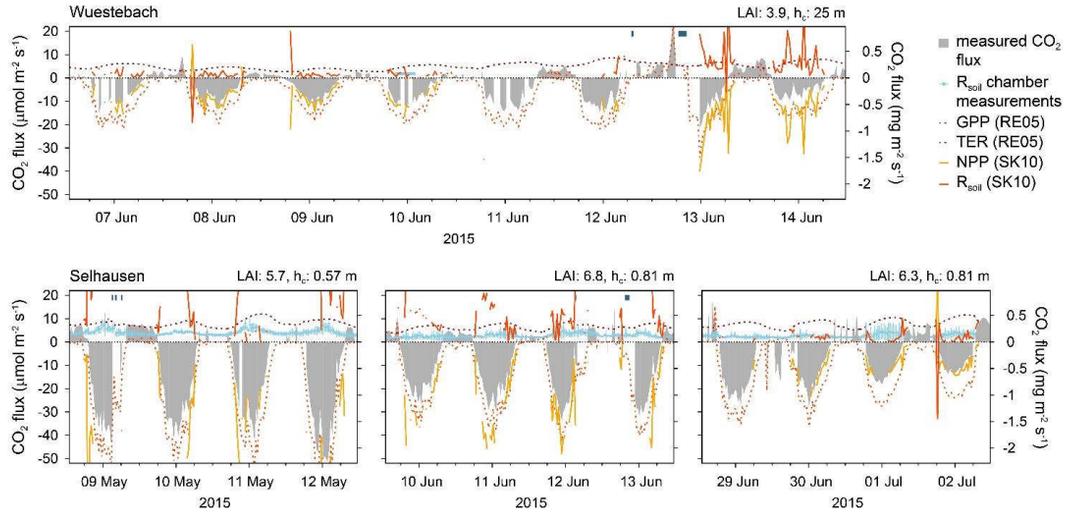

Fig. 3.3: Comparison of source partitioning results of the approaches after Reichstein et al. (2005; RE05) and after Scanlon and Kustas (2010; SK10) for CO_2 fluxes at the two study sites Wüstebach (forest; *top*) and Selhausen (cropland; *bottom*) for varying time periods (GPP: gross primary production; NPP: net primary production; TER: total ecosystem respiration; R_{soil}: soil respiration; LAI: leaf area index; h_c: canopy height; *blue bars*: precipitation events). *Light blue bar* in Wüstebach on June 10th, 2015 shows time-space-average of R_{soil} chamber measurements.

0.9 for winter wheat depending on the crop cover, in which our findings belonged to the lower ranges.

Results of the CO_2 partitioning showed more scatter at both study sites (Fig. 3.3). While the partitioning model after Reichstein et al. (2005) has different target flux components than SK10 (see 3.1. Introduction), its respiration (TER) can be used as an upper limit for the validation of the SK10-based R_{soil}. Here, R_{soil} often exceeded TER (correspondingly NPP exceeded GPP) and chamber measurements, and peaked in implausible magnitudes, especially in the cropland for the two chosen time periods earlier in the year. In the latter time period, when the winter wheat matured, NEE measurements decreased and SK10 results appeared more reasonable. Compared to R_{soil} chamber measurements, the estimated soil source by SK10 matched measurements very well on June 30th, but was often underestimated in early July. Weather conditions were similar in the three considered time periods, thus, the ecosystem WUE differing between the time periods seemed to have an effect on the partitioning performance. T and NPP results particularly differed between the last two time periods, which were similar in plant height and LAI, but differed in maturity of the crop. A direct relationship of T and NPP to plant height or LAI could not be observed, also because these canopy properties only varied slightly between the considered time periods (Fig. 3.2, 3.3). At the forest site, the obtained CO_2 flux components had a reasonable magnitude, except after the precipitation events. The significant increase of the flux components could be caused by the presence of interception, so the SK10 procedure could not differentiate between T and evaporation of interception water, thus, overestimating T and NPP with an unchanged WUE.

The median of the partitioning fraction R_{soil}/NEE was -0.29 for the forest and between -0.74 and -0.14 for the cropland.

Reasons for the relatively poor performance of SK10 at our study sites could include a wrong functioning of the partitioning method, such as finding a wrong solution for $\rho_{cp'c_{r'}}$, excluding not enough/too many levels of large-scale fluctuations, or a falsified WUE estimation. Also, inapplicable micrometeorological and environmental conditions, such as a non-identical sink-source-distribution of H_2O and CO_2 fluxes, horizontal canopy heterogeneity, insufficient vertical spacing between stomatal and non-stomatal processes, and deviations of these processes from flux-variance similarity theory, could cause the improbable results. Also, not all processes could be incorporated in the method, e.g., such as respiratory fluxes of a forest understory or woody tissue and refixation of respiratory CO_2 in the canopy.

The correct exclusion of large-scale fluctuations was checked with a modified SK10 method by searching for the best solution in all eddy scales and not stopping at the first valid solution. This did not improve partitioning results significantly (not shown). Thus, we assumed that the application of the wavelet transform and the exclusion of low frequency processes were efficient. By removing large-scale fluctuations it was assumed that the removed part had a composition of H_2O and CO_2 that was proportional to the remaining data (Scanlon and Sahu 2008). At our cropland site, the fraction of the H_2O and CO_2 fluxes transported by large-scale eddies was very small and very similar between water vapor and CO_2. The number of removed wavelet levels for each time step decreased on average with maturity of the crop. At our forest site, the proportions of the fluxes were larger for low frequency processes and some differences between H_2O and CO_2 fractions were observed, but the partitioning performance did not seem to be dependent. But the spikes in the CO_2 components observed before the precipitation events at the forest site were provoked by the removal of more than ten wavelet

Tab. 3.1: Root mean square error (RMSE), bias in µmol m^{-2} s^{-1}, and number of found solutions (N) of the source partitioning results for soil respiration after the approach of Scanlon and Kustas (2010) with various water use efficiencies (WUE; including input parameters for WUE estimation: T_f: foliage temperature; c_i: internal CO_2 concentration; meanT: measured mean air temperature; MOST: Monin-Obukhov similarity theory; OLR: outgoing longwave radiation; see text for description) compared to chamber measurements at the two study sites Selhausen (cropland) and Wüstebach (forest). Outliers were excluded which deviated from the mean by more than ten times the standard deviation.

	T_f	c_i (ppm)	Selhausen, cropland			Wüstebach, forest		
			RMSE	bias	N*	RMSE	bias	N*
$WUE_{mean\ T}$	meanT	270	16.77	6.810	184	1.39	-0.255	7
$WUE_{mean\ T\ -2\ K}$	meanT – 2 K	270	27.69	5.459	215	1.55	0.510	8
$WUE_{mean\ T\ +2\ K}$	meanT + 2 K	270	19.70	0.052	215	9.81	-7.806	8
WUE_{MOST}	via MOST	270	14.37	5.909	174	1.07	-0.876	5
WUE_{OLR}	via OLR	270	18.56	5.068	142	0.87	-0.866	3
WUE_{MAX}	meanT – 2 K	200	36.62	14.895	163	NaN	NaN	0
WUE_{MIN}	meanT + 5 K	300	26.76	3.460	114	NaN	NaN	0

* number of time steps with available chamber measurements: 280 in Selhausen, 8 in Wüstebach.

levels in these time steps, so flux fractions were not represented realistically anymore and the partitioning method could not work properly.

As observed by Scanlon and Albertson (2001), at our forest site the largest proportions of the

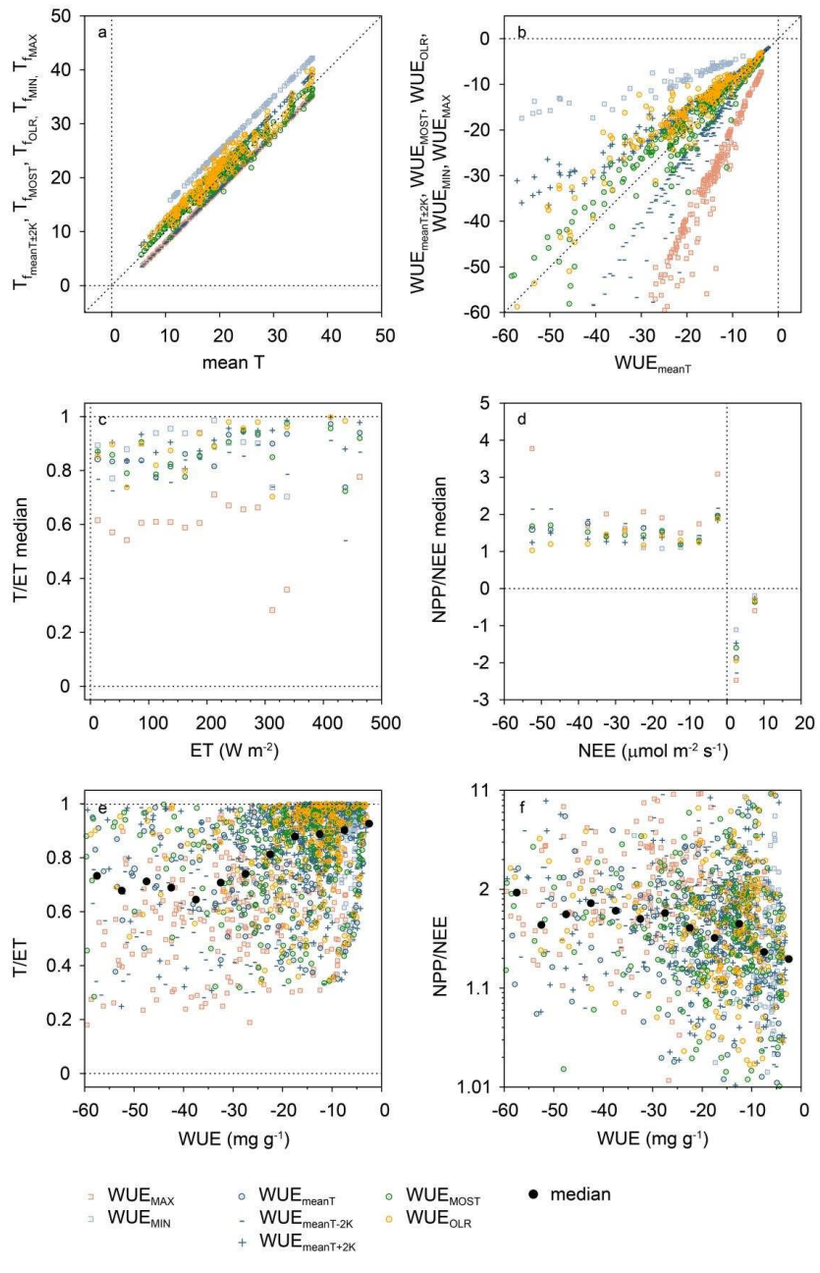

Fig. 3.4: Comparison of source partitioning results of the approach after Scanlon and Kustas (2010) depending on different water use efficiency (WUE) inputs for both study sites (see text for description; T_f: foliage temperature; ET: evapotranspiration; T: transpiration; NEE: net ecosystem exchange; NPP: net primary production).

vertical H_2O and CO_2 fluxes were also mostly transported by eddies in the order of four times the canopy height. At the cropland site, the eddies transporting the largest flux fractions were up to ten or even more times larger than the canopy. This and the very small distance between canopy and soil surface sink/sources (relative to the measurement height) could cause the unsatisfactory performance of SK10 for the cropland. Besides, EC measurements were obtained at between 3 and 4.3 h_c at the crop site on the considered days and at 1.52 h_c at the forest site. Assuming the roughness sublayer ranges up to 1.5 to 3 h_c (Williams et al. 2007), measurements at the latter site were more likely obtained within or close to the roughness sublayer, resulting in a lower scalar-scalar-correlation $\rho_{q'c'}$ and more information for SK10. At both study sites degraded $\rho_{q'c'}$ were observed for the excluded large-scale eddies, e.g., due to entrainment, and for eddy scales smaller than the canopy height, so $\rho_{q'c'}$ was possibly influenced by the sink-source-distribution (Huang et al. 2013; Scanlon and Sahu 2008; Williams et al. 2007). The signals were well correlated at the intermediate scales.

A crucial issue of SK10 is currently ascribed to the input of the WUE estimation (Anderson et al. 2018; Palatella et al. 2014; Sulman et al. 2016). To investigate the sensitivity of the partitioning approach to WUE input, differing T_f were used for the calculation. Figures 3.4a and 3.4b show how these modified temperatures and the corresponding WUEs deviated from mean air temperature and WUE_{meanT}. T_f calculated by considering a logarithmic mean profile implementing MOST varied in the range of mean air temperature ± 2 K (this certain range of temperature was suggested by Scanlon and Sahu 2008). T_f calculated by means of measured outgoing longwave radiation was mostly higher than mean air temperatures during the day (up to 3 K at forest and 6 K at crop site). The magnitudes of corresponding WUEs decreased/increased (were less/more negative) with higher/lower temperature as stated before. WUE_{MOST} and WUE_{OLR} were within the range of $WUE_{meanT-2K}$ and $WUE_{meanT+2K}$, WUE_{OLR} usually being less negative. Also shown are WUE_{MIN} and WUE_{MAX} not only differing in used temperature, but also in c_i, which represented the outer reasonable margins for WUE input. With $WUE_{MIN,}$ SK10 found valid solutions less often for both study sites – on many days only in the morning or evening hours (see Fig. B.1, B.2 in Appendix B). Also, the morning and evening hours usually produced WUEs of large magnitudes. Figures 3.4c and 3.4d show the median of the partitioning fractions for H_2O and CO_2 fluxes in relation to the measured net fluxes (T/ET, NPP/NEE) grouped into classes of 25 W m^{-2} or 5 µmol m^{-2} s^{-1}, respectively, of the total fluxes. With larger measured ET the medians of T/ET increased slightly and converged towards 1. Such a clear trend was not observed for the medians of NPP/NEE in dependence on the magnitude of NEE. Furthermore, partitioning fractions for H_2O and CO_2 were closer to unity with a less negative WUE. With a more negative WUE, as e.g. WUE_{MAX}, the medians of the partitioning fractions decreased for H_2O, so estimated T and E converged, and increased for CO_2, such that both R_{soil} and the magnitude of NPP increased. Sulman et al. (2016) have made the same observations. Figures 3.4e and 3.4f show all half-hourly partitioning fractions for both scalars as a function of the WUE obtained with the different T_f

estimations. While single values scatter widely due to varying factors affecting partitioning in each half-hour, the median over WUE classes of 5 mg g^{-1} revealed a general trend in the partitioning result. With increasing magnitude of WUE the fraction of T in ET decreased, and both CO_2 flux components became larger. For our sites and chosen time periods, the medians of the partitioning fractions ranged between 0.6 and 1 for T/ET, and between 1.1 and 2 for NPP/NEE. Thus, T usually represented the larger fraction of the total water vapor flux. Further, the large range of NPP/NEE indicates a larger impact of uncertain WUE in the CO_2 partitioning than for H_2O, as also reported by Scanlon and Sahu (2008). Furthermore, the differing WUE inputs caused a bigger difference for the cropland than for the forest (Fig. B.1, B.2 in Appendix B). In general, usage of WUE_{MOST} or WUE_{OLR} improved the estimation of R_{soil} compared to the chamber measurements regarding the *RMSE* and *bias* (Tab. 3.1). However, these error quantities were highly sensitive towards outliers.

3.3.2 Large Eddy Simulations

The vertical profiles of wind velocity, momentum flux, second-order moments, and skewness produced by the LES are shown in Figure 3.5, and they compared qualitatively well with profiles shown by Edburg et al. (2012) and Ouwersloot et al. (2016). Here, no oscillations between canopy and free air above could be observed in the velocity components due to the smooth transition of the PAD at canopy top, as prescribed by Ouwersloot et al. (2016). We also conducted short test runs on the one hand with higher resolution (grid size of 0.05 h_c x 0.05 h_c x 0.05 h_c) and on the other hand with a larger domain size (doubled in x-, y-,

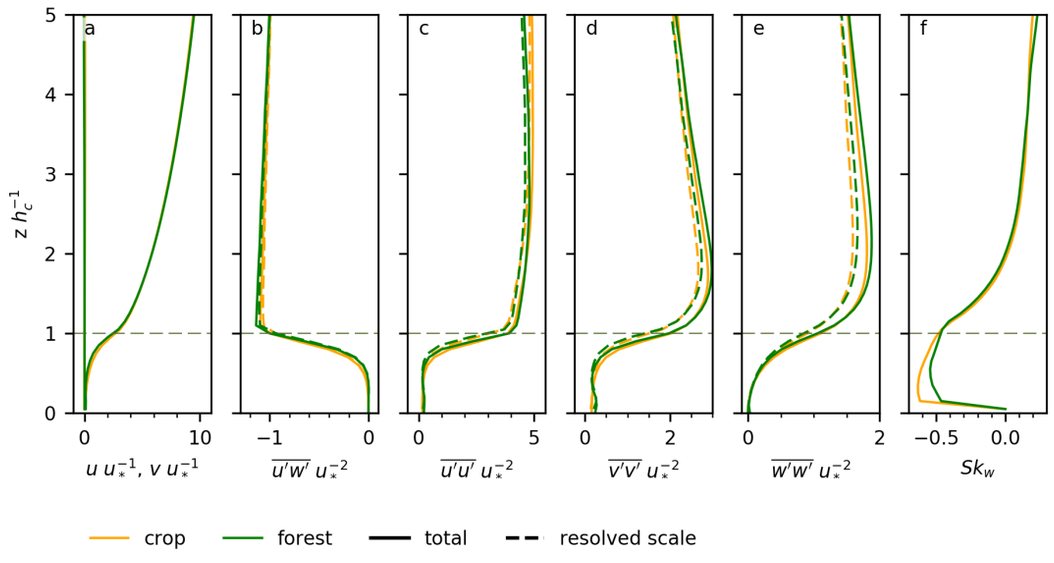

Fig. 3.5: Mean vertical profiles of streamwise and crosswise velocity (u, v), vertical momentum flux ($\overline{u'w'}$), variances of u, v, and vertical wind velocity (w), and skewness of vertical wind (Sk_w), scaled by friction velocity (u_*) at canopy top. Shown are profiles of the simulations with the crop and forest canopy.

and z-direction) to test if our main LES experiments described the turbulence and scalar transport sufficiently, especially near the surface. Even though the costly test runs had a short runtime during which they did not converge, a clear independence of the domain size could be observed. Small discrepancies between the original LES and the one with higher resolution could be found, in which flux profiles adjusted quicker in the latter. The proportion of the resolved scale of the second-order moments was well below 15% in the original LES except in the region below 1.5 h_c. Thus, we assumed that the conducted LES simulated canopy flows and scalar transport reasonably well. Because the simulated turbulences and the associated calculated fluxes did not show large differences between the two canopy types, only results of the crop canopy are shown in the following (corresponding results of the forest canopy in Fig. B.5-B.11 in Appendix B). Thus, differences in scalar-scalar-correlations and flux profiles between the various cases were caused solely by the differing sink-source-distributions (shape and relative strength of the soil source) and not by differences in the turbulence. Examples of the sampled synthetic high frequency data of *q'* and *c'* are shown in Appendix B for different 'measurement' heights and for the two sink-source-distributions ModelV and ModelB each with the strong soil source (Fig. B.3).

The vertical profiles of the total fluxes of H_2O and CO_2 were very similar and did not show large differences above the canopy between the different sink-source-distributions (ModelV or ModelB) and soil CO_2 source strengths (Fig. 3.6a, d). The profiles showed differences of typically less than 1% above 1.5 h_c. For CO_2 the varying soil surface sources could be distinguished in the flux profiles of the components originating from the canopy or soil surface (Fig. 3.6b, c). Vertical profiles of the correlation between *q'* and *c'* showed only larger discrepancies (larger than 1%) between the various experiments up to a measurement height of 3.2 h_c (Fig. 3.7a). The correlation between fluctuations of H_2O components ($\rho_{q_t'q_e'}$) or of CO_2 components ($\rho_{c_p'c_r'}$) and the transport efficiencies $\rho_{w'q_t'}$ and $\rho_{w'c_p'}$ were dependent on the sink-source-distribution (Fig. 3.7b, d, e), in which discrepancies vanished above a height of 8 h_c (not shown). The transport efficiencies of the soil sources $\rho_{w'q_e'}$ and $\rho_{w'c_r'}$ were naturally independent of the sink-source-distribution in the canopy and of the source strength. When comparing $\rho_{w'q_t'}$, $\rho_{w'q_e'}$, $\rho_{w'c_p'}$, and $\rho_{w'c_r'}$ with each other for each sink-source-distribution, differences (larger than 1%) between these transport efficiencies disappeared above 7 h_c.

SK10 was applied to the sampled data at every virtual measurement height. SK10 generally underestimated the magnitudes of CO_2 fluxes originating from the soil surface and the canopy (Fig. 3.6b, c). Accordingly, the canopy H_2O flux source was underestimated, and the soil source overestimated. Above a height of 1.5 h_c for the low CO_2 soil source and above 2.5 h_c for the strong source, almost no differences between ModelV and ModelB were visible, such that in Figures 3.6b, 3.6c, 3.6e, and 3.6f data points of ModelB are hidden under data points of ModelV. Above a height of 5 h_c larger discrepancies between the various experiments emerged again (not shown), probably related to the fact that $\rho_{q'c'}$ converged to -1 with increasing height. Below these heights, partitioning results of ModelV converged towards the

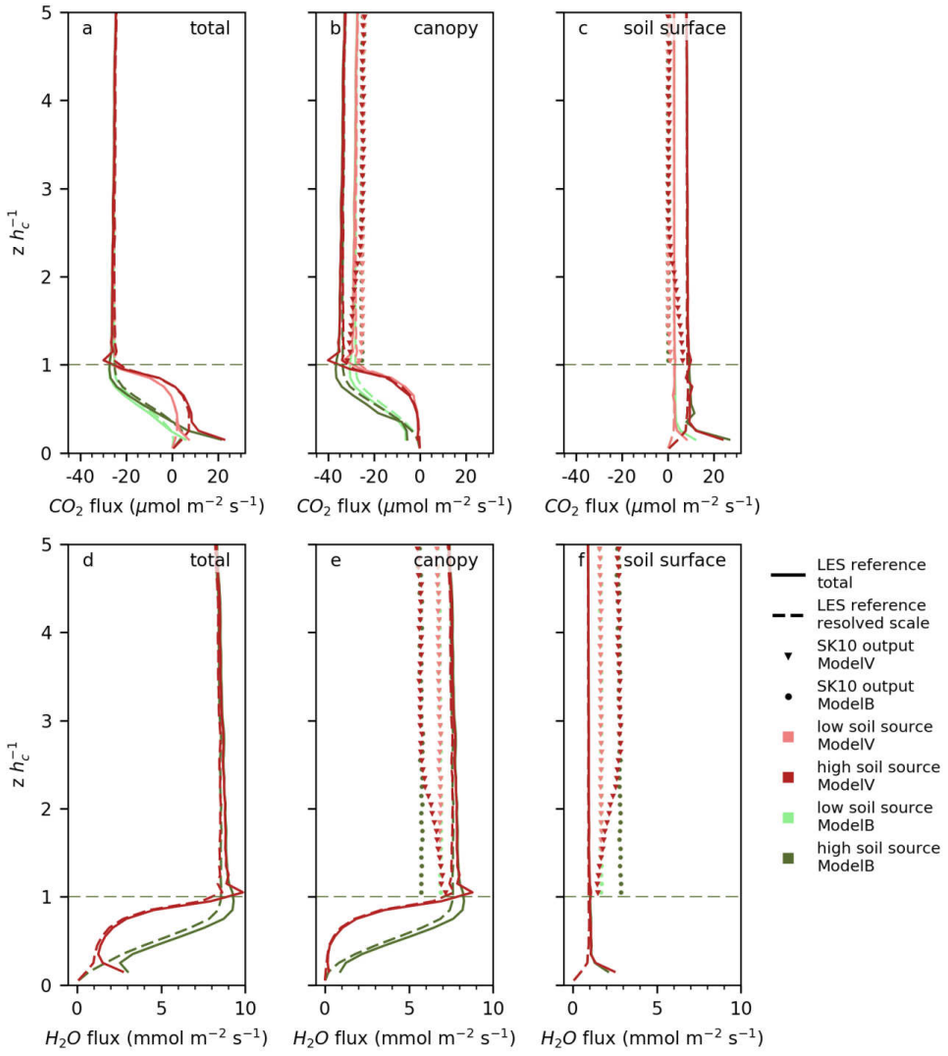

Fig. 3.6: Vertical profiles of H_2O and CO_2 flux, and their components resulting from LES scaled with the four variations of sink-source-distributions (ModelV or ModelB; low or high soil source) for the crop canopy. Also shown are the partitioning results of the approach after Scanlon and Kustas (2010; SK10) for each grid height.

known input fluxes of the scaled LES. These better results seemed to be connected with the stronger decorrelation between q' and c' observed in the corresponding heights ($|\rho_{q'c'}| < 0.975$; Fig. 3.7a). Furthermore, the height-dependence of the SK10-estimated flux components was very similar for all four sink-source-distributions (with exception of the lower few h_c of ModelV). Differences between soil source strengths were not detected. However, SK10 produced a difference in the H_2O flux profiles depending on soil source strength, contradicting the differences in the scaling input. This can also be seen in the scatter plots of Figure 3.8 showing partitioning results for the height of 2.5 h_c. Also, the SK10-based $\rho_{cp'cr'}$, and $\sigma_{cp'}^2$

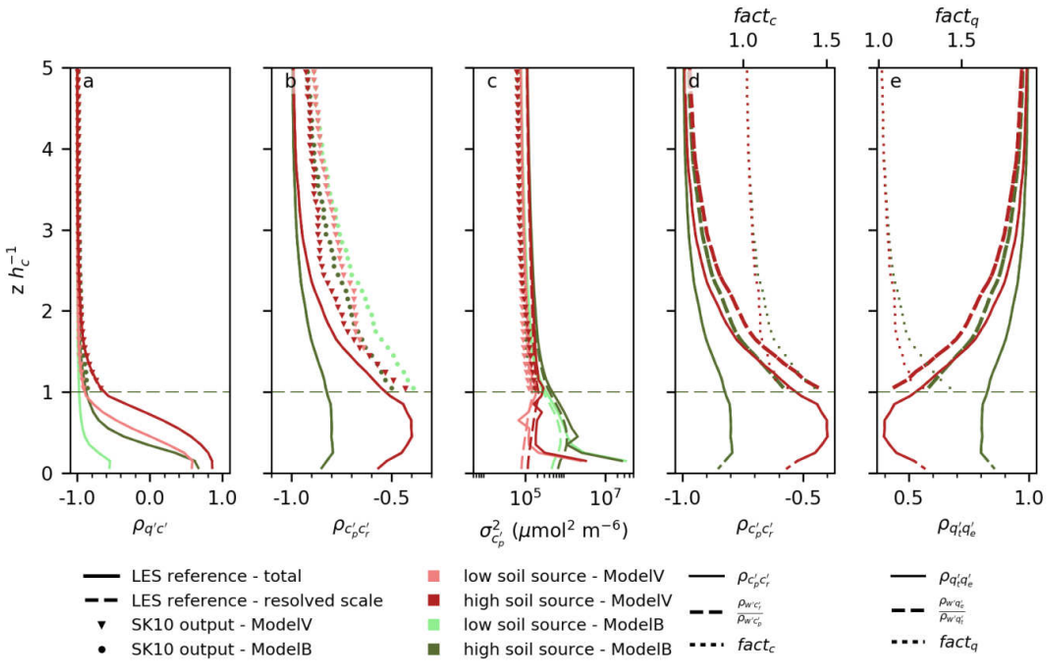

Fig. 3.7: a)-c) Vertical profiles of $\rho_{q'c'}$, $\rho_{cp'cr'}$, and $\sigma_{cp'}^2$ resulting from LES scaled with the four variations of sink-source-distributions (ModelV or ModelB; low or high soil source) for the crop canopy (*lines*), compared to results of the approach after Scanlon and Kustas (2010; SK10) (*dots*). d)-e) Comparison of the two sides of Equations 3.2 and 3.3 checking the transfer assumption and corresponding correction factors ($fact_q$, $fact_c$, defined in Equation 3.5 and 3.6).

deviated from the known input (Fig. 3.7b, c, 3.8d, e). The permitted error between the known $\rho_{q'c'}$ of the synthetic high frequency data and the by SK10 calculated $\rho_{q'c'}$ was set to a maximum of 0.1 (Fig. 3.7a, 3.8c).

Up to this point we can conclude that SK10 was not able to infer the correct partitioning, even if the correct leaf-level WUE was used. The magnitude of the difference between ecosystem- and canopy-level WUE did not seem to affect the partitioning performance, otherwise both experiments of ModelV and ModelB with the stronger soil source would have yielded better results than the sink-source-distributions with the lower soil source. A certain degree of decorrelation between *q'* and *c'* is needed for the method to work: $\rho_{q'c'}$ converged slower to -1 with increasing height for ModelV than for ModelB caused by a larger separation of soil source and canopy sink/source. The impact of the WUE input could also have been compensated by the impact of the decorrelation. In the next paragraph we inquire an additional influencing factor for the partitioning performance of SK10.

For the LES analysis, the falsified partitioning by SK10 could not be caused by an uncertain WUE input, as was assumed for our field data, because the correct WUE from the scaled LES experiments was used. As seen in Figures 3.7d and 3.7e, the approximations made in Equations 3.2 and 3.3 (transfer assumption) were invalid for our synthetic experiments,

possibly causing the erroneous partitioning results. In the next step, we conducted the source partitioning with SK10 again, including correction factors $fact_q$ and $fact_c$ in Equations 3.2 and 3.3, which were known from the scaled LES experiments (Fig. 3.7d, e).

$$\rho_{q_t' q_e'} = \frac{\rho_{w' q_e'}}{\rho_{w' q_t'}} \cdot fact_q \tag{3.5}$$

$$\rho_{c_p' c_r'} = \frac{\rho_{w' c_r'}}{\rho_{w' c_p'}} \cdot fact_c \tag{3.6}$$

Thus, we made sure that the approximations were valid. These correction factors had to be included in the complete system of equations of the SK10 method, because all equations are derived based on these approximations. For ModelB the correction factors had to be larger than for ModelV, which could explain the better results for the latter (Fig. 3.7d, e). Figures 3.8 and 3.9 show updated source partitioning results by SK10 including these correction factors. In this case, SK10 almost perfectly matched the known input of the scaled LES experiments. Small discrepancies were observed above a height of 2 h_c especially for ModelB. For the forest-like canopy, the correction of the transfer assumption brought perfect partitioning results up to a height of 4 h_c (Fig. B.9 in Appendix B) This was due to the fact that the necessary decorrelation between *q'* and *c'* reached higher in the simulation with the forest canopy than with the crop canopy.

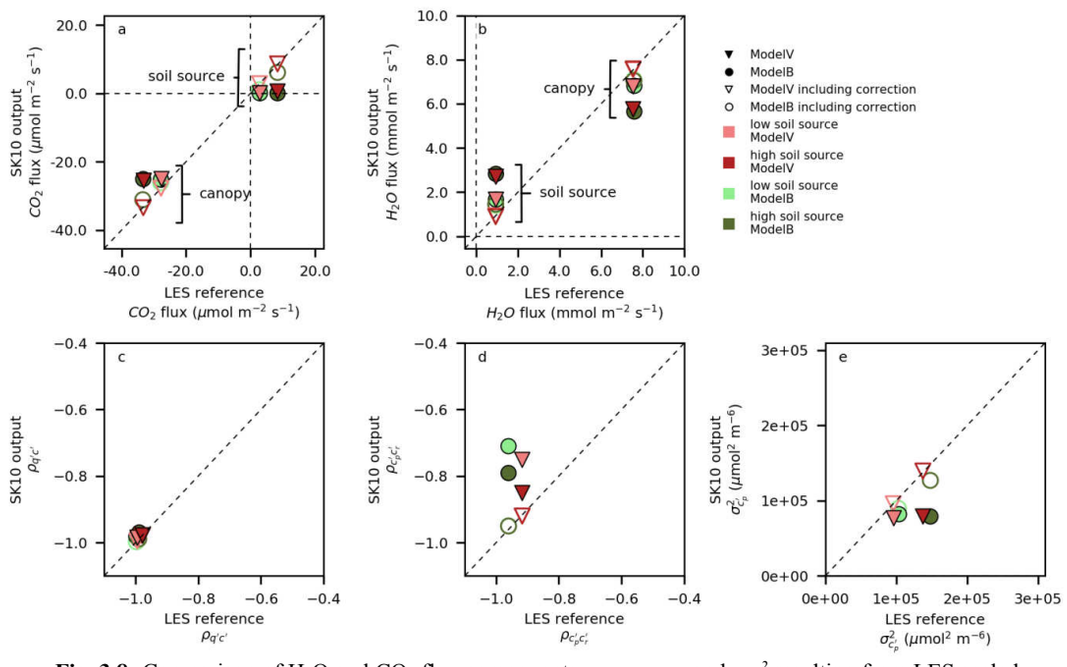

Fig. 3.8: Comparison of H_2O and CO_2 flux components, $\rho_{q'c'}$, $\rho_{c_p'c_r'}$, and $\sigma_{c_p}^2$ resulting from LES scaled with the four variations of sink-source-distributions (ModelV or ModelB; low or high soil source) and the partitioning results of the approach after Scanlon and Kustas (2010; SK10) at a 'measurement' height of 2.5 canopy heights for the crop canopy. Shown are results of the partitioning procedure without and with correction of the transfer assumption.

To transfer these results from the LES experiments to study sites, the SK10 method would benefit from an EC measurement height in the lower roughness sublayer to ensure a certain degree of decorrelation of the scalars (which is not a measurement height usually chosen for high-quality net flux measurements). At the same time, however, a larger measurement height would ensure more likely the validity of the transfer assumption. A comparison of Figures 3.6, 3.7d, and 3.7e indicates that the latter factor compensates the former to some degree, such that without known correction factors for the transfer assumption, no measurement height is ideal. However, the better performance of ModelV close to the canopy in Figure 3.6 indicates that the net effect of both factors leads to better results with measurements low above the canopy.

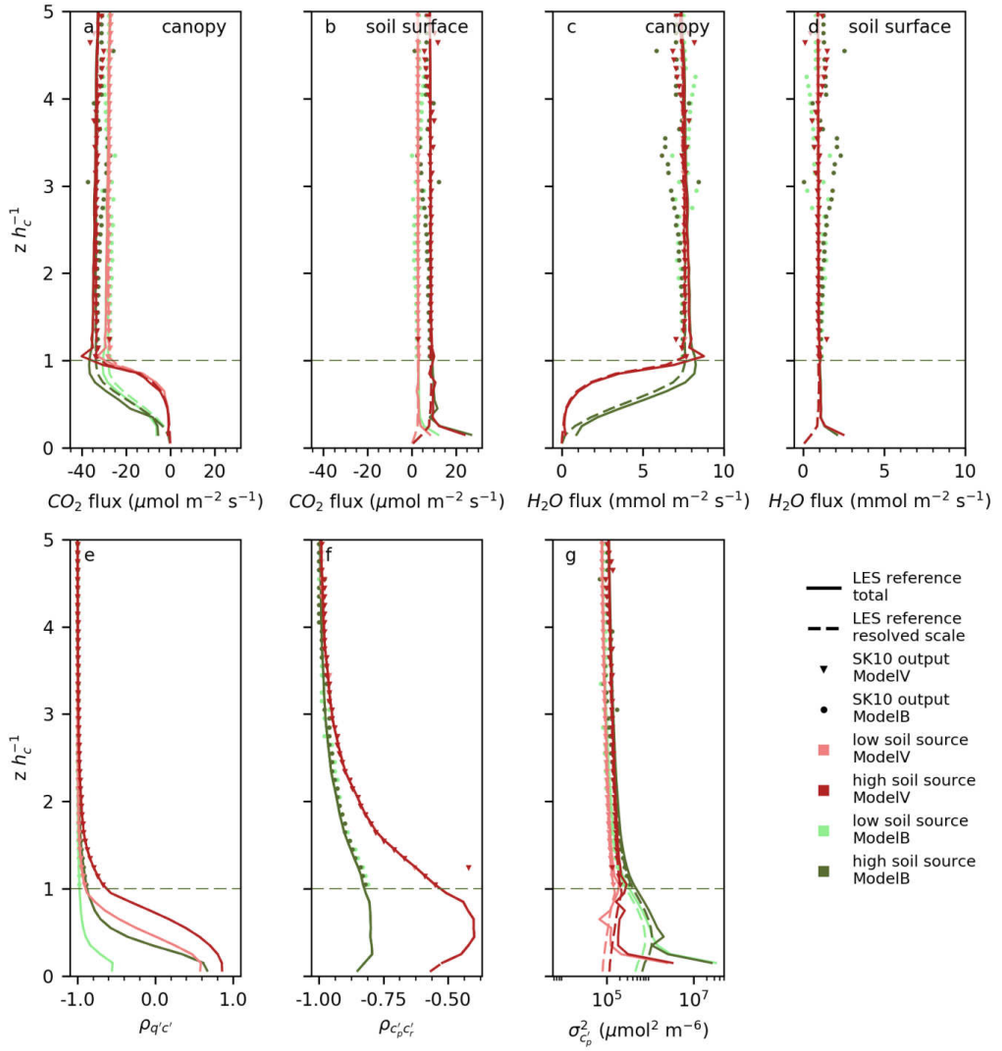

Fig. 3.9: Vertical profiles of H_2O and CO_2 flux components, $\rho_{q'c'}$, $\rho_{c_p'c_r'}$, and $\sigma_{c_p'}^2$ resulting from LES scaled with the four variations of sink-source-distributions (ModelV or ModelB; low or high soil source) for the crop canopy. Also, the partitioning results of the approach after Scanlon and Kustas (2010; SK10) including the correction of the transfer assumption are shown for each grid height.

To further investigate the influence of the turbulence and the canopy on the partitioning performance, additional LES runs with e.g., larger LAI would be necessary. With changed turbulence the transport efficiencies and scalar-scalar-correlations would differ. Huang et al. (2013) stated that the correlation between *q'* and *c'* increased with increasing canopy density in their LES studies. LAI might therefore have a similarly ambiguous effect on SK10's performance as measurement height. This conundrum could only be solved if a way was found to estimate correction factors for $\rho_{cp'c_{r'}}$ and $\rho_{qt'q_{e'}}$ in field studies.

At our cropland and forest study sites, WUE inputs varied between one third of and three times of WUE_{meanT} depending on the calculation of T_f and the magnitude of c_i (Fig. 3.4). In order to put the sensitivity to WUE input in context to the possible error in the transfer assumption discussed above, we repeated the SK10-based analysis of the LES data with corrected transfer assumption and with the variability of WUE input as seen in the field data analysis. However, no valid solutions could be found by the algorithm below a height of 4 h_c. Instead, WUE input could only be changed by up to minus 90% or plus 24% while still obtaining an effectual amount of partitioning solutions. In Figure 3.10 partitioning fractions of the H_2O and CO_2 fluxes are shown as a function of WUE input for each sink-source-distribution at a virtual measurement height of 2.5 h_c. Other than at our study sites (Fig. 3.4e, f), in this case the true WUE and partitioning fractions were known. The transfer assumption was applied in its original form (Eqs. 3.2, 3.3; *filled markers* in Fig. 3.10) and with correction factors (Eqs. 3.5, 3.6; *non-filled markers*), such that the combined effect of both sources of error (wrong WUE input and invalid transfer assumption) on the partitioning result could be seen (also see Fig. B.4, B.11 in Appendix B). Both sink-source-distributions, ModelV and ModelB, show the same trends in the relation of T/ET and NPP/NEE with WUE. With the correct WUE and including the correction factors, small discrepancies between true and estimated partitioning factors were observed for ModelB, as described above (Fig. 3.8, 3.9). For H_2O, the range of T/ET for varying WUEs was smaller with a corrected transfer assumption than without. Thus, the potential error made with wrong WUE inputs was smaller. An overestimation of the magnitude of WUE (more negative) led to an overestimation of T with corrected, and an underestimation with uncorrected transfer assumption. Figure 3.10 also indicates that without correction of the transfer assumption, typically a slightly underestimated magnitude of WUE will lead to a partitioning fraction close to the truth. For CO_2, the variability in NPP/NEE was larger for the applications with corrected transfer assumption than without (note the logarithmic y-axes), which is contrary to the behavior of T/ET. NPP/NEE was very small with the incorrect transfer assumption. At our study sites we often observed an overestimation of the CO_2 components (Fig. 3.3). In contrast, in the LES-based analysis NPP/NEE was underestimated without correction factors, even with the correct WUE. With a correct WUE input the errors made by an invalid transfer assumption were mostly smaller for the low soil source than for the high soil source.

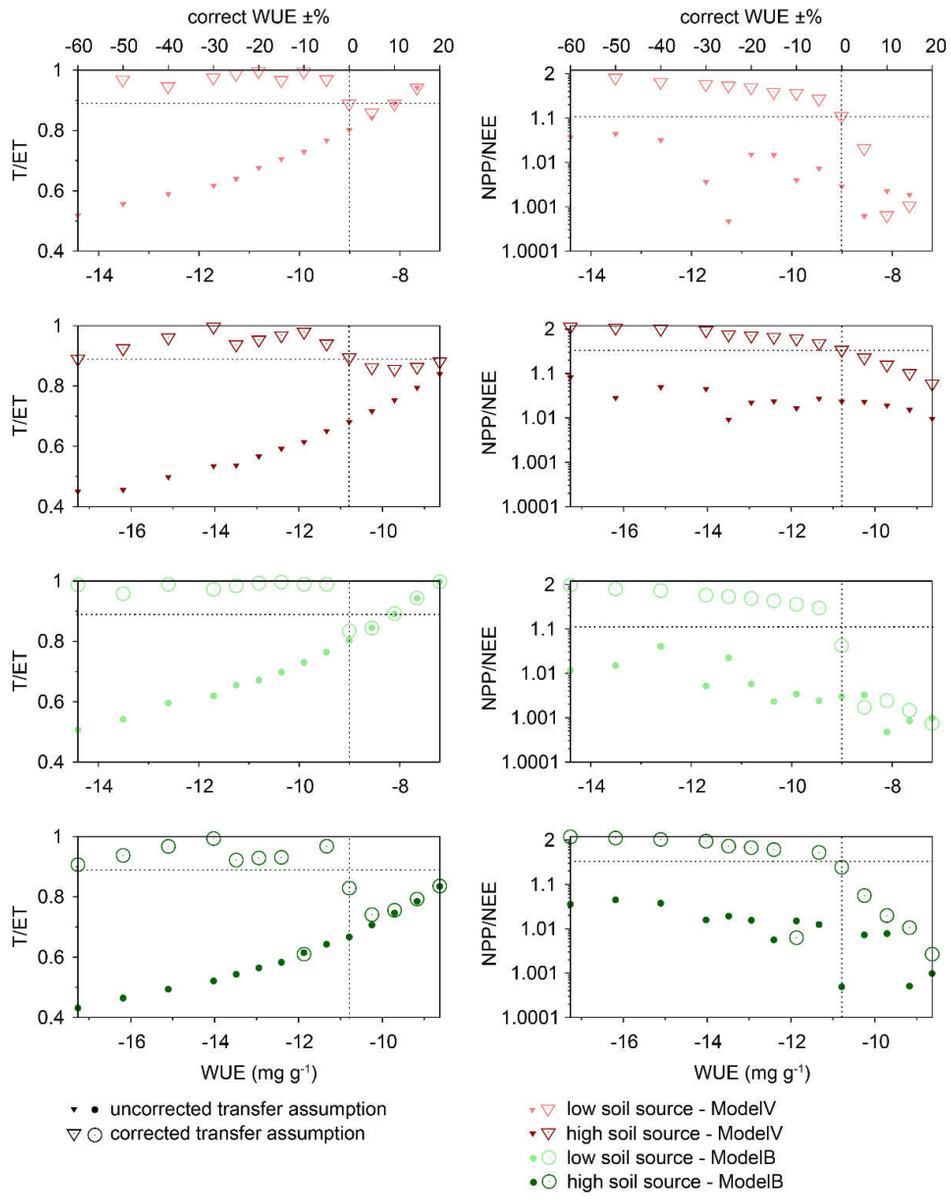

Fig. 3.10: Results of partitioning fractions for H_2O (T/ET, *left*) and CO_2 (NPP/NEE, *right*) fluxes in relation to the input water use efficiency (WUE). The source partitioning approach after Scanlon and Kustas (2010) was applied to synthetic high frequency data from LES scaled with the four variations of sink-source-distributions (ModelV or ModelB; low or high soil source) at a 'measurement' height of 2.5 canopy heights for the crop canopy with corrected and uncorrected transfer assumption. The true known partitioning factors and WUE input are indicated by the *dashed lines*.

Considering the medians in Figure 3.4e and 3.4f, E, R_{soil}, and |NPP| increased and T decreased by increasing the magnitude of WUE (more negative) at our study sites, thus, describing a

similar behavior as the partitioning factors derived by SK10 with an incorrect transfer assumption in the LES-based analysis. But the range of the varying WUE was larger at our study sites than the possible range in the LES-based analysis, and at the study sites differing WUEs of multiple half-hours on various days with varying weather conditions and different canopies were compared.

Sulman et al. (2016) reported a higher sensitivity of E and R_{soil} to the WUE input than of T and NPP. By varying WUE, the absolute change of stomatal and non-stomatal processes of H_2O or CO_2 were identical, because they were summing up to the unchanged, measured net fluxes. But the relative change differed because of the much smaller magnitude of non-stomatal processes than of stomatal processes (Sulman et al. 2016). We also observed that the differing input of WUE had a larger relative effect on soil source fluxes than on fluxes originating from the canopy (relative residuals in Fig. B.4, B.11 in Appendix B). The errors in the final flux partitioning obtained when not using the true known WUE input, were on the same order of magnitude as those obtained when ignoring the correction of the transfer assumption (Fig. 3.10).

3.4. SUMMARY AND CONCLUSIONS

In this study, we applied the source partitioning method SK10 to data of our study sites and analyzed how the partitioning results depend on the WUE input. Compared to R_{soil} chamber measurements and to E_{soil} calculated based on Beer's law depending on LAI, the partitioning results for the forest site in Wüstebach were more satisfying than for the cropland in Selhausen for the respective study periods. The partitioning method's performance was sensitive to precipitation events and to the maturity of the crop, connected to the photosynthetic activity and the relation between stomatal and non-stomatal processes in the crop canopy. With a less active canopy, relative stronger soil sources, or with a higher distance between canopy and soil sink/sources, SK10 performed better at our study sites. The estimation of WUE input based on T_f derived with measurements of outgoing longwave radiation (WUE_{OLR}) or by considering a logarithmic mean profile implementing MOST (WUE_{MOST}) improved the partitioning performance compared to R_{soil} measurements. Inclusion of direct measurements of WUE on leaf-level would improve the method's performance (Anderson et al. 2018; Sulman et al. 2016), but such measurements are not available at most study sites.

In a next step, we applied SK10 to synthetic high frequency data generated by LES and analyzed the partitioning performance depending on canopy type, measurement height, and given sink-source-distributions. Primarily, approximations involved in SK10 (Eqs. 3.2, 3.3; transfer assumption) were checked in the LES. Furthermore, for the synthetic data the dependence of the partitioning result to WUE input was analyzed as well. Because simulated turbulence did not differ much between PAD types, also SK10's performance did not differ significantly. The performance was sensitive to the virtual 'measurement' height and to the

corresponding decorrelation between *q'* and *c'*. The decorrelation above the canopy was stronger and reached higher for the forest canopy, for the v-shaped sink-source-distribution (and thus for a higher separation between soil sources and canopy sink/source), and/or for the distributions with high soil sources, resulting in slightly lower residuals between known input and SK10 output. To further investigate the influence of the canopy architecture and resulting turbulence on the partitioning performance, additional LES runs with e.g., larger LAI would be necessary. Similar behavior of SK10's performance depending on differing input of WUE could be reproduced with the synthetic experiments as observed at the study sites. Primarily, our LES study indicated that next to a precise WUE estimation, the validity of the transfer assumption was a crucial point for a correct application of SK10. Therefore, a thorough assessment of the conditions at study sites affecting the validity of the transfer assumption would be necessary. These conditions could include measurement height above the canopy, separation between soil sources and canopy sink/source, and the corresponding transport efficiencies.

3.5. ACKNOWLEDGEMENTS

This research was supported by the German Federal Ministry of Education and Research BMBF, project IDAS-GHG [grant number 01LN1313A]. The measurement infrastructure providing observational data was supported by the German Research Foundation DFG through the Transregional Collaborative Research Centre 32 (TR 32) and Terrestrial Environmental Observatories (TERENO). The computational facilities have been provided by the Netherlands Science Foundation under contract NWO 15774 (SH-312-15). The authors thank all technicians, engineers, and laboratory assistances in TR32 and TERENO for providing measurements of the test sites.

4

SOURCE PARTITIONING OF H_2O AND CO_2 FLUXES BASED ON HIGH FREQUENCY EDDY COVARIANCE DATA: A STUDY SITES COMPARISON

This chapter is based on a journal article published as:
Klosterhalfen, A., Graf, A., Brüggemann, N., Drüe, C., Esser, O., González-Dugo, M.P., Heinemann, G., Jacobs, C.M.J., Mauder, M., Moene, A.F., Ney, P., Pütz, T., Rebmann, C., Ramos Rodrìguez, M., Scanlon, T.M., Schmidt, M., Steinbrecher, R., Thomas, C.K., Valler, V., Zeeman, M.J., Vereecken, H., 2019. Source partitioning of H_2O and CO_2 fluxes based on high-frequency eddy covariance data: a comparison between study sites. Biogeosciences 16, 1111-1132, https://doi.org/10.5194/bg-16-1111-2019.

4.1. INTRODUCTION

The eddy covariance (EC) method is a micrometeorological technique commonly used to measure the energy, water vapor, and carbon dioxide exchange between biosphere and atmosphere across a large spectrum in time and space (Baldocchi et al. 2001; Reichstein et al. 2012). The measurements help to understand the temporal and spatial variations of these fluxes at the land-atmosphere interface. For a better consideration, assessment, and prediction of climate change by scientists, policy-makers, and citizens, a further understanding of the soil and vegetation flux components of H_2O and CO_2 and their interaction with physical conditions and physiological functioning of plants and ecosystems is necessary (Baldocchi et al. 2001). To obtain magnitudes of transpiration (T), evaporation (E), photosynthesis, and respiration by soil and vegetation, certain measurements with additional instrumentation independent of the EC technique can be conducted. Alternatively or additionally, so-called source partitioning approaches can be applied to the net fluxes obtained with the EC method: the evapotranspiration (ET) and net ecosystem exchange (NEE). For instance, with the notion that during night no CO_2 is assimilated by plants, respiratory fluxes are often estimated based on semi-empirical models describing the relationship between a physical driver (e.g., temperature) and respiration (Lloyd and Taylor 1994; Reichstein et al. 2005, 2012). To estimate soil surface fluxes of both H_2O and CO_2 directly from high frequency EC data without assumptions on such drivers, two new partitioning approaches were developed by Scanlon and Sahu (2008), Scanlon and Kustas (2010), and Thomas et al. (2008). Both approaches imply that the high frequency scalar concentrations available in the framework of EC measurements contain information about the strength of sinks and sources in and below the canopy, which can be quantified by applying the flux-variance similarity theory or conditional sampling strategies. Thus, scalar dissimilarities have to be apparent above the canopy. The scalar-scalar-correlations of H_2O and CO_2, their concentration profiles, and fluxes are dependent on height (atmospheric surface layer, roughness sublayer), surface heterogeneity (Williams et al. 2007), canopy density, sink-source-distributions, and coherent structures (Edburg et al. 2012; Huang et al. 2013).

The source partitioning approach after Scanlon and Sahu (2008) and Scanlon and Kustas (2010) was applied to data of a corn field (eastern USA; Scanlon and Kustas 2012), compared to isotopic H_2O flux partitioning (Good et al. 2014) and to the Noah Land Surface Model (Wang et al. 2016) both for grasslands, and evaluated on a forest site in a decadal time scale (Sulman et al. 2016). Zeeman et al. (2013) further investigated the partitioning approach after Thomas et al. (2008) in association with coherent structures. To better assess these two approaches and their theoretical background, an intercomparison at a variety of study sites is necessary (Anderson et al. 2018).

The objective of this study was to compare and evaluate the source partitioning approaches after Scanlon and Kustas (2010) and after Thomas et al. (2008) by applying them to high

frequency flux measurements of various study sites in different ecosystems. Next to testing slight modifications of these partitioning methods, conditions and characteristics of study sites are identified under which the methods perform best. Based on findings of the above-mentioned authors and the large eddy simulation (LES) study in Chapter 3, we hypothesize that the methods' performance is dependent on the canopy height (h_c), which should represent the vertical separation of sinks and sources of H_2O and CO_2 between canopy top and soil surface, on the canopy density (LAI, LAI h_c^{-1}), and on the ratio between measurement height (z) and h_c. All these factors affect the degree of mixing of the scalars when they reach the EC sensors. With a high (low) and sparse (dense) canopy and a low (high) z h_c^{-1}, we assume a larger dissimilarity between scalar fluctuations and a more precise (less sufficient) partitioning result of both source partitioning approaches. To summarize, goals of this study are:

- The comparison and evaluation of the partitioning results obtained with the approaches after Scanlon and Kustas (2010) and after Thomas et al. (2008) for various ecosystems, and testing slight modifications of the approaches
- An analysis of the two approaches with respect to their dependence on their underlying assumptions
- The description of the interrelations between turbulence characteristics, site characteristics (such as canopy type, h_c, z h_c^{-1}, LAI, and LAI h_c^{-1}), and performance of the partitioning methods
- The identification of characteristics of a data set (i.e. of study site and period properties), which lead to a sufficient performance of the partitioning methods, if such characteristics exist.

4.2. MATERIAL AND METHODS

4.2.1. Source Partitioning after Scanlon and Kustas (2010) - SK10

To estimate the contributions of T, E, photosynthesis, and soil respiration ($R_{soil,}$ autotrophic and heterotrophic sources) to the measured total fluxes, Scanlon and Sahu (2008) and Scanlon and Kustas (2010) proposed a source partitioning method using high frequency time series from a typical EC station. This method (SK10 in the following) is based on the spatial separation and relative strength of sinks and sources of water vapor and CO_2 among the sub-canopy, canopy, and atmosphere. Assuming that air from those sinks and sources is not yet perfectly mixed before reaching EC sensors, partitioning is estimated based on the separate application of the flux-variance similarity theory to the stomatal and non-stomatal components of the regarded scalars, as well as on additional assumptions on stomatal water use efficiency (WUE). The correlation between the two scalars ($\rho_{q'c'}$) usually deviates from -1 during daytime. This reduction of correlation and its deviation from WUE at leaf-level is used to estimate the composition and magnitudes of the measured fluxes (Scanlon and Kustas 2010; Scanlon and Sahu 2008). For a detailed analytical description of SK10 see Palatella et al.

(2014), Scanlon and Albertson (2001), Scanlon and Kustas (2010, 2012), and Scanlon and Sahu (2008). SK10 was applied to high frequency EC data and the flux components were estimated as prescribed in Chapter 3.

As mentioned before, the WUE at leaf-level has to be estimated for the application of SK10. WUE at leaf-level describes the relation between the amount of CO_2 uptake through stomata (photosynthesis) and the corresponding amount of H_2O loss (T). One way to derive WUE (without additional measurements at leaf-level) is to relate the difference in mean CO_2 concentration between air outside the leaf and stomata to the difference in mean humidity concentration between air and stomata including a factor that accounts for the difference in diffusion between H_2O and CO_2 through the stomatal aperture (see Eq. 3.4; Campbell and Norman 1998). The mean H_2O and CO_2 concentrations just outside the leaf can be inferred from EC measurements by considering logarithmic mean concentration profiles implementing Monin-Obukhov similarity theory (MOST; Scanlon and Kustas 2010, 2012; Scanlon and Sahu 2008). For the internal CO_2 concentration a constant value of 270 or 130 ppm was presumed, typical for C3 or C4 plants, respectively (Campbell and Norman 1998; Špunda et al. 2005; Williams et al. 1996; Xue et al. 2004). Values for the internal water vapor concentration were estimated based on 100% relative humidity at foliage temperature (T_f). Measurements of T_f were not available at the study sites, so for the source partitioning T_f was set equal to measured air temperature (WUE_{meanT}; Scanlon and Sahu 2008). Additionally, to investigate the sensitivity of WUE, T_f was also derived by means of measured outgoing longwave radiation (WUE_{OLR}; with a surface emissivity of 0.98), or calculated similar to the external concentrations by considering a logarithmic mean profile implementing MOST (WUE_{MOST}). Thus, three different approaches of SK10 with differing inputs for WUE were applied to all study sites.

4.2.2. Source Partitioning after Thomas et al. (2008) - TH08

Thomas et al. (2008) presented a new method (TH08 in the following) to estimate daytime sub-canopy respiration of forests directly from EC raw data by conditional sampling. At the same time, evaporation can be quantified by exchanging *c'* with *q'* in the equations given by Thomas et al. (2008, equations 1-11, pages 1212-1215). The method assumes that occasionally air parcels moving upward (vertical wind fluctuations $w' > 0$) carry unaltered H_2O/CO_2 concentration combinations of the sub-canopy. Looking at the fluctuations *q'* and *c'*, both normalized over the corresponding standard deviation, respiration/evaporation signals should occur within the plane, where *q'* and *c'* are both positive, i.e. in the first quadrant in the *q'-c'* plane. Additionally, Thomas et al. (2008) introduced a hyperbolic threshold criterion within quadrant 1, thus sampling all data points above this hyperbola. Thomas et al. (2008) found realistic respiration estimates with a hyperbolic threshold of 0.25, which was also applied here. To estimate daytime evaporation and respiration from the sampled *w'*, *q'*, and *c'* time series

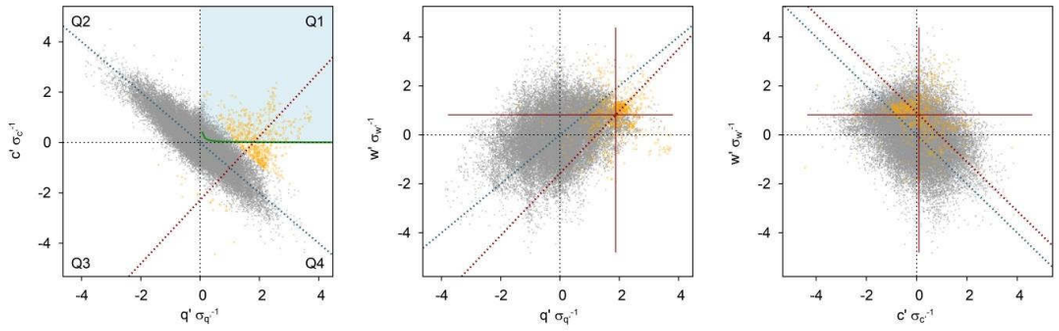

Fig. 4.1: Exemplary scatterplots of w', q', and c' from WU_FR, May 18th, 2015, 12:00-12:30 p.m. including results of the cluster analysis by Gaussian Mixture Model (*orange data points*) for the conditional sampling. Also shown are the hyperbolic threshold (H = 0.25, *green line*) after Thomas et al. (2008), the averages of w, q, and c only considering data points of the respiration/evaporation 'cloud' (*red lines*), and reduced major axis regression lines after Webster (1997) for all data points (*blue dashed lines*) and only 'cloud' data points (*red dashed lines*).
In this example, calculating the covariance for w and c considering the averages of the 'cloud' yielded a negative soil flux (negative correlation). Thus, only 'cloud' data points within quadrant 1 in the original q'-c' plane were considered for flux calculation using averages of all data points.

the conditional average of the covariance between *w'* and corresponding scalar can be calculated. Furthermore, the turbulent H_2O and CO_2 flux can be represented by the relaxed eddy accumulation (REA) technique (Businger and Oncley 1990). Therefore, Thomas et al. (2008) applied four different conditional sampling approaches, sampling the respiration/evaporation 'cloud' in quadrant 1 (Q1) or using the hyperbola threshold criterion (H), and then calculating the fluxes for each case by the covariances (CV) or the REA technique.

For some averaging periods in our data, a potential respiration/evaporation 'cloud' was evident but did not occur within quadrant 1 (Fig. 4.1). As a modification of the conditional sampling strategy and a more tolerant detection of respiration/evaporation events, a distribution-based cluster analysis was conducted (fifth approach, GMM). With the Gaussian Mixture Model using the Expectation-Maximization Algorithm, two clusters or components, respectively, were defined for each averaging period: the respiration/evaporation 'cloud' and all further points associated to T and photosynthesis independent of the sign of *w'*. The GMM method is based on taking random samples from each component and fitting a certain number of Gaussian distributions to the samples, optimizing their parameters iteratively to model the data (Canty 2010). Soil surface fluxes were calculated by CV, where the deviations from the averages of all sampled cluster data points were used for *w'*, *q'*, and *c'*. Because the sampled respiration/evaporation 'cloud' by GMM would not always lie within quadrant 1 (often in quadrant 1 and 4, or in 1 and 2), and *q'* and/or *c'* of the defined 'cloud' could correlate negatively with *w'*, the corresponding surface flux would often be of negative magnitude (Fig. 4.1). If this was the case for H_2O and/or CO_2 soil fluxes, the corresponding flux was recalculated considering the deviations from the averages of all data points for *w'*, *q'*, and *c'*, and only including data points within quadrant 1 of the original *q'-c'* plane and with $w' > 0$.

This recalculated flux represented only a minimal fraction of the corresponding flux component. Also, as a result of this procedure the number of data points could differ between H_2O and CO_2 for TH08 CV GMM depending on the used calculation step.

4.2.3. Study Sites and Data Processing

For the application and evaluation of the source partitioning methods, various study sites with differing canopy types, canopy densities (regarding the leaf area index LAI), and measurement heights were chosen (Tab. 4.1). Almost all study sites are part of the FLUXNET network (Baldocchi et al. 2001). Detailed site and measurement descriptions can be found in the listed references. Next to coniferous and deciduous forests, grasslands, and croplands, some sites represent special canopy types: in SC_FR (for site abbreviations see Tab. 4.1) EC measurements have been conducted above an Mediterranean oak savanna (dehesa; Andreu et al. 2018); in Wüstebach an area of about 9 ha was deforested in 2013 and so measurements were obtained above the still present spruce forest (WU_FR) and the deforested area (WU_GL), where grass, shrubs, and young deciduous trees are regrowing swiftly; and in LA_FR a coniferous forest is regrowing gradually after a non-cleared windthrow in 2007 (Matiu et al. 2017). These three study sites represent the most heterogeneous landcover types in this study.

For each study site, measurements from days with a high-productive state of the vegetation and fair-weather conditions were selected to exclude factors interfering with the performance of the partitioning. Time periods with precipitation events were excluded. Furthermore, the quality assessment scheme after Mauder et al. (2013) was applied to each data set and source partitioning was only conducted for time periods with the highest or intermediate quality flag levels assigned by this scheme. We only considered partitioning results of daytime data, because both methods require the presence of photosynthesis. Here, daytime was determined by calculating sunrise and sunset times by means of local time. Additionally, the TH08 method was only applied to time periods with a negative $\rho_{q'c'}$, and if less than 1% of the total data points in one half-hour time period were sampled as the respiration/evaporation ‘event’, the partitioning result was disregarded.

The high frequency H_2O and CO_2 time series of all study sites were pre-processed and prepared for the application of the source partitioning approaches as prescribed in Chapter 3. For each study site, physically impossible values and spikes were excluded in the high frequency EC data of vertical wind, total H_2O and CO_2 concentrations, the time delay was corrected, missing raw data in one half-hour period was gap-filled by linear interpolation, and a planar-fit rotation was conducted. Then, the source partitioning approaches were applied to half-hourly time series of these pre-processed high frequency data, partitioning factors (E/ET or R_{soil}/NEE, respectively) were calculated, and applied to the post-processed half-hourly EC data.

Tab. 4.1: Study sites and their characteristics (organized by first canopy type and second latitude; FR: forest; GL: grassland; CL: cropland).

abbrevi-ation	site	Latitude Longitude	elevation (m a.s.l.)	canopy type	period	LAI (m^2 m^{-2})	canopy height (m)	EC meas height (m)	meas resol-ution (Hz)	mean annual Temp (°C)	mean annual P sum (mm a^{-1})	references
LO_FR	**Loobos** Gelderland, NL	52.166581 5.743556	25	**FR** (pine)	08.-14. July 2003	1.9	18.6	24.0	10	10.0	966	Dolman et al. 2002 Elbers et al. 2011
HH_FR	**Hohes Holz** ST, DE	52.085306 11.222233	210	**FR** (deciduous broadleaf)	03.-09. July 2016	6.0	33.0	49.0	20	9.8	516	Wollschläger et al. 2017
WU_FR	**Wüstebach (forest)** NRW, DE	50.504907 6.331019	610	**FR** (spruce)	18.-24. May 2015	3.9	25.0	38.0	20	7.5	1220	Ney et al. (in press) Wiekenkamp et al. 2016
WA_FR	**Waldstein** BY, DE	50.14194 11.86694	775	**FR** (spruce)	04.-10. July 2016	5.5	25.0	36.0	20	5.8	885	Babel et al. 2017 Foken et al. 2017
LA_FR	**Lackenberg** BY, DE	49.0996177 13.304667	1308	**FR** (spruce/grass)	24.-30. September 2017	-	3.0	9.0	10	3.7	1480	Lindauer et al. 2014 Matiu et al. 2017
MMP_FR	**Metolius Mature Pine** PNW, US	44.4523 -121.5574	1253	**FR** (pine)	06.-12. June 2014	2.4	17.0	33.5	20	6.3	523	Thomas et al. 2009 Vickers et al. 2012
SC_FR	**Sta. Clotilde** ES	38.210142 -4.287495	736	**FR** (oak savanna)	01.-07. April 2017	1.0	8.5	18.0	10	15.3	720	Andreu et al. 2018
RO_GL	**Rollesbroich** NRW, DE	50.621914 6.304126	515	**GL**	15.-21. July 2013	5.9	0.19	2.6	20	7.7	1033	Borchard et al. 2015 Gebler et al. 2015
WU_GL	**Wüstebach (clear cut)** NRW, DE	50.503046 6.335946	610	**GL** (deforested area)	18.-24. May 2015	< 2.5	0.25	2.5	20	7.5	1220	Ney et al. (in press) Wiekenkamp et al. 2016
FE_GL	**Fendt** BY, DE	47.8329 11.0607	595	**GL**	11.-17. July 2015	3.5	0.25	3.5	20	8.4	1081	Brosy et al. 2017 Zeeman et al. 2017
DI_CL_MA_06	**Dijkgraaf**	51.992061	9	**CL** (maize)	14.-16. June 2007	0.35	0.35	4.0	10	10.5	803	Jans et al. 2010
DI_CL_MA_07	Gelderland, NL	5.645944			14.-16. July 2007	3.5	1.70					
DI_CL_MA_08					04.-06. August 2007	3.0	2.80					
SE_CL_WW	**Selhausen**	50.8658339	103	**CL** (winter wheat)	03.-05. June 2015	6.1	0.79	2.4	20	9.9	698	Eder et al. 2015
SE_CL_BA	NRW, DE	6.4473888		(barley)	27.-29. May 2016	5.1	0.95					Ney and Graf 2018
SE_CL_IC				(intercrop)	23.-25. September 2016	1.0	0.22					
SE_CL_SB_06				(sugar beet)	20.-22. June 2017	2.3	0.37					
SE_CL_SB_08					02.-04. August 2017	5.2	0.46					
SE_CL_SB_09					04.-06. September 2017	4.3	0.50					

LAI: leaf area index; EC: eddy covariance; meas: measurement; Temp: temperature; P: precipitation

4.2.4 Evaluation of Source Partitioning Results

The evaluation of the source partitioning performance was preceded in multiple ways for the various study sites depending on data-availability (Fig. 4.6). At some study sites, R_{soil} was measured additionally with closed-chamber measurements independently of the EC measurements. In RO_GL and SE_CL, continuous measurements of multiple longterm-chambers were available for the considered time periods (half-hourly at SE_CL and hourly interpolated to half-hourly at RO_GL). In DI_CL, WU_FR, and WU_GL, R_{soil} was measured with survey-chambers at several measurement points on one day during the considered time periods, so spatial and temporal averages for the hours in question could be calculated. For all study sites (except for LA_FR), soil evaporation E_{soil} was estimated as a fraction of measured ET based on Beer's law depending on LAI (E_{soil} = ET exp(-0.6 LAI); Campbell and Norman 1998; Denmead et al. 1996). Thus, the root mean square error (*RMSE*) and the *bias* could be calculated between the partitioning results for E or R_{soil} and the estimated E_{soil} or chamber measurements, respectively. *RMSE* was sensitive to outliers and the distribution of errors was prone to be asymmetric. A method overestimating the magnitude of a flux component may earn a larger *RMSE* than an underestimating one. Therefore, we also calculated a version of the *RMSE* based on log-transformed data ($RMSE_{ln}$; data transformed with ln(x +1)) before computing differences between estimated and reference E or R_{soil}. One has to keep in mind that the measurements of R_{soil} and LAI can also contain errors and that E_{soil} is only a rough model approximation.

Furthermore, partitioned CO_2 fluxes were compared to results of the established partitioning approach after Reichstein et al. (2005) if available; even though this approach targets other flux components (total ecosystem respiration TER and gross primary production GPP). Here, the estimated NPP and R_{soil} for every time step were classified as reasonable if their magnitudes were smaller than the calculated GPP or TER, respectively. Since all data sets were from the main growing season and weather conditions favorable of high respiration, R_{soil} should additionally be larger than 1 µmol m^{-2} s^{-1}. In the following, NPP and R_{soil} estimates meeting these criteria ("hits in range") will be counted as HiR GPP and HiR TER. Again, within this evaluation step two models including their different assumptions and uncertainties were examined and compared, and the results have to be handled with care. An evaluation of the estimated flux magnitudes was also possible for some study sites by means of former publications.

4.2.5 Analysis of Source Partitioning Approaches

To compare SK10 and TH08 and to gain a better insight in their functionality and dependencies on turbulence and site characteristics, a correlation analysis was conducted between HiR GPP or HiR TER and the variables z, h_c, z h_c^{-1}, LAI, or LAI h_c^{-1}. All study sites,

only forest sites, or only cropland and grassland sites were considered to calculate the correlations.

Furthermore, we developed a conceptual model to generate simple, synthetic data sets of *w'*, *q'*, and *c'* with different degrees of mixing between scalar sinks and sources from the soil, canopy, and boundary layer (Fig. 4.7 *upper panels*). We considered no mixing, complete mixing, and partial mixing between scalars originating from soil and canopy (with positive *w'*), all three sets excluding mixing with scalars originating from boundary layer (with negative *w'*). Averages of fluctuations were all specified as zero, and each scalar sink/source strength was determined such that the net H_2O flux equates to 1 mmol m^{-2} s^{-1} and the net CO_2 flux to -1 µmol m^{-2} s^{-1}. Each generated data point of *q'* and *c'* was scaled with a random number to simulate additional sources of variance not related to the degree of mixing. TH08 was applied to these synthetic data sets and could be validated with the true known partitioning factors, while SK10 was already thoroughly analyzed and validated by means of the synthetic high frequency data derived by LES in Chapter 3.

4.3. RESULTS AND DISCUSSION

For each study site, the number of half-hourly time steps during daylight per considered time period is shown in Table C.1 in Appendix C. Also, the relative fraction of daylight time steps of high-quality (HQ) which were used in the application of SK10 and TH08 are shown, where for SK10 only a good or intermediate quality flag (after Mauder et al. 2013) and no precipitation, and for TH08 additionally a negative $\rho_{q'c'}$ had to be given. Furthermore, the relative fraction of these HQ-time steps, for which partitioning solutions were found, is shown for each method version. With TH08 by sampling in the first quadrant (Q1) a partitioning result could be obtained for almost every time step (minimum of 98.2%). With the hyperbolic threshold criteria and with GMM fewer solutions could be found, because quite often the number of sampled data points was less than 1% of the total number in one half-hour time period. SK10 sometimes could not find a partitioning solution, when the measured and estimated $\rho_{q'c'}$ were not equal and removing large-scale processes by Wavelet-transform could not help either to solve the system of equations. The most solutions were found for MMP_FR and the least for RO_GL. For DI_CL_MA and SE_CL_SB the number of solutions with SK10 increased with development stage of the maize or sugar beet, respectively, while the ratio between measurement height and h_c decreased. At the same time the number of solutions for TH08 with hyperbolic threshold and GMM decreased or in case of the conditional sampling in Q1 was not affected. Generally, for the grasslands and the lower crop canopies more solutions were obtained with TH08 than SK10. An exception was the low intercrop in Selhausen (SE_CL_IC).

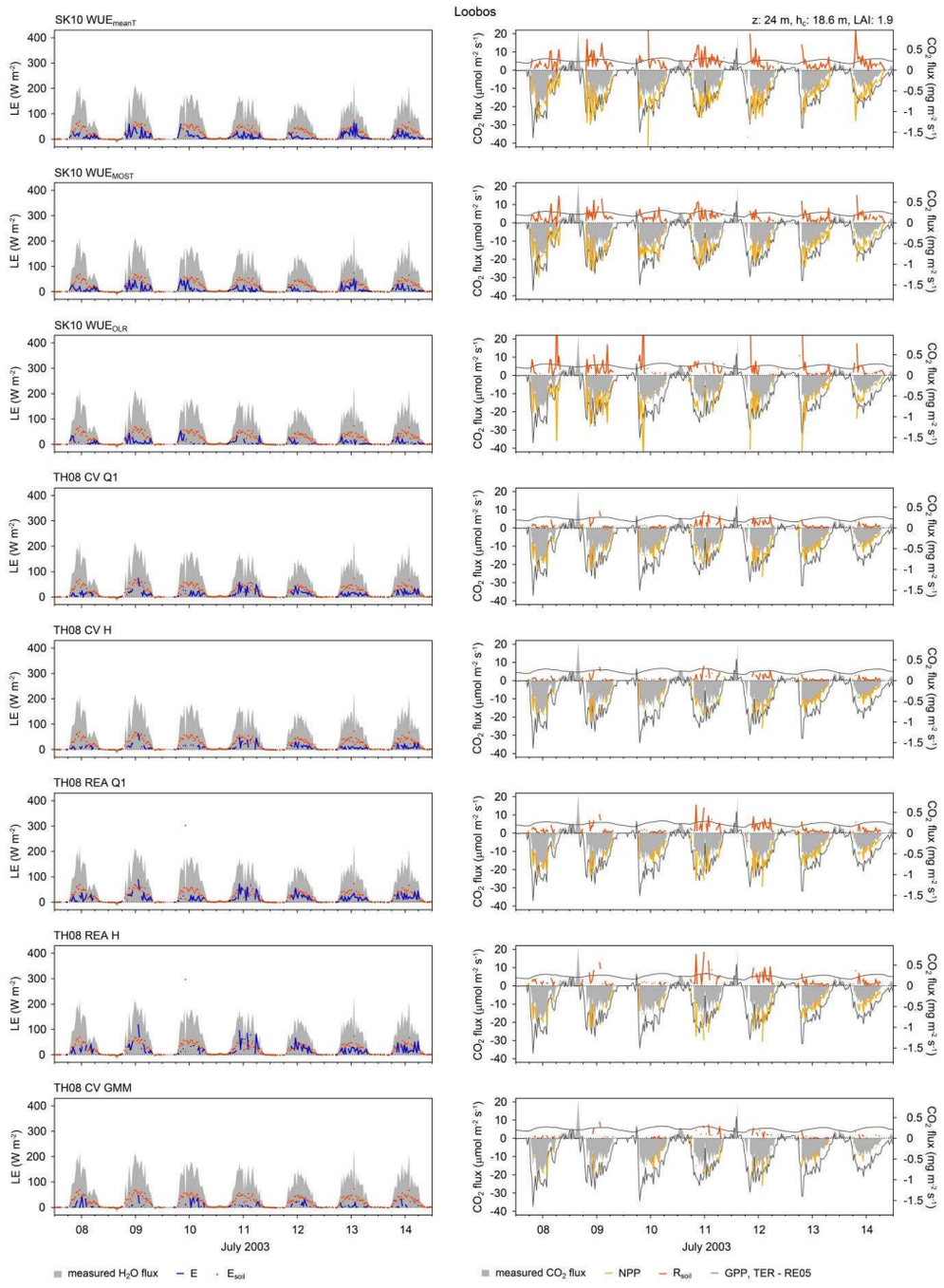

Fig. 4.2: Source partitioning results of H_2O (*left*) and CO_2 (*right*) fluxes in half-hourly time steps for the Loobos study site (forest) in The Netherlands and for every method version (see text for description). CO_2 flux estimates by Reichstein et al. (2005; RE05) are also included (LE: latent heat flux; E: evaporation; E_{soil}: estimated evaporation based on Beer's law; GPP: gross primary production; NPP: net primary production; TER: total ecosystem respiration; R_{soil}: soil respiration; z: measurement height; h_c: canopy height; LAI: leaf area index).

4.3.1. Evaluation of Source Partitioning Results

In Figure 4.2 the source partitioning results for H_2O and CO_2 fluxes for LO_FR are shown in half-hourly time steps as an example. The partitioning results for all sites and all method versions are shown in Appendix C (Fig. C.1-C.12) including E_{soil} estimations based on Beer's law, R_{soil} chamber measurements, and partitioning results after Reichstein et al. (2005). The diurnal dynamics of H_2O and CO_2 fluxes, their components, and WUE for WA_FR and all method versions are shown in Figure 4.3, and for every study site and just the method application SK10 with WUE_{OLR} and TH08 with REA H in Figure 4.4. In Figure 4.5 the total average of the flux components of each considered time period is shown on the one hand for MMP_FR and for every method version (*top panel*), and on the other hand for every site and for SK10 with WUE_{OLR} and TH08 with REA H (*lower panels*). For the calculation of these diurnal dynamics and averages large spikes in the estimated flux components (deviation from the mean by more than ten times of the standard deviation) were excluded. Figure 4.6 shows the error quantities, $RMSE_{ln}$ and *bias* regarding R_{soil} chamber measurements, HiR GPP, HiR TER, and $RMSE_{ln}$ and *bias* regarding E_{soil} estimation, for each site and method version. Timestamps in all following figures are in local time.

In general, SK10 and TH08 gave differing results for each study site and performed disparately between method versions. In Figures 4.2-4.5 it is apparent that TH08 mostly resulted in lower magnitudes of the flux components originating from the soil surface or sub-canopy, than SK10. The source partitioning results of LO_FR (Fig. 4.2) were a small exception to this rule. For this study site the partitioning fractions of SK10 and TH08 were very similar and thus entail a very low uncertainty for the results. For the other study sites larger discrepancies could be observed between SK10 and TH08.

Considering the equations of the various TH08 approaches, more data points are sampled in Q1 than with the hyperbolic threshold, which might suggest that the magnitudes of the flux components should be larger (fluxes due to CV Q1 > CV H, and REA Q1 > REA H). However, with less sampled data points the calculation of the fluxes via REA yielded larger fluxes than via CV, thus the largest magnitudes were obtained by using REA with the hyperbolic threshold (REA H) and the smallest by using CV H. In some time steps, no respiration/evaporation 'cloud' was apparent in the *q'-c'* plane, thus, the applied conditional sampling strategies could not be effective as intended and an assessment of a correct sampling was not possible. Compared to the magnitude of GPP and TER estimated by the gap-filling model after Reichstein et al. (2005), components estimated by TH08 almost always were within this prescribed range because of their small resulting fluxes, whereby R_{soil} was often below the defined minimal threshold of 1 µmol m^{-2} s^{-1} and thus underestimated (Fig. 4.6, C.1-C.12 in Appendix C). Regarding the error quantities in Figure 4.6, TH08 REA H performed best. Partitioning results obtained by TH08 CV GMM were not systematically different from the other method versions but showed no extreme spikes in the soil flux components.

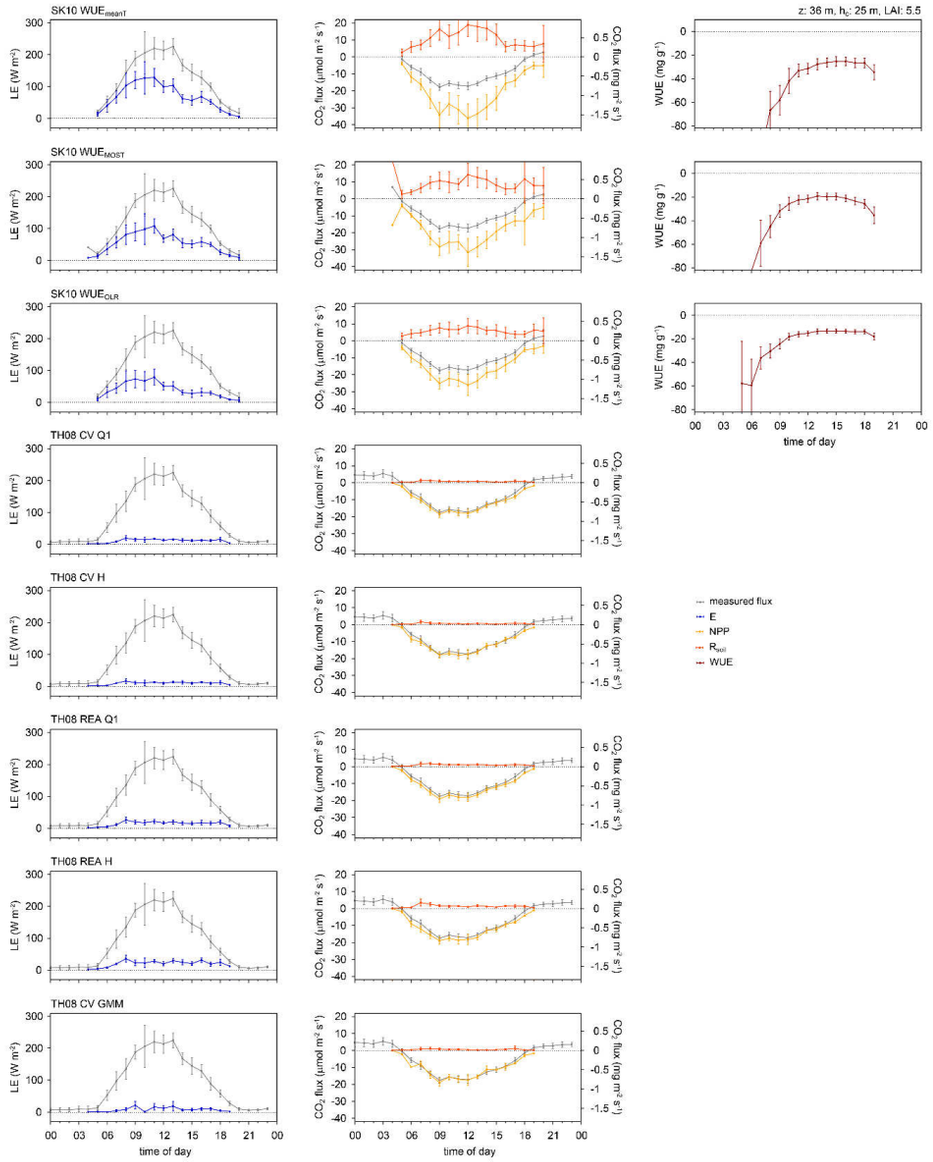

Fig. 4.3: Diurnal dynamics of source partitioning results of H_2O (*left*) and CO_2 (*middle*) fluxes and water use efficiency (WUE, *right*) for the Waldstein study site (forest) in Germany for 4-10 July, 2016 and for every method version (see text for description; LE: latent heat flux; E: evaporation; NPP: net primary production; R_{soil}: soil respiration; z: measurement height; h_c: canopy height; LAI: leaf area index). *Error bars* indicate the 95% confidence intervals of the mean values.

The SK10 approach had the tendency to produce very high magnitudes of the soil flux components. Considering the diurnal dynamics and averages (Fig. 4.3-4.5), results of SK10 were more reasonable and satisfactory. For most of the study sites, the magnitudes and variances of the soil flux components were decreased by using WUE_{MOST} or WUE_{OLR} instead of WUE_{meanT}. The differing WUE inputs had a larger effect on the CO_2 flux components than

on H_2O. Considering the error quantities in Figure 4.6, SK10 with WUE_{OLR} very often gave the best results.

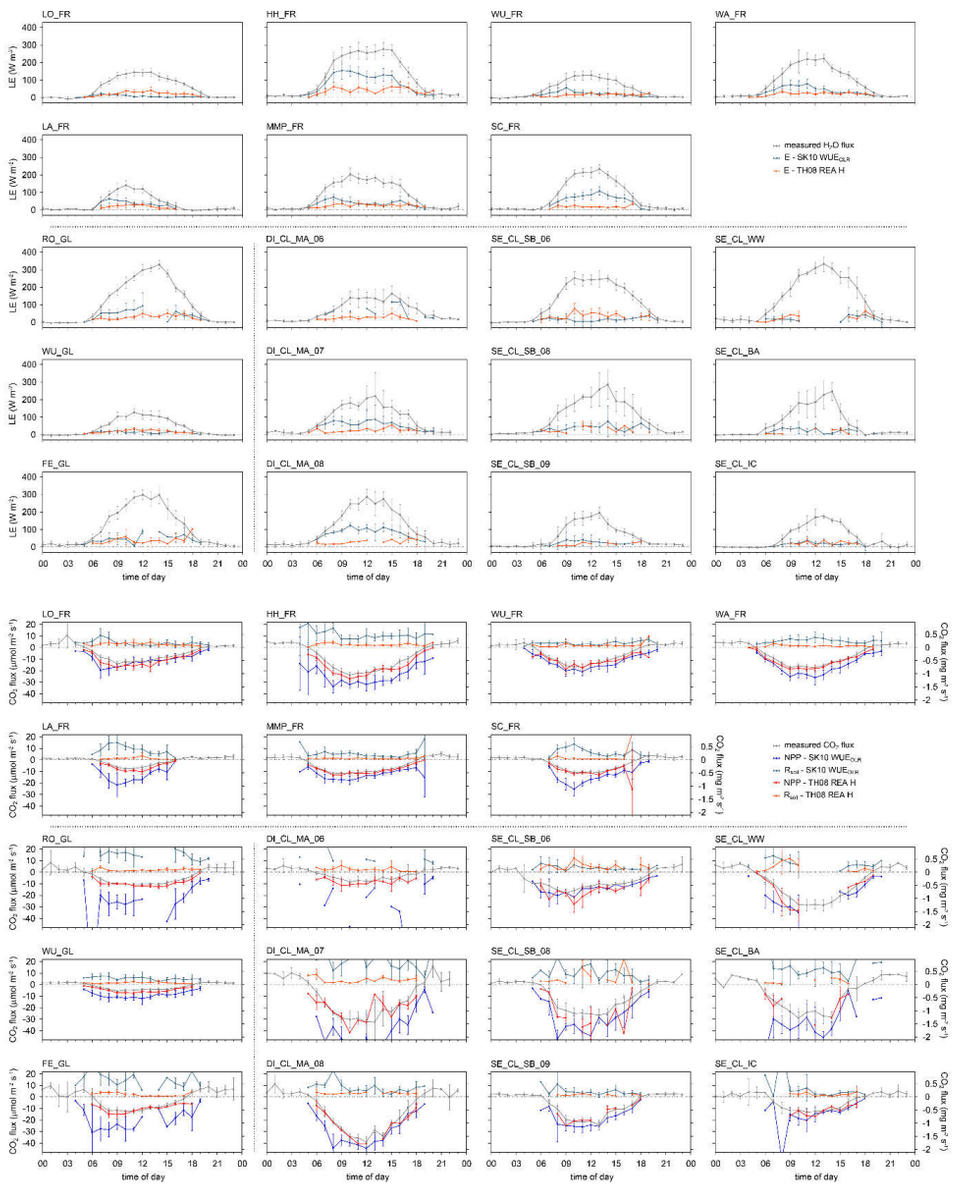

Fig. 4.4: Diurnal dynamics of source partitioning results of H_2O (*upper panels*) and CO_2 (*lower panels*) fluxes for all study sites and for the approach after Scanlon and Kustas (2010; SK10) with WUE_{OLR} and after Thomas et al. (2008; TH08) with REA H (see text for description; LE: latent heat flux; E: evaporation; NPP: net primary production; R_{soil}: soil respiration). *Error bars* indicate the 95% confidence intervals of the mean values.

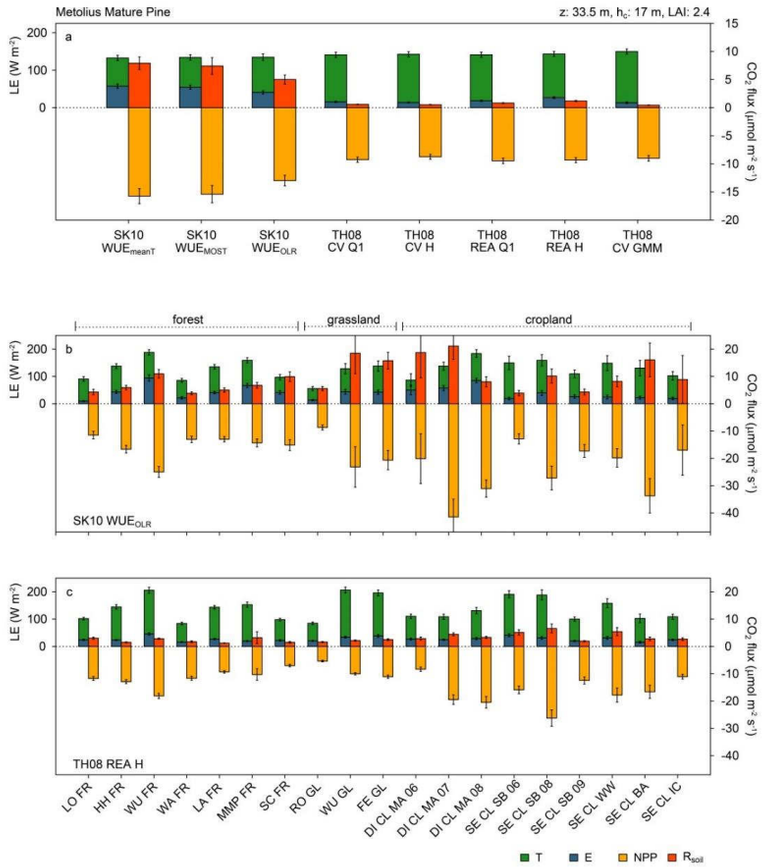

Fig. 4.5: Averages of source partitioning results of H_2O and CO_2 fluxes, a) for the Metolius Mature Pine study site (forest) in US and for every method version, b) for all study sites and for the approach after Scanlon and Kustas (2010; SK10) with WUE_{OLR}, and c) after Thomas et al. (2008; TH08) with REA H (see text for description; LE: latent heat flux; E: evaporation; NPP: net primary production; R_{soil}: soil respiration; z: measurement height; h_c: canopy height; LAI: leaf area index). *Error bars* indicate the 95% confidence intervals of the mean values.

The partitioned CO_2 fluxes generally showed a higher variability and more spikes than the partitioned H_2O fluxes for all sites. Jans et al. (2010) reported a mean R_{soil} measurement of 3.16 µmol m^{-2} s^{-1} and a peak event of 23 µmol m^{-2} s^{-1} for DI_CL_MA in 2007. R_{soil} estimates by SK10 were often as large as this peak, but the maximum observed by Jans et al. (2010) was triggered by precipitation, which does not apply for our considered time periods (Fig. C.10 in Appendix C). For LO_FR in 1997, Dolman et al. (2002) reported a peak respiration measurement of 12 µmol m^{-2} s^{-1}, Falge et al. (2002) a seasonal maximum GPP of -24 µmol m^{-2} s^{-1} and seasonal maximum TER of 5.3 µmol m^{-2} s^{-1}, and chamber measurements from June 2003 had a magnitude of 17.3 µmol m^{-2} s^{-1}. All these quantities support our partitioning results for LO_FR based on SK10, TH08, and the approach after Reichstein et al. (2005) (Fig. 4.2). For MMP_FR, Thomas et al. (2009) derived from sap flux

measurements a T/ET ratio of 50%, which agrees well with the partitioning results by SK10 (Fig. C.5 in Appendix C). Results by TH08 and estimated E_{soil} imply a larger fraction of T. For WU_GL, TH08 yielded results matching comparatively well to the modeled estimate E_{soil} and the gap-filling approach after Reichstein et al. (2005) (Fig. C.8 in Appendix C). As mentioned before, WU_GL is a very heterogeneous site with regrowing vegetation of grasses, shrubs, and trees on dry and wet areas. Thus, the measured signals could display fluxes coming from different sinks and sources distributed horizontally rather than vertically. The present variety of plant types increased the uncertainty in the estimation of WUE, where the usage of WUE_{OLR} improved the partitioning by SK10 significantly, but the overestimation of R_{soil} (compared to chamber measurements and TER) was not averted. For LA_FR we observed the similar behavior as for WU_GL. Here too, a forest is regrowing, but trees are already more frequent and larger. At SC_FR the impact of water stress on the application of source partitioning methods could be observed. For a very dry period in August 2016 both partitioning approaches were not applicable, because transpiration and photosynthesis almost ceased due to water stress and the correlations between H_2O and CO_2 fluxes were almost always positive (not shown). For a period in April 2017 partitioning results could be obtained, where an increase in SK10 estimated R_{soil} and a decrease in estimated E was evident during the regarded time period (Fig. C.6 in Appendix C). Spring in 2017 was considered as relatively dry in this region and the last precipitation event was five days before the regarded time period, such that it can be assumed that water stress increased steadily in April. TH08 underestimated soil fluxes substantially, because no respiration/evaporation events were apparent, which could be caused by the sub-canopy of the oak savanna. For WA_FR, SK10-derived E and R_{soil} were relatively large but for one day (July 8th, 2016) with smaller magnitudes of the CO_2 flux components (Fig. C.3 in Appendix C). On this day no significant differences in weather conditions or scalar statistics were apparent compared to the other days. The only noticeable difference was that SK10 found partitioning results for less negative $\rho_{c_p'c_r'}$ than on the other days. In RO_GL the continuous R_{soil} chamber measurements and TER estimated with the approach after Reichstein et al. (2005) did not agree well, where the latter decreased steadily over the seven days and was mostly lower than measured R_{soil}. Compared to both quantities, SK10 still overestimated and TH08 underestimated R_{soil} fluxes.

A clear pattern in the performance of the source partitioning depending on method version or on study site characteristics could not be identified in the error quantities (Fig. 4.6). The following statements can be made: the *RMSE* in R_{soil} was usually larger for SK10 than for TH08 (not shown). Considering $RMSE_{ln}$ in R_{soil}, SK10 performed better at forest sites than TH08, and slightly worse at crop- and grasslands (Fig. 4.6). The *bias* in R_{soil} was always positive for SK10 (except for WU_FR) and often negative for TH08 (except for TH08 REA H). Therefore, SK10 has the tendency to overestimate and TH08 to underestimate R_{soil} compared to respiration chamber measurements. The lowest *RMSE*, $RMSE_{ln}$, and *bias* were found for the SK10 method versions in WU_FR and for TH08 in WU_FR, WU_GL, and

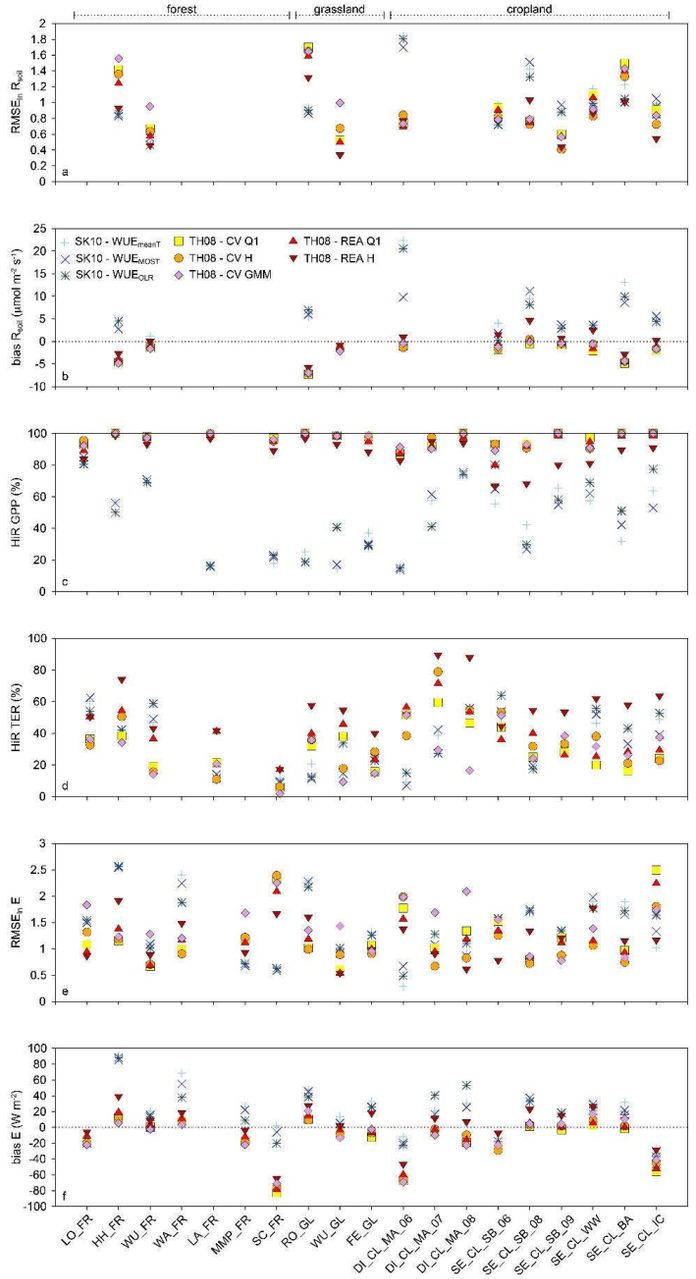

Fig. 4.6: Error quantities of source partitioning results for each study site and method version (see text for description). a)-b) Root mean square error in log-transformed data ($RMSE_{ln}$) and bias considering soil respiration chamber measurements, c)-d) relative fraction of time steps with partitioning results in range (HiR) of estimated gross primary production (GPP) and total ecosystem respiration (TER) by the approach after Reichstein et al. (2005), e)-f) $RMSE_{ln}$ and bias considering E_{soil} estimated based on Beer's law.

SE_CL_SB_09. In comparison to the gap-filling model after Reichstein et al. (2005),

HiR GPP were relatively frequent for TH08 with a minimum of 66.7% for SE_CL_SB_06, and HiR GPP for SK10 were usually rarer. For HiR TER both methods converged. While SK10 mostly overestimated TER, TH08 often estimated soil fluxes smaller than the minimal R_{soil} threshold of 1 µmol m^{-2} s^{-1}. TH08 REA H gave usually the best results for HiR TER and the worst for HiR GPP within the method versions of TH08. Also, the performance of SK10 improved for CO_2 in DI_CL_MA with increasing crop height and lower LAI (Fig. 4.4, 4.6). The *RMSE* (not shown), $RMSE_{ln}$, and *bias* in E (compared to the modeled estimate E_{soil} after Beer's law) were mostly similar or slightly larger for SK10 than for TH08 except for the short crop canopies, LO_FR, MMP_FR, and SC_FR. These sites also have a relatively low LAI. Both quantities were low in WU_FR and WU_GL for SK10 and TH08 (Fig. 4.6). The worst performance regarding E could be found in HH_FR for SK10, and in SC_FR, DI_CL_MA_06, and SE_CL_IC for TH08. The *bias* indicated that SK10 underestimated E for all canopies with a LAI lower than 2.3 (LO_FR, SC_FR, DI_CL_MA_06, SE_CL_SB_06, SE_CL_IC, the latter three have relatively short canopies). This could also be explained by the larger E_{soil} estimates based on Beer's law due to the smaller LAIs, thus preventing an overestimation by SK10.

4.3.2. Analysis of Source Partitioning Approaches

With a correlation analysis we studied the interrelations between partitioning performance (regarding HiR GPP and HiR TER) and site characteristics such as canopy height h_c, LAI and

Tab. 4.2: Correlation coefficients between partitioning performance of each method version regarding HiR GPP (see text for description) and study site characteristics (h_c: canopy height; LAI: leaf area index; z: measurement height) considering all, only forest, or only crop- and grassland sites. *Green* (*blue*) *lettering* indicate highest positive (negative) correlation, and *green* (*red*) *cell filling* highest (lowest) magnitude of correlation.

variable	SK10 WUE_{meanT}	SK10 WUE_{MOST}	SK10 WUE_{OLR}	TH08 CV Q1	TH08 CV H	TH08 REA Q1	TH08 REA H	TH08 CV GMM
all								
h_c	0.52	0.56	0.44	0.21	0.27	0.28	0.45	0.22
LAI	0.15	0.12	0.02	0.43	0.21	0.43	0.12	0.22
z	0.48	0.52	0.40	0.23	0.27	0.31	0.48	0.26
z h_c^{-1}	-0.51	-0.60	-0.45	-0.11	-0.15	-0.13	-0.15	0.04
LAI h_c^{-1}	-0.44	-0.53	-0.47	0.19	0.05	0.11	-0.11	0.15
forests								
h_c	0.64	0.63	0.56	0.20	0.21	0.21	0.27	0.11
LAI	0.35	0.32	0.26	0.61	0.74	0.68	0.70	0.64
z	0.62	0.60	0.55	0.37	0.31	0.36	0.41	0.26
z h_c^{-1}	-0.74	-0.75	-0.68	0.27	0.25	0.28	0.20	0.38
LAI h_c^{-1}	0.35	0.33	0.34	0.77	0.78	0.81	0.83	0.78
croplands, grasslands								
h_c	0.54	0.64	0.33	0.07	0.23	0.12	0.31	0.02
LAI	0.07	0.05	-0.10	0.40	0.10	0.37	-0.03	0.10
z	0.02	0.07	-0.29	-0.44	-0.11	-0.17	0.37	-0.17
z h_c^{-1}	-0.58	-0.71	-0.51	-0.01	-0.01	0.03	0.17	0.24
LAI h_c^{-1}	-0.37	-0.49	-0.46	0.37	0.21	0.32	0.16	0.33

LAI h_c^{-1} as proxy for canopy density, measurement height z, and z h_c^{-1} (Tab. 4.2, 4.3). h_c should represent the vertical separation of sinks and sources of passive scalars between canopy top and soil surface. LAI can correlate with h_c of a study site, thus to distinguish between their impacts on partitioning performance separately, LAI h_c^{-1} was also considered. z was constant for each cropland, DI_CL_MA or SE_CL, for all considered time periods, thus the correlation coefficients with z have to be handled with care. All these site characteristics also affect the degree of mixing of the scalars, when they reach the EC sensor, where we assume that with increasing LAI, LAI h_c^{-1}, and z h_c^{-1} and decreasing h_c the dissimilarity between *q'* and *c'* decreases and EC measurements contain less information for the partitioning approaches (Edburg et al. 2012; Huang et al. 2013; Williams et al. 2007). Results in Chapter 3 suggest a decreasing performance of SK10 with increasing z h_c^{-1}. Correlation coefficients were calculated for all sites at once, for only forests, or for only crop- and grasslands, respectively.

For the SK10 method versions, the correlation coefficients showed similar relations between variables and partitioning results for both HiR GPP and HiR TER, because SK10 had the tendency to overestimate both NPP and R_{soil}. For the TH08 method versions, relations slightly differ between HiR GPP and HiR TER, because TH08 had the tendency to underestimate R_{soil} fluxes, thus HiR TER were smaller than HiR GPP. Only considering forest sites, the correlations were relatively high between variables and partitioning performance. The performance of all SK10 method versions correlated negatively with z h_c^{-1} and positively with

Tab. 4.3: Correlation coefficients between partitioning performance of each method version regarding HiR TER (see text for description) and study site characteristics (h_c: canopy height; LAI: leaf area index; z: measurement height) considering all, only forest, or only crop- and grassland sites. *Green* (*blue*) *lettering* indicate highest positive (negative) correlation, and *green* (*red*) *cell filling* highest (lowest) magnitude of correlation.

variable	SK10 WUE_{meanT}	SK10 WUE_{MOST}	SK10 WUE_{OLR}	TH08 CV Q1	TH08 CV H	TH08 REA Q1	TH08 REA H	TH08 CV GMM
all								
h_c	0.52	0.52	0.47	-0.12	-0.18	0.17	0.01	-0.24
LAI	0.11	0.16	0.07	-0.17	0.13	-0.02	0.33	-0.05
z	0.48	0.47	0.44	-0.17	-0.24	0.12	-0.06	-0.29
z h_c^{-1}	-0.47	-0.57	-0.42	0.08	-0.01	-0.14	-0.15	0.29
LAI h_c^{-1}	-0.42	-0.50	-0.47	-0.08	0.03	-0.21	-0.06	0.15
forests								
h_c	0.63	0.63	0.63	0.59	0.68	0.56	0.76	0.40
LAI	0.34	0.38	0.41	0.53	0.51	0.65	0.82	0.34
z	0.60	0.59	0.64	0.46	0.60	0.41	0.72	0.26
z h_c^{-1}	-0.72	-0.73	-0.66	-0.48	-0.52	-0.39	-0.47	-0.33
LAI h_c^{-1}	0.32	0.36	0.46	0.19	0.10	0.33	0.61	-0.05
croplands, grasslands								
h_c	0.54	0.59	0.34	0.42	0.61	0.50	0.85	-0.31
LAI	0.01	0.06	-0.13	-0.49	-0.04	-0.33	0.03	-0.28
z	0.04	0.01	-0.23	0.64	0.59	0.70	0.48	-0.09
z h_c^{-1}	-0.48	-0.66	-0.47	-0.16	-0.45	-0.20	-0.59	0.09
LAI h_c^{-1}	-0.34	-0.47	-0.47	-0.36	-0.30	-0.31	-0.37	-0.10

h_c and z. The correlation coefficients regarding LAI, also positive, were the weakest, where for the forest sites LAI was more important than for the remaining sites. LAI h_c^{-1} correlated always negatively with performance of SK10 except for the forest sites, where the coefficients of LAI and LAI h_c^{-1} were similar. For the TH08 method versions LAI had larger, and h_c, z h_c^{-1}, and LAI h_c^{-1} smaller effects on partitioning performance than for SK10 method versions, and a few signs changed. For HiR TER and only forests or only crop- and grasslands, h_c was more important again in TH08 method versions (especially while neglecting the correlation with z). Correlation coefficients of LAI and LAI h_c^{-1} were mostly positive with a few exceptions (e.g., regarding HiR TER for crop- and grasslands). For forest sites and TH08, only positive correlations were evident except for the relationship between HiR TER and z h_c^{-1}. Also, the impacts of h_c and LAI h_c^{-1} were reversed between HiR GPP and HiR TER. Apparently, a dense forest canopy yielded too low sub-canopy fluxes derived by TH08, and a high canopy less reasonable canopy fluxes.

The variable LAI usually correlated positively for SK10 and TH08 method versions and all canopies, making it the sole variable which clearly contradicted our initial hypotheses. Also, the correlation between partitioning performance and LAI h_c^{-1} at forest sites was contradictory. Next to canopy density, LAI could also be connected to larger sinks and sources of canopy fluxes (T and photosynthesis) relative to soil surface fluxes due to larger biomass, and to the appearance and frequency of coherent structures. A dense canopy prevents frequent ejections of air parcels from the sub-canopy, but provokes higher scalar concentrations in such air parcels because of a longer accumulation under the canopy. Respiration/evaporation events could occur less frequent but be of higher magnitude. Also, small gaps in an otherwise dense canopy can play an important role regarding ejection events. Thus, how canopy density affects scalar-scalar-correlation measured above the canopy (and connected to that the partitioning performance), cannot be assessed easily. In this study, canopy density and partitioning performance correlated negatively at crop- and grassland sites and positively at the forest sites. Assuming gaps in the canopy can be more expected in forests than in crop- or grasslands, these results support the above-mentioned aspects. For further assessments, an estimate about the (large-scale) heterogeneity and density of the study sites' vegetation has to be made and included in this analysis.

SK10 was already thoroughly analyzed and validated by means of the synthetic high frequency data derived by LES in Chapter 3. Here, TH08 was applied to various synthetic *w'*-, *q'*-, and *c'*-data sets including soil, canopy, and boundary layer scalar sink/sources derived by a simple conceptual model as described above (Fig. 4.7 *top panel*). For each data set, different degrees of mixing of the soil and canopy sink/source were implied (no, complete, and partial mixing), where the resulting net fluxes for each set was specified to 1 mmol m^{-2} s^{-1} for H_2O and to -1 µmol m^{-2} s^{-1} for CO_2. Defined by the conditional sampling concept, we hypothesized that TH08 would work perfectly with no mixing of the scalars from the three different origins, would not obtain any partitioning factors in case of the complete mixing, and would

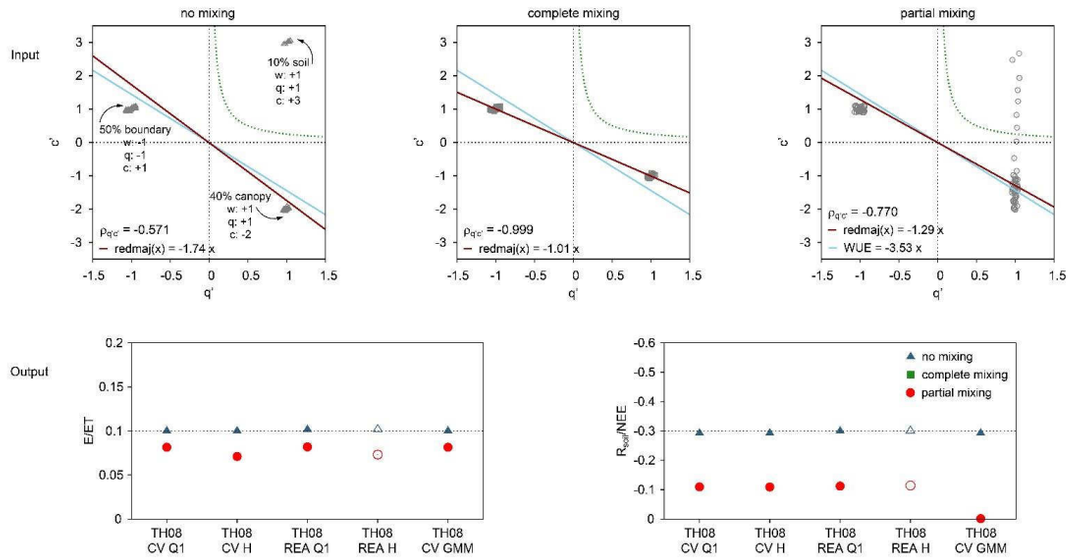

Fig. 4.7: a)-c) Setup of conceptual model for synthetic fluctuations (q' and c') originating from soil, canopy, or boundary layer with differing degrees of mixing (no, complete, or partial mixing between soil and canopy sink/source) including water use efficiency (mg g^{-1}; *blue line*), reduced major axis regression (*red line*) after Webster (1997), hyperbolic threshold criteria after Thomas et al. (2008; TH08) (H = 0.25; *green dashed line*) and correlation coefficient between q' and c' ($\rho_{q'c'}$). d)-e) True known partitioning ratios (*dashed line*) and source partitioning results of all TH08 method versions (see text for description) for each degree of mixing.

underestimate the soil fluxes in case of partial mixing. TH08 behaved as assumed except for TH08 REA H (see below; Fig. 4.7 *bottom panel*). For the partial mixing a small difference in TH08-derived partitioning factors (especially for H_2O) was observed between the sampling in Q1 and with H, because one data point was not sampled with the hyperbolic threshold, but laid within Q1. TH08 REA H did not yield any partitioning results in case of no or partial mixing. This is due to the different definitions of β in the application of REA with the sampling in Q1 or with H (Thomas et al. 2008, equation 4, page 1213 and statement page 1215). β is an empirical constant and can be approximated by the ratio between the standard deviation of *w'* ($\sigma_{w'}$) and the difference between the mean vertical velocities in updrafts and downdrafts ($\overline{w_+} - \overline{w_-}$). For the conditional sampling approach within Q1, β is derived including all data points (disregarding the sign of *q'* or *c'*). For the approach including the hyperbolic threshold criterion, β is derived from *w'* data points which satisfy the hyperbolic threshold criterion for positive *q'* and *c'*. In case of our conceptual model for the partial mixing, no data point with negative *w'* satisfied this criterion, so without $\overline{w_-}$ β and a partitioning factor could not be calculated. Figure 4.7 shows the partitioning factors for TH08 REA H while applying β as calculated in TH08 REA Q1 (*non-filled markers*). TH08 CV GMM performed similar to the other method versions, sampled the correct respiration/evaporation 'cloud' in case of no mixing, no 'cloud' in case of complete mixing, but all data points with $q' > 0$ in case of partial

mixing. For the latter, the covariances using the averages of w, q, or c of the sampled cluster, and considering only data points with $w' > 0$, was very small for CO_2 (Fig. 4.7) and negative for E (not shown). Thus, E was recalculated with the covariances using the averages of w and q considering all data points, and including only data points with $w' > 0$, within quadrant 1, and within the sampled cluster, which resulted in a similar partitioning fraction as the other method versions.

4.4. CONCLUSIONS

The partitioning approaches after Scanlon and Kustas (2010; SK10) and after Thomas et al. (2008; TH08) gave differing results for each study site and performed disparately between method versions. TH08 mostly resulted in lower magnitudes of the flux components originating from the soil surface than SK10, and had the tendency to underestimate these flux components compared to soil respiration flux measurements and estimates of E_{soil} based on Beer's law. SK10 usually had the tendency to overestimate soil flux components and yielded larger error quantities, because the distribution of errors was prone to be asymmetric. A method overestimating the magnitude of a flux component may earn a larger *RMSE* than an underestimating one. Decreasing the weight of outliers by log-transforming R_{soil} chamber observations and partitioning estimations revealed a lower $RMSE_{ln}$ for SK10 at forest sites than for TH08. Also, estimating input WUE based on foliage temperature derived by means of measured outgoing longwave radiation often enhanced the partitioning performance of SK10. Applying a Gaussian Mixture Model for the conditional sampling approach in TH08 did not improve partitioning performance significantly, because to obtain a positive and correct flux estimation was difficult from data points not within quadrant 1 in the q'-c' plane. For TH08, conditional sampling including a hyperbolic threshold and calculating flux components based on the relaxed eddy accumulation technique yielded the best partitioning results. The partitioned CO_2 fluxes generally showed a higher variability and more spikes than the partitioned H_2O fluxes for all sites and both methods. Also, mean diurnal cycles averaged over each site's regarded time period yielded more satisfactory results for both approaches.

The dependencies of the partitioning performance on turbulence and site characteristics were analyzed based on a correlation analysis and the application of TH08 to synthetic, conceptual data sets of scalar fluctuations. Foremost, the performance of SK10 correlated negatively with the ratio between measurement and canopy height. The performance of TH08 was more dependent on canopy height and leaf area index. Canopy density and partitioning performance of both methods correlated negatively at crop- and grassland sites and positively at the forest sites. All site characteristics which increase dissimilarities between scalars enhance partitioning performance for SK10 and TH08. For the forest site Loobos in The Netherlands, SK10 and TH08 obtained similar partitioning results and sufficient error quantities indicating a low uncertainty. At this site with a relatively low LAI, high canopy, and low ratio between

measurement and canopy height, conditions for both partitioning approaches seemed to be appropriate.

4.5. ACKNOWLEDGEMENTS

This research was supported by the German Federal Ministry of Education and Research BMBF, project IDAS-GHG [grant number 01LN1313A]. The measurement infrastructure providing observational data was supported by the German Research Foundation DFG through the Transregional Collaborative Research Centre 32 (TR 32) and Terrestrial Environmental Observatories (TERENO). The authors thank Nicolas Brüggemann, Clemens Drüe, Odilia Esser, Günther Heinemann, Thomas Pütz, Veronika Valler, all technicians, engineers, and laboratory assistances in TR32, TERENO, and elsewhere for providing measurements of the test sites.

5

FINAL CONCLUSIONS

In Chapter 2 we introduced the process-based model AgroC and demonstrated that it can be used to simulate the CO_2 exchange in agroecosystems. After optimizing the model for soil moisture, crop development, and soil respiration (R_{soil}), the simulation of hourly net ecosystem exchange (NEE) agreed well with eddy covariance (EC) measurements at three crop sites in Western Germany. Further, AgroC reproduced the flux dynamics very effectively after sudden changes in the grassland canopy due to mowing. An additional calibration of AgroC based on EC measurements further improved model performance and reduced the systematic error between observations and simulations. The combination of EC data and R_{soil} chamber measurements as constraints for the calibration procedure gave the best results regarding model performance criteria. But we also showed, that particularly the cumulative NEE over the entire simulation period (carbon balance) was strongly affected by the choice of optimization strategy, even though the model performance regarding error quantities between optimization strategies did not diverge substantially. Thus, carbon balances obtained via calibration and gap-filling methods are associated with considerable uncertainty, which can be decreased by including additional information/measurements about flux components.

Gaps in the data record of EC measurements often occur systematically during certain atmospheric conditions, especially during nighttime. Commonly used gap-filling and source partitioning approaches use regressed relationships between nighttime flux measurements and physical drivers, and extrapolate these relationships to daytime conditions making certain assumptions necessary (e.g., approach after Reichstein et al. 2005). The various non-linear regression gap-filling methods differ in choice of functional form, parameter fitting, and time window size, and usually do not include additional drivers, such as nutrient levels or sudden changes in the canopy due to harvest or cutting. For gap-filling and source partitioning purposes, AgroC describes multiple carbon flux components precisely for each crop organ and respiration source (R_{soil}, terrestrial ecosystem respiration TER, respiration by heterotrophs R_h, respiration by autotrophs R_a, rhizosphere respiration R_{rhizo}, root respiration R_{root}) including the desired interrelations with various environmental drivers, physical conditions, and biological factors. Various (empirical) functional relationships and parameters can be chosen for this description, so simulations can differ substantially. In general, the usage of process-based models for source partitioning is very time-consuming. Several assumptions have to be made, and various site-specific measurements and parameters are necessary for calibration and evaluation. The assessment of structural errors in models (wrong or missing description of processes), or the risk of over-parameterization and equifinality stay a challenge for model users.

In Chapter 3 and 4 we applied the source partitioning approaches after Scanlon and Kustas (2010) and after Thomas et al. (2008) to high frequency EC measurements of various ecosystems (croplands, grasslands, and forests) to estimate the flux components transpiration (T), evaporation (E), net primary production (NPP), and R_{soil}. Partitioning results could be evaluated based on individual measurements or estimates of flux components and on the

comparison to the commonly used partitioning approach after Reichstein et al. (2005). Furthermore, we tested the partitioning approach after Scanlon and Kustas (2010) by applying it to synthetic high frequency data generated by large eddy simulations (LES; Chapter 3). The dependency of the partitioning performance on canopy type, measurement height, and given sink-source-distributions of the scalars was analyzed. The partitioning approach needed a certain degree of decorrelation of H_2O and CO_2 fluctuations, which was enhanced for observations within the roughness sublayer, as well as by a larger separation between soil sources and canopy sink/sources. Also, the expected dependence of the partitioning results on the water use efficiency (WUE) input was observed. Furthermore, another possible error source, which was so far not yet discussed in the literature, could be detected for the partitioning approach. The method assumes that the correlation coefficient between stomatal and non-stomatal scalar fluctuations can be estimated by the ratio of the transport efficiencies of these scalar components (transfer assumption). The LES-based analysis revealed a violation of this assumption in the simulations, yielding an incorrect partitioning by the approach. The known true partitioning could only be attained after introducing a correction factor for the transfer assumption, which was known however only in the special case of the LES experiments. While applying the approach after Scanlon and Kustas (2010) to the field data, it can only be assumed that the transfer assumption is approximately correct for the given meteorological conditions. As also suggested by Anderson et al. (2018) and Sulman et al. (2016), the method's performance would improve by including direct measurements of WUE on leaf-level, but such measurements are usually not available at most study sites.

In Chapter 4 the source partitioning approaches after Scanlon and Kustas (2010) and after Thomas et al. (2008) including slight modifications were compared and evaluated for various study sites. The methods are both based on joint higher-order statistics of the H_2O and CO_2 fluctuations in EC measurements, while the approaches and procedures differ. The partitioning results were analyzed considering their half-hourly and diurnal dynamics, and the variations of the averaged flux ratios between ecosystems. The approach after Scanlon and Kustas (2010) tended to overestimate half-hourly soil fluxes, while the approach after Thomas et al. (2008) tended to underestimate. The differences were more apparent in the partitioning of CO_2 fluxes than for H_2O. For the approach after Scanlon and Kustas (2010), the estimation of WUE input based on foliage temperature (T_f) derived with measurements of outgoing longwave radiation (compared to just using the air temperature) improved the partitioning performance at most study sites. An implemented modification of the approach after Thomas et al. (2008), by applying a cluster analysis for the conditional sampling of respiration/evaporation events, performed sufficiently, but did not result in significant advantages compared to the other method versions. Both partitioning approaches yielded sufficient diurnal dynamics and averaged partitioning ratios.

Conditions and characteristics of common EC study sites were identified under which both source partitioning methods perform best. Under additional consideration of the findings in

Chapter 3, the source partitioning was affected by canopy density (leaf area index LAI), canopy height (which represents the vertical separation of sinks and sources between canopy and soil surface), and the ratio between measurement and canopy height. All these factors affect the degree of mixing of the scalars when they reach the EC sensors. From a correlation analysis and application of the partitioning approach after Thomas et al. (2008) to synthetic data derived with a conceptual model, we could conclude that the source partitioning performance of both approaches improved with a larger dissimilarity between the passive scalars (less mixing). A sufficient partitioning would be obtained for study sites with a high canopy (especially for the application of the approach after Thomas et al. (2008) on crop- and grasslands and for the approach after Scanlon and Kustas (2010) on all canopies) and a low ratio between measurement and canopy height (especially for the application of the approach after Scanlon and Kustas 2010). A high canopy density would be of advantage for forests and a low density for crop- and grasslands.

In this study, the application of various source partitioning methods including their various approaches, involved assumptions, required input data and work effort showed that still uncertainties and unknowns prevail for the source partitioning of water vapor and CO_2 fluxes. Modifications and improvements have been described and tested. An assessment and evaluation of a partitioning's sufficiency was conducted with additional measurements of flux components on differing spatial and temporal scales independent of the EC measurements. Furthermore, the source partitioning methods using high frequency data were tested and validated based on synthetic data generated by large eddy simulations and a conceptual model. The performance of a complex agroecosystem model was thoroughly analyzed by various calibration exercises. The application of multiple partitioning methods (usage of an ensemble) to the same data can give an idea about uncertainties in the results. For a more precise partitioning, a mixture between the approaches used in this study, the complex agroecosystem model AgroC and the data-driven methods after Scanlon and Kustas (2010), Thomas et al. (2008), and Reichstein et al. (2005), is preferable. Flux estimations from a data-driven approach combined with the simplest physiological model is desirable, that relies on as few assumptions as possible. This approach should be able to describe the interrelations between flux components and the biogeochemical and physical environment (e.g., temperature, soil moisture, nutrient level) sufficiently. Varying parameters should be included to allow for rapid, seasonal, or interannual changes in canopy structure. Also, easily obtainable input data and a minimal effort should be required for its application across global EC station networks.

APPENDIX A

A. The AgroC Model

Hourly Time Step

The SOILCO2/RothC model has a flexible time stepping scheme, however the original SUCROS model explicitly runs at a daily time step. Since net ecosystem exchange (NEE) typically shows distinct diurnal variations, the SUCROS code was adapted to work with an hourly time step. Only the calculation of development stage DVS (-) still relies on the original approach based on the effective temperature sum. In the SUCROS model, daily total gross assimilation is obtained by three-point Gauss integration of the instantaneous assimilation rates per unit leaf area over the daylight period. This integration was omitted in the AgroC model with an hourly time step. Hourly gross assimilation is computed from the hourly average inputs of global radiation and mean temperature using the same approach that was used for the instantaneous assimilation rate in the original code. Major changes were required for the estimation of the photosynthetic active radiation (PAR) flux at the top of the canopy. In SUCROS, instantaneous PAR (J $[L]^{-2}$ $[T]^{-1}$) is estimated from the sine of solar inclination *sinB* (-) and the daily integral of *sinB* including a correction of lower atmospheric transmittance at lower solar elevation *dsinBE* (s d^{-1}). The integral daily value *dsinBE* is approximated and *sinB* is estimated for the day of the year in dependence of the geographic position. In AgroC, the hourly integral of the sine of solar inclination *dsinB* (s h^{-1}) is now calculated using the trapezoidal rule according to:

$$dsinB = 0.5\left(sinB_{t-1} + \left(\sin(\delta)\ \sin(\varphi) + \cos(\delta)\ \cos(\omega)\ \cos(\varphi)\right)\right) t_s \qquad (A.1)$$

where instantaneous $sinB_{t-1}$ $(= \sin(\delta)\sin(\varphi) + \cos(\delta)\cos(\omega)\cos(\varphi))$ is the sine of solar elevation of the previous hour, δ (°) is the sun declination angle, φ (°) is the geographic latitude, ω (°) is the hour angle, and t_s (s) is the number of seconds with astronomically possible solar radiation within one hour (3600 during day, 0 during night, and a value in between for the two hours that include sunrise and sunset). The value of *dsinBE* is then estimated as:

$$dsinBE = \sin\left(\arcsin\left(0.5\ (sinB_{t-1} + sinB)\right) + 0.4\left(0.5\ (sinB_{t-1} + sinB)\right)\right) t_s \qquad (A.2)$$

where 0.4 is the regression coefficient between transmission and solar angle (Supit et al. 1994).

Water Fluxes

The coupling between SOILCO2 and SUCROS involves two hydrological processes: rainfall interception and root water uptake. Interception loss is estimated according to the single-big-leaf concept (Rutter et al. 1971). The canopy interception storage capacity S_i ([L]) was assumed to be proportional to the total leaf area index LAI ([L^2 L^{-2}]). Water is removed from the interception storage by evaporation E_i ([L T^{-1}]):

$$E_i = \left(ET_{p,crop} - E_p\right)\frac{C_i}{S_i} \tag{A.3}$$

where C_i ([L]) represents the interception storage at a certain time step, $ET_{p,crop}$ ([L T^{-1}]) is the potential crop evapotranspiration, and E_p ([L T^{-1}]) is the potential soil evaporation. The amount of interception N_i ([L T^{-1}]) is then estimated according to:

$$N_i = \begin{cases} 0 & \text{for } N_0 = 0 \\ S_i - C_i & \text{for } S_i - C_i < N_0 \\ N_0 & \text{for } S_i - C_i > N_0 \end{cases} \tag{A.4}$$

where N_0 ([L T^{-1}]) represents precipitation. The amount of precipitation entering the soil N_p ([L T^{-1}]) is calculated as the difference between N_0 and N_i.

In SUCROS, $ET_{p,crop}$ is computed by scaling the potential grass reference evapotranspiration (Penman-Monteith approach; Allen et al. 1998) with the dimensionless crop conversion factor K_c. On the basis of Beer's law, $ET_{p,crop}$ is split into potential soil evaporation E_p ([L T^{-1}]) and potential transpiration T_p ([L T^{-1}]) in dependence of LAI:

$$E_p = ET_{p,crop}\exp(-0.6 \cdot LAI) \tag{A.5}$$

$$T_p = ET_{p,crop} - E_p - E_i \tag{A.6}$$

The potential soil evaporation is passed to SOILCO2, where it is used to prescribe the potential upward water flux as upper boundary condition. Potential transpiration is distributed over soil depth according to the relative root density distribution to provide the potential sink term for root water uptake. The depth-specific actual root water uptake is computed by scaling the potential root water uptake with reduction factor α (-) in dependence of soil pressure head h ([L]) following the approach of Feddes et al. (1978):

$$\alpha(h) = \begin{cases} \frac{h_0 - h}{h_0 - h_1} & \text{for } h_0 \le h \le h_1 \\ 1 & \text{for } h_1 \le h \le h_2 \\ 10^{\frac{h_2 - h}{h_3}} & \text{for } h_2 \le h \le h_3 \end{cases} \tag{A.7}$$

where h_0, h_1, h_2, and h_3 ([L]) are prescribed threshold pressure heads (Vanclooster et al. 1995), which are plant dependent (Tab. A.2). Integration of the actual root water uptake over depth

provides the actual transpiration T_a ([L T^{-1}]). The reduction of stomatal conductance due to water stress was assumed to correspond to the ratio between actual and potential transpiration T_a/T_p.

Carbon Fluxes

In this study, carbon fluxes from the atmosphere to the ecosystem (downward) are defined as negative fluxes, and upward fluxes are defined as positive. The water stress ratio (T_a/T_p) is used to scale gross carbon assimilation and to account for the effect of limited soil water availability on crop activity in terms of gross primary productivity *GPP* (mol CO_2 [L]$^{-2}$ [T]$^{-1}$):

$$GPP = -\frac{G_{phot}}{Mol_{CH_2O}} \cdot \frac{T_a}{T_p} \tag{A.8}$$

where G_{phot} (kg CH_2O [L]$^{-2}$ [T]$^{-1}$) is the glucose equivalent of the total gross assimilation per time step (Spitters et al. 1989), and Mol_{CH_2O} is the molar mass of CH_2O (= 0.030 kg mol^{-1}). The net primary productivity *NPP* (mol CO_2 [L]$^{-2}$ [T]$^{-1}$) is defined as:

$$NPP = GPP + R_{gr} + R_m \tag{A.9}$$

where R_{gr} (mol CO_2 [L]$^{-2}$ [T]$^{-1}$) is the total growth respiration, and R_m (mol CO_2 [L]$^{-2}$ [T]$^{-1}$) is the maintenance respiration. Net ecosystem exchange *NEE* (mol CO_2 [L]$^{-2}$ [T]$^{-1}$) is computed as:

$$NEE = NPP + R_h \tag{A.10}$$

where R_h (mol CO_2 [L]$^{-2}$ [T]$^{-1}$) is the depth-integral of the heterotrophic CO_2 source term provided by the RothC module.

Maintenance and Growth Respiration

In a first step, the total maintenance respiration demand at 25°C $R_{m,r}$ (kg CH_2O [L]$^{-2}$ [T]$^{-1}$) is computed as a glucose equivalent according to:

$$R_{m,r} = \sum_{o=1}^{4} f_{m,o}\, W_o\, f_t \tag{A.11}$$

where $f_{m,o}$ (kg CH_2O kg^{-1} DM [T]$^{-1}$) is the maintenance coefficient with index o looping over the four plant organs leaves, stems, roots, and storage organs with coefficients of 0.03, 0.015, 0.015, and 0.01, respectively (Spitters et al. 1989), W_o (kg DM [L]$^{-2}$) is the respective organ dry weight, and f_t (-) is a time conversion factor accounting for the use of an hourly or daily

time step. In a second step, $R_{m,r}$ is corrected for temperature to estimate total maintenance respiration $R_{m,c}$ (kg CH_2O $[L]^{-2}$ $[T]^{-1}$) as described by Spitters et al. (1989) and converted to CO_2 equivalent maintenance respiration R_m (mol CO_2 $[L]^{-2}$ $[T]^{-1}$) by dividing with Mol_{CH_2O}. Total growth respiration R_{gtot} (kg CH_2O $[L]^{-2}$ $[T]^{-1}$) in glucose equivalents is estimated as:

$$R_{gtot} = \left(G_{phot} \cdot \frac{T_a}{T_p} - R_{m,c}\right) - \Delta W \cdot C_{cont} \cdot \frac{Mol_{CH_2O}}{Mol_C} \quad \text{(A.12)}$$

where ΔW (kg DM $[L]^{-2}$ $[T]^{-1}$) is the overall dry matter growth rate, C_{cont} (g C g^{-1} DM) is the conversion factor between carbon and biomass dry matter weight, and Mol_C is the molar mass of C (= 0.012 kg mol^{-1}). Growth respiration for each plant organ $R_{gr,o}$ (mol CO_2 $[L]^{-2}$ $[T]^{-1}$) is computed from R_{gtot} according to:

$$R_{gr,o} = \frac{R_{gtot} \cdot f_o}{Mol_{CH_2O}} \quad \text{(A.13)}$$

where index o loops over the four plant organs, and f_o (-) is the organ-specific partitioning factor. Total growth respiration R_{gr} (mol CO_2 $[L]^{-2}$ $[T]^{-1}$) is finally computed as the sum of all $R_{gr,o}$. The sum of maintenance and growth respiration of the roots represents the autotrophic source term of soil CO_2 and is distributed over the soil profile according to the time-variable relative root density distribution.

Root Exudation and Root Decay

In SUCROS, the daily or hourly glucose assimilation rate G_{phot} (kg CH_2O $[L]^{-2}$ $[T]^{-1}$) is partitioned in dependence of the DVS into the fraction for the shoot and for the root system to build up biomass. According to labelling experiments performed by Swinnen et al. (1995) for winter wheat, 18.2% of net assimilation is transferred to the roots, 7.1% are used to build up root biomass, and 5.3% are released as young photosynthetate rhizodeposition. This translates into fractions of 0.39 and 0.29 for root biomass build-up and exudates, respectively, relative to net assimilation transferred to the roots. The remaining fraction consists of root respiration and root decay. The relative root exudation factor f_{exu} (-) thus equals 0.43 (= 0.29 / (0.39 + 0.29)). In AgroC, the root exudation rate Rt_{exu} (kg C $[L]^{-2}$ $[T]^{-1}$) is computed according to this partitioning factor from the dry matter root growth rate ΔW_{rt} (kg DM $[L]^{-2}$ $[T]^{-1}$):

$$Rt_{exu} = \Delta W_{rt} \cdot f_{rt} \cdot f_{exu} \cdot 0.467 \quad \text{(A.14)}$$

where f_{rt} is the dimensionless partitioning factor for roots, and 0.467 kg C kg^{-1} DM is the root-specific dry matter carbon content (Goudriaan et al. 1997). Using this approach, the simulated root exudation shows diurnal variations due to the dependence on the assimilation rate, as suggested by Hopkins et al. (2013) and Kuzyakov (2006) amongst others.

Swinnen et al. (1995) reported that 3.1% of the net assimilation ends up as dead roots. In relation to the 18.2% transferred to the roots, this equals a relative fraction of 0.17. In order to account for this, a root death factor f_{dea} (-) was introduced. It was assumed that f_{dea} is lower during the crop juvenile stages than at flowering:

$$f_{dea} = \begin{cases} 0 & DVS < 0.2 \\ \frac{f_{deamax}(DVS-0.2)}{0.5-0.2} & \text{for } 0.2 \leq DVS \leq 0.5 \\ f_{deamax} & DVS > 0.5 \end{cases} \quad \text{(A.15)}$$

where f_{dea} is the root death factor in relation to the total amount of roots, and f_{deamax} (-) is the maximum value of the root death factor. For winter wheat, a f_{deamax} of 0.43 was used, which approximately reproduced the cumulative fraction of dead roots of 0.17 of net assimilation determined by Swinnen et al. (1995). The rate of root death in orders of carbon release Rt_{dea} (kg C $[L]^{-2}$ $[T]^{-1}$) is computed as:

$$Rt_{dea} = \Delta W_{rt} \cdot f_{rt} \cdot f_{dea} \cdot 0.467 \quad \text{(A.16)}$$

ΔW_{rt} is reduced according to the loss of root exudates and dead roots. The total amount of root exudates and dead roots is again distributed over depth according to the relative root density profile. The carbon equivalent of the root exudates is transferred to the depth-specific decomposable plant material pool (DPM) of the RothC subroutine because of the expected rapid decomposition of these labile substances by rhizosphere microorganisms. The carbon equivalent of the dead roots is split into the DPM and the resistant plant material (RPM) pool according to the original RothC partitioning factor for incoming plant material of 0.59 and 0.41 (Coleman and Jenkinson 2008), respectively.

For winter wheat and barley, harvest residues are also considered. At the time of harvest, root biomass and 25% of stem biomass is added to the DPM and RPM pool up to a user-specified soil depth (i.e. ploughing depth). Figure 2.1 provides a summary of the carbon cycling in AgroC.

Grassland

The original SUCROS code is not capable of simulating managed grassland, which are characterized by multiple mowing events over the season. Mowing is associated with the transfer of glucose from roots and stubble to the leaves, which allows for a faster compensation of defoliation. The routines implemented in AgroC for the simulation of the above-mentioned processes follow the sink/source approach suggested by Schapendonk et al. (1998) for the grassland productivity model LINGRA.

At prescribed mowing dates, the current green leaf area index LAI_g is set to a fixed post-mowing leaf area index LAI_{post} (in this study we set $LAI_{post} = 0.35$ based on LAI

measurements). The ratio between pre-mowing LAI and post-mowing LAI_{post} is used to compute the respective loss of dry matter biomass:

$$f_{lai} = \frac{LAI_g}{LAI_{post}} \tag{A.17}$$

$$w_{post,i} = \frac{w_{pre,i}}{f_{lai}} \tag{A.18}$$

where f_{lai} (-) is the pre-/post-mowing LAI ratio, w_{pre} (kg DM $[L]^{-2}$) is the biomass prior to mowing, and w_{post} (kg DM $[L]^{-2}$) is the respective biomass after mowing. The index i loops over leaves, stems, and storage organs/inflorescence. At each mowing event, DVS is also reset to a prescribed value of $DVS_{reset} = 0.5$. In order to simulate the transfer of glucose after defoliation, we implemented a glucose storage that is filled between a DVS_{lo} of 0.6 and a DVS_{hi} of 1.0. The rate of glucose storage increase λ_{s+} (kg CH_2O $[L]^{-2}$ $[T]^{-1}$) is computed as a fraction f_{stor} (-) of global net glucose production:

$$\lambda_{s+} = \left(G_{phot} \cdot \frac{T_a}{T_p} - R_{m,c}\right) \cdot f_{stor} \tag{A.19}$$

The part of global net glucose production (= $G_{phot} \cdot T_a/T_p - R_{m,c}$) available for biomass growth and respiration is reduced accordingly by λ_{s+}. The storage fraction is computed in dependence of DVS:

$$f_{stor} = \begin{cases} 0 & DVS \leq DVS_{lo} \\ \frac{f_{stormax}(DVS - DVS_{lo})}{(DVS_{hi} - DVS_{lo})} & \text{for} \quad DVS_{lo} < DVS < DVS_{hi} \\ f_{stormax} & DVS \geq DVS_{hi} \end{cases} \tag{A.20}$$

where $f_{stormax}$ (-) is the user-specified maximum storage fraction. Thus, the glucose storage $S_{stor,t}$ (kg CH_2O $[L]^{-2}$) increases by λ_{s+} until a user-defined maximum value of $S_{stormax}$ (kg CH_2O $[L]^{-2}$) is reached. After that, $S_{stor,t}$ remains constant. After mowing, the dry matter transfer rate λ_{s-} ($[T^{-1}]$) from $S_{stor,t}$ to the shoot is estimated as:

$$\lambda_{s-} = \frac{\log(100)}{t_{stor}} \tag{A.21}$$

where t_{stor} ([T]) is a user-specified time required to reach a value of 1% of the storage at the time of mowing. According to Gonzales et al. (1989) and Prud'homme et al. (1992), the mobilization of carbohydrates in ryegrass is highest during the first 6 days after defoliation and levels out in a second phase that lasts until 29 days after defoliation. In this study, t_{stor} was set to 15 days, which results in a λ_{s-} of 0.31 d^{-1}. Correspondingly, $S_{stor,t}$ is reduced down to a limiting value of zero according to:

$$S_{stor,t+1} = S_{stor,t}\,(1 - \lambda_{s-}) \tag{A.22}$$

The additional dry matter growth rate ΔW_{stor} (kg DM $[L]^{-2}$ $[T]^{-1}$) resulting from the declining $S_{stor,t}$ is added to the dry matter growth rate of the shoot ΔW_{sh} (kg DM $[L]^{-2}$ $[T]^{-1}$), which is the outcome of the photosynthetic activity of the plant. The additional shoot growth rate ΔW_{stor} is computed as:

$$\Delta W_{stor} = \frac{S_{stor,t}\ \lambda_{s-}}{f_{sh}\,(1.46\ f_{lv} + 1.51\ f_{st})} \qquad (A.23)$$

where f_{sh}, f_{lv}, and f_{st} are the dimensionless partitioning factors for shoot, leaves, and stems, respectively. The assimilate requirement coefficients of 1.46 and 1.51 in Equation A.23 have a unit of kg CH_2O kg^{-1} DM (Spitters et al. 1989).

As suggested by Schapendonk et al. (1998), a mechanism was implemented by which the specific leaf area (ha leaf kg^{-1} DM) varies over the season as a function of DVS. Furthermore, a mechanism to distinguish between vegetative and reproductive development of grass was introduced as suggested by Barrett et al. (2004). These two stages of development differ in the productivity of grass and in several major physiological processes that alter the response of the plant to environmental drivers (e.g., Anslow and Green 1967; Leafe et al. 1974; Parsons 1988; Robson et al. 1988).

Tab. A.1: Site-specific soil properties (C_{org}: organic carbon content) and calibrated hydraulic parameters (θ_r: residual water content; θ_s: saturated water content; α: inverse of the bubbling pressure; n: shape parameter; K_s: saturated hydraulic conductivity; van Genuchten 1980).

	soil profile horizons	sand (%)	silt (%)	clay (%)	C_{org} (%)	θ_r ($cm^3\ cm^{-3}$)	θ_s ($cm^3\ cm^{-3}$)	α (cm^{-1})	n (-)	K_s ($cm\ h^{-1}$)
Selhausen	0-15 cm	15.4	67.5	17.1	1.03	0.069	0.504	0.0056	1.68	0.01
	15-33 cm	15.6	67.7	16.6	0.96	0.109	0.504	0.0059	1.92	0.05
	33-57 cm	16.2	63.1	23.1	0.34	0.000	0.463	0.0061	1.28	0.35
	57-120 cm	12.3	64.0	23.7	0.24	0.044	0.441	0.0013	1.69	0.05
Merzen-hausen	0-12 cm	6.4	78.2	15.4	1.0	0.001	0.462	0.0031	1.69	0.30
	12-40 cm	6.4	78.2	15.4	1.0	0.001	0.571	0.0039	1.63	0.41
	40-60 cm	1.0	77.1	21.9	0.4	0.057	0.418	0.0034	1.21	0.64
	60-110 cm	0.5	73.4	26.1	0.3	0.103	0.367	0.0017	1.88	0.13
Rollesbroich	0-5 cm	22.0	60.8	17.2	4.82	0.034	0.443	0.0082	2.83	2.16
	5-14 cm	22.0	60.8	17.2	4.82	0.056	0.380	0.0077	2.84	2.04
	14-34 cm	23.1	59.1	17.8	2.49	0.039	0.379	0.0109	1.68	1.75
	34-60 cm	23.2	59.3	17.5	0.81	0.038	0.340	0.0160	1.33	0.84
	60-100 cm	23.2	59.3	17.5	0.0	0.037	0.375	0.0131	1.06	0.71

Tab. A.2: Selection of most important fitted plant parameters for the calibration of the plant growth module of AgroC. (WW: winter wheat; WB: winter barley; GL: grassland; DVS: development stage; DM: dry matter).

	Selhausen	**Merzenhausen**			**Rollesbroich**
	WW 2009	**WW 2012**	**WW 2013**	**WB 2014**	**GL 2013**
prescribed threshold pressure heads h_0, h_1, h_2, and h_3 for scaling the root water uptake (cm)	-10, -100, -300, -800	-100, -400, -1000, -10000	-100, -400, -1000, -10000	-100, -400, -1000, -10000	-5, -70, -150, -800
specific leaf area of new leaves (ha leaf kg^{-1} DM)	0.0024	0.0024	0.0023	0.0033	0.003
potential CO_2 assimilation rate of a unit leaf area for light saturation (kg CO_2 ha^{-1} leaf h^{-1})	47.0	60.0	53.0	48.0	75.0
initial light use efficiency ((kg CO_2 ha^{-1} leaf h^{-1})(J m^{-2} s^{-1})$^{-1}$)	0.5	0.5	0.5	0.45	0.36
DVS against reduction factor of the maximal light assimilation rate	0.0 1.0 1.0 1.0 2.0 0.4	0.0 1.0 1.0 1.0 2.0 0.5	0.0 1.0 1.0 1.0 2.0 0.4	0.0 1.0 1.0 1.0 2.0 0.3	0.0 1.0 0.4 1.0 1.0 0.9 1.2 0.9 1.5 0.9 1.8 0.9
daily average daytime temperature against reduction factor of the maximal light assimilation rate	0.0 0.05 4.0 0.3 10.0 0.6 15.0 0.8 20.0 1.0 30.0 0.0	0.0 0.01 6.0 0.3 10.0 0.7 17.0 1.0 25.0 0.5 35.0 0.4	0.0 0.05 6.0 0.1 10.0 0.5 20.0 1.0 25.0 0.7 35.0 0.6	0.0 0.6 5.0 0.7 15.0 0.9 18.0 1.0 25.0 0.6 40.0 0.3	0.0 0.4 5.0 0.6 10.0 1.0 15.0 1.0 20.0 0.8 35.0 0.2
DVS against fraction of dry matter allocated to the shoot	0.0 0.33 0.1 0.33 0.2 0.42 0.4 0.67 0.5 0.78 0.7 0.85 0.9 0.92 1.2 1.0 2.0 1.0	0.0 0.24 0.1 0.24 0.2 0.33 0.4 0.58 0.5 0.64 0.7 0.72 0.9 0.80 1.5 0.91 2.0 1.0	0.0 0.24 0.1 0.24 0.2 0.33 0.4 0.58 0.5 0.64 0.7 0.72 0.9 0.80 1.5 0.91 2.0 1.0	0.0 0.34 0.51 0.44 0.72 0.84 1.7 0.99 2.0 1.00	0.0 0.62 0.2 0.52 0.4 0.49 0.7 0.57 1.0 0.64 1.3 0.47 2.0 0.55

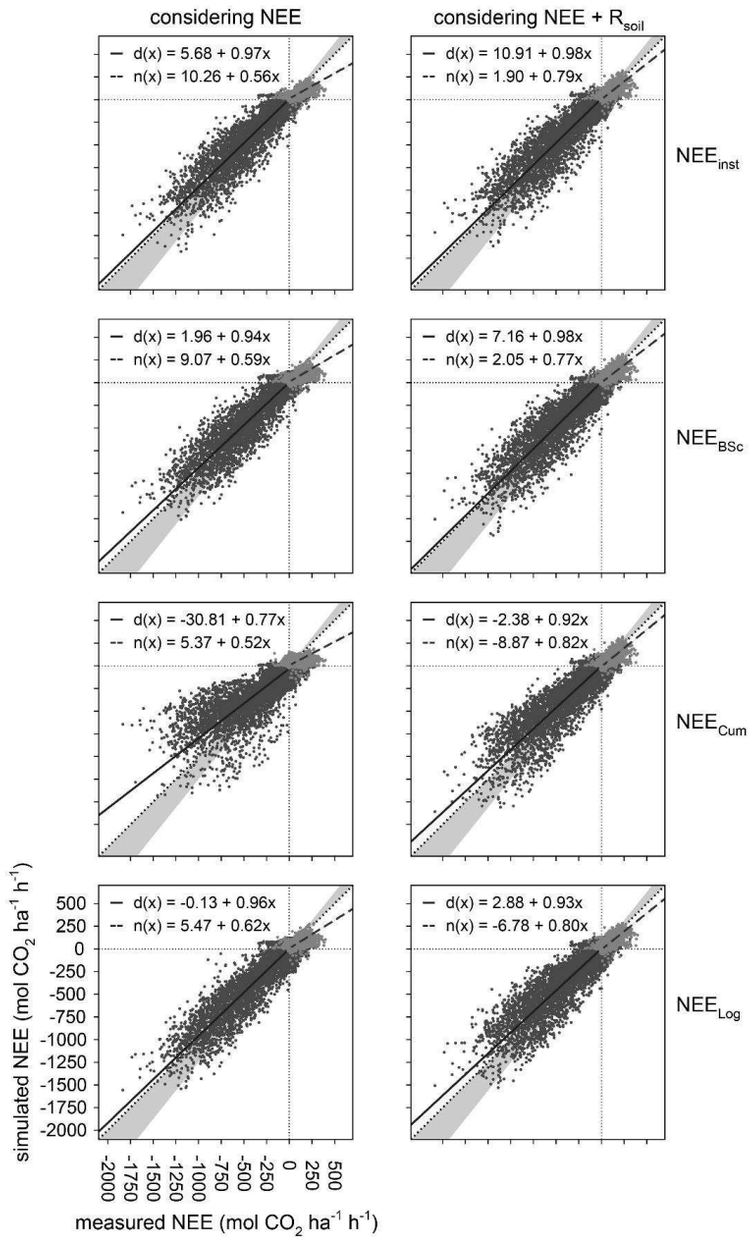

Fig. A.1: Correlations between observed and simulated net ecosystem exchange (NEE) for all optimization strategies at test site Merzenhausen. Reduced major axis regression was derived for each strategy distinguished between day- (d) and nighttime (n) CO_2 fluxes, whereat nighttime was designated to a measured global radiation lower than 20 W m^{-2}. For description of optimization strategies see Chapter 2.

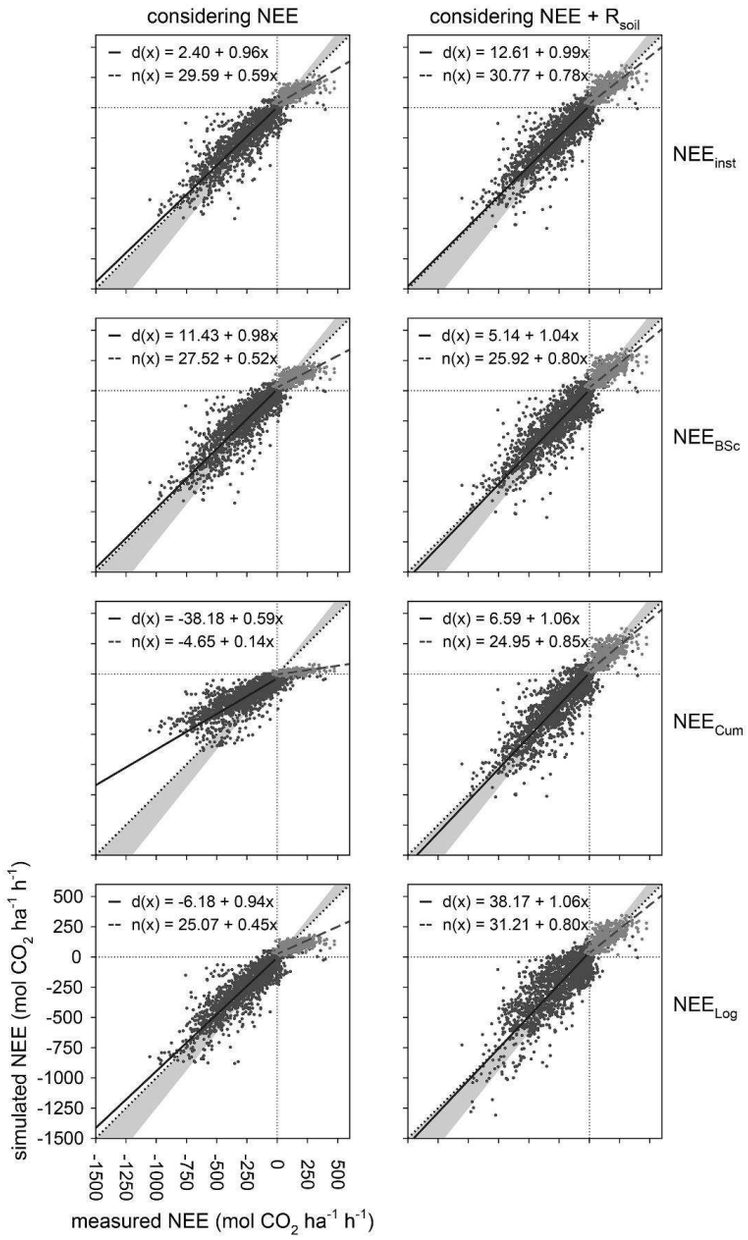

Fig. A.2: Correlations between observed and simulated net ecosystem exchange (NEE) for all optimization strategies at test site Rollesbroich. Reduced major axis regression was derived for each strategy distinguished between day- (d) and nighttime (n) CO_2 fluxes, whereat nighttime was designated to a measured global radiation lower than 20 W m^{-2}. For description of optimization strategies see Chapter 2.

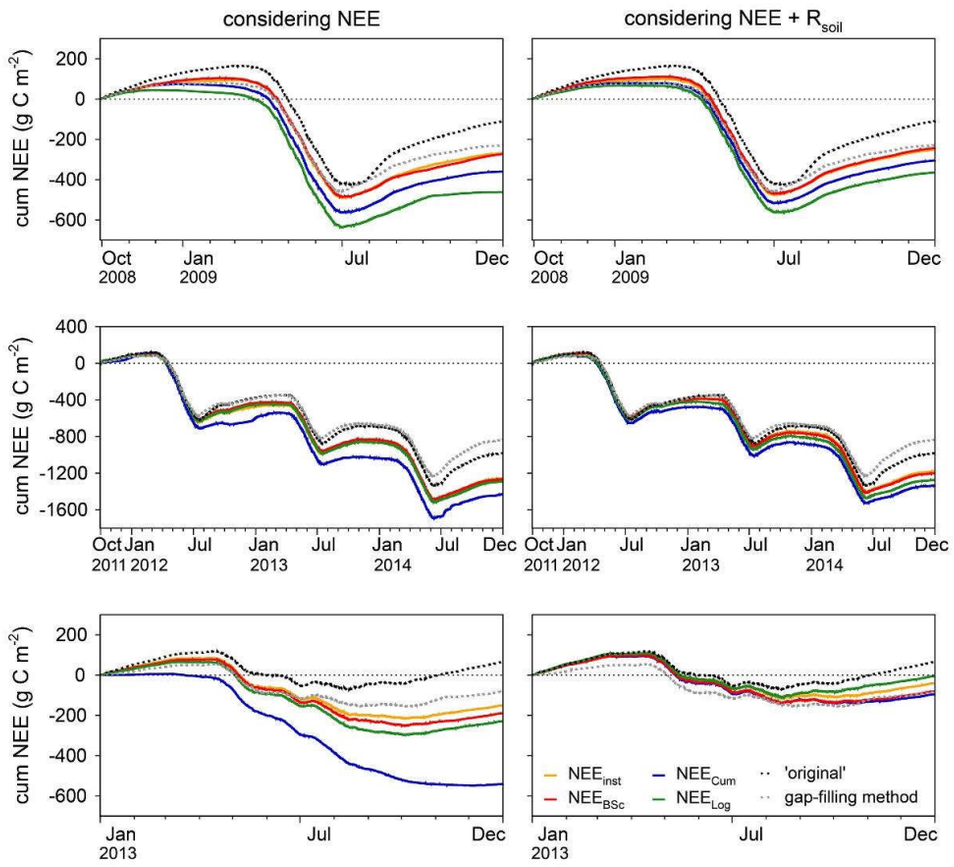

Fig. A.3: Cumulated net ecosystem exchange (cum NEE) over simulation time period, calculated in "gap-filling mode", for each optimization strategy, for the simulation without calibration to NEE ('original'), and for the gap-filling method after Reichstein et al. (2005) (gap-filling method) in Selhausen (*top*), Merzenhausen (*middle*), and Rollesbroich (*bottom*). For description of optimization strategies see Chapter 2.

APPENDIX B

B. Source Partitioning Based on High Frequency Data

Scanlon and Sahu (2008) and Scanlon and Kustas (2010) provided a system of equations for the source partitioning of H_2O and CO_2 fluxes including following essential equation, which was further modified and reported by Palatella et al. (2014, Equation 29, page 331) as follows:

$$\mathrm{WUE} = \frac{\overline{w'c'}}{\overline{w'q'}} \frac{1 - \rho^2_{c_p' c_r'} + \sqrt{\rho^2_{c_p' c_r'} \left(\rho^2_{c_p' c_r'} - 1 + \frac{\mathrm{WUE}^2 \, \sigma^2_{q'}}{\sigma^2_{c_p'}} \right)}}{1 - \rho^2_{c_p' c_r'} \pm \sqrt{\rho^2_{c_p' c_r'} \left(\rho^2_{c_p' c_r'} - 1 + \frac{\sigma^2_{c'}}{\sigma^2_{c_p'}} \right)}} \qquad \text{(B.1)}$$

where WUE is the water use efficiency on leaf-level (defined as negative), which can be estimated with Equation 3.4, $\overline{w'q'}$ and $\overline{w'c'}$ are the measured H_2O and CO_2 flux of the regarded time period, ρ and σ^2 are the correlation and variance of the indicated scalars (subscribes q, c, c_p, c_r represent H_2O, CO_2, photosynthesis, and R_{soil}, respectively). The two parameters $\rho_{cp'cr'}$ and $\sigma_{cp'}^2$ in the equation are the only unknowns and the denominator implies two possible solutions, for what Palatella et al. (2014) implemented a globally convergent Newton's method searching for plausible solutions. As follows, we manipulated Equation B.1 further to solve for $\sigma_{cp'}^2 = f(\rho_{cp'cr'})$, leaving only $\rho_{cp'cr'}$ as unknown parameter, so that we could do without the numerical routine.

$$\mathrm{A} = \mathrm{WUE}^2 \left(\frac{\overline{w'q'}}{\overline{w'c'}} \right)^2 \left(2\,\rho^4_{c_p' c_r'} - 3\,\rho^2_{c_p' c_r'} + 1 \right) - \mathrm{WUE} \left(\frac{\overline{w'q'}}{\overline{w'c'}} \right) \left(2\,\rho^4_{c_p' c_r'} - 4\,\rho^2_{c_p' c_r'} + 2 \right) - \rho^2_{c_p' c_r'} + 1$$

$$\mathrm{B} = 2\,\mathrm{WUE} \left(\frac{\overline{w'q'}}{\overline{w'c'}} \right) \left(\mp\,\mathrm{WUE} \left(\frac{\overline{w'q'}}{\overline{w'c'}} \right) \rho^2_{c_p' c_r'} \pm \mathrm{WUE} \left(\frac{\overline{w'q'}}{\overline{w'c'}} \right) \pm \rho^2_{c_p' c_r'} \mp 1 \right)$$

Only one branch of this equation is necessary, because B is always squared in the following equations. Both branches give the same solution for B^2.

$$\mathrm{C} = \mathrm{WUE}^2 \, \rho^2_{c_p' c_r'} \left(\left(\frac{\overline{w'q'}}{\overline{w'c'}} \right)^2 \sigma^2_{c'} - \sigma^2_{q'} \right)$$

$$\mathrm{D} = 2\,\frac{\mathrm{A\,C}}{\mathrm{B}^2} - \sigma^2_{c'}\,\rho^2_{c_p' c_r'}$$

$$\mathrm{E} = \frac{\mathrm{A}^2}{\mathrm{B}^2} - \rho^4_{c_p' c_r'} + \rho^2_{c_p' c_r'}$$

$$\sigma^2_{c_p'_{1,2}} = -\frac{1}{2}\frac{\mathrm{D}}{\mathrm{E}} \pm \sqrt{\left(\frac{1}{2}\frac{\mathrm{D}}{\mathrm{E}} \right)^2 - \frac{\mathrm{C}^2}{\mathrm{B}^2\,\mathrm{E}}} \qquad \text{(B.2)}$$

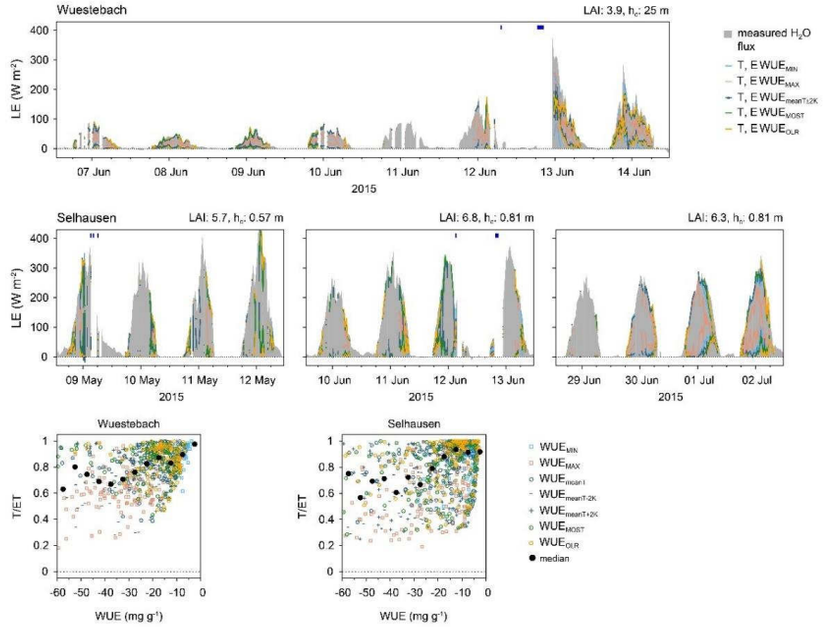

Fig. B.1: Source partitioning results of the approach after Scanlon and Kustas (2010) for H_2O fluxes with various water use efficiency (WUE) inputs (see Chapter 3 for description) at the two study sites Wüstebach (forest; *top*) and Selhausen (cropland; *bottom*) for varying time periods (LE: latent heat flux; ET: evapotranspiration; T: transpiration; E: evaporation; LAI: leaf area index; h_c: canopy height; *blue bars*: precipitation events).

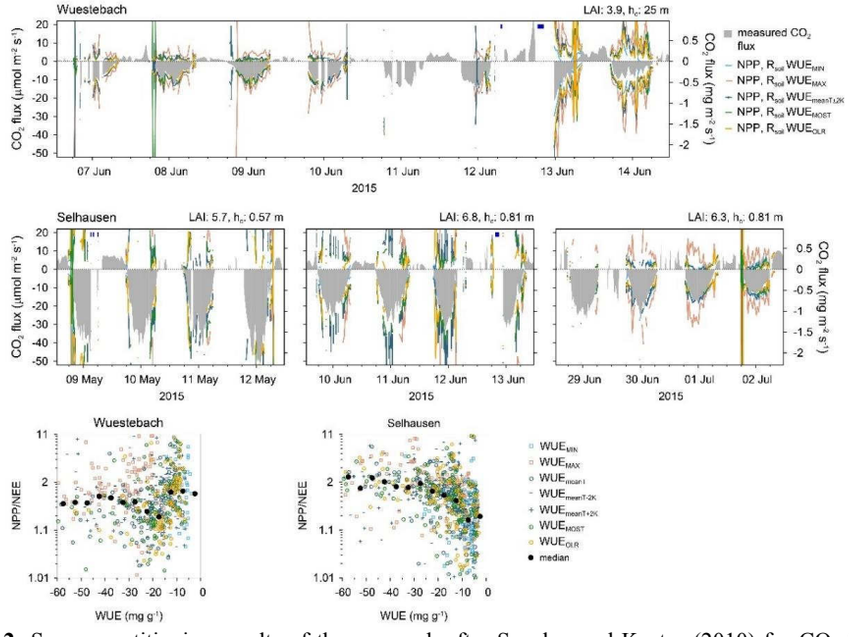

Fig. B.2: Source partitioning results of the approach after Scanlon and Kustas (2010) for CO_2 fluxes with various water use efficiency (WUE) inputs (see Chapter 3 for description) at the two study sites Wüstebach (forest; *top*) and Selhausen (cropland; *bottom*) for varying time periods (NEE: net ecosystem exchange; NPP: net primary production; R_{soil}: soil respiration; LAI: leaf area index; h_c: canopy height; *blue bars*: precipitation events).

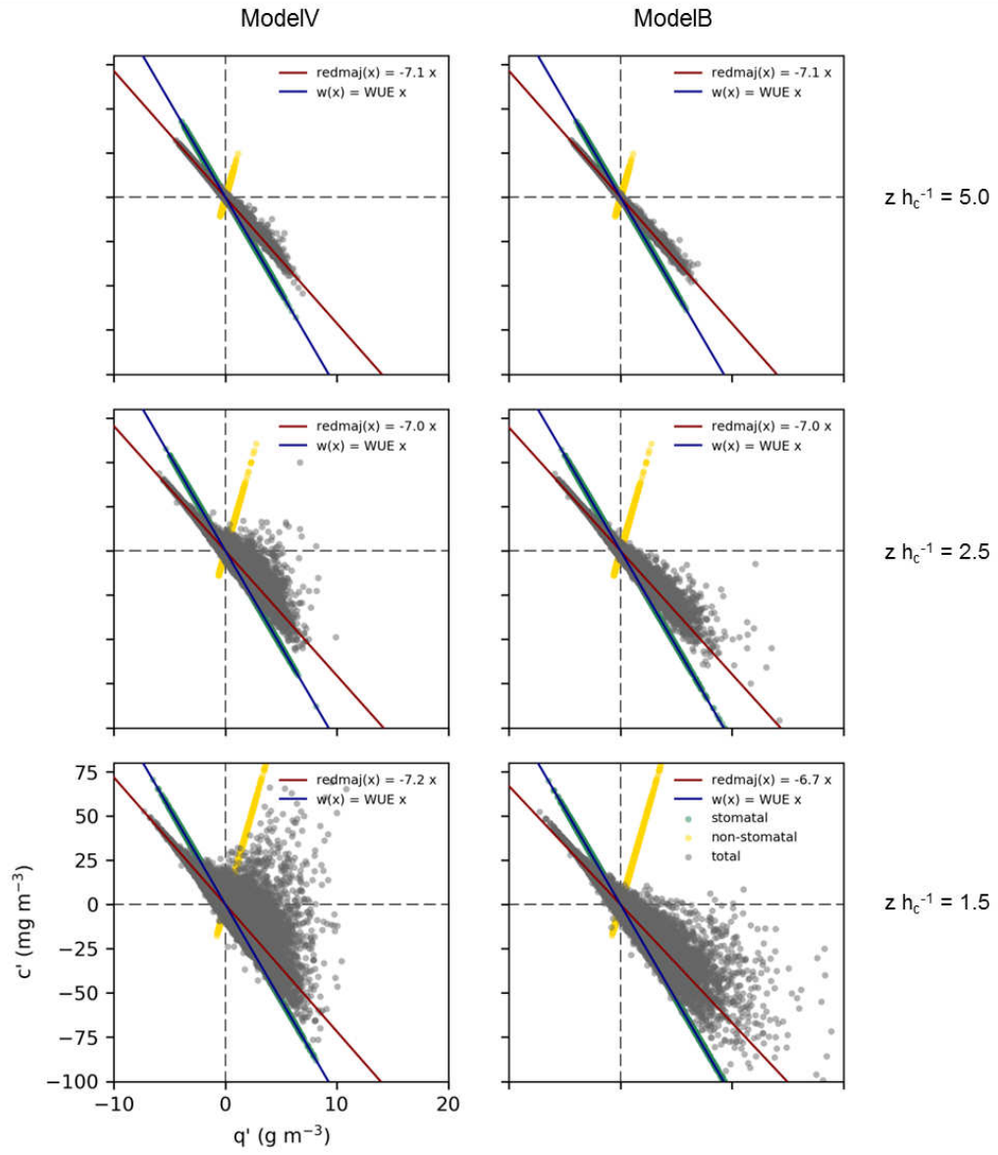

Fig. B.3: Examples of sampled synthetic high frequency data of H_2O (q') and CO_2 fluctuations (c') for the crop canopy in different 'measurement' heights and for the two sink-source-distributions ModelV (*left*) and ModelB (*right*) each with the strong soil source. In the LES-derived data it could be differentiated between scalars originating from stomatal (*green dots*) and non-stomatal (*yellow dots*) processes. The *blue line* presents the water use efficiency (WUE) and the *red line* the reduced major axis regression between total q' and c' (h_c: canopy height; z: height above soil surface).

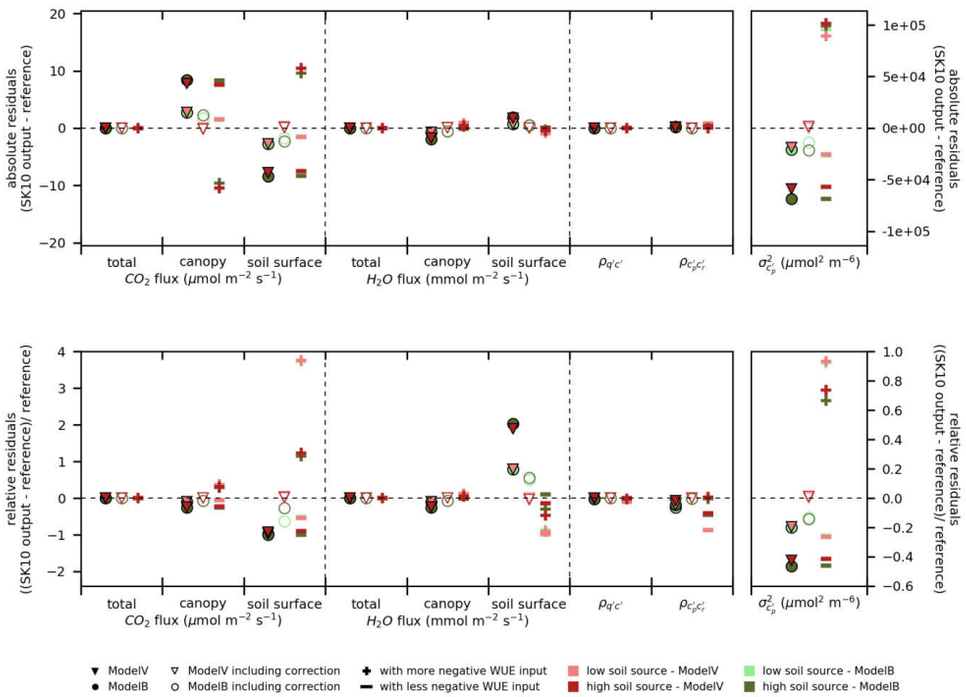

Fig. B.4: Absolute (*top*) and relative (*bottom*) residuals between H_2O and CO_2 flux components, $\rho_{q'c'}$, $\rho_{c_p'c_r'}$, and $\sigma_{c_p}^2$ resulting from LES scaled with the four variations of sink-source-distributions (ModelV or ModelB; low or high soil source) and the partitioning results of the approach after Scanlon and Kustas (2010; SK10) at a 'measurement' height of 2.5 canopy heights for the crop canopy. Shown are results of the partitioning procedure i) including correct water use efficiency (WUE) input known from LES, but without the correction of the transfer assumption (*filled markers*), ii) including correct WUE and corrected transfer assumption (*non-filled markers*), and iii) with corrected transfer assumption, but with a changed WUE of ±24% (*plus and minus signs*).

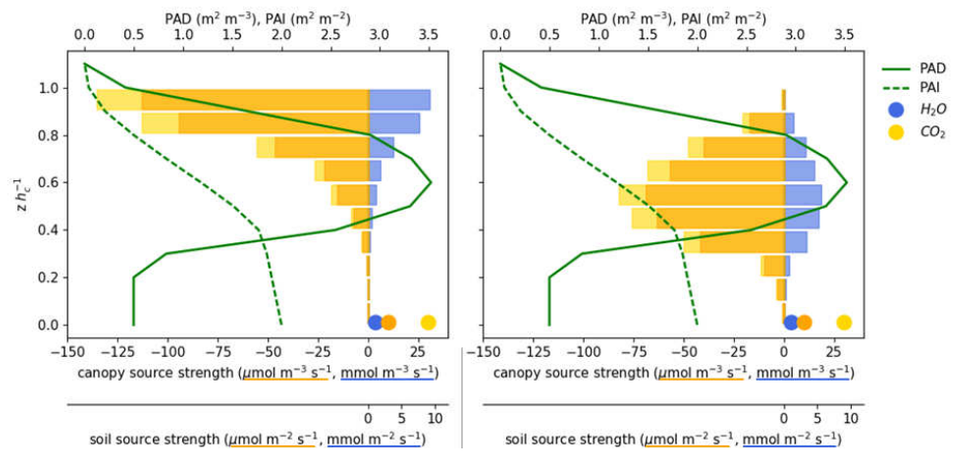

Fig. B.5: Vertical profiles of the forest plant area density (PAD), cumulative plant area index (PAI), and variations of sink-source-distributions for H_2O and CO_2 used to scale the LES scalar fields (*left*: ModelV, after Sellers et al. 1992; *right*: ModelB, after Ney et al. 2017), each with ten canopy sinks/sources (*bars*) and one soil source (*circle*). For CO_2, two different soil sources and accordingly differing canopy sinks were used, in which the flux at canopy top for each distribution is the same.

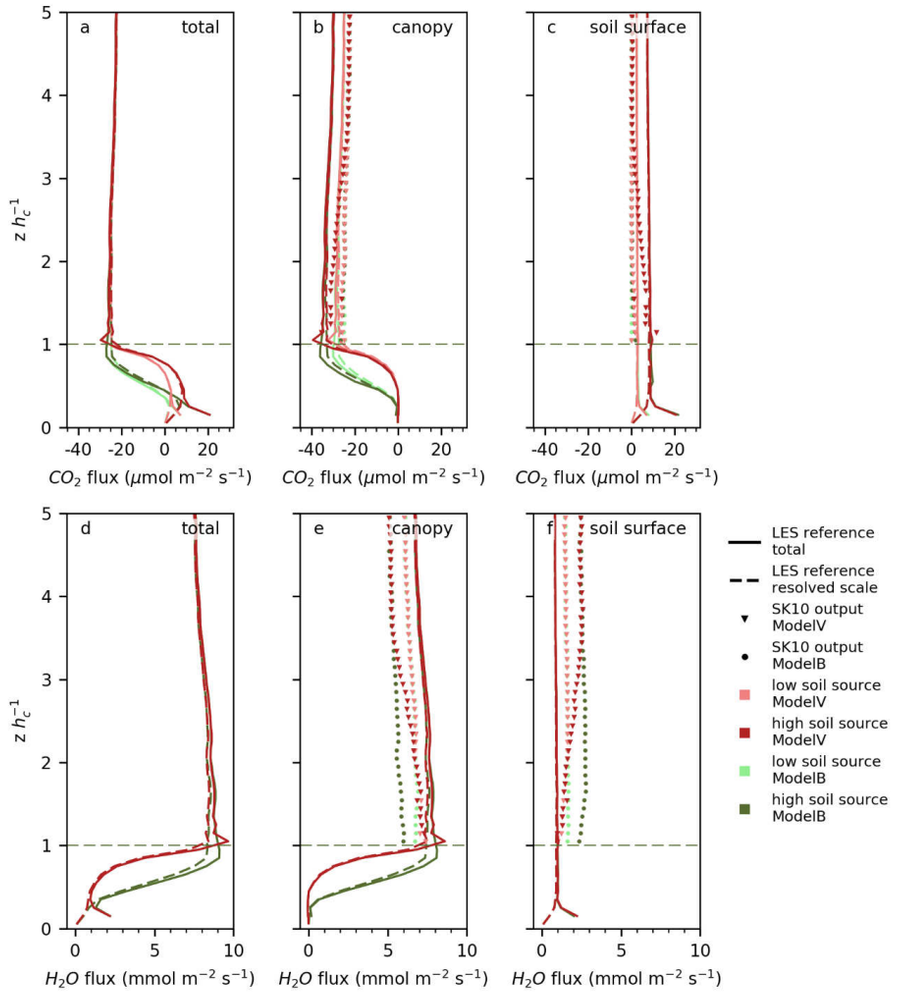

Fig. B.6: Vertical profiles of H_2O and CO_2 flux, and their components resulting from LES scaled with the four variations of sink-source-distributions (ModelV or ModelB; low or high soil source) for the forest canopy. Also shown are the partitioning results of the approach after Scanlon and Kustas (2010; SK10) for each grid height.

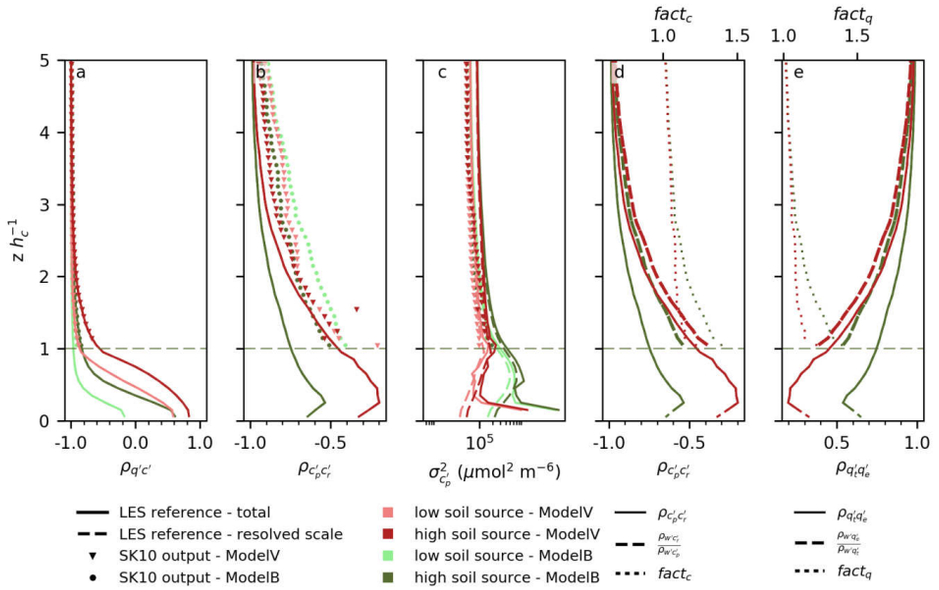

Fig. B.7: a)-c) Vertical profiles of $\rho_{q'c'}$, $\rho_{c_p'c_r'}$, and $\sigma_{c_p}^2$ resulting from LES scaled with the four variations of sink-source-distributions (ModelV or ModelB; low or high soil source) for the forest canopy (*lines*), compared to results of the approach after Scanlon and Kustas (2010; SK10) (*dots*). d)-e) Comparison of the two sides of Equation 3.2 and 3.3 checking the transfer assumption and corresponding correction factors ($fact_q$, $fact_c$, defined in Equation 3.5 and 3.6).

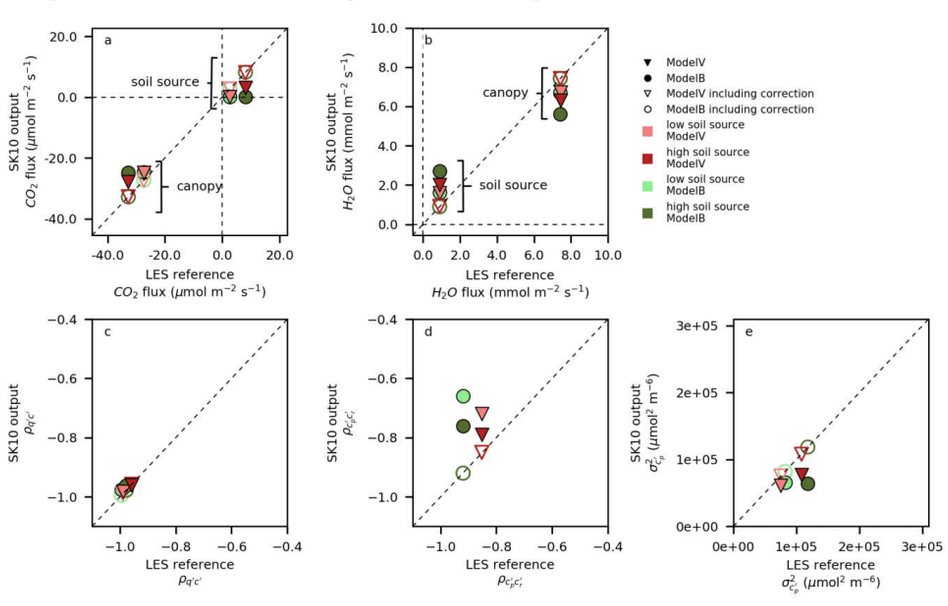

Fig. B.8: Comparison of H_2O and CO_2 flux components, $\rho_{q'c'}$, $\rho_{c_p'c_r'}$, and $\sigma_{c_p}^2$ resulting from LES scaled with the four variations of sink-source-distributions (ModelV or ModelB; low or high soil source) and the partitioning results of the approach after Scanlon and Kustas (2010; SK10) at a 'measurement' height of 2.5 canopy heights for the forest canopy. Shown are results of the partitioning procedure without and with correction of the transfer assumption.

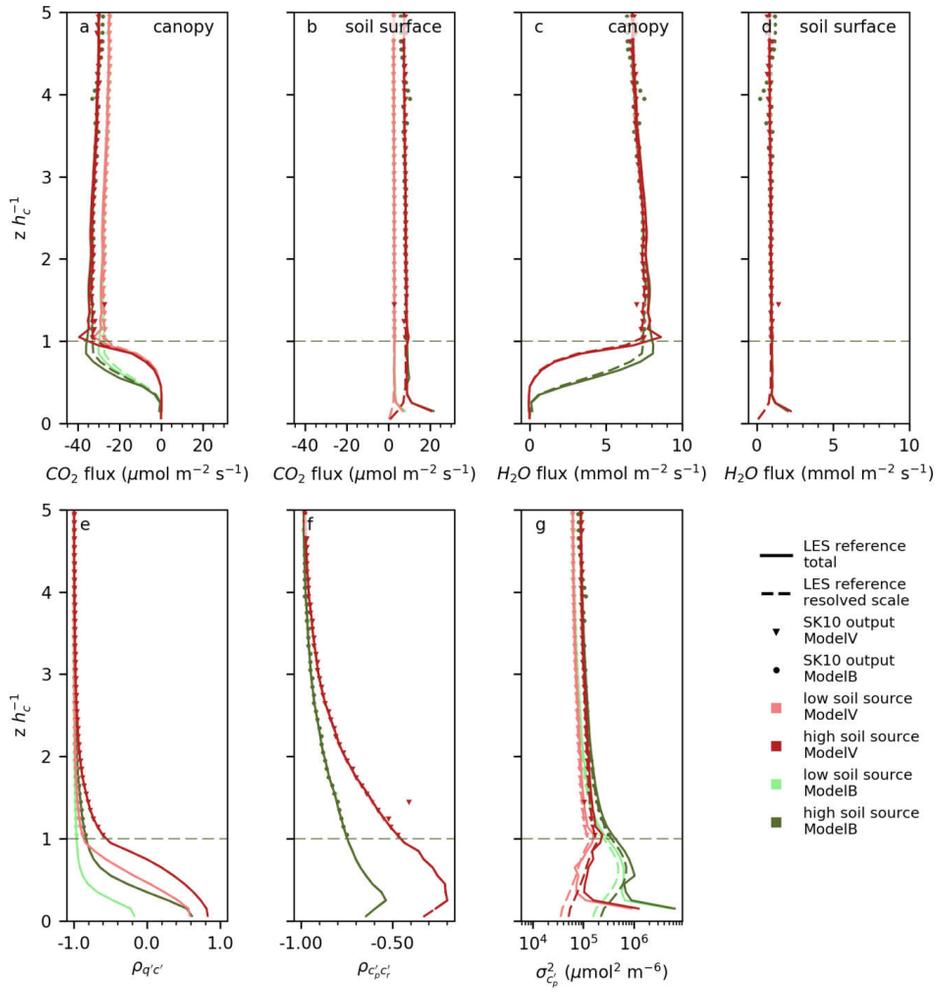

Fig. B.9: Vertical profiles of H_2O and CO_2 flux components, $\rho_{q'c'}$, $\rho_{c_p'c_r'}$, and $\sigma_{c_p}^2$ resulting from LES scaled with the four variations of sink-source-distributions (ModelV or ModelB; low or high soil source) for the forest canopy. Also, the partitioning results of the approach after Scanlon and Kustas (2010; SK10) including the correction of the transfer assumption are shown for each grid height.

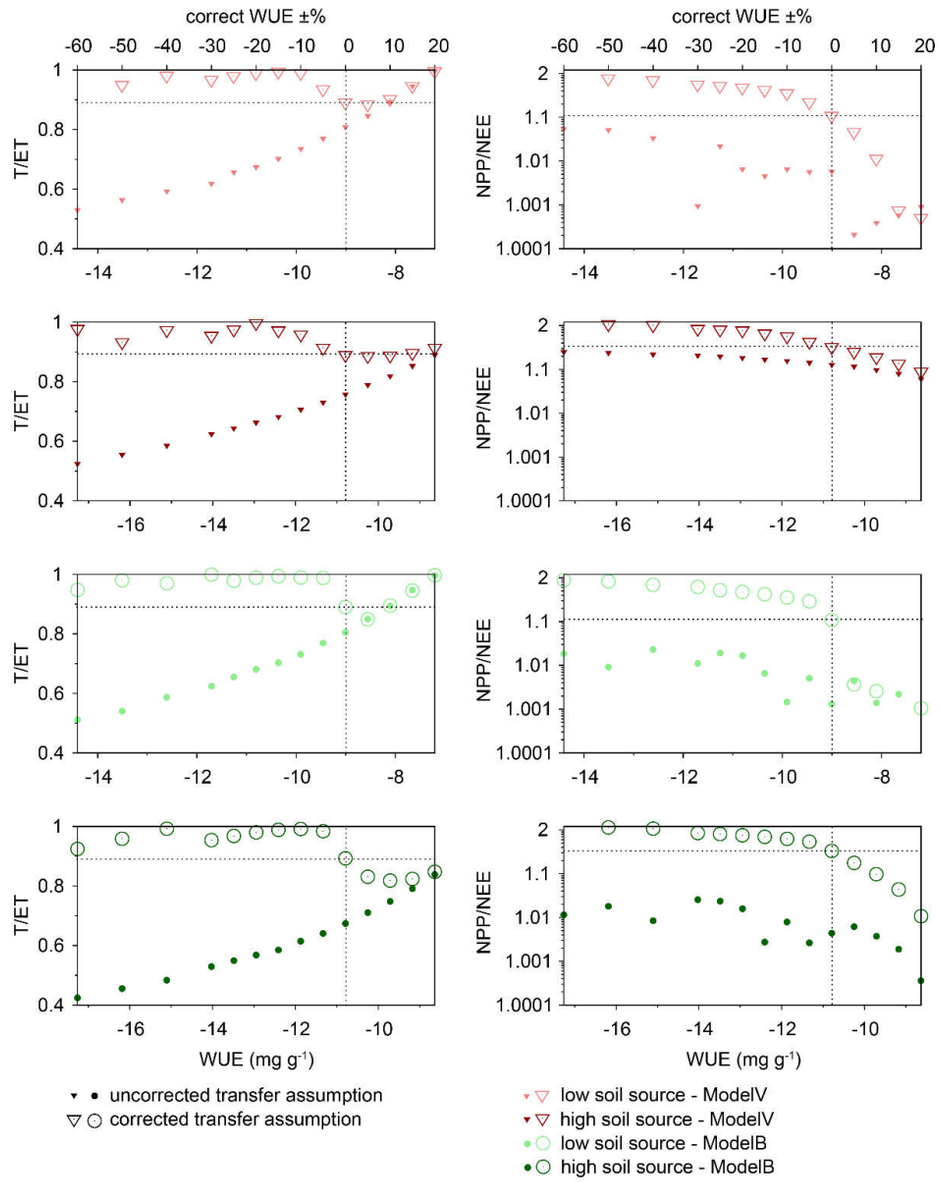

Fig. B.10: Results of partitioning fractions for H_2O (T/ET, *left*) and CO_2 (NPP/NEE, *right*) fluxes in relation to the input water use efficiency (WUE). The source partitioning approach after Scanlon and Kustas (2010) was applied to synthetic high frequency data from LES scaled with the four variations of sink-source-distributions (ModelV or ModelB; low or high soil source) at a 'measurement' height of 2.5 canopy heights for the forest canopy with corrected and uncorrected transfer assumption. The true known partitioning factors and WUE input are indicated by the *dashed lines*.

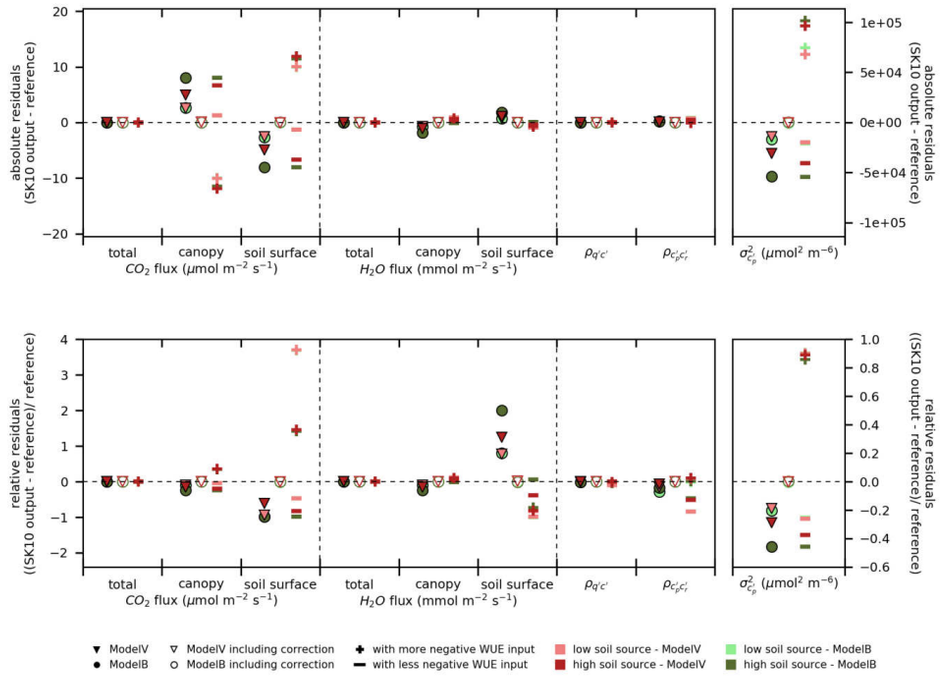

Fig. B.11: Absolute (*top*) and relative (*bottom*) residuals between H_2O and CO_2 flux components, $\rho_{q'c'}$, $\rho_{c_p'c_r'}$, and $\sigma_{c_p}^2$ resulting from LES scaled with the four variations of sink-source-distributions (ModelV or ModelB; low or high soil source) and the partitioning results of the approach after Scanlon and Kustas (2010; SK10) at a 'measurement' height of 2.5 canopy heights for the forest canopy. Shown are results of the partitioning procedure i) including correct water use efficiency (WUE) input known from LES, but without the correction of the transfer assumption (*filled markers*), ii) including correct WUE and corrected transfer assumption (*non-filled markers*), and iii) with corrected transfer assumption, but with a changed WUE of ±24% (*plus and minus signs*).

APPENDIX C

C. Study Sites Comparison

Tab. C.1: Count of half-hourly time steps during daylight (CoD) per considered time period for each study site, corresponding relative fractions of CoD of high-quality (HQ) and relative fractions of these HQ-time steps with a partitioning solution for each method version. *Green* (*red*) *lettering* indicates the highest (lowest) fraction of solutions for each site. *Green* (*red*) *cell filling* indicates the highest (lowest) fraction for each method version.

method	site time period	CoD	rel CoD used (HQ)	rel HQ with partitioning solution	site time period	CoD	rel CoD used (HQ)	rel HQ with partitioning solution
SK10 WUE$_{meanT}$				84.4				26.2
SK10 WUE$_{MOST}$			91.8	82.1			84.8	34.5
SK10 WUE$_{OLR}$	**LO_FR**	231		65.6	**DI_CL_MA_06**	99		23.8
TH08 CV Q1, REA Q1	08.-14.07.2003			99.4	14.-16.06.2007			98.4
TH08 CV H, REA H			68.0	86.0			63.6	82.5
TH08 CV GMM				57.3				55.6
SK10 WUE$_{meanT}$				75.7				90.4
SK10 WUE$_{MOST}$			89.2	76.2			97.9	88.3
SK10 WUE$_{OLR}$	**HH_FR**	231		74.8	**DI_CL_MA_07**	96		77.7
TH08 CV Q1, REA Q1	03.-09.07.2016			100.0	14.-16.07.2007			98.7
TH08 CV H, REA H			59.7	55.8			78.1	50.7
TH08 CV GMM				48.6				48.0
SK10 WUE$_{meanT}$				80.6				95.3
SK10 WUE$_{MOST}$			78.0	78.8			94.5	94.2
SK10 WUE$_{OLR}$	**WU_FR**	218		70.6	**DI_CL_MA_08**	91		89.5
TH08 CV Q1, REA Q1	18.-24.05.2015			100.0	04.-06.08.2007			100.0
TH08 CV H, REA H			55.5	74.4			80.2	45.2
TH08 CV GMM				48.8				49.3
SK10 WUE$_{meanT}$				88.3				57.3
SK10 WUE$_{MOST}$			92.8	91.7			92.7	57.3
SK10 WUE$_{OLR}$	**WA_FR**	222		89.3	**SE_CL_SB_06**	96		52.8
TH08 CV Q1, REA Q1	04.-10.07.2016			100.0	20.-22.06.2017			98.6
TH08 CV H, REA H			75.2	65.9			76.0	58.9
TH08 CV GMM				46.7				49.3
SK10 WUE$_{meanT}$				33.3				72.9
SK10 WUE$_{MOST}$			84.1	38.4			77.8	71.4
SK10 WUE$_{OLR}$	**LA_FR**	164		56.5	**SE_CL_SB_08**	90		72.9
TH08 CV Q1, REA Q1	24.-30.09.2017			100.0	02.-04.08.2017			100.0
TH08 CV H, REA H			54.9	93.3			62.2	37.5
TH08 CV GMM				57.8				48.2
SK10 WUE$_{meanT}$				95.0				80.6
SK10 WUE$_{MOST}$			84.8	95.0			92.3	81.9
SK10 WUE$_{OLR}$	**MMP_FR**	211		93.3	**SE_CL_SB_09**	78		81.9
TH08 CV Q1, REA Q1	06.-12.06.2014			100.0	04.-06.09.2017			98.3
TH08 CV H, REA H			73.0	70.8			76.9	25.0
TH08 CV GMM				60.4				20.0

(continued)

Tab. C.1 continued:

method	site time period	CoD	rel CoD used (HQ)	rel HQ with partitioning solution	site time period	CoD	rel CoD used (HQ)	rel HQ with partitioning solution
SK10 WUE$_{meanT}$				73.9				56.7
SK10 WUE$_{MOST}$			87.4	75.2			93.8	52.2
SK10 WUE$_{OLR}$	**SC_FR**	175		77.1	**SE_CL_WW**	96		46.7
TH08 CV Q1, REA Q1	01.-07.04.2017			99.3	03.-05.06.2015			98.6
TH08 CV H, REA H			77.7	47.1			77.1	25.7
TH08 CV GMM				39.7				27.0
SK10 WUE$_{meanT}$				21.1				50.6
SK10 WUE$_{MOST}$			91.7	32.7			82.3	51.9
SK10 WUE$_{OLR}$	**RO_GR**	217		28.6	**SE_CL_BA**	96		58.2
TH08 CV Q1, REA Q1	15.-21.07.2013			100.0	27.-29.05.2016			98.5
TH08 CV H, REA H			73.3	53.5			67.7	26.2
TH08 CV GMM				49.1				26.2
SK10 WUE$_{meanT}$				31.3				64.6
SK10 WUE$_{MOST}$			82.1	38.0			91.5	70.8
SK10 WUE$_{OLR}$	**WU_GR**	218		40.8	**SE_CL_IC**	71		73.8
TH08 CV Q1, REA Q1	18.-24.05.2015			100.0	23.-25.09.2016			98.2
TH08 CV H, REA H			58.7	90.6			80.3	35.1
TH08 CV GMM				89.8				24.6
SK10 WUE$_{meanT}$				34.8				
SK10 WUE$_{MOST}$			82.0	36.0				
SK10 WUE$_{OLR}$	**FE_GR**	217		39.9				
TH08 CV Q1, REA Q1	11.-17.07.2015			100.0				
TH08 CV H, REA H			58.5	46.5				
TH08 CV GMM				60.6				

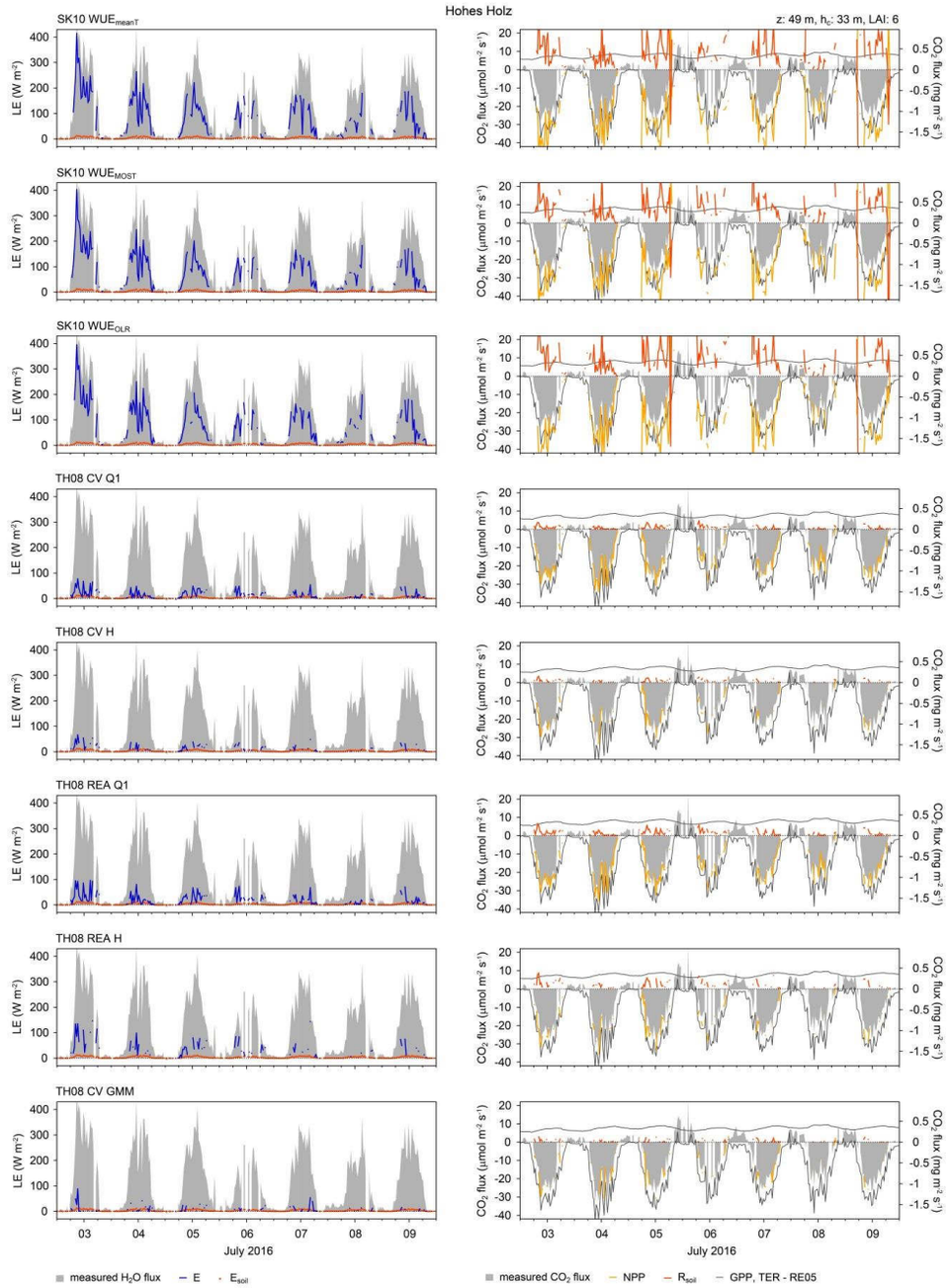

Fig. C.1: Source partitioning results of H_2O (*left*) and CO_2 (*right*) fluxes in half-hourly time steps for the Hohes Holz study site (forest) in Germany and for every method version (see Chapter 4 for description). CO_2 flux estimates by Reichstein et al. (2005; RE05) are also included (LE: latent heat flux; E: evaporation; E_{soil}: estimated evaporation based on Beer's law; GPP: gross primary production; NPP: net primary production; TER: total ecosystem respiration; R_{soil}: soil respiration; z: measurement height; h_c: canopy height; LAI: leaf area index).

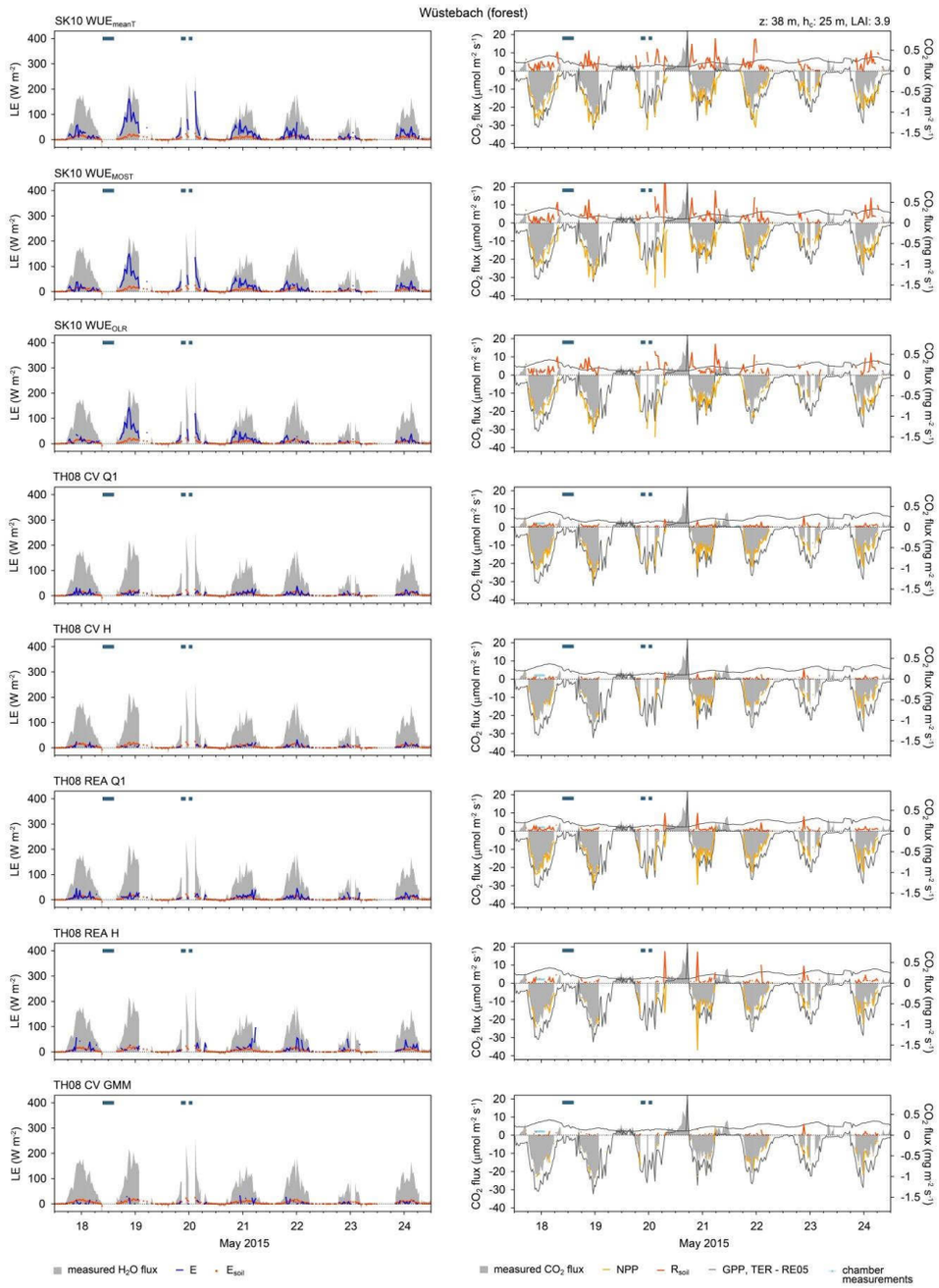

Fig. C.2: Source partitioning results of H_2O (*left*) and CO_2 (*right*) fluxes in half-hourly time steps for the Wüstebach study site (forest) in Germany and for every method version (see Chapter 4 for description). CO_2 flux estimates by Reichstein et al. (2005; RE05) and R_{soil} chamber measurements are also included (LE: latent heat flux; E: evaporation; E_{soil}: estimated evaporation based on Beer's law; GPP: gross primary production; NPP: net primary production; TER: total ecosystem respiration; R_{soil}: soil respiration; z: measurement height; h_c: canopy height; LAI: leaf area index; *blue bars*: precipitation events).

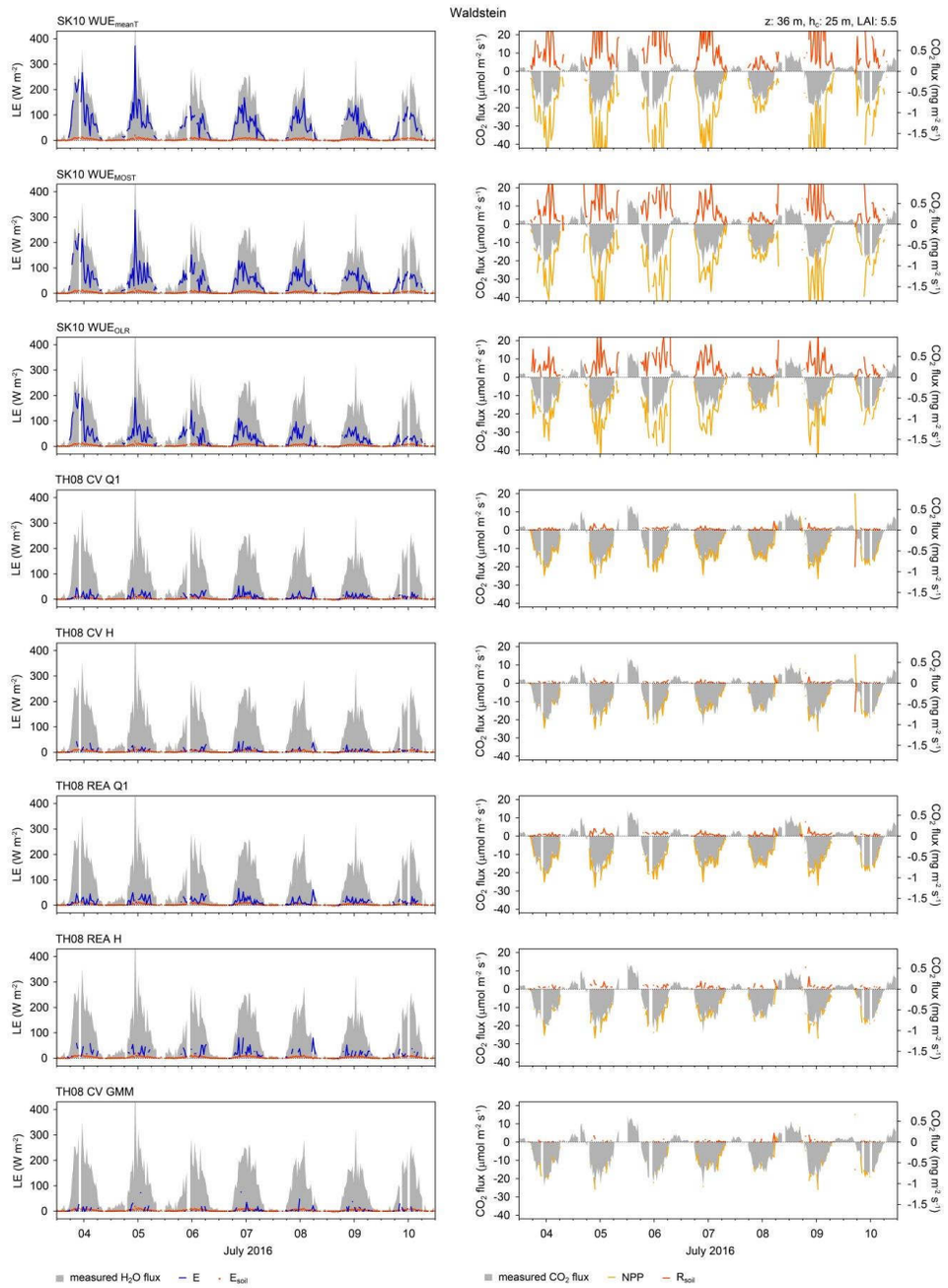

Fig. C.3: Source partitioning results of H_2O (*left*) and CO_2 (*right*) fluxes in half-hourly time steps for the Waldstein study site (forest) in Germany and for every method version (see Chapter 4 for description; LE: latent heat flux; E: evaporation; E_{soil}: estimated evaporation based on Beer's law; NPP: net primary production; R_{soil}: soil respiration; z: measurement height; h_c: canopy height; LAI: leaf area index).

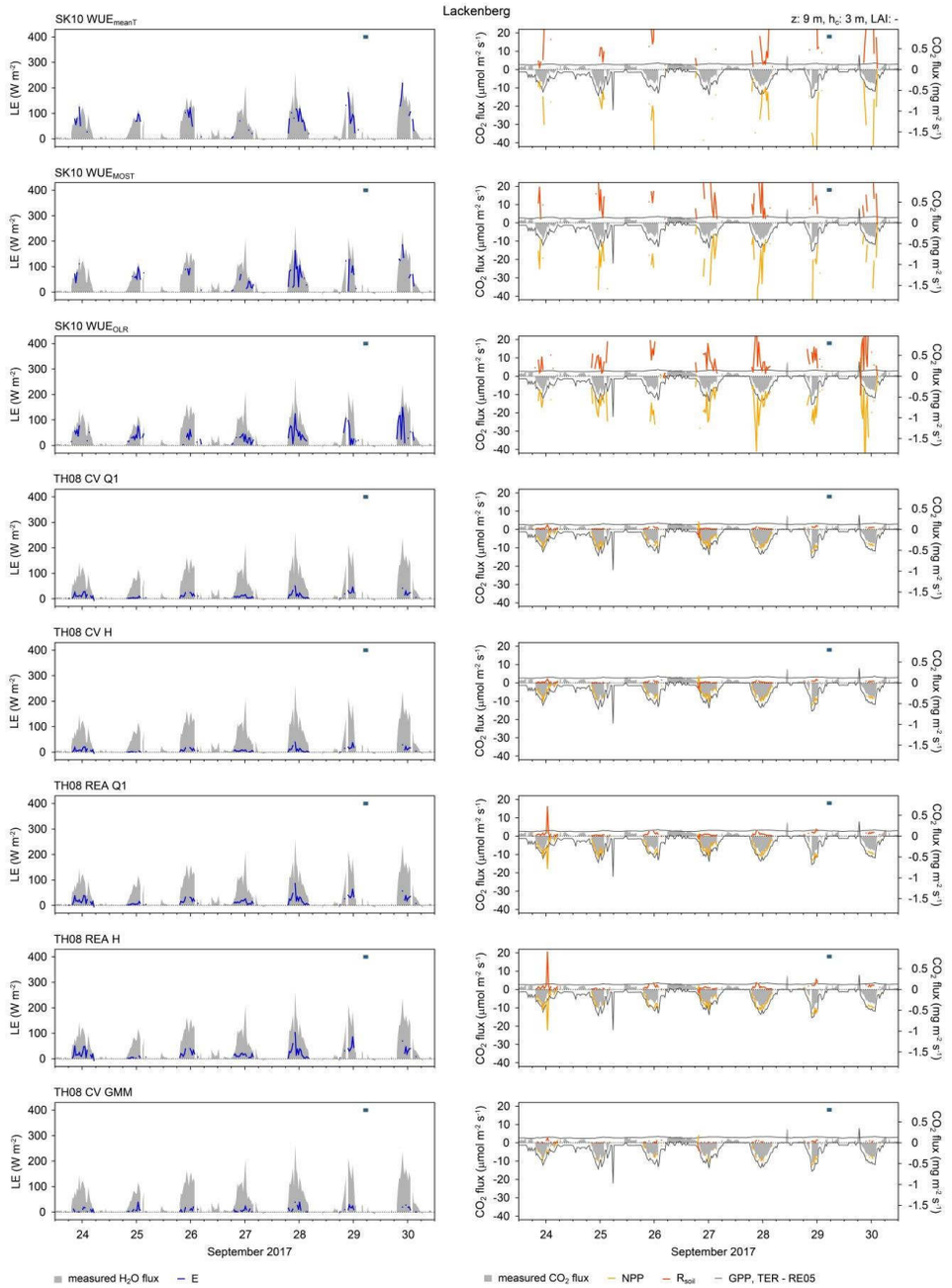

Fig. C.4: Source partitioning results of H_2O (*left*) and CO_2 (*right*) fluxes in half-hourly time steps for the Lackenberg study site (forest) in Germany and for every method version (see Chapter 4 for description). CO_2 flux estimates by Reichstein et al. (2005; RE05) are also included (LE: latent heat flux; E: evaporation; GPP: gross primary production; NPP: net primary production; TER: total ecosystem respiration; R_{soil}: soil respiration; z: measurement height; h_c: canopy height; LAI: leaf area index; *blue bars*: precipitation events).

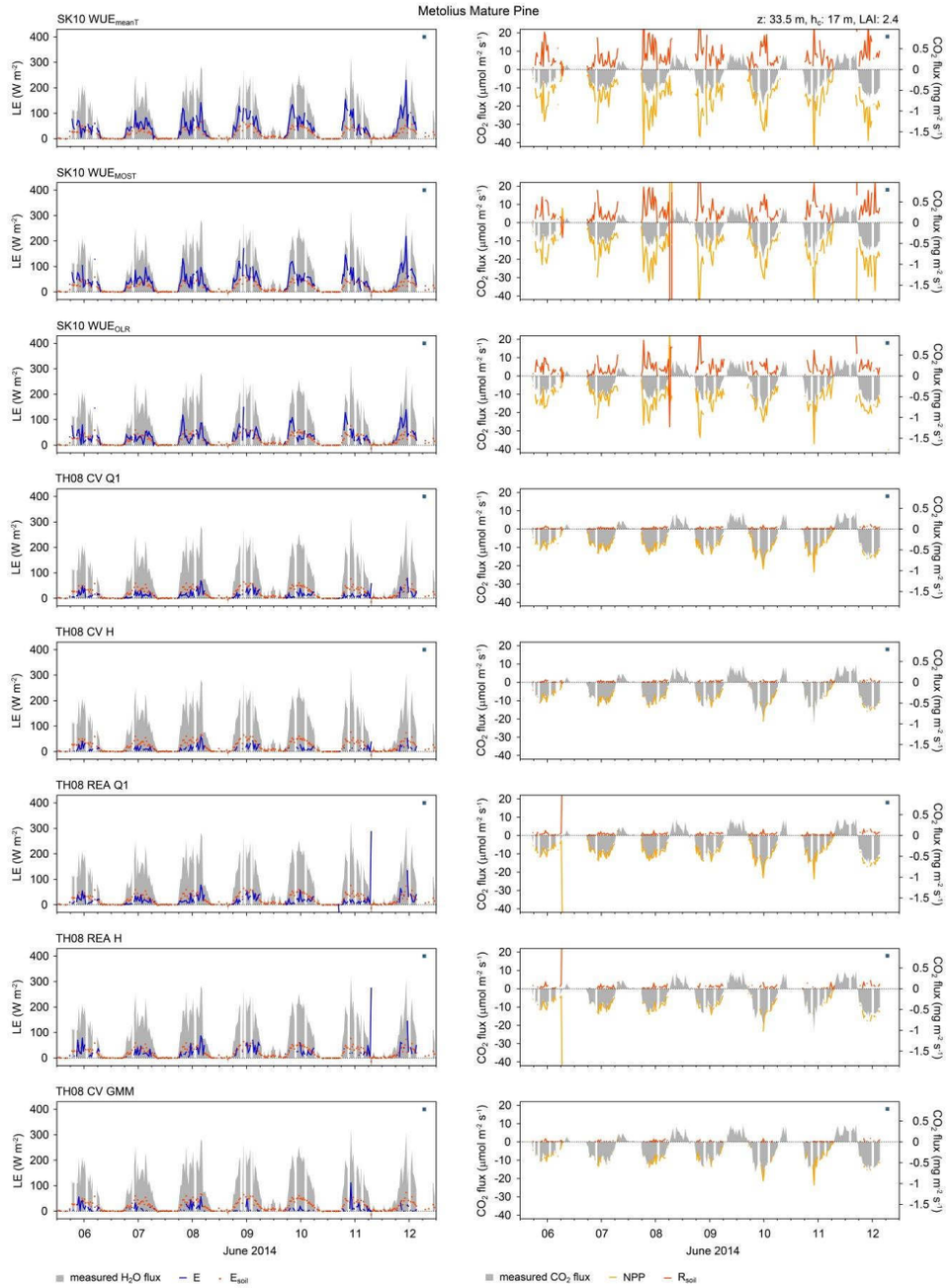

Fig. C.5: Source partitioning results of H_2O (*left*) and CO_2 (*right*) fluxes in half-hourly time steps for the Metolius Mature Pine study site (forest) in United States and for every method version (see Chapter 4 for description; LE: latent heat flux; E: evaporation; E_{soil}: estimated evaporation based on Beer's law; NPP: net primary production; R_{soil}: soil respiration; z: measurement height; h_c: canopy height; LAI: leaf area index; *blue bars*: precipitation events).

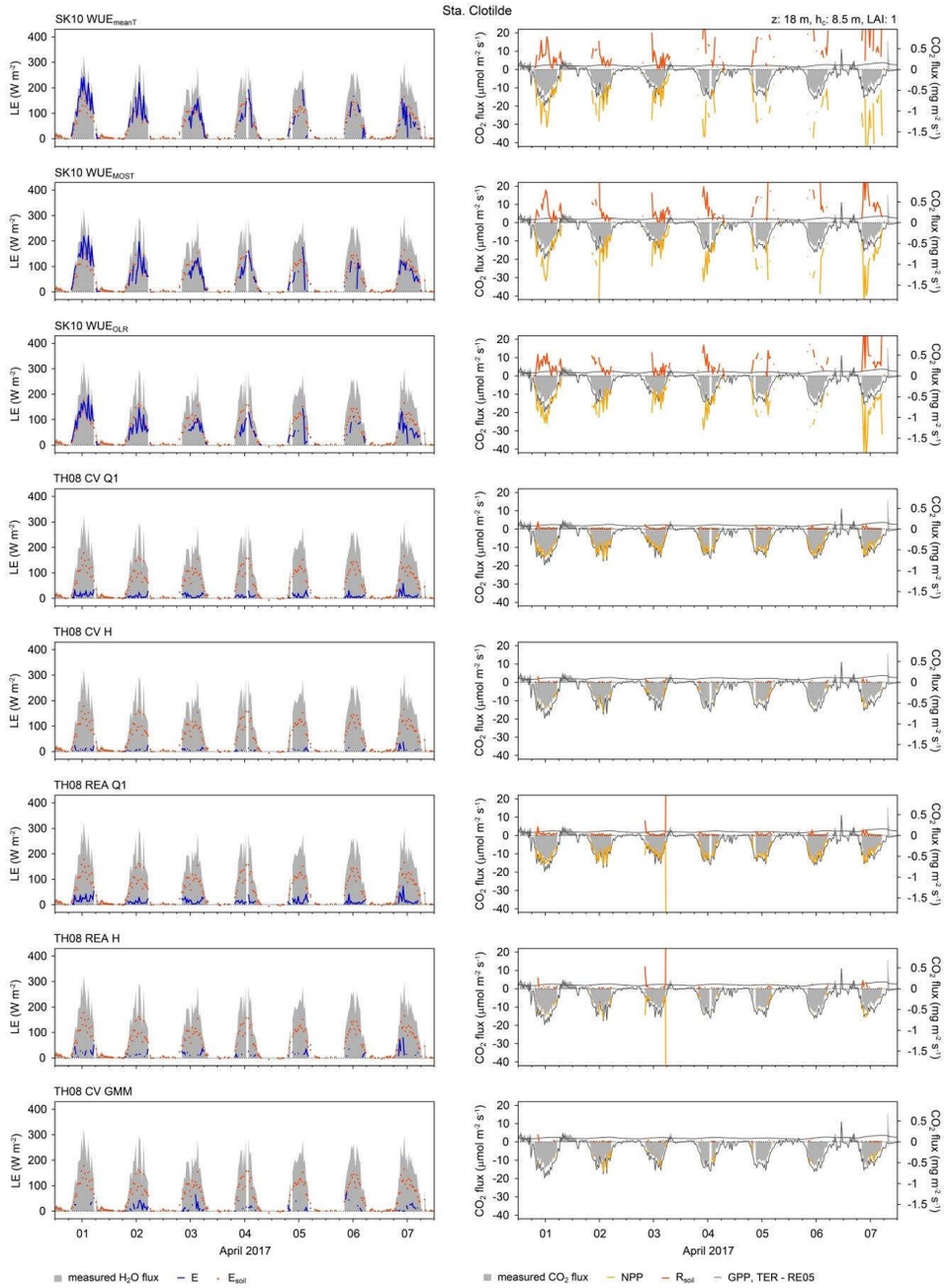

Fig. C.6: Source partitioning results of H_2O (*left*) and CO_2 (*right*) fluxes in half-hourly time steps for the Sta. Clotilde study site (forest) in Spain and for every method version (see Chapter 4 for description). CO_2 flux estimates by Reichstein et al. (2005; RE05) are also included (LE: latent heat flux; E: evaporation; E_{soil}: estimated evaporation based on Beer's law; GPP: gross primary production; NPP: net primary production; TER: total ecosystem respiration; R_{soil}: soil respiration; z: measurement height; h_c: canopy height; LAI: leaf area index).

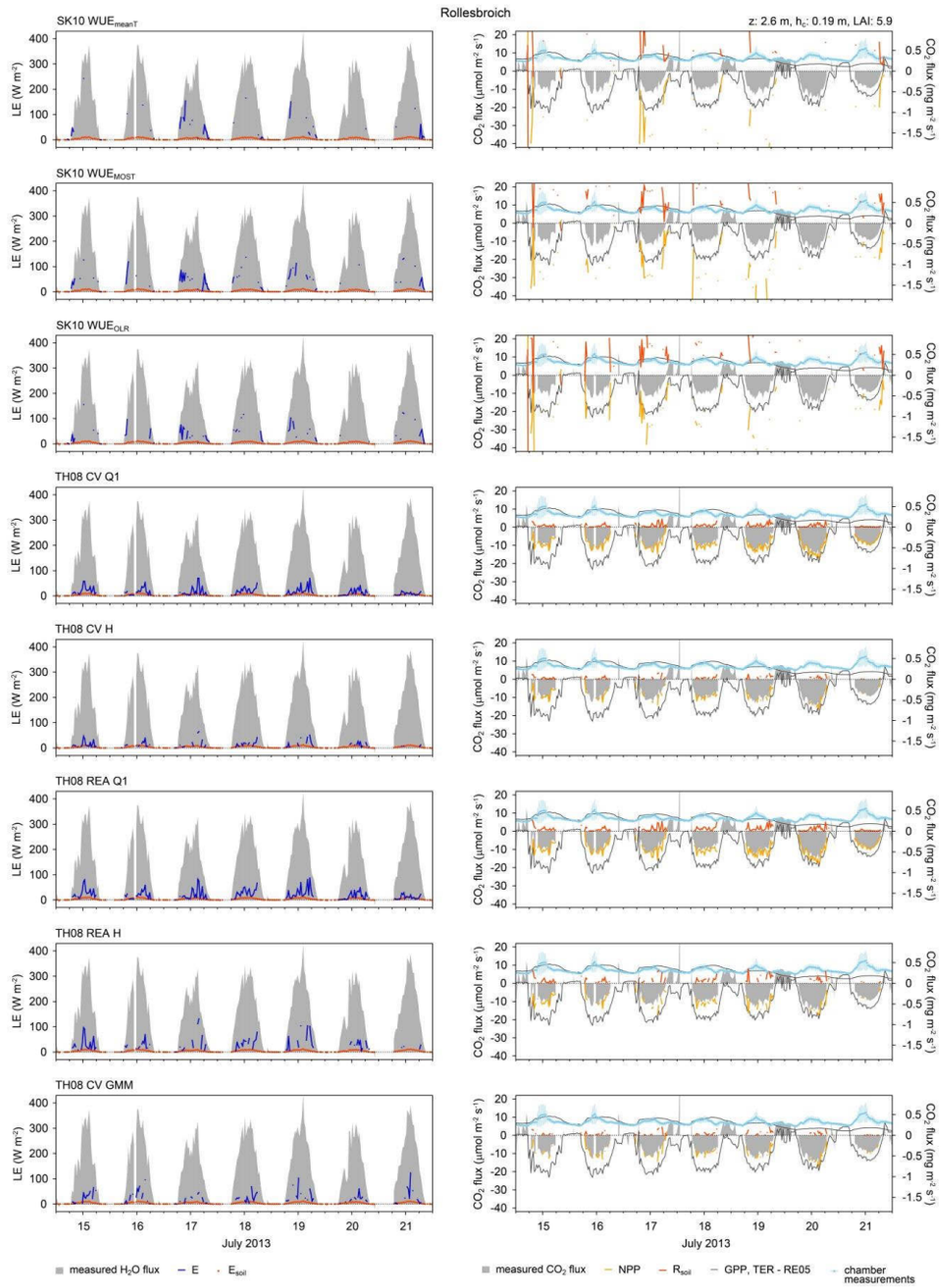

Fig. C.7: Source partitioning results of H_2O (*left*) and CO_2 (*right*) fluxes in half-hourly time steps for the Rollesbroich study site (grassland) in Germany and for every method version (see Chapter 4 for description). CO_2 flux estimates by Reichstein et al. (2005; RE05) and R_{soil} chamber measurements are also included (LE: latent heat flux; E: evaporation; E_{soil}: estimated evaporation based on Beer's law; GPP: gross primary production; NPP: net primary production; TER: total ecosystem respiration; R_{soil}: soil respiration; z: measurement height; h_c: canopy height; LAI: leaf area index).

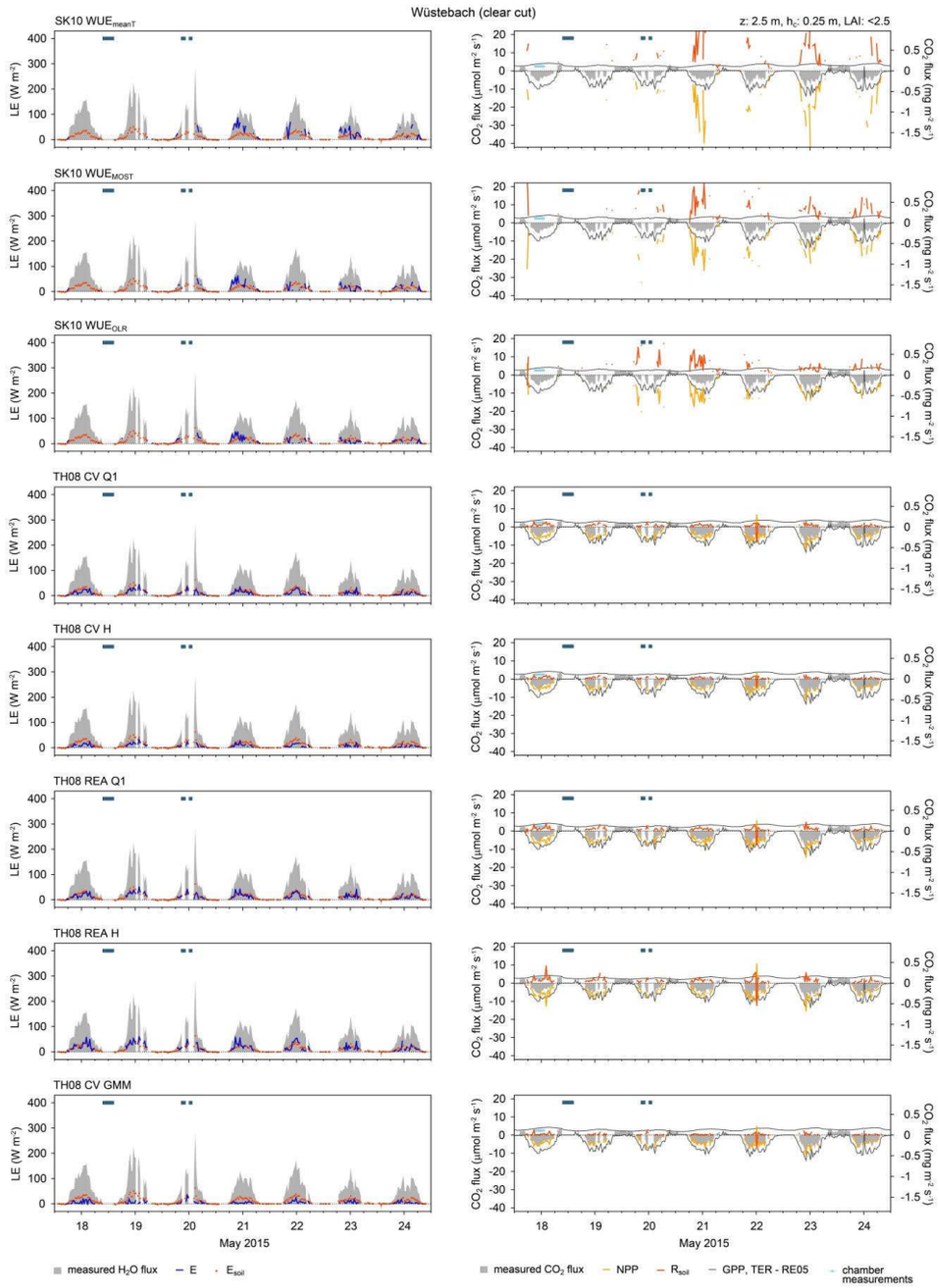

Fig. C.8: Source partitioning results of H_2O (*left*) and CO_2 (*right*) fluxes in half-hourly time steps for the Wüstebach study site (clear cut) in Germany and for every method version (see Chapter 4 for description). CO_2 flux estimates by Reichstein et al. (2005; RE05) and R_{soil} chamber measurements are also included (LE: latent heat flux; E: evaporation; E_{soil}: estimated evaporation based on Beer's law; GPP: gross primary production; NPP: net primary production; TER: total ecosystem respiration; R_{soil}: soil respiration; z: measurement height; h_c: canopy height; LAI: leaf area index; *blue bars*: precipitation events).

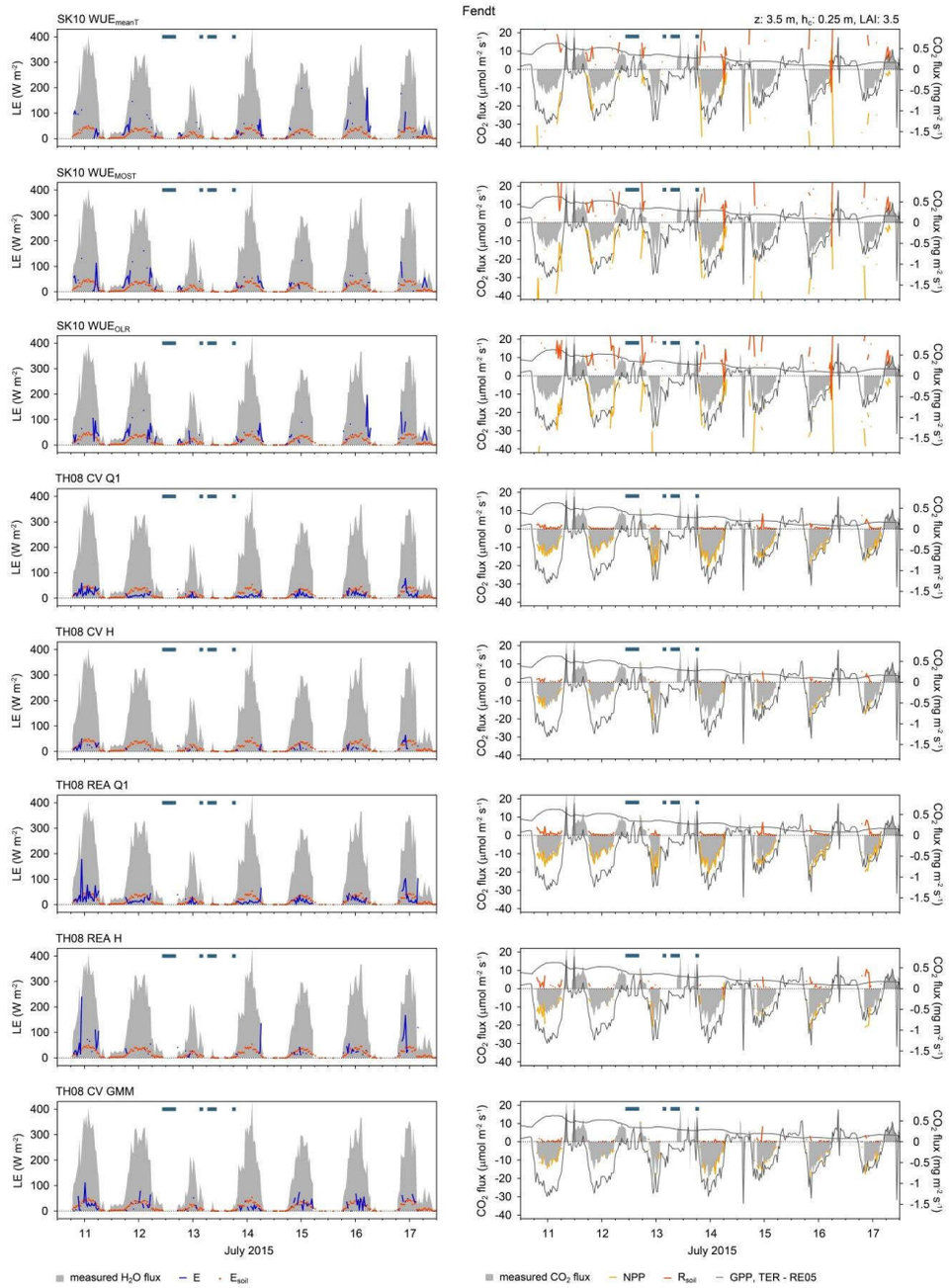

Fig. C.9: Source partitioning results of H_2O (*left*) and CO_2 (*right*) fluxes in half-hourly time steps for the Fendt study site (grassland) in Germany and for every method version (see Chapter 4 for description). CO_2 flux estimates by Reichstein et al. (2005; RE05) are also included (LE: latent heat flux; E: evaporation; E_{soil}: estimated evaporation based on Beer's law; GPP: gross primary production; NPP: net primary production; TER: total ecosystem respiration; R_{soil}: soil respiration; z: measurement height; h_c: canopy height; LAI: leaf area index; *blue bars*: precipitation events).

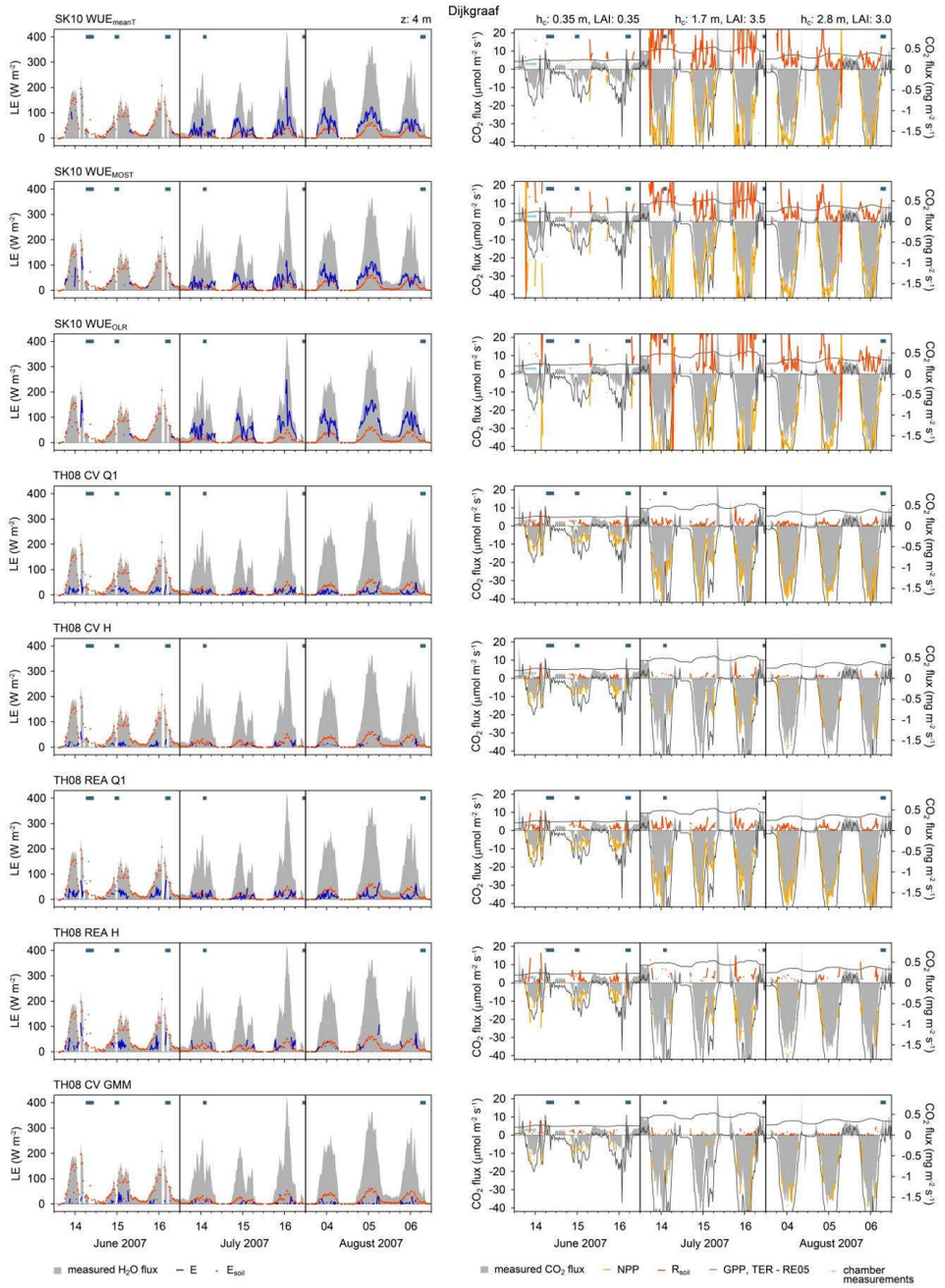

Fig. C.10: Source partitioning results of H_2O (*left*) and CO_2 (*right*) fluxes in half-hourly time steps for the Dijkgraaf study site (cropland, maize) in The Netherlands and for every method version (see Chapter 4 for description). CO_2 flux estimates by Reichstein et al. (2005; RE05) and R_{soil} chamber measurements are also included (LE: latent heat flux; E: evaporation; E_{soil}: estimated evaporation based on Beer's law; GPP: gross primary production; NPP: net primary production; TER: total ecosystem respiration; R_{soil}: soil respiration; z: measurement height; h_c: canopy height; LAI: leaf area index; *blue bars*: precipitation events).

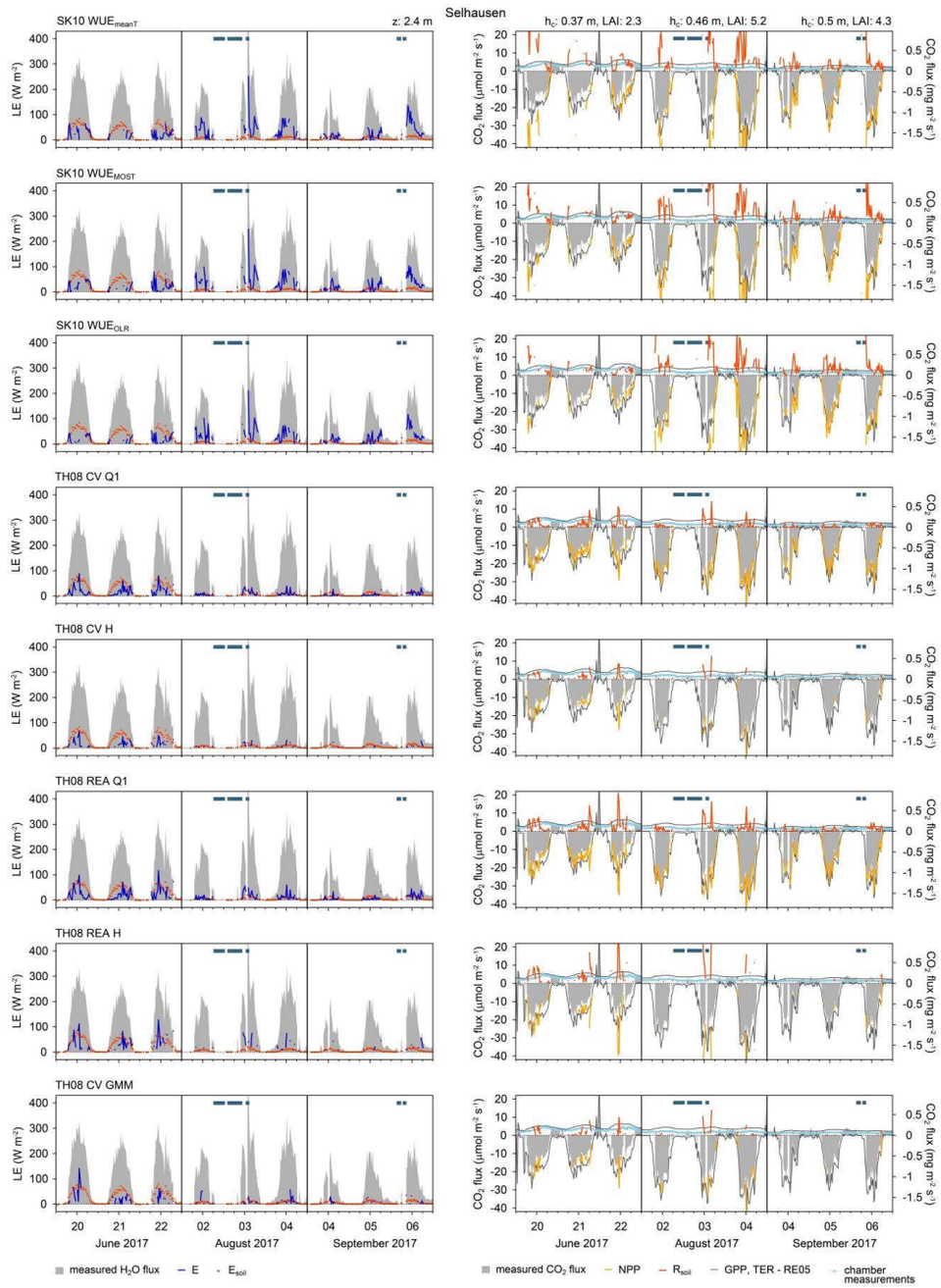

Fig. C.11: Source partitioning results of H_2O (*left*) and CO_2 (*right*) fluxes in half-hourly time steps for the Selhausen study site (cropland, sugar beet) in Germany and for every method version (see Chapter 4 for description). CO_2 flux estimates by Reichstein et al. (2005; RE05) and R_{soil} chamber measurements are also included (LE: latent heat flux; E: evaporation; E_{soil}: estimated evaporation based on Beer's law; GPP: gross primary production; NPP: net primary production; TER: total ecosystem respiration; R_{soil}: soil respiration; z: measurement height; h_c: canopy height; LAI: leaf area index; *blue bars*: precipitation events).

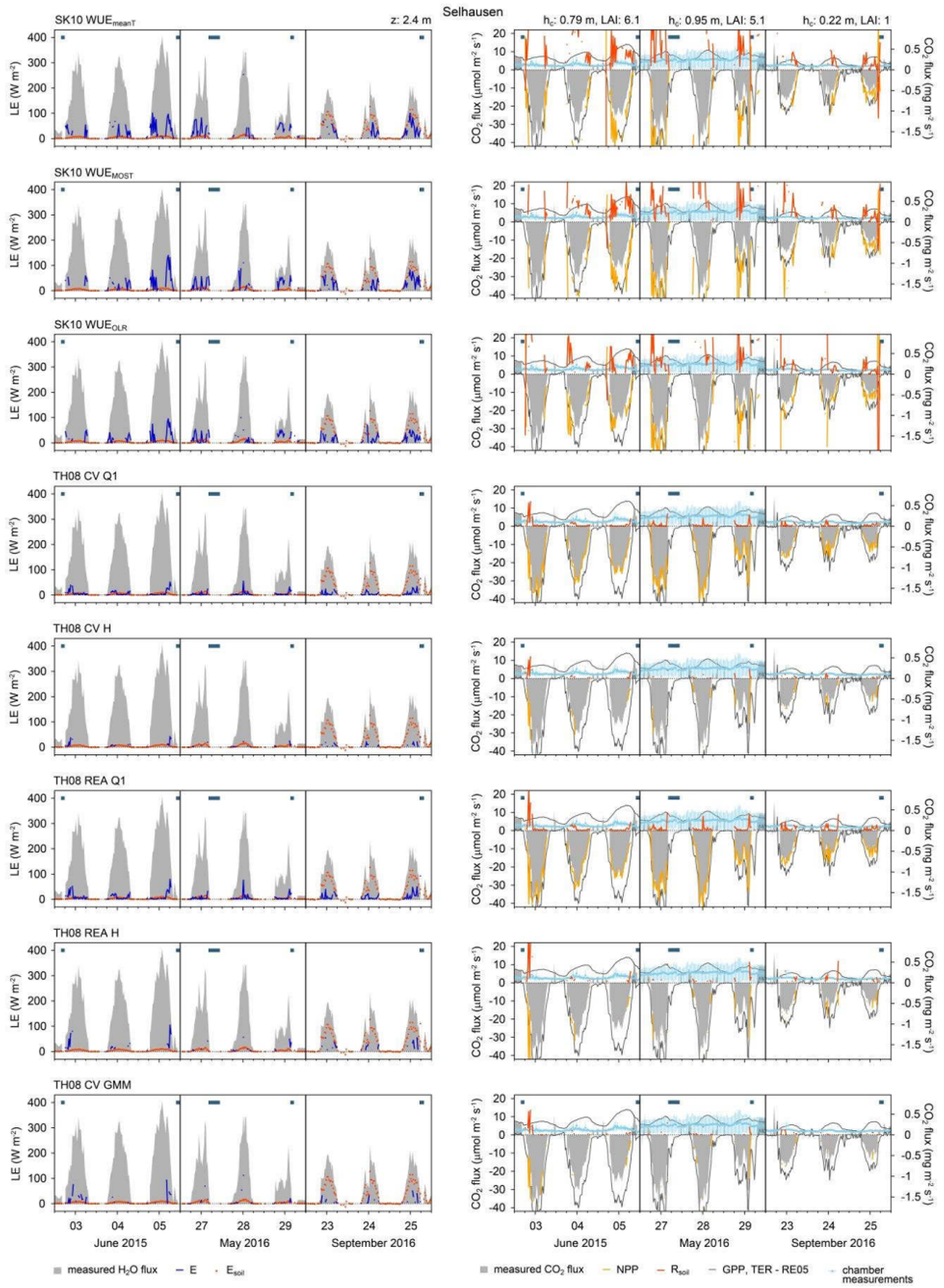

Fig. C.12: Source partitioning results of H_2O (*left*) and CO_2 (*right*) fluxes in half-hourly time steps for the Selhausen study site (cropland, 06/2015: winter wheat, 05/2016: barley, 09/2016: intercrop) in Germany and for every method version (see Chapter 4 for description). CO_2 flux estimates by Reichstein et al. (2005; RE05) and R_{soil} chamber measurements are also included (LE: latent heat flux; E: evaporation; E_{soil}: estimated evaporation based on Beer's law; GPP: gross primary production; NPP: net primary production; TER: total ecosystem respiration; R_{soil}: soil respiration; z: measurement height; h_c: canopy height; LAI: leaf area index; *blue bars*: precipitation events).

REFERENCES

Allen, R.G., Pereira, L.S., Raes, D., Smith, M., 1998. Crop evapotranspiration. Guidelines for computing crop water requirements. FAO Irrigation and Drainage Paper No. 56. Food and Agriculture Organization of the United Nations (FAO), Rome, pp. 300.

Anderson, R.G., Zhang, X., Skaggs, T.H., 2018. Measurement and partitioning of evapotranspiration for application to vadose zone studies. Vadose Zone J. 16 (13), 1-9, https://doi.org/10.2136/vzj2017.08.0155.

Andreu, A., Kustas, W.P., Polo, M.J., Carrara, A., González-Dugo, M.P., 2018. Modeling surface energy fluxes over a dehesa (oak savanna) ecosystem using a thermal based two-source energy balance model (TSEB) I. Remote Sens. 10 (4), 567, pp. 27, https://doi.org/10.3390/rs10040567.

Anslow, R.C., Green, J.O., 1967. The seasonal growth of pasture grasses. J. Agric. Sci. 68, 109-122.

Anthoni, P.M., Freibauer, A., Kolle, O., Schulze, E.-D., 2004. Winter wheat carbon exchange in Thuringia, Germany. Agric. For. Meteorol. 121 (1-2), 55-67, https://doi.org/10.1016/S0168-1923(03)00162-X.

Babel, W., Lüers, J., Hübner, J., Rebmann, C., Wichura, B., Thomas, C.K., Serafimovich, A., Foken, T., 2017. Long-term carbon and water vapour fluxes. In: Foken, T. (Ed.), Energy and matter fluxes of a spruce forest ecosystem. Ecological Studies 229, Springer, pp. 73-96, https://doi.org/10.1007/978-3-319-49389-3_4.

Baldocchi, D., Falge, E., Gu, L., Olson, R., Hollinger, D., Running, S., Anthoni, P., Bernhofer, C., Davis, K., Evans, R., Fuentes, J., Goldstein, A., Katul, G., Law, B., Lee, X., Malhi, Y., Meyers, T., Munger, W., Oechel, W., Paw U, K.T., Pilegaard, K., Schmid, H.P., Valentini, R., Verma, S., Vesala, T., Wilson, K., Wofsy, S., 2001. FLUXNET: A new tool to study the temporal and spatial variability of ecosystem-scale carbon dioxide, water vapor, and energy flux densities. Bull. Am. Meteorol. Soc. 82 (11), 2415-2434, https://doi.org/10.1175/1520-0477(2001)082<2415:FANTTS>2.3.CO;2.

Baldocchi, D.D., 2003. Assessing the eddy covariance technique for evaluating carbon dioxide exchange rates of ecosystems: past, present and future. Global Change Biol. 9 (4), 479-492, https://doi.org/10.1046/j.1365-2486.2003.00629.x.

Bales, R.C., 2002. Hydrology. In: Holton, J.R., Curry, J. (Eds.), Encyclopedia of atmospheric sciences. Academic Press, Oxford, pp. 968-973, https://doi.org/10.1016/B0-12-227090-8/00476-0.

Barrett, P.D., Laidlaw, A.S., Mayne, C.S., 2004. An evaluation of selected perennial ryegrass growth models for development and integration into a pasture management decision support system. J. Agric. Sci. 142, 327-334, https://doi.org/10.1017/s0021859604004289.

Bauer, J., Herbst, M., Huisman, J.A., Weihermüller, L., Vereecken, H., 2008. Sensitivity of simulated soil heterotrophic respiration to temperature and moisture reduction functions. Geoderma 145 (1-2), 17-27, https://doi.org/0.1016/j.geoderma.2008.01.026.

Bauer, J., Weihermüller, L., Huisman, J.A., Herbst, M., Graf, A., Séquaris, J.-M., Vereecken, H., 2012. Inverse determination of heterotrophic soil respiration response to temperature and water content under field conditions. Biogeochemistry 108 (1-3), 119-134, https://doi.org/10.1007/s10533-011-9583-1.

Bink, N.J., Meesters, A.G.C.A., 1997. Comment on 'Estimation of surface heat and momentum fluxes using the flux-variance method above uniform and non-uniform terrain' by Katul et al. (1995). Boundary-Layer Meteorol. 84 (3), 497-502, https://doi.org/10.1023/A:1000427431944.

Bogena, H.R., Bol, R., Borchard, N., Brüggemann, N., Diekkrüger, B., Drüe, C., Groh, J., Gottselig, N., Huisman, J.A., Lücke, A., Missong, A., Neuwirth, B., Pütz, T., Schmidt, M., Stockinger, M., Tappe, W., Weihermüller, L., Wiekenkamp, I., Vereecken, H., 2015. A terrestrial observatory approach to the integrated investigation of the effects of deforestation on water, energy, and matter fluxes. Science China: Earth Sciences 58 (1), 6175, https://doi.org/10.1007/s11430-014-4911-7.

Bolinder, M.A., Angers, D.A., Dubuc, J.P., 1997. Estimating shoot to root ratios and annual carbon inputs in soils for cereal crops. Agric. Ecosyst. Environ. 63 (1), 61-66, https://doi.org/10.1016/s0167-8809(96)01121-8.

Bolinder, M.A., Angers, D.A., Bélanger, G., Michaud, R., Laverdière, M.R., 2002. Root biomass and shoot to root ratios of perennial forage crops in eastern Canada. Can. J. Plant Sci. 82 (4), 731-737.

Boons-Prins, E.R., de Koning, G.H.J., van Diepen, C.A., Penning de Vries, F.W.T., 1993. Crop-specific simulation parameters for yield forecasting across the European Community. Simulation Reports CABO-TT, No 32. CABO-DLO, Wageningen, pp. 43.

Borchard, N., Schirrmann, M., von Hebel, C., Schmidt, M., Baatz, R., Firbank, L., Vereecken, H., Herbst, M., 2015. Spatio-temporal drivers of soil and ecosystem carbon fluxes at field scale in an upland grassland in Germany. Agric. Ecosyst. Environ. 211, 84-93, https://doi.org/10.1016/j.agee.2015.05.008.

Brosy, C., Krampf, K., Zeeman, M., Wolf, B., Junkermann, W., Schäfer, K., Emeis, S., Kunstmann, H., 2017. Simultaneous multicopter-based air sampling and sensing of meteorological variables. Atmos. Meas. Tech. 10 (8), 2773-2784, https://doi.org/10.5194/amt-10-2773-2017.

Businger, J.A., Oncley, S.P., 1990. Flux measurement with conditional sampling. J. Atmos. Ocean. Technol. 7 (2), 349-352, https://doi.org/10.1175/1520-0426(1990)007<0349:FMWCS>2.0.CO;2.

Campbell, G.S., Norman, J.M., 1998. An introduction to environmental biophysics. Springer, New York, pp. 286.

Canty, M.J., 2010. Image analysis, classification and change detection in remote sensing, with algorithms for ENVI/IDL. CRC Press, Boca Raton, FL, pp. 441.

Cassiani, M., Katul, G.G., Albertson, J.D., 2008. The effects of canopy leaf area index on airflow across forest edges: large-eddy simulation and analytical results. Boundary-Layer Meteorol. 126 (3), 433-460, https://doi.org/10.1007/s10546-007-9242-1.

Coleman, K., Jenkinson, D.S., 2008. RothC-26.3. A model for the turnover of carbon in soil. Model description and windows users guide. IACR-Rothamsted, Harpenden, pp. 47.

de Noblet-Ducoudré, N., Gervois, S., Ciais, P., Viovy, N., Brisson, N., Seguin, B., Perrier, A., 2004. Coupling the Soil-Vegetation-Atmosphere-Transfer Scheme ORCHIDEE to the agronomy model STICS to study the influence of croplands on the European carbon and water budgets. Agronomie 24 (6-7), 397-407, https://doi.org/10.1051/agro:2004038.

Denmead, O.T., Dunin, F.X., Leuning, R., Raupach, M.R., 1996. Measuring and modelling soil evaporation in wheat crops. Phys. Chem. Earth 21 (3), 97-100, https://doi.org/10.1016/S0079-1946(97)85567-X.

Desai, A.R., Richardson, A.D., Moffat, A.M., Kattge, J., Hollinger, D.Y., Barr, A., Falge, E., Noormets, A., Papale, D., Reichstein, M., Stauch, V.J., 2008. Cross-site evaluation of eddy covariance GPP and RE decomposition techniques. Agric. For. Meteorol. 148 (6-7), 821-838, https://doi.org/10.1016/j.agrformet.2007.11.012.

Detto, M., Katul, G.G., 2007. Simplified expressions for adjusting higher-order turbulent statistics obtained from open path gas analyzers. Boundary-Layer Meteorol. 122 (1), 205-216, https://doi.org/10.1007/s10546-006-9105-1.

Dickinson, R.E., 2002. Land-atmosphere interactions, overview. In: Holton, J.R., Curry, J. (Eds.), Encyclopedia of atmospheric sciences. Academic Press, Oxford, pp. 1116-1120, https://doi.org/10.1016/B0-12-227090-8/00476-0.

Dolman, A.J., Moors, E.J., Elbers, J.A., 2002. The carbon uptake of a mid latitude pine forest growing on sandy soil. Agric. For. Meteorol. 111 (3), 157-170, https://doi.org/10.1016/S0168-1923(02)00024-2.

Duan, Q.Y., Gupta, V.K., Sorooshian, S., 1993. Shuffled complex evolution approach for effective and efficient global minimization. J. Optimiz. Theory App. 76 (3), 501-521, https://doi.org/10.1007/bf00939380.

Dupont, S., Brunet, Y., 2008. Influence of foliar density profile on canopy flow: a large-eddy simulation study. Agric. For. Meteorol. 148 (6-7), 976-990, https://doi.org/10.1016/j.agrformet.2008.01.014.

Eamus, D., 2001. How does ecosystem water balance influence net primary productivity? - a discussion. In: Kirschbaum, M.U.F., Mueller, R. (Eds.), Net ecosystem exchange. Workshop Proceedings, 18-20 April 2001, Cooperative Research Centre for Greenhouse Accounting, Canberra, pp. 62-70.

Edburg, S.L., Stock, D., Lamb, B.K., Patton, E.G., 2012. The effect of the vertical source distribution on scalar statistics within and above a forest canopy. Boundary-Layer Meteorol. 142 (3), 365-382, https://doi.org/10.1007/s10546-011-9686-1.

Eder, F., Schmidt, M., Damian, T., Traumner, K., Mauder, M., 2015. Mesoscale eddies affect near-surface turbulent exchange: evidence from Lidar and tower measurements. J. Appl. Meteor. Climatol. 54 (1), 189-206, https://doi.org/10.1175/JAMC-D-14-0140.1.

Elbers, J.A., Jacobs, C.M.J., Kruijt, B., Jans, W.W.P., Moors, E.J., 2011. Assessing the uncertainty of estimated annual totals of net ecosystem productivity: a practical approach applied to a mid latitude temperate pine forest. Agric. For. Meteorol. 151 (12), 1823-1830, https://doi.org/10.1016/j.agrformet.2011.07.020.

Evans, G.T., 2003. Defining misfit between biogeochemical models and data sets. J. Mar. Syst. 40-41, 49-54, https://doi.org/10.1016/s0924-7963(03)00012-5.

Falge, E., Baldocchi, D., Olson, R., Anthoni, P., Aubinet, M., Bernhofer, C., Burba, G., Ceulemans, R., Clement, R., Dolman, H., Granier, A., Gross, P., Grünwald, T., Hollinger, D., Jensen, N.-O., Katul, G., Keronen, P., Kowalski, A., Lai, C.T., Law, B.E., Meyers, T., Moncrieff, J., Moors, E., Munger, J.W., Pilegaard, K., Rannik, Ü., Rebmann, C., Suyker, A., Tenhunen, J., Tu, K., Verma, S., Vesala, T., Wilson, K., Wofsy, S., 2001. Gap filling strategies for defensible annual sums of net ecosystem exchange. Agric. For. Meteorol. 107 (1), 43-69, https://doi.org/10.1016/S0168-1923(00)00225-2.

Falge, E., Baldocchi, D., Tenhunen, J., Aubinet, M., Bakwin, P., Berbigier, P., Bernhofer, C., Burba, G., Clement, R., Davis, K.J., Elbers, J.A., Goldstein, A.H., Grelle, A., Granier, A., Guðmundsson, J., Hollinger, D., Kowalski, A.S., Katul, G., Law, B.E., Malhi, Y., Meyers, T., Monson, R.K., Munger, J.W., Oechel, W., Paw U, K.T., Pilegaard, K., Rannik, Ü., Rebmann, C., Suyker, A., Valentini, R., Wilson, K., Wofsy, S., 2002. Seasonality of ecosystem respiration and gross primary production as derived from FLUXNET measurements. Agric. For. Meteorol. 113 (1-4), 53-74, https://doi.org/10.1016/S0168-1923(02)00102-8.

Falloon, P., Smith, P., Coleman, K., Marshall, S., 1998. Estimating the size of the inert organic matter pool from total soil organic carbon content for use in the Rothamsted carbon model. Soil Biol. Biochem. 30 (8-9), 1207-1211, https://doi.org/10.1016/s0038-0717(97)00256-3.

Feddes, R.A., Kowalik, P.J., Zaradny, H., 1978. Simulation of field water use and crop yield. Simulation Monographs, Wageningen, pp. 188.

Finnigan, J.J., Shaw, R.H., Patton, E.G., 2009. Turbulence structure above a vegetation canopy. J. Fluid Mech. 637, 387-424, https://doi.org/10.1017/S0022112009990589.

Foken, T., 2006. Angewandte Meteorologie. Mikrometeorologische Methoden. Springer, Berlin, Heidelberg, New York, pp. 325.

Foken, T., Gerstberger, P., Köck, K., Siebicke, L., Serafimovich, A., Lüers, J., 2017. Description of the Waldstein measuring site. In: Foken, T. (Ed.), Energy and matter fluxes of a spruce forest ecosystem. Ecological Studies 229, Springer, pp. 19-38, https://doi.org/10.1007/978-3-319-49389-3_2.

Food and Agriculture Organization (FAO) of the United Nations, Regional Office for Europe and Central Asia, 2014. FAO statistical yearbook 2014. Europe and Central Asia, Food and Agriculture. FAO, Budapest, pp 113.

Gebler, S., Hendricks Franssen, H.J., Pütz, T., Post, H., Schmidt, M., Vereecken, H., 2015. Actual evapotranspiration and precipitation measured by lysimeters: a comparison with eddy covariance and tipping bucket. Hydrol. Earth Syst. Sci. 19 (5), 2145-2161, https://doi.org/10.5194/hess-19-2145-2015.

Gonzales, B., Boucaud, J., Salette, J., Langlois, J., Duyme, M., 1989. Changes in stubble carbohydrate content during regrowth of defoliated perennial ryegrass (*Lolium perenne* L.) on two nitrogen levels. Grass Forage Sci. 44 (4), 411-415, https://doi.org/10.1111/j.1365-2494.1989.tb01940.x.

Good, S.P., Soderberg, K., Guan, K., King, E.G., Scanlon, T.M., Caylor, K.K., 2014. δ^2H isotopic flux partitioning of evapotranspiration over a grass field following a water pulse and subsequent dry down. Water Resour. Res. 50 (2), 1410-1432, https://doi.org/10.1002/2013WR014333.

Goudriaan, J., van Keulen, H., van Laar, H.H., 1997. Crop growth model for potential production (SUCROS1). In: van Laar, H.H., Goudriaan, J., van Keulen, H. (Eds.), SUCROS97: Simulation of crop growth for potential and water-limited production situations. As applied to spring wheat. Quantitative Approaches in Systems Analysis, AB-DLO, Wageningen, pp. 1-20.

Graf, A., Herbst, M., Weihermüller, L., Huisman, J.A., Prolingheuer, N., Bornemann, L., Vereecken, H., 2012. Analyzing spatiotemporal variability of heterotrophic soil respiration at the field scale using orthogonal functions. Geoderma 181, 91-101, https://doi.org/10.1016/j.geoderma.2012.02.016.

Graf, A., Werner, J., Langensiepen, M., van de Boer, A., Schmidt, M., Kupisch, M., Vereecken, H., 2013. Validation of a minimum microclimate disturbance chamber for net ecosystem flux measurements. Agric. For. Meteorol. 174-175, 1-14, https://doi.org/10.1016/j.agrformet.2013.02.001.

Gspaltl, M., Bauerle, W., Binkley, D., Sterba, H., 2013. Leaf area and light use efficiency patterns of Norway spruce under different thinning regimes and age classes. Forest Ecol. Manag. 288, 49-59, https://doi.org/10.1016/j.foreco.2011.11.044.

Herbst, M., Fialkiewicz, W., Chen, T., Pütz, T., Thiéry, D., Mouvet, C., Vachaud, G., Vereecken, H., 2005. Intercomparison of flow and transport models applied to vertical drainage in cropped lysimeters. Vadose Zone J. 4 (2), 240-254, https://doi.org/10.2136/vzj2004.0070.

Herbst, M., Hellebrand, H.J., Bauer, J., Huisman, J.A., Šimůnek, J., Weihermüller, L., Graf, A., Vanderborght, J., Vereecken, H., 2008. Multiyear heterotrophic soil respiration: evaluation of a coupled CO_2 transport and carbon turnover model. Ecol. Model. 214 (2-4), 271-283, https://doi.org/10.1016/j.ecolmodel.2008.02.007.

Hess, T.F., Schmidt, S.K., 1995. Improved procedure for obtaining statistically valid parameters estimates from soil respiration data. Soil Biol. Biochem. 27 (1), 1-7, https://doi.org/10.1016/0038-0717(94)00166-X.

Heus, T., van Heerwaarden, C.C., Jonker, H.J.J., Pier Siebesma, A., Axelsen, S., van den Dries, K., Geoffroy, O., Moene, A.F., de Roode, S.R., Vilà-Guerau de Arellano, J., 2010. Formulation of the Dutch Atmospheric Large-Eddy Simulation (DALES) and overview of its applications. Geosci. Model Dev. 3 (2), 415-444, https://doi.org/10.5194/gmd-3-415-2010.

Hill, R.J., 1989. Implications of Monin-Obukhov Similarity Theory for scalar quantities. J. Atmos. Sci. 46 (14), 2236-2244.

Hopkins, F., Gonzalez-Meler, M.A., Flower, C.E., Lynch, D.J., Czimczik, C., Tang, J., Subke, J.-A., 2013. Ecosystem-level controls on root rhizosphere respiration. New Phytol. 199 (2), 339-351, https://doi.org/10.1111/nph.12271.

Houghton, R.A., 2014. The contemporary carbon cycle. In: Holland, H.D., Turekian, K.K. (Eds.), Treatise on geochemistry. Elsevier, Oxford, pp. 399-435, https://doi.org/10.1016/B978-0-08-095975-7.00810-X.

Huang, J., Katul, G., Albertson, J., 2013. The role of coherent turbulent structures in explaining scalar dissimilarity within the canopy sublayer. Environ. Fluid Mech. 13 (6), 571-599, https://doi.org/10.1007/s10652-013-9280-9.

I.U.S.S. Working Group WRB, 2006. World reference base for soil resources 2006. A framework for international classification, correlation and communication. World Soil Resources Reports No. 103. FAO, Rome, pp. 128.

Ingwersen, J., Imukova, K., Högy, P., Streck, T., 2015. On the use of the post-closure methods uncertainty band to evaluate the performance of land surface models against eddy covariance flux data. Biogeosciences 12 (8), 2311-2326, https://doi.org/10.5194/bg-12-2311-2015.

Jans, W.W.P., Jacobs, C.M.J., Kruijt, B., Elbers, J.A., Barendse, S., Moors, E.J., 2010. Carbon exchange of a maize (*Zea mays* L.) crop: influence of phenology. Agric. Ecosyst. Environ. 139 (3), 316-324, https://doi.org/10.1016/j.agee.2010.06.008.

Jones, H.G., Rotenberg, E., 2001. Energy, radiation and temperature regulation in plants. In: Encyclopedia of Life Sciences. John Wiley & Sons, Ltd, pp. 8, https://doi.org/10.1002/9780470015902.a0003199.pub2.

Katul, G., Goltz, S.M., Hsieh, C., Cheng, Y., Mowry, F., Sigmon, J., 1995. Estimation of surface heat and momentum fluxes using the flux-variance method above uniform and non-uniform terrain. Boundary-Layer Meteorol. 74 (3), 237-260, https://doi.org/10.1007/BF00712120.

Kirschbaum, M.U.F., Eamus, D., Gifford, R.M., Roxburgh, S.H., Sands, P.J., 2001. Definitions of some ecological terms commonly used in carbon accounting. In: Kirschbaum, M.U.F., Mueller, R. (Eds.), Net ecosystem exchange. Workshop Proceedings, 18-20 April 2001, Cooperative Research Centre for Greenhouse Accounting, Canberra, pp. 2-5.

Kool, D., Agam, N., Lazarovitch, N., Heitmann, J.L., Sauer, T.J., Ben-Gal, A., 2014. A review of approaches for evapotranspiration partitioning. Agric. For. Meteorol. 184, 56-70, https://doi.org/10.1016/j.agrformet.2013.09.003.

Kormann, R., Meixner, F.X., 2001. An analytical footprint model for non-neutral stratification. Boundary-Layer Meteorol. 99 (2), 207-224, https://doi.org/10.1023/A:1018991015119.

Kristensen, A.H., Thorbjørn, A., Jensen, M.P., Pedersen, M., Moldrup, P., 2010. Gas-phase diffusivity and tortuosity of structured soils. J. Contam. Hydrol. 115 (1-4), 26-33, https://doi.org/10.1016/j.jconhyd.2010.03.003.

Kuzyakov, Y., Domanski, G., 2000. Carbon input by plants into the soil. Review. J. Plant Nutr. Soil Sci. 163 (4), 421-431, https://doi.org/0.1002/1522-2624(200008)163:4<421::aid-jpln421>3.0.co;2-r.

Kuzyakov, Y., 2006. Sources of CO_2 efflux from soil and review of partitioning methods. Soil Biol. Biochem. 38 (3), 425-448, https://doi.org/10.1016/j.soilbio.2005.08.020.

Lamaud, E., Irvine, M., 2006. Temperature-humidity dissimilarity and heat-to-water-vapour transport efficiency above and within a pine forest canopy: the role of the Bowen ratio. Boundary-Layer Meteorol. 120 (1), 87-109, https://doi.org/10.1007/s10546-005-9032-6.

Lasslop, G., Reichstein, M., Papale, D., Richardson, A.D., Arneth, A., Barr, A., Stoy, P., Wohlfahrt, G., 2010. Separation of net ecosystem exchange into assimilation and respiration using a light response curve approach: critical issues and global evaluation. Global Change Biol. 16 (1), 187-208, https://doi.org/10.1111/j.1365-2486.2009.02041.x.

Leafe, E.L., Stiles, W., Dickinson, S.E., 1974. Physiological processes influencing the pattern of productivity of the intensively managed grass sward. Sectional Papers, 12th International Grassland Congress (congress proceedings - June 11-20, 1974), Vol. 1, Part I, 442-457.

Li, C., Frolking, S., Xiao, X., Moore III, B., Boles, S., Qiu, J., Huang, Y., Salas, W., Sass, R., 2005. Modeling impacts of farming management alternatives on CO_2, CH_4 and N_2O emissions: a case study for water management of rice agriculture in China. Global Biogeochem. Cy. 19 (3), 1-10, https://doi.org/10.1029/2004GB002341.

Lindauer, M., Schmid, H.P., Grote, R., Mauder, M., Steinbrecher, R., Wolpert, B., 2014. Net ecosystem exchange over a non-cleared wind-throw-disturbed upland spruce forest - Measurements and simulations. Agric. For. Meteorol. 197, 219-234, https://doi.org/10.1016/j.agrformet.2014.07.005.

Lloyd, J., Taylor, A., 1994. On the temperature dependence of soil respiration. Funct. Ecol. 8 (3), 315-323, https://doi.org/10.2307/2389824.

López, I.F., Kemp, P.D., Dörner, J., Descalzi, C.A., Balocchi, O.A., García, S., 2013. Competitive strategies and growth of neighbouring *Bromus valdivianus* Phil. and *Lolium perenne* L. plants under water restriction. J. Agron. Crop Sci. 199 (6), 449-459, https://doi.org/10.1111/jac.12032.

Mandel, J., 1957. Fitting a straight line to certain types of cumulative data. J. Am. Stat. Assoc. 52 (280), 552-566, https://doi.org/10.2307/2281706.

Massman, W.J., Lee, X., 2002. Eddy covariance flux corrections and uncertainties in long-term studies of carbon and energy exchanges. Agric. For. Meteorol. 113 (1-4), 121-144, https://doi.org/10.1016/s0168-1923(02)00105-3.

Matiu, M., Bothmann, L., Steinbrecher, R., Menzel, A., 2017. Monitoring succession after a non-cleared windthrow in a Norway spruce mountain forest using webcam, satellite vegetation indices and turbulent CO_2 exchange. Agric. For. Meteorol. 244-245, 72-81, https://doi.org/10.1016/j.agrformet.2017.05.020.

Mauder, M., Cuntz, M., Drüe, C., Graf, A., Rebmann, C., Schmid, H.P., Schmidt, M., Steinbrecher, R., 2013. A strategy for quality and uncertainty assessment of long-term eddy-covariance measurements. Agric. For. Meteorol. 169, 122-135, https://doi.org/10.1016/j.agrformet.2012.09.006.

Moene, A.F., Schüttemeyer, D., 2008. The effect of surface heterogeneity on the temperature-humidity correlation and the relative transport efficiency. Boundary-Layer Meteorol. 129, 99-113, https://doi.org/10.1007/s10546-008-9312-z.

Moene, A.F., van Dam, J.C., 2014. Transport in the atmosphere-vegetation-soil continuum. Cambridge University Press, Cambridge, New York, pp. 436.

Moffat, A.M., Papale, D., Reichstein, M., Hollinger, D.Y., Richardson, A.D., Barr, A.G., Beckstein, C., Braswell, B.H., Churkina, G., Desai, A.R., Falge, E., Gove, J.H., Heimann, M., Hui, D., Jarvis, A.J., Kattge, J., Noormets, A., Stauch, V.J., 2007. Comprehensive comparison of gap-filling techniques for eddy covariance net carbon fluxes. Agric. For. Meteorol. 147 (3-4), 209-232, https://doi.org/10.1016/j.agrformet.2007.08.011.

Moureaux, C., Debacq, A., Hoyaux, J., Suleau, M., Tourneur, D., Vancutsem, F., Bodson, B., Aubinet, M., 2008. Carbon balance assessment of a Belgian winter wheat crop (*Triticum aestivum* L.). Global Change Biol. 14 (6), 1353-1366, https://doi.org/10.1111/j.1365-2486.2008.01560.x.

Moyano, F.E., Vasilyeva, N., Bouckaert, L., Cook, F., Craine, J., Curiel Yuste, J., Don, A., Epron, D., Formanek, P., Franzluebbers, A., Ilstedt, U., Kätterer, T., Orchard, V., Reichstein, M., Rey, A., Ruamps, L., Subke, J.-A., Thomson, I.K., Chenu, C., 2012. The moisture response of soil heterotrophic respiration: interaction with soil properties. Biogeosciences 9 (3), 1173-1182, https://doi.org/10.5194/bg-9-1173-2012.

Nash, J.E., Sutcliffe, J.V., 1970. River flow forecasting through conceptual models. Part I - a discussion of principles. J. Hydrol. 10 (3), 282-290, https://doi.org/10.1016/0022-1694(70)90255-6.

Nelder, J.A., Mead, R., 1965. A simplex method for function minimization. Comput. J. 7 (4), 308-313.

Ney, P., Schmidt, M., Klosterhalfen, A., Graf, A., 2017. A high-resolution measurement technique for vertical CO_2 and H_2O profiles within and above crop canopies and its use for flux partitioning. Poster presentation, EGU General Assembly 2017, Vienna, Austria, 23-28 Apr 2017.

Ney, P., Graf, A., 2018. High-resolution vertical profile measurements for carbon dioxide and water vapour concentrations within and above crop canopies. Boundary-Layer Meteorol. 166, 449-473, https://doi.org/10.1007/s10546-017-0316-4.

Ney, P., Graf, A., Bogena, H., Diekkrüger, B., Drüe, C., Esser, O., Heinemann, G., Klosterhalfen, A., Pick, K., Pütz, T., Schmidt, M., Valler, V., Vereecken, H., in press. CO_2 fluxes before and after partial deforestation of a Central European spruce forest. Agric. For. Meteorol.

Ouwersloot, H.G., Moene, A.F., Attema, J.J., Vilà-Guerau de Arellano, J., 2016. Large-Eddy Simulation comparison of neutral flow over a canopy: sensitivities to physical and numerical conditions, and similarity to other representations. Boundary-Layer Meteorol. 162 (1), 71-89, https://doi.org/10.1007/s10546-016-0182-5.

Palatella, L., Rana, G., Vitale, D., 2014. Towards a flux-partitioning procedure based on the direct use of high-frequency eddy-covariance data. Boundary-Layer Meteorol. 153 (2), 327-337, https://doi.org/10.1007/s10546-014-9947-x.

Palosuo, T., Foereid, B., Svensson, M., Shurpali, N., Lehtonen, A., Herbst, M., Linkosalo, T., Ortiz, C., Todorovic, G.R., Marcinkonis, S., Li, C., Jandl, R., 2012. A multi-model comparison of soil carbon assessment of a coniferous forest stand. Environ. Modell. Softw. 35, 38-49, https://doi.org/10.1016/j.envsoft.2012.02.004.

Parsons, A.J., Robson, M.J., 1981. Seasonal changes in the physiology of S24 perennial ryegrass (*Lolium perenne* L.). 3. Partition of assimilates between root and shoot during the transition from vegetative to reproductive growth. Ann. Bot. 48 (5), 733-744.

Parsons, A.J., 1988. The effects of season and management on the growth of grass swards. In: Jones, M.B., Lazenby, A. (Eds.), The grass crop. The physiological basis of production. Chapman and Hall, London, New York, pp. 129-177.

Patton, E.G., Finnigan, J.J., 2012. Canopy turbulence. In: Fernando, H.J.S. (Ed.), Handbook of environmental fluid dynamics, Volume 1. CRC Press, Boca Raton, pp. 311-327.

Post, H., Hendricks Franssen, H.J., Graf, A., Schmidt, M., Vereecken, H., 2015. Uncertainty analysis of eddy covariance CO_2 flux measurements for different EC tower distances using an extended two-tower approach. Biogeosciences 12 (4), 1205-1221, https://doi.org/10.5194/bg-12-1205-2015.

Prolingheuer, N., Scharnagl, B., Graf, A., Vereecken, H., Herbst, M., 2014. On the spatial variation of soil rhizospheric and heterotrophic respiration in a winter wheat stand. Agric. For. Meteorol. 195-196, 24-31, https://doi.org/10.1016/j.agrformet.2014.04.016.

Prud'homme, M.-P., Gonzalez, B., Billard, J.-P., Boucaud, J., 1992. Carbohydrate content, fructan and sucrose enzyme activities in roots, stubble and leaves of ryegrass (*Lolium perenne* L.) as affected by source/sink modification after cutting. J. Plant Physiol. 140, 282-291.

Quade, M., Klosterhalfen, A., Graf, A., Brüggemann, N., Hermes, N., Vereecken, H., Rothfuss, Y., 2019. In-situ monitoring of soil water isotopic composition for partitioning of evapotranspiration during one growing season of sugar beet (*Beta vulgaris*). Agric. For. Meteorol. 266-267, 53-64, https://doi.org/10.1016/j.agrformet.2018.12.002.

Reichstein, M., Falge, E., Baldocchi, D., Papale, D., Aubinet, M., Berbigier, P., Bernhofer, C., Buchmann, N., Gilmanov, T., Granier, A., Grünwald, T., Havránková, K., Ilvesniemi, H., Janous, D., Knohl, A., Laurila, T., Lohila, A., Loustau, D., Matteucci, G., Meyers, T., Miglietta, F., Ourcival, J.-M., Pumpanen, J., Rambal, S., Rotenberg, E., Sanz, M., Tenhunen, J., Seufert, G., Vaccari, F., Vesala, T., Yakir, D., Valentini, R., 2005. On the separation of net ecosystem exchange into assimilation and ecosystem respiration: review and improved algorithm. Global Change Biol. 11 (9), 1424-1439, https://doi.org/10.1111/j.1365-2486.2005.001002.x.

Reichstein, M., Stoy, P.C., Desai, A.R., Lasslop, G., Richardson, A.D., 2012. Partitioning of net fluxes. In: Aubinet, M., Vesala, T., Papale, D. (Eds.), Eddy covariance. A practical guide to measurement and data analysis. Springer, Dordrecht, Heidelberg, London, New York, pp. 263-289.

Richardson, A.D., Williams, M., Hollinger, D.Y., Moore, D.J.P., Dail, D.B., Davidson, E.A., Scott, N.A., Evans, R.S., Hughes, H., Lee, J.T., Rodrigues, C., Savage, K., 2010. Estimating parameters of a forest ecosystem C model with measurements of stocks and fluxes as joint constraints. Oecologia 164 (1), 25-40, https://doi.org/10.1007/s00442-010-1628-y.

Robson, M.J., Ryle, G.J.A., Woledge, J., 1988. The grass plant - its form and function. In: Jones, M.B., Lazenby, A. (Eds.), The grass crop. The physiological basis of production. Chapman and Hall, London, New York, pp. 25-83.

Rustad, L.E., Huntington, T.G., Boone, R.D., 2000. Controls on soil respiration: implications for climate change. Biogeochemistry 48 (1), 1-6, https://doi.org/10.1023/A:1006255431298.

Rutter, A.J., Kershaw, K.A., Robins, P.C., Morton, A.J., 1971. A predictive model of rainfall interception in forests, 1. Derivation of the model from observations in a plantation of Corsican pine. Agric. Meteorol. 9, 367-384, https://doi.org/10.1016/0002-1571(71)90034-3.

Scanlon, T.M., Albertson, J.D., 2001. Turbulent transport of carbon dioxide and water vapor within a vegetation canopy during unstable conditions: identification of episodes using wavelet analysis. J. Geophys. Res. 106 (D7), 7251-7262, https://doi.org/10.1029/2000JD900662.

Scanlon, T.M., Sahu, P., 2008. On the correlation structure of water vapor and carbon dioxide in the atmospheric surface layer: a basis for flux partitioning. Water Resour. Res. 44 (10), W10418, pp. 15, https://doi.org/10.1029/2008WR006932.

Scanlon, T.M., Kustas, W.P., 2010. Partitioning carbon dioxide and water vapor fluxes using correlation analysis. Agric. For. Meteorol. 150 (1), 89-99, https://doi.org/10.1016/j.agrformet.2009.09.005.

Scanlon, T.M., Kustas, W.P., 2012. Partitioning evapotranspiration using an eddy covariance-based technique: improved assessment of soil moisture and land-atmosphere exchange dynamics. Vadose Zone J. 11 (3), https://doi.org/10.2136/vzj2012.0025.

Schapendonk, A.H.C.M., Stol, W., van Kraalingen, D.W.G., Bouman, B.A.M., 1998. LINGRA, a sink/source model to simulate grassland productivity in Europe. Eur. J. Agron. 9, 87-100, https://doi.org/10.1016/S1161-0301(98)00027-6.

Scharnagl., B., Vrugt, J.A., Vereecken, H., Herbst, M., 2011. Inverse modelling of in situ soil water dynamics: investigating the effect of different prior distributions of the soil hydraulic parameters. Hydrol. Earth Syst. Sci. 15 (10), 3043-3059, https://doi.org/10.5194/hess-15-3043-2011.

Schlesinger, W.H., Jasechko, S., 2014. Transpiration in the global water cycle. Agric. For. Meteorol. 189-190, 115-117, https://doi.org/10.1016/j.agrformet.2014.01.011.

Schmidt, M., Reichenau, T.G., Fiener, P., Schneider, K., 2012. The carbon budget of a winter wheat field: an eddy covariance analysis of seasonal and inter-annual variability. Agric. For. Meteorol. 165, 114-126, https://doi.org/10.1016/j.agrformet.2012.05.012.

Schmitt, M., Bahn, M., Wohlfahrt, G., Tappeiner, U., Cernusca, A., 2010. Land use affects the net ecosystem CO_2 exchange and its components in mountain grasslands. Biogeosciences 7 (8), 2297-2309, https://doi.org/10.5194/bg-7-2297-2010.

Sellers, P.J., Berry, J.A., Collatz, G.J., Field, C.B., Hall, F.G., 1992. Canopy reflectance, photosynthesis, and transpiration. III. A reanalysis using improved leaf models and a new canopy integration scheme. Remote Sens. Environ. 42 (3), 187-216, https://doi.org/10.1016/0034-4257(92)90102-P.

Séquaris, J.-M., Klumpp, E., Vereecken, H., 2013. Colloidal properties and potential release of water-dispersible colloids in an agricultural soil depth profile. Geoderma 193, 94-101, https://doi.org/10.1016/j.geoderma.2012.10.014.

Šimůnek, J., Suarez, D.L., 1993. Modeling of carbon dioxide transport and production in soil 1. Model development. Water Resour. Res. 29 (2), 487-497, https://doi.org/10.1029/92WR02225.

Šimůnek, J., Suarez, D.L., Šejna, M., 1996. The UNSATCHEM Software Package for simulating the one-dimensional variably saturated water flow, heat transport, carbon dioxide production and transport, and multicomponent solute transport with major ion equilibrium and kinetic chemistry, Version 2.0. Research Report No. 141. U.S. Salinity Laboratory, Agricultural Research Service, U.S. Department of Agriculture, Riverside, California, pp. 186.

Skaggs, T.H., Anderson, R.G., Alfieri, J.G., Scanlon, T.M., Kustas, W.P., 2018. Fluxpart: Open source software for partitioning carbon dioxide and water vapor fluxes. Agric. For. Meteorol. 253-254, 218-224, https://doi.org/10.1016/j.agrformet.2018.02.019.

Skjemstad, J.O., Spouncer, L.R., Cowie, B., Swift, R.S., 2004. Calibration of the Rothamsted organic carbon turnover model (RothC ver. 26.3), using measurable soil organic carbon pools. Aust. J. Soil Res. 42 (1), 79-88, https://doi.org/10.1071/sr03013.

Skopp, J., Jawson, M.D., Doran, J.W., 1990. Steady-state aerobic microbial activity as a function of soil water content. Soil Sci. Soc. Am. J. 54 (6), 1619-1625.

Soussana, J.F., Allard, V., Pilegaard, K., Ambus, P., Amman, C., Campbell, C., Ceschia, E., Clifton-Brown, J., Czobel, S., Domingues, R., Flechard, C., Fuhrer, J., Hensen, A., Horvath, L., Jones, M., Kasper, G., Martin, C., Nagy, Z., Neftel, A., Raschi, A., Baronti, S., Rees, R.M., Skiba, U., Stefani, P., Manca, G., Sutton, M., Tuba, Z., Valentini, R., 2007. Full accounting of the greenhouse gas (CO_2, N_2O, CH_4) budget of nine European grassland sites. Agric. Ecosyst. Environ. 121 (1-2), 121-134, https://doi.org/10.1016/j.agee.2006.12.022.

Spitters, C.J.T., van Keulen, H., van Kraalingen., D.W.G., 1989. A simple and universal crop growth simulator, SUCROS87. In: Rabbinge, R., Ward, S.A., van Laar, H.H., (Eds.), Simulation and systems management in crop protection. Simulation Monographs 32, PUDOC, Wageningen, pp. 147-181.

Špunda, V., Kalina, J., Urban, O., Luis, V.C., Sibisse, I., Puértolas, J., Šprtová, M., Marek, M.V., 2005. Diurnal dynamics of photosynthetic parameters of Norway spruce trees cultivated under ambient and elevated CO_2: the reasons of midday depression in CO_2 assimilation. Plant Sci. 168 (5), 1371-1381, https://doi.org/10.1016/j.plantsci.2005.02.002.

Stadler, A., Rudolph, S., Kupisch, M., Langensiepen, M., van der Kruk, J., Ewert, F., 2015. Quantifying the effects of soil variability on crop growth using apparent soil electrical conductivity measurements. Eur. J. Agron. 64, 8-20, https://doi.org/10.1016/j.eja.2014.12.004.

Stoy, P.C., Katul, G.G., Siqueira, M.B.S., Juang, J.-Y., Novick, K.A., Uebelherr, J.M., Oren, R., 2006. An evaluation of models for partitioning eddy covariance-measured net ecosystem exchange into photosynthesis and respiration. Agric. For. Meteorol. 141 (1), 2-18, https://doi.org/10.1016/j.agrformet.2006.09.001.

Subke, J.-A., Inglima, I., Cotrufo, M.F., 2006. Trends and methodological impacts in soil CO_2 efflux partitioning: a metaanalytical review. Global Change Biol. 12 (6), 921-943, https://doi.org/10.1111/j.1365-2486.2006.01117.x.

Suleau, M., Moureaux, C., Dufranne, D., Buysse, P., Bodson, B., Destain, J.-P., Heinesch, B., Debacq, A., Aubinet, M., 2011. Respiration of three Belgian crops: partitioning of total ecosystem respiration in its heterotrophic, above- and below-ground autotrophic components. Agric. For. Meteorol. 151 (5), 633-643, https://doi.org/10.1016/j.agrformet.2011.01.012.

Sulman, B.N., Roman, D.T., Scanlon, T.M., Wang, L., Novick, K.A., 2016. Comparing methods for partitioning a decade of carbon dioxide and water vapor fluxes in a temperate forest. Agric. For. Meteorol. 226-227, 229-245, https://doi.org/10.1016/j.agrformet.2016.06.002.

Supit, I., Hooijer, A.A., van Diepen, C.A., 1994. System description of the WOFOST 6.0 Crop Simulation Model implemented in CGMS. Volume 1: theory and algorithms. EUR 15956 EN, Joint Research Centre, European Commission, Luxembourg, pp. 146.

Sus, O., Williams, M., Bernhofer, C., Béziat, P., Buchmann, N., Ceschia, E., Doherty, R., Eugster, W., Grünwald, T., Kutsch, W., Smith, P., Wattenbach, M., 2010. A linked carbon cycle and crop developmental model: description and evaluation against measurements of carbon fluxes and carbon stocks at several European agricultural sites. Agric. Ecosyst. Environ. 139 (3), 402-418, https://doi.org/10.1016/j.agee.2010.06.012.

Swinnen, J., van Veen, J.A., Merckx, R., 1995. Carbon fluxes in the rhizosphere of winter wheat and spring barley with conventional vs integrated farming. Soil Biol. Biochem. 27 (6), 811-820, https://doi.org/10.1016/0038-0717(94)00230-X.

Thomas, C., Martin, J.G., Goeckede, M., Siqueira, M.B., Foken, T., Law, B.E., Loescher, H.W., Katul, G., 2008. Estimating daytime subcanopy respiration from conditional sampling methods applied to multi-scalar high frequency turbulence time series. Agric. For. Meteorol. 148 (8-9), 1210-1229, https://doi.org/10.1016/j.agrformet.2008.03.002.

Thomas, C.K., Law, B.E., Irvine, J., Martin, J.G., Pettijohn, J.C., Davis, K.J., 2009. Seasonal hydrology explains interannual and seasonal variation in carbon and water exchange in a semiarid mature ponderosa pine forest in central Oregon. J. Geophys. Res. 114, G04006, pp. 22, https://doi.org/10.1029/2009JG001010.

Trudinger, C.M., Raupach, M.R., Rayner, P.J., Kattge, J., Liu, Q., Pak, B., Reichstein, M., Renzullo, L., Richardson, A.D., Roxburgh, S.H., Styles, J., Wang, Y.P., Briggs, P., Barrett, D., Nikolova, S., 2007. OptIC: An intercomparison of optimization techniques for parameter estimation in terrestrial biogeochemical models. J. Geophys. Res. 112, G02027, pp. 17, https://doi.org/10.1029/2006jg000367.

Twine, T.E., Kustas, W.P., Norman, J.M., Cook, D.R., Houser, P.R., Meyers, T.P., Prueger, J.H., Starks, P.J., Wesely, M.L., 2000. Correcting eddy-covariance flux underestimates over a grassland. Agric. For. Meteorol. 103 (3), 279-300, https://doi.org/10.1016/s0168-1923(00)00123-4.

van de Boer, A., Moene, A.F., Graf, A., Schüttemeyer, D., Simmer, C., 2014. Detection of entrainment influences on surface-layer measurements and extension of Monin-Obukhov Similarity Theory. Boundary-Layer Meteorol. 152, 19-44, https://doi.org/10.1007/s10546-014-9920-8.

van Genuchten, M.T., 1980. A close-form equation for predicting the hydraulic conductivity of unsaturated soils. Soil Sci. Soc. Am. J. 44 (5), 892-898.

van Keulen, H., Goudriaan, J., Stroosnijder, L., Lantinga, E.A., van Laar, H.H., 1997. Crop growth model for water-limited conditions (SUCROS2). In: van Laar, H.H., Goudriaan, J., van Keulen, H. (Eds.), SUCROS97: Simulation of crop growth for potential and water-limited production situations. As applied to spring wheat. Quantitative Approaches in Systems Analysis, AB-DLO, Wageningen, pp. 21-58.

Vanclooster, M., Viaene, P., Diels, J., Christiaens, K., 1995. WAVE: A mathematical model for simulating water and agrochemicals in the soil and vadose environment: reference and user's manual (release 2.0). Institute for Land and Water Management, Katholieke Universiteit, Leuven, Belgium, pp. 154.

Vickers, D., Thomas, C.K., Pettijohn, C., Martin, J.G., Law, B.E., 2012. Five years of carbon fluxes and inherent water-use efficiency at two semi-arid pine forests with different disturbance histories. Tellus B Chem. Phys. Meteorol. 64, 17159, pp. 14, https://doi.org/10.3402/tellusb.v64i0.17159.

Wang, W., Fang, J., 2009. Soil respiration and human effects on global grasslands. Global Planet. Change 67 (1-2), 20-28, https://doi.org/10.1016/j.gloplacha.2008.12.011.

Wang, W., Smith, J.A., Ramamurthy, P., Baeck, M.L., Bou-Zeid, E., Scanlon, T.M., 2016. On the correlation of water vapor and CO_2: application to flux partitioning of evapotranspiration. Water Resour. Res. 52 (12), 9452-9469, https://doi.org/10.1002/2015WR018161.

Wang, Y.-P., Trudinger, C.M., Enting, I.G., 2009. A review of applications of model-data fusion to studies of terrestrial carbon fluxes at different scales. Agric. For. Meteorol. 149 (11), 1829-1842, https://doi.org/10.1016/j.agrformet.2009.07.009.

Wattenbach, M., Sus, O., Vuichard, N., Lehuger, S., Gottschalk, P., Li, L., Leip, A., Williams, M., Tomelleri, E., Kutsch, W.L., Buchmann, N., Eugster, W., Dietiker, D., Aubinet, M., Ceschia, E., Béziat, P., Grünwald, T., Hastings, A., Osborne, B., Ciais, P., Cellier, P., Smith, P., 2010. The carbon balance of European croplands: a cross-site comparison of simulation models. Agric. Ecosyst. Environ. 139 (3), 419-453, https://doi.org/10.1016/j.agee.2010.08.004.

Webster, R., 1997. Regression and functional relations. Eur. J. Soil Sci. 48 (3), 557-566, https://doi.org/10.1046/j.1365-2389.1997.00099.x.

Weihermüller, L., Huisman, J.A., Lambot, S., Herbst, M., Vereecken, H., 2007. Mapping the spatial variation of soil water content at the field scale with different ground penetrating radar techniques. J. Hydrol. 340 (3-4), 205-216, https://doi.org/10.1016/j.jhydrol.2007.03.013.

Weihermüller, L., Huisman, J.A., Graf, A., Herbst, M., Séquaris, J.-M., 2009. Multistep outflow experiments to determine soil physical and carbon dioxide production parameters. Vadose Zone J. 8 (3), 772-782, https://doi.org/10.2136/vzj2008.0041.

Weihermüller, L., Graf, A., Herbst, M., Vereecken, H., 2013. Simple pedotransfer functions to initialize reactive carbon pools of the RothC model. Eur. J. Soil Sci. 64 (5), 567-575, https://doi.org/10.1111/ejss.12036.

Weiskittel, A.R., Kershaw Jr., J.A., Hofmeyer, P.V., Seymour, R.S., 2009. Species differences in total and vertical distribution of branch- and tree-level leaf area for the five primary conifer species in Maine, USA. Forest Ecol. Manag. 258 (7), 1695-1703, https://doi.org/10.1016/j.foreco.2009.07.035.

Wiekenkamp, I., Huisman, J.A., Bogena, H.R., Graf, A., Lin, H.S., Drüe, C., Vereecken, H., 2016. Changes in measured spatiotemporal patterns of hydrological response after partial deforestation in a headwater catchment. J. Hydrol. 542, 648-661, https://doi.org/10.1016/j.jhydrol.2016.09.037.

Williams, C.A., Scanlon, T.M., Albertson, J.D., 2007. Influence of surface heterogeneity on scalar dissimilarity in the roughness sublayer. Boundary-Layer Meteorol. 122 (1), 149-165, https://doi.org/10.1007/s10546-006-9097-x.

Williams, M., Rastetter, E.B., Fernandes, D.N. Goulden, M.L., Wofsy, S.C., Shaver, G.R., Melillo, J.M., Munger, J.W., Fan, S.-M., Nadelhoffer, K.J., 1996. Modelling the soil-plant-atmosphere continuum in a Quercus-Acer stand at Harvard Forest: the regulation of stomatal conductance by light, nitrogen and soil/plant hydraulic properties. Plant Cell Environ. 19 (8), 911-927, https://doi.org/10.1111/j.1365-3040.1996.tb00456.x.

Williams, M., Richardson, A.D., Reichstein, M., Stoy, P.C., Peylin, P., Verbeeck, H., Carvalhais, N., Jung, M., Hollinger, D.Y., Kattge, J., Leuning, R., Luo, Y., Tomelleri, E., Trudinger, C.M., Wang, Y.-P., 2009. Improving land surface models with FLUXNET data. Biogeosciences 6 (7), 1341-1359.

Wohlfahrt, G., Hammerle, A., Haslwanter, A., Bahn, M., Tappeiner, U., Cernusca, A., 2008. Seasonal and inter-annual variability of the net ecosystem CO_2 exchange of a temperate mountain grassland: effects of weather and management. J. Geophys. Res. 113, D08110, pp. 14, https://doi.org/10.1029/2007JD009286.

Wollschläger, U., Attinger, S., Borchardt, D., Brauns, M., Cuntz, M., Dietrich, P., Fleckenstein, J.H., Friese, K., Friesen, J., Harpke, A., Hildebrandt, A., Jäckel, G., Kamjunke, N., Knöller, K., Kögler, S., Kolditz, O., Krieg, R., Kumar, R., Lausch, A., Liess, M., Marx, A., Merz, R., Mueller, C., Musolff, A., Norf, H., Oswald, S.E., Rebmann, C., Reinstorf, F., Rode, M., Rink, K., Rinke, K., Samaniego, L., Vieweg, M., Vogel, H.-J., Weitere, M., Werban, U., Zink, M., Zacharias, S., 2017. The Bode hydrological observatory: a platform for integrated, interdisciplinary hydro-ecological research within the TERENO Harz/Central German Lowland Observatory. Environ. Earth Sci. 76 (1), 29, pp. 25, https://doi.org/10.1007/s12665-016-6327-5.

Wu, X., Luo, Y., Weng, E., White, L., Ma, Y., Zhou, X., 2009. Conditional inversion to estimate parameters from eddy-flux observations. J. Plant Ecol. 2 (2), 55-68, https://doi.org/10.1093/jpe/rtp005.

Xue, Q., Weiss, A., Arkebauer, T.J., Baenziger, P.S., 2004. Influence of soil water status and atmospheric vapor pressure deficit on leaf gas exchange in field-grown winter wheat. Environ. Exp. Bot. 51 (2), 167-179, https://doi.org/10.1016/j.envexpbot.2003.09.003.

Yuan, W., Liang, S., Liu, S., Weng, E., Luo, Y., Hollinger, D., Zhang, H., 2012. Improving model parameter estimation using coupling relationships between vegetation production and ecosystem respiration. Ecol. Model. 240, 219-240, https://doi.org/10.1016/j.ecolmodel.2012.04.027.

Zacharias, S., Bogena, H., Samaniego, L., Mauder, M., Fuß, R., Pütz, T., Frenzel, M., Schwank, M., Baessler, C., Butterbach-Bahl, K., Bens, O., Borg, E., Brauer, A., Dietrich, P., Hajnsek, I., Helle, G., Kiese, R., Kunstmann, H., Klotz, S., Munch, J.C., Papen, H., Priesack, E., Schmid, H.P., Steinbrecher, R., Rosenbaum, U., Teutsch, G., Vereecken, H., 2011. A network of terrestrial environmental observatories in Germany. Vadose Zone J. 10 (3), 955-973, https://doi.org/10.2136/vzj2010.0139.

Zeeman, M.J., Eugster, W., Thomas, C.K., 2013. Concurrency of coherent structures and conditionally sampled daytime sub-canopy respiration. Boundary-Layer Meteorol. 146, 1-15, https://doi.org/10.1007/s10546-012-9745-2.

Zeeman, M.J., Mauder, M., Steinbrecher, R., Heidbach, K. Eckart, E., Schmid, H.P., 2017. Reduced snow cover affects productivity of upland temperate grasslands. Agric. For. Meteorol. 232, 514-526, https://doi.org/10.1016/j.agrformet.2016.09.002.

Zimmermann, M., Leifeld, J., Schmidt, M.W.I., Smith, P., Fuhrer, J., 2007. Measured soil organic matter fractions can be related to pools in the RothC model. Eur. J. Soil Sci. 58 (3), 658-667, https://doi.org/10.1111/j.1365-2389.2006.00855.x.

ACKNOWLEDGEMENTS

This work was supported by the German Federal Ministry of Education and Research BMBF, project IDAS-GHG [grant number 01LN1313A]. Most measurement infrastructure providing observational data was supported by the German Research Foundation DFG through the Transregional Collaborative Research Centre 32 (TR32) and Terrestrial Environmental Observatories (TERENO).

I would like to express my gratitude to my doctoral supervisor Prof. Dr. Harry Vereecken, head of the Institute of Bio- and Geosciences - Agrosphere (IBG-3) at the Forschungszentrum Jülich, for our discussions on my work, your precious time and input, and for all the opportunities (and little pushes) you have given me during my time at the institute. Furthermore, I thank Prof. Dr. Bernd Diekkrüger of the University of Bonn, Department of Geography, for taking on the co-supervision.

My deepest gratitude goes to my supervisor Dr. Alexander Graf of IBG-3. Thank you for this opportunity to write this thesis with you and for all challenges you have given me. Further, thank you for all your efforts, time and patience, great teaching skills, cheerfulness, and your numerous and extraordinary ideas. You are an amazing person! And thank you for sharing large amounts of chocolate.

I am very grateful to Dr. Arnold F. Moene, whom I visited for three months at Wageningen University and Research, Meteorology and Air Quality Group. Thank you for introducing me to large eddy simulations and thus, opening new possibilities to my studies. Moreover, thank you for your time, support, large efforts, your spontaneity, and valuable ideas!

This work would not have been possible without the support of many colleagues at IBG-3. I thank all secretaries, IT specialists, and further management personal for their patient and quick support in everyday business. I am also grateful to all technicians, engineers, and laboratory assistants in TR32, TERENO, and elsewhere for providing measurements of the test sites. I am grateful to Dr. Michael Herbst and PD Dr. Lutz Weihermüller of IBG-3 (It is their fault that I stranded in Jülich). Thank you for introducing me to programming, modelling, and the world of science. Moreover, thank you for your time, patience, humor, and many Streuselbrötchen.

Furthermore, I thank my colleagues and friends, who joined me for numerous enjoyable lunch breaks, cake sessions, ice cream and coffee breaks, field campaigns, conferences, pub visits, dinners, travels, board game sessions, …Thank you for the great time at the institute! Also, I thank my friends from school, university, and sports for their constant support and the amazing adventures we have experienced (and still will in the future).

Finally, I thank my family, especially my parents Stephanie and Hartwig, my brother Jan, and my grandparents Anneliese, Günther, and Elisabeth for their continuous support, their love, and encouragement! Thank you for teaching me so much! Also, I thank Julian for always being there for me. Thank you for always understanding, encouraging, and taking care of me! I am very grateful to have you in my life!

Band / Volume 448
3D simulation of impurity transport in a fusion edge plasma using a massively parallel Monte-Carlo code
J. Romazanov (2018), xvi, 149 pp
ISBN: 978-3-95806-377-8

Band / Volume 449
Projektbericht Adelheid – aus dem Labor heraus in die Lüfte
R. Peters, J. Pasel, R. C. Samsun, A. Tschauder, C. Wiethege, F. Scharf, D. Stolten (2018), xxi, 321 pp
ISBN: 978-3-95806-378-5

Band / Volume 450
Microstructure and Thermomechanical Properties of $SrTi_{1-x}Fe_xO_{3-\delta}$ Oxygen Transport Membranes and Supports
R. Oliveira Silva (2019), vi, 148 pp
ISBN: 978-3-95806-381-5

Band / Volume 451
Sodium Ion Conducting Ceramics for Sodium Ion Batteries
S. Naqash (2019), vii, 134 pp
ISBN: 978-3-95806-382-2

Band / Volume 452
Quantitative Analyse der Trocknungsverläufe von Katalysatordispersionen
F. Scheepers (2019), VIII, 191 pp
ISBN: 978-3-95806-384-6

Band / Volume 453
Neue Optionen für einen wirtschaftlichen Betrieb von Wasserstoffzügen durch Nutzung der LOHC-Technologie?
P. Wasserscheid, T. Grube, D. Sternfeld, M. Essl, M. Robinius, D. Stolten (2019), II, 88 pp
ISBN: 978-3-95806-386-0

Band / Volume 454
Reformierung von BtL-Kraftstoffen für die HT-PEFC in luftfahrttechnischen Systemen
C. Wilbrand (2019), IV, 312 pp
ISBN: 978-3-95806-387-7

Band / Volume 455
Entwicklung von thermischen Spritzprozessen für fortschrittliche Schutz- und Funktionsschichten
G. Mauer (2019), vi, 57 pp
ISBN: 978-3-95806-388-4

Band / Volume 456
Columnar Structured Thermal Barrier Coatings Deposited by Axial Suspension Plasma Spraying
D. Zhou (2019), VI, 126 pp
ISBN: 978-3-95806-391-4

Band / Volume 457
Modellierung zeitlich aufgelöster Ladeenergienachfragen von batterie-elektrischen Fahrzeugen und deren Abbildung in einem Energiesystemmodell
J. F. Linßen (2019), VIII, 189 pp
ISBN: 978-3-95806-395-2

Band / Volume 458
Synthesis and Analysis of Spinel Cathode Materials for High Voltage Solid-State Lithium Batteries
A. Windmüller (2019), iv, 142 pp
ISBN: 978-3-95806-396-9

Band / Volume 459
Monazite-type ceramics as nuclear waste form: Crystal structure, microstructure and properties
Y. Arinicheva (2019), 194 pp
ISBN: 978-3-95806-397-6

Band / Volume 460
Coupling a Solid Oxide Fuel Cell with a Biomass Gasifier: Degradation Mechanisms and Alternative Anode Materials
H. Jeong (2019), II, 112 pp
ISBN: 978-3-95806-398-3

Band / Volume 461
Model-based Source Partitioning of Eddy Covariance Flux Measurements
A. Klosterhalfen (2019), XVI, 132 pp
ISBN: 978-3-95806-401-0

Weitere ***Schriften des Verlags im Forschungszentrum Jülich*** unter
http://wwwzb1.fz-juelich.de/verlagextern1/index.asp

Energie & Umwelt / Energy & Environment
Band / Volume 461
ISBN 978-3-95806-401-0

Mitglied der Helmholtz-Gemeinschaft

JÜLICH
Forschungszentrum